University of South-Eastern Norway
Faculty of Technology, Natural Sciences and Maritime Studies
—
Doctoral dissertation no. 118
2022

Ramesh Timsina

Modelling and simulations of bubbling fluidized bed and entrained flow biomass gasification reactors

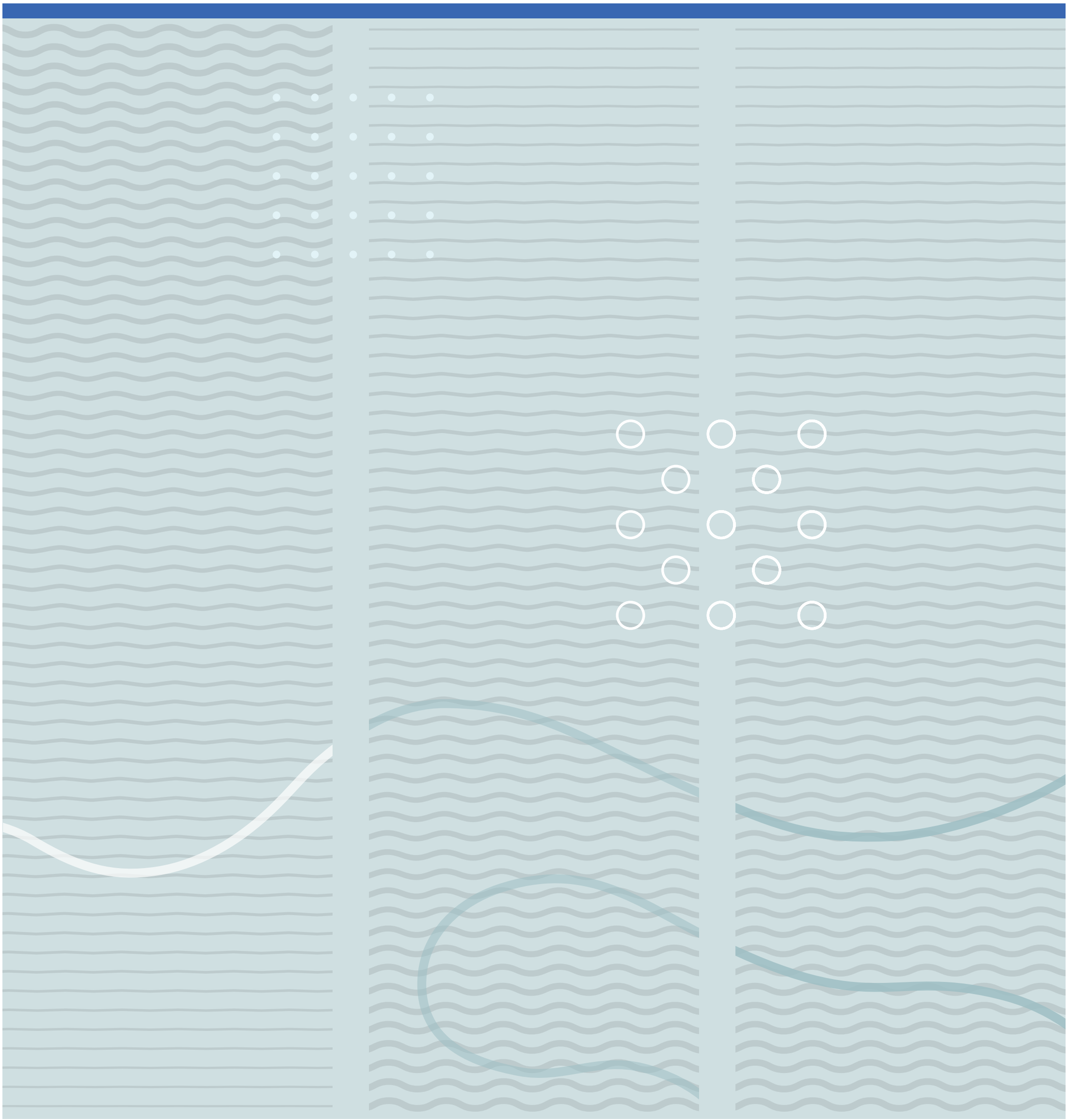

Ramesh Timsina

Modelling and simulations of bubbling fluidized bed and entrained flow biomass gasification reactors

A PhD dissertation in
Process, Energy and Automation Engineering

© 2022 Ramesh Timsina
Faculty of Technology, Natural Sciences and Maritime Studies
University of South-Eastern Norway
Porsgrunn, 2022

Doctoral dissertations at the University of South-Eastern Norway no. 118

ISSN: 2535-5244 (print)
ISSN: 2535-5252 (online)

ISBN: 978-82-7206-644-3 (print)
ISBN: 978-82-7206-645-0 (online)

This publication is, except otherwise stated, licenced under Creative Commons. You may copy and redistribute the material in any medium or format. You must give appropriate credit provide a link to the license, and indicate if changes were made.
http://creativecommons.org/licenses/by-nc-sa/4.0/deed.en

Print: University of South-Eastern Norway

I dedicate this to,

My beloved parents…

Supervisors and teachers…

Family and friends…

all those who have brought me to this stage…

Preface

This thesis is submitted to the University of South-Eastern Norway (USN) for the degree of Philosophiae doctor (PhD). This dissertation is based on the research work carried at USN Porsgrunn. Norwegian ministry of education and research financed this work through the PhD program in Process, Energy and Automation Engineering at USN. The research is supported by the Norwegian centre for sustainable bio-based fuels and energy (Bio4Fuels).

In regard to my background, I have a bachelor's degree in mechanical engineering from the National Institute of Technology Durgapur India (2013) and a master's degree in process technology from USN (2017).

This PhD work is a continuation of the previous studies carried out at USN Porsgrunn (Agu, 2019; Bandara, 2021; Rautenbach, 2012; Thapa, 2015). Several literatures were studied to gain the knowledge and ideas of the current research and developments in the same field.

USN provided the simulation tools for this project: Barracuda VR for the computational fluid dynamics (CFD) simulations and Aspen Plus for process simulations. USN gave access to the cold flow models for bubbling fluidized bed (BFB) and a pilot-scale BFB gasification reactor. The cold flow models are used to predict the fluidization behaviour whereas the gasifiers are used to optimize the gasification process of biomass.

Acknowledgements

From Nepal to India and eventually, to Norway, the quest to pursue a doctorate has been demanding and overwhelming to me. I would like to thank all the people for helping me directly or indirectly to achieve this goal. It would not have been possible without the help and support of many people. I deeply appreciate my main supervisor Professor Marianne S. Eikeland and my co-supervisors Professor Britt M. E. Moldestad and Dr Rajan K. Thapa for providing me with a comfortable working environment and supports whenever needed. I am also grateful for their continuous guidance, support, encouragement, and keeping the patient throughout this project. It is a great pleasure to work with such persons with expertise in the field of gasification, CFD, process simulations, and many more. I would like to thank USN for giving me an opportunity to carry out this project and express my sincere gratitude to the university for the research funding for this project. I would also like to thank the library staff and the IT department of the university for providing various supports whenever required.

I would like to express my sincere gratitude to Rajan K. Thapa for inspiring and sharing his knowledge in this field to get started on the research project. I owe special thanks to him for his guidance, support, encouragement, and motivation during my hard time both in professional and in private life. My humble appreciation goes to my fellow researchers Rajan Jaiswal, Janitha Bandara, Cornelius Agu, Nora C. I. Furuvik, and Nastaran Ahmadpour Samani from USN for sharing their knowledge and time.

Ramesh Timsina (Porsgrunn, Norway / 06 October 2021)

Abstract

The world needs sustainable energy solutions to replace fossil fuels. Climate change is the defining challenge of our time. New reports from the International Energy Agency (IEA, 2021)[1] have developed a roadmap for max 1.5°C global warming and net zero emissions by 2050 from the energy sector. The roadmap recommends increasing efforts and a clear political action to invest in renewable energy extensively and immediately. Biomass contributes to more than 10% of the global energy demand and has the potential to contribute to a renewable energy supply. Gasification is a thermal conversion of biomass into higher energy gases such as carbon monoxide (CO), hydrogen (H_2), and methane (CH_4), and the gases can be used directly or synthesized into biofuel and higher value chemicals.

This thesis contains the experimental results for a cold flow model for bubbling fluidized bed (BFB) and a pilot scale BFB gasifier. The reactor hydrodynamics and the mixing behaviour of the bed were investigated using the cold flow model study. The experimental studies in BFB gasifier include the gasification of wood chips, wood pellets and grass pellets at different air flow rates and biomass feed rates. The product gas compositions and the gasifier performance (based on the mass balance of N_2 in the inlet and outlet gas) were measured and analyzed. Increasing the equivalence ratio (ER) gave an increased gas yield per kilogram of biomass, however, the lower heating value (LHV) of the product gas decreased due to the dilution of the product gas with N_2. Gasification of grass pellets was challenging due to the formation of agglomerates and gave a low carbon conversion. Wood chips showed reasonable results at a temperature of around 850°C with a carbon conversion of around 60%.

Computational particle fluid dynamics (CPFD) models were developed for the cold flow model for BFB, BFB gasifier and entrained flow (EF) gasifier. The models were validated against the experimental results from the corresponding reactor/gasifiers. The results

---

[1] https://www.iea.org/reports/net-zero-by-2050

from the model showed that bed hydrodynamics plays a significant role in biomass conversion in the BFB gasifier. The bubbling behaviour of the bed influenced the heat and particle distribution, thus affecting the gasification behaviour. For a case with birch wood, the CO concentration decreased from 25 to 13.2 mole % and the CO_2 concentration increased from 17 to 19.5 mole % when the ER increased from 0.2 to 0.3.

Simulation results for the EF gasifier showed that the Char- O_2 and char-H_2O reactions are significant in the gasifier entrance region, whereas the char-CO_2 reaction is prevalent throughout the reactor elevation. Particles in the central region show high carbon conversion compared to the particles in the other zones. The ratio of product gas to biomass was calculated as 3.61 Nm^3/kg of biomass. The average gas fractions on a volume basis were 0.038 of CH_4, 0.457 of CO, 0.226 of CO_2, and 0.275 of H_2. The lower heating value of the product gas is calculated as 7.8 MJ/kg.

A process simulation model was developed to study the BFB biomass gasification in Aspen Plus. The model was used to predict the gasifier performance for different operating conditions, i.e., temperature, steam to biomass ratio (STBR), biomass types, and biomass loadings. Hydrogen production was around 50% for all types of biomass while CO production varies from 8% (Pig manure) to 24.5% (Olive residue) at 700°C. H_2/CO ratio increased with an increase in STBR for all types of biomass. H_2 concentration increased from 46 % to 54% and CO concentration decreases from 30% to 20% with an increase in STBR from 0.6 to 1 for the wood residue.

The results obtained from this study can be useful for the operational control and the optimization of the biomass gasification reactors. The proposed model for the BFB gasifier can be extended into a dual circulating fluidized bed (DCFB), which gives the product gas free from nitrogen (N_2). The models for gasifiers accept different possible inputs to the gasifiers, which can be useful in determining the optimal operating conditions for efficient biomass conversion.

Keywords: fluidized bed, biomass gasification, entrained flow, process simulation, CFD simulation, CPFD, biofuels

List of tables

List of figures

Table of contents

A. Overview

2

1 Introduction

Energy demand is steadily increasing due to the continuous increase in population, industry, and increase in the living quality of people. This leads to an increase in greenhouse gas (GHG) emissions as well as an increase in municipal solid waste. Therefore, sustainable energy supply and waste management are the two main challenges of our generation. Waste management, industrial activities, and household activities should be based on the principles of circular economy, i.e., minimize the waste of any materials, energy, and economy (X. Zhang *et al.*, 2020).

Both on national and international levels, efforts are made to limit greenhouse gas emissions (IEA, 2019). For example, European Union (EU) has set a target of 60% emission reduction to achieve carbon neutrality by 2050 through a share of renewable energy sources and hydrogen up to 53% and 24% respectively (Voultsos et al., 2020).

Nearly one-fourth of the global emissions in 2016 were from the transport sector, of which the road and aviation industry made up to 86% as shown in Figure 1-1 (Guo, 2020). This is due to the fact that the transport sector is primarily driven by fossil fuels. There are several attempts to address this problem. Liquid biofuel is one of the options. The produced biofuels can be more or less integrated into the current infrastructure compared to other renewable technologies such as batteries and fuel cells (Güell et al., 2013). This is very relevant for the conventional conservative industries such as aviation and marine (Köhler et al., 2014).

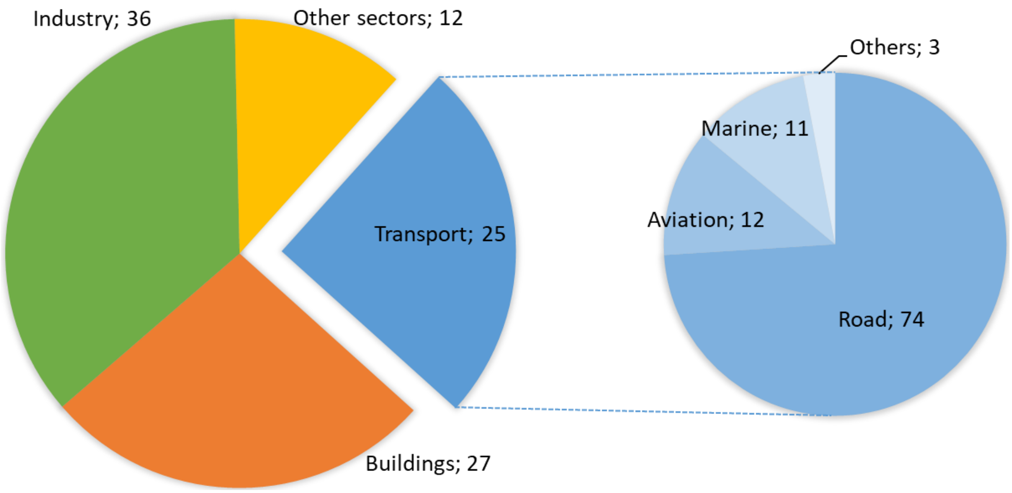

Figure 1-1. Global CO_2 emissions (in percentage) (Guo, 2020)

1.1 Background

Biomass is a renewable energy source with hydrocarbon origin and has the potential to replace fossil-fuel-based products, commonly known as biofuel. In addition, biofuels could potentially fill the gap bridge between the transition of the current use of fossil fuel to future electric and battery propelled vehicles. Apart from emission reduction, mass plantation of energy crops and trees improve the ecosystem and biodiversity. Biomass is a natural sink for carbon: the higher the trees grown, the higher will be the CO_2 capture (Zanchi et al., 2012).

USN is a partner in the research centre for environment friendly energy (FME), Bio4fuels, and has the responsibility for the work package «Preparing for piloting» within the subproject «Gasification Processes» (NMBU, 2020). This PhD project is a direct contribution to this work package. Bio4Fuels is focused on developing viable conversion technologies for the conversion of biomass and organic residue to transportation fuels, along with added value chemicals, heat, and power. The Bio4Fuels project has five subprojects focusing on bioresources acquisition, biomass conversion technologies (gasification processes, biochemical processes, and liquefaction process) and process design and end-use.

In the subproject gasification processes, SINTEF Energy has the responsibility for the development of the gasification technology. SINTEF Energy has a pilot-scale entrained flow biomass gasifier whereas USN has a pilot-scale bubbling fluidized bed biomass gasifier. Norwegian University of Science and Technology has the responsibility for gas conditioning and the Fischer-Tropsch synthesis (Gavrilović et al., 2021; Pandey et al., 2021). Based on the resources and the responsibility for the project, this PhD work is focused on the bubbling fluidized bed and entrained flow biomass gasification as well as a process simulation for the conversion of syngas to methanol.

Among different biomass conversion technologies, biomass gasification is a thermal breakdown of biomass particles into combustible gases, tars, char, and ash in a limited supply of oxidizing agents (steam, air, or oxygen). The major gas components from biomass gasification are CO, H_2, carbon dioxide (CO_2), and CH_4 (Basu, 2018). The main objective of this work is to obtain a higher value product from biomass via biomass gasification, a thermochemical conversion technology.

Bubbling fluidized bed gasifiers use inert or catalytic bed material at a fluidized state which enhances the heat and biomass distribution inside the gasifier. The fluidized beds are characterized by the lower pressure drop and low-temperature gradient inside the bed (Rhodes, 1990). Bubbling fluidized bed gasifiers operate between 700°C and 1100°C. Entrained Flow biomass gasifier operates at elevated temperature (1000-1400 °C) and pressure (20-70 bar) (Basu, 2018). Fuel, as well as the gasifying agent, are introduced concurrently into the gasifier and the product gas leaves from the bottom half of the reactor. The range of applications for the different types of biomass gasifiers are different. For example, entrained flow gasifiers have the capacity in the range of 50 MW to 1000 MW and fluidized bed gasifiers have the capacity in the range of 2 MW to 100MW (Basu, 2018).

The product gas produced during the gasification process has different applications, from heating and power generation to biofuel and higher-value chemicals synthesis. Figure 1-2 shows the conversion steps of biomass into biofuels via gasification.

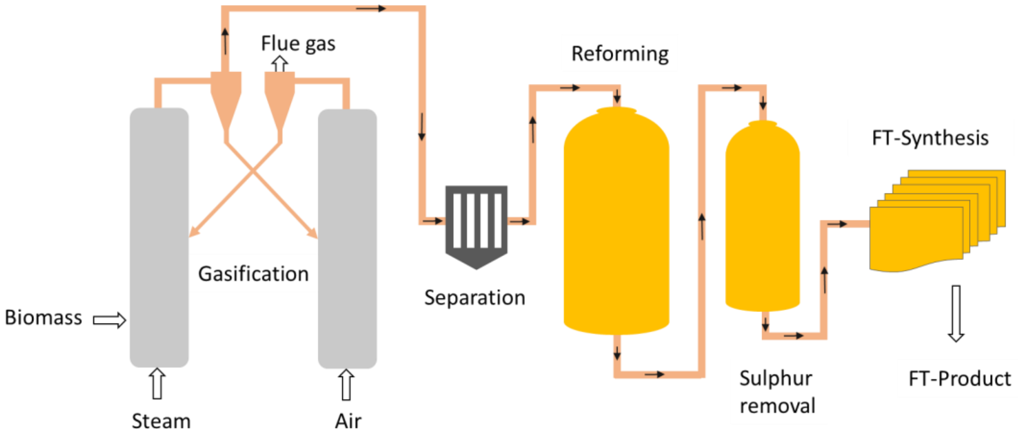

Figure 1-2. Different steps for the conversion of biomass to biofuels via gasification

The figure shows different steps involved in the conversion of biomass into biofuels. The product gas from the biomass gasification reactor enters the separation stage where solid particles are filtered out and the removal of CH_4 and CO_2 is carried out. The clean product gas consisting of CO and H_2 (called syngas) enters a reforming reactor where a particular ratio of H_2/CO is achieved. The gas is then passed through a sulphur removal unit to remove sulphur (if any) present in the syngas. The syngas then enters gas to liquid (GtL) process (for example FT-synthesis, methanol synthesis) to give the liquid product.

1.2 The problem statements

Biomass gasification is still in a developing stage at an industrial scale. A consensus on the optimal approach is not yet established. The physical and chemical behaviour of biomass in a gasifier varies between each gasification reactor, even for the same types of biomass. The published literature does not account for all the possible variables change at once, rather focuses on a particular parameter for a particular gasifier. This gives different fluidization conditions and operational conditions, giving a different gasification behaviour from one another. Therefore, new experiments and studies are important for the possible improvements of the gasifiers for successful commercialization.

Biomass particles conversion is challenging due to its low density, irregularity in shape and fibrous structure. There are still some challenges concerning the hydrodynamics and the thermochemical properties of a biomass gasifier, both in a fluidized bed and entrained flow reactors. The reactor hydrodynamics and the thermochemical behaviour are not fully understood yet. Therefore, continuous research and studies are required for the simultaneous optimization of the reactor hydrodynamics and the operational conditions such as equivalence ratio, temperatures, pressures etc.

Computational fluid dynamics modelling and simulation has become a useful tool for system optimization and upscaling. Multiphase modelling and simulation are very complex and time consuming compared to single phase systems. Computational particle fluid dynamics is a novel development in the field of CFD which is built on a multiphase particle-in-cell (MP-PIC) approach. CPFD model validation against the experimental results is an essential step due to the fact that these models have a certain level of simplification, empirical models and approximation techniques. Therefore, the models developed during this study have been validated against the experimental results.

1.3 Objective and scope

The primary objective for this PhD work was to develop CFD and process simulation models as a basis for process design, piloting, and upscaling for the conversion of biomass into biofuels. The objective is divided into three main tasks:

1. Experimental study of biomass gasification in fluidized bed reactors.
2. Development of CFD models for the study of biomass gasification in a fluidized bed and entrained flow gasification reactor.
3. Development of a process model using Aspen Plus for the study of the conversion of syngas to methanol.

1.4 Limitations

- The experimental results for biomass gasification require more experiments for a generalized product gas performance.
- Devolatilization is defined as a one-step global reaction. Mass fractions of volatile components and char were taken from literature.
- Minor elements in biomass such as sulphur and nitrogen are neglected during modelling and all the tar formed during the process is assumed to convert into CO, CO_2, and CH_4.
- Gas properties were calculated using the ideal gas law.
- The inputs to the simulation model for the methanol synthesis were assumed as clean syngas at a specified ratio and the detailed study of the intermediate steps from the gasification reactor to the feed of the synthesis reactor was beyond the scope of this thesis.
- Aspen Plus lacks the library model to simulate a fluidized bed gasifier and different unit operations were combined to represent the biomass gasification as close as possible.

1.5 Main contribution

As stated in the objective of this current research, the major focus was on the study of gasification behaviour in BFB and EF biomass gasifiers. A study of the gas to liquid process was also performed based on the developed model in Aspen Plus. The major contribution is divided into three major categories (experimental studies, CPFD studies and Aspen Plus simulation) and can be summarised as follows:

1. Experimental studies of biomass gasification were performed in an air blown atmospheric BFB gasifier located at USN. The study gave a detailed insight into the biomass gasification process in such types of reactors. Experiments were performed in a cold flow model of the BFB to study the reactor hydrodynamics and the mixing behaviour of the biomass with the bed material. The experiments in the cold flow model were used to calculate the minimum fluidization velocity at cold conditions. The calculated minimum fluidization velocity is cross calculated for the hot bed conditions for the pilot-scale BFB gasifier in order to operate in the bubbling fluidized regime.
2. A CPFD model is developed for both the cold flow model and the pilot-scale BFB gasifier. The models were validated with the results obtained from the experiments. The developed model is efficient in terms of saving time and resources.
3. A CPFD model is developed to study the biomass gasification behaviour in an EF gasifier. The CPFD model for the EF biomass gasifier was validated against the results published in the literature for a pressurized entrained-flow biomass gasifier (PEBG) plant present at the Energy Technology Centre (ETC) in Piteå Sweden. The major focus was to optimize the flow behaviour and thermochemical behaviour inside the reactor.
4. A process model in Aspen Plus was developed to study the conversion of syngas into methanol. The model was used to optimize some of the operating parameters in a methanol synthesis plant (distillation column) and provides an overview of the overall conversion steps and efficiency.

5. A process model in Aspen Plus was developed to study the gasification of biomass. Such models offer a convenient way to study gasification behaviour in a relatively short time. Aspen Plus has been widely used for different chemical reactors on an industrial scale. In these models, reaction kinetics is unknown, and the products of gasification are estimated based on the minimization of Gibbs's free energy. The model was used to study the product gas composition for different feedstocks, at different temperatures and biomass feed loadings.

Figure 1-3 summarizes the summary of work performed during the PhD period.

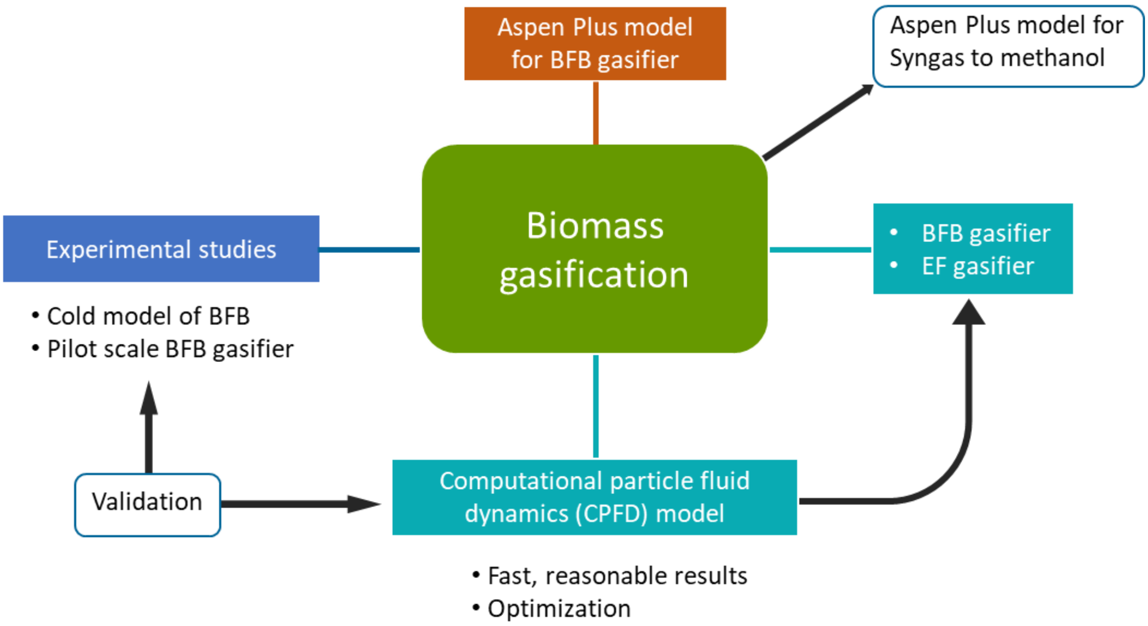

Figure 1-3. Summary of the project work

1.6 Thesis Layout

The thesis contains two parts. The first part includes a brief background of the study, the materials and methods used, and a summary of the findings. The second part contains a detailed analysis of the results enclosed in the form of different publications. The literature reviews and the previous works reported in this thesis are a summary of those contained in different papers. All the symbols and narration used in this thesis are the same as those in the relevant paper and therefore no symbol narration lists are provided. New symbols and narrations are clearly defined in their first appearances.

1.7 List of publications

- **Timsina R.**, Moldestad B., Eikeland M.S. and Thapa R.K. (2019). Simulation of air-biomass gasification in a bubbling fluidized bed using CPFD model. Presented at the 60th SIMS Conference on Simulation and Modelling, August 12-16, Västerås, Sweden. *Linköping University Electronic Press*, Issue no. 170, pp. 145-150. doi.org/10.3384/ecp20170145.
- **Timsina R.**, Thapa R.K. and Eikeland M.S. (2019). Aspen Plus simulation of biomass gasification for different types of biomass. Presented at the 60th SIMS Conference on Simulation and Modelling, August 12-16, Västerås, Sweden. *Linköping University Electronic Press*, Issue no. 170, pp. 151-157. doi.org/10.3384/ecp20170151.
- **Timsina R.**, Thapa R.K., Moldestad B.M. and Eikeland M.S. (2019). Effect of particle size on flow behaviour in fluidized beds. *International Journal of Energy Production and Management*, 4(4), 287-297. doi.org/10.2495/EQ-V4-N4-287-297.
- **Timsina R.**, Thapa R.K., Moldestad B.M. and Eikeland M.S. (2020). Experiments and computational particle fluid dynamics simulations of biomass gasification in an air-blown fluidized bed gasifier. *International Journal of Energy Production and Management*, 5(2), 102-114. doi.org/10.2495/EQ-V5-N2-102-114.
- **Timsina R.**, Thapa R.K., Moldestad B.M. and Eikeland M.S. (2020). Simulation of entrained flow gasification reactor with Multi Phase Particle in Cell (MP-PIC) approach. Presented at the 61st SIMS Conference on Simulation and Modelling, September 22-24, Online Conference. *Linköping University Electronic Press*, Issue no. 176, pp. 428-434. doi.org/10.3384/ecp20176428.
- **Timsina R.**, Thapa R.K., Moldestad B.M. and Eikeland M.S. (2021). Computational particle fluid dynamics simulation of biomass gasification in an entrained flow gasifier. *Chemical Engineering Science: X,* 12, 100112. doi.org/10.1016/j.cesx.2021.100112.
- **Timsina R.**, Thapa R.K., Moldestad B.M. and Eikeland M.S. (2021). Methanol synthesis from syngas: a process simulation. Presented at the SIMS EUROSIM 2021, September 21-23, Online Conference.
- **Timsina R.**, Jaiswal R., Thapa R.K., Moldestad, B.M.E., Bhattarai A., Jecmenica M. and Eikeland, M.S. (2021). Experimental evaluation of wood and grass pellets in a bubbling fluidized bed gasifier. Submitted to *Chemical Science*.

2 Literature studies

This chapter provides an overview of the theory and the principle used throughout this work. It gives a brief introduction to biomass properties, biomass gasification and its application, and the modelling of biomass gasification.

2.1 Biomass properties

Biomass can come from a wide range of sources. Biomass is composed of cellulose, hemicellulose, lignin, organic polymers, pectins, proteins, and minerals. Biomass contains 40-60% of cellulose, 15-25% of hemicellulose, and 15-25% of lignin (Pecha et al., 2019; Vassilev et al., 2010). Cellulose is the most linear of the three, contributing to the fibrous nature of biomass. Lignin is the least linear among the three. Hemicellulose and lignin act as a binding material for cellulose in the cell wall of the plant (Pecha et al., 2019).

Coal and biomass both share a conceptual similarity. Both of them consists of moisture, volatiles matter, fixed carbon, ash, etc. However, the composition varies a lot between coal and biomass. Biomass has higher amounts of volatiles, oxygen content and moisture but low carbon content, heating value and ash compared to coal. (Vassilev et al., 2015). Further, the sulphur content in biomass is mostly less than 0.5 wt%. The major components of biomass ash are potassium, calcium and phosphorous. It also contains iron, sodium, magnesium, silicon, and some trace elements. The biomass ash has a lower melting point as compared to coal ash (Qin, 2012).

The non-spherical nature of biomass particles influences the particle motion, heat, and mass transfer inside a reactor. Heat transfer within a biomass particle is anisotropic due to its fibrous structure (Pecha et al., 2019). Therefore, the pre-treatment of biomass is often needed to increase homogeneity in size and composition for most of the thermal conversion process.

Different types of biomass such as Norwegian spruce, pulverized miscanthus, beechwood, etc. are irregular in shape (T. Li *et al.*, 2015; Panahi *et al.*, 2017). Under non-reactive conditions, the particle shape affects the reactor/bed hydrodynamics. For different particles with different shapes, the particle surface area to volume ratio varies, which affects the heat and mass transfer process. Li and Zhang (J. Li & Zhang, 2017) demonstrated that the char combustion rate increases with an increase in the particle aspect ratio from 0.3 to 0.9. Lu et al. (Lu et al., 2010) have shown that the particle shape affects the particle devolatilization rate. Near-spherical particles gave lower volatiles and higher tar yields relative to aspherical particles under similar conditions for a given mass. The volatile yields decreased with increasing particle size for particles of all shapes (Lu et al., 2010). Therefore, the biomass particle shape affects the overall conversion process and should be properly defined while modelling the biomass gasification process. Misrepresenting the shape of biomass particles could make the simulation results misrepresentative of reality.

There are also studies on improving the biomass feedstocks quality by optimizing lignin levels and reduction of ash and moisture contents. This can be achieved by breeding/developing a new species, specially targeted for energy production in a larger quantity (Tanger et al., 2013). Algal biomass is being investigated for different conversion technologies because of its fast-growing capacity and has no competition with agricultural food and feed production (Chowdhury & Loganathan, 2019; Demirbas, 2007; Wang et al., 2017).

2.2 Biomass gasification

Biomass gasification is the partial oxidation of carbonaceous fuels (biomass) into syngas (a mixture of mainly CO and H_2) in the presence of air, oxygen and/or steam. The gasification process involves a series of heterogeneous as well as homogeneous reactions. The other major components from biomass gasification are CO_2, and CH_4 (Basu, 2018).

As the biomass enters the reactor different physical, chemical, and thermal processes may occur simultaneously or subsequently depending upon the fuel types, gasifier types and operating conditions. Figure 2-1 shows major steps occurring during the biomass gasification process. The major reaction taking place during a biomass gasification process is presented in Table 2-1.

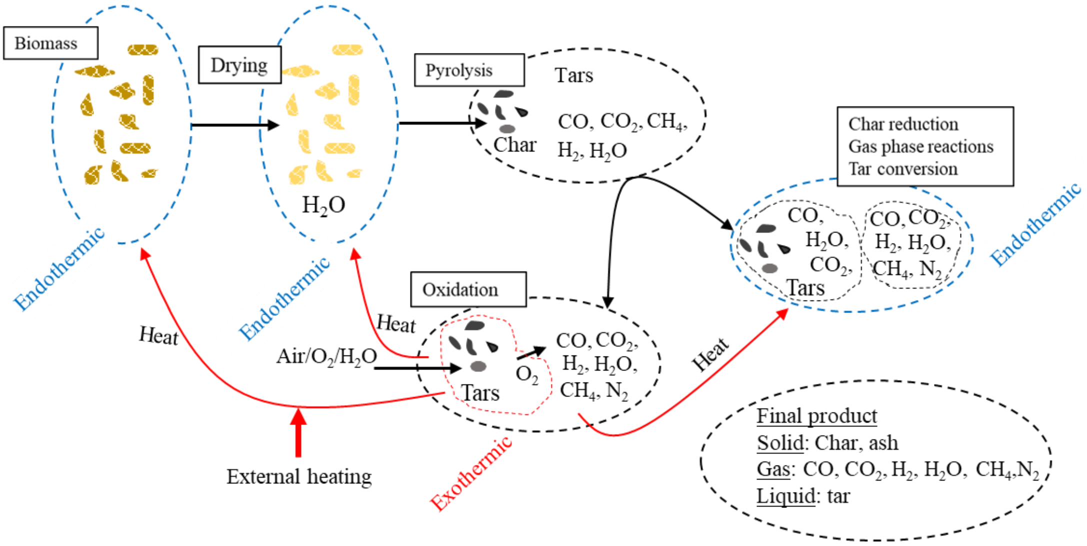

Figure 2-1. Major steps in biomass gasification

Table 2-1. Principal reaction during a biomass gasification process (Basu, 2018)

Reaction	Name	Enthalpy (kJ/mol)	
	Heterogeneous reactions		
$C(s) + 0.5O_2 \rightarrow CO$	Char partial oxidation	-111	R2.1
$C(s) + H_2O \leftrightarrow CO + H_2$	Steam gasification	+131	R2.2
$C(s) + CO_2 \leftrightarrow 2CO$	Boudouard reaction	+172	R2.3
$C(s) + 2H_2 \leftrightarrow CH_4$	Methanation	-75	R2.4
$C(s) + O_2 \rightarrow CO_2$	Char combustion	-394	R2.5
	Homogeneous reactions		
$H_2 + 0.5O_2 \rightarrow H_2O$	H_2 oxidation	-242	R2.6
$CO + 0.5O_2 \rightarrow CO_2$	CO oxidation	-283	R2.7
$CH_4 + 1.5O_2 \rightarrow CO + 2H_2O$	CH_4 oxidation		R2.8
$CO + H_2O \leftrightarrow CO_2 + H_2$	Water-gas shift	-41	R2.9
$CH_4 + H_2O \leftrightarrow CO + 3H_2$	Methane reforming	+206	R2.10

2.2.1 Drying and devolatilization

Moisture is the first component to release from the biomass when it enters the operating gasifiers.

$$biomass + heat = dry\ biomass + H_2O \qquad 2.1$$

When the temperature of the dry biomass increases around 300-400°C, devolatilization (also known as pyrolysis step in some literature) takes place and the dry biomass converts into char as well as tar and volatiles (Qin, 2012). Fuel particles can lose up to 80% of their weight during the devolatilization process (Smoot & Smith, 1985). The volatiles undergo a series of homogeneous reactions both within the bed and in the freeboard region.

$$dry\ biomass + heat = volatiles + char + soot \qquad 2.2$$

The volatile components may include CO, H_2, CO_2, CH_4, C_2H_4, H_2O, C_2H_6, H_2S, NH_3, olefins, aromatics and tar depending on the biomass and the gasifier specification (Qin, 2012). Char is the solid particles consisting of organic material (carbon) and inorganic materials (ash). Drying and devolatilization could occur simultaneously as well as instantly depending on the heating rate in the gasifier.

2.2.2 Oxidation and gasification

As a principle, a limited amount of oxygen is introduced into the gasifier as an oxidizing agent. A certain ratio of the product formed during the devolatilization process gets oxidized to provide the thermal energy required for the gasification reactions.

Different reactions have different reaction rates depending on the gasification system; allothermal or autothermal gasification (Kaur *et al.*, 2019; Qin, 2012). Allothermal gasification requires an external heating source to fulfil the energy required for gasification. In autothermal gasification, the required heat is generated directly by partial oxidation inside a gasifier. The indirect use of a heat exchanger or the circulation of hot bed materials between the combustion and gasification zone is an example of an autothermal process. Dual fluidized bed gasification is an autothermal gasification process (Kaur *et al.*, 2019).

Above a temperature of around 700°C, char can be gasified by H_2O and CO_2. Further char can be gasified by H_2 at elevated pressure. As compared to the devolatilization and the oxidation reactions, heterogeneous gasification reactions are much slower, controlling the product formation (Qin, 2012). At the same time, the homogeneous reaction occurs between the different gases present inside the reactor. One of the most important reactions during a gasification process is the water gas shift reaction (WGS), which is particularly important as it can be used to shift the ratio of H_2 and CO. Lower temperature is favourable for the forward WGS and high temperature is favourable for the backward WGS and methane reforming reactions. Backward methane reforming reaction is also favourable at high pressure. In addition, at sufficiently high temperatures, tar may decompose into non-condensable gases and secondary tars.

$$Primary\ tar\ (\mathrm{CH}_x\mathrm{O}_y) \rightarrow CO, CO_2, CH_4, H_2, C_2H_4, secondary\ tar \qquad 2.3$$

2.2.3 Char conversion/reactivity

As discussed in Chapter 2.2, char particles are produced during the devolatilization process in biomass gasification. The reactions R2.2, R2.3 and R2.5 are the main chemical reactions involving char particles. Reactions R2.1 and R2.4 are less significant compared to the former char reactions. Char conversion is a slow process as compared to the devolatilization step and is often referred to as a rate-limiting step in a gasification process. The reaction rate depends upon the form of carbonaceous material being reacted, its specific surface area and its corresponding activation energy. This is particularly important for entrained flow gasifiers where the particle residence time is very short (Molino *et al.*, 2016; Qin *et al.*, 2013). Char reactivity plays an important role in determining the reaction rate for heterogeneous reactions. The reactivity of char is given by:

$$r_m = -\frac{1}{m_c}\frac{dm_c}{dt} = \frac{1}{(1-x_c)}\frac{dx_c}{dt} \qquad 2.4$$

where m_c and x_c are the mass of carbon contained in the sample and its conversion rate at time t (Gómez-Barea and Leckner, 2010).

2.2.4 BFB gasifier and EF gasifier

There are different types of gasification reactors. The most common types of gasification technologies are fixed beds, fluidized beds, and entrained flow reactors. As this work is focused on the bubbling fluidized gasifier and entrained flow gasifiers, the details of these reactors are provided in this chapter.

Fluidized bed gasifiers use inert or catalytic bed material at a fluidized state to enhance the heat and biomass distribution inside the gasifier. The fluidized beds are characterized by the lower pressure drop and low temperature gradient inside the bed (Rhodes, 1990). Fluidized bed gasifiers are divided into bubbling fluidized bed (BFB), circulating fluidized bed (CFB) and dual fluidized bed (DFB) gasifiers. A DFB gasifier configuration consists of an interconnected BFB column and a CFB riser. Biomass gasification takes place in the BFB column, and the combustion of char residue and additional fuel (if required) takes place in the CFB riser. The main purpose of these types of reactors is to transfer the heat released during the combustion process in the riser back into the BFB column to aid the gasification process. The DFB reactor is extensively used for the steam gasification of biomass in different parts of the world. For example, the SilvaGas biomass gasification process in Atlanta, United States America (Paisley & Overend, 2002), biomass gasification plant located in Gussing, Austria (Hofbauer *et al.*, 2002; Kirnbauer & Hofbauer, 2011) and DFB gasification reactor located at the Chalmers University of Technology (Larsson, 2014) are based on the principle of DFB gasifier. Air gasification in a BFB gasifier dilutes the product gas with nitrogen, which can be eliminated easily using a dual circulating fluidized bed (DCFB) gasifier.

The bubbling fluidized bed technology operates in the temperature range of 700-1100°C (Franco et al., 2003). A fluidizing agent such as air or steam is introduced from the bottom of the bed and the reactors operate within the bubbling fluidization regime. Superficial velocity is usually kept around twice the minimum fluidization velocity to minimize particle elutriation. Biomass is fed either from the top or from the side of a bed in a BFB gasifier.

Figure 2-2 shows the particle scale mechanism in a BFB gasification reactor. Several complex physical and chemical transformations occur over time and space in a BFB gasifier. Bubbles rising through the solid bed and the circulating solids play an important role in the hydrodynamic of the bed. Solid-gas flow in a BFB is characterized as a random mixing of the two phases. Under ideal conditions, the random mixing, and the high heat capacity of the bed material result in a higher rate of heat transfer to the biomass particles. Bubble hydrodynamics, particle-particle and fluid-particle mixing have a great impact on the gasification behaviour of the BFB gasification reactor.

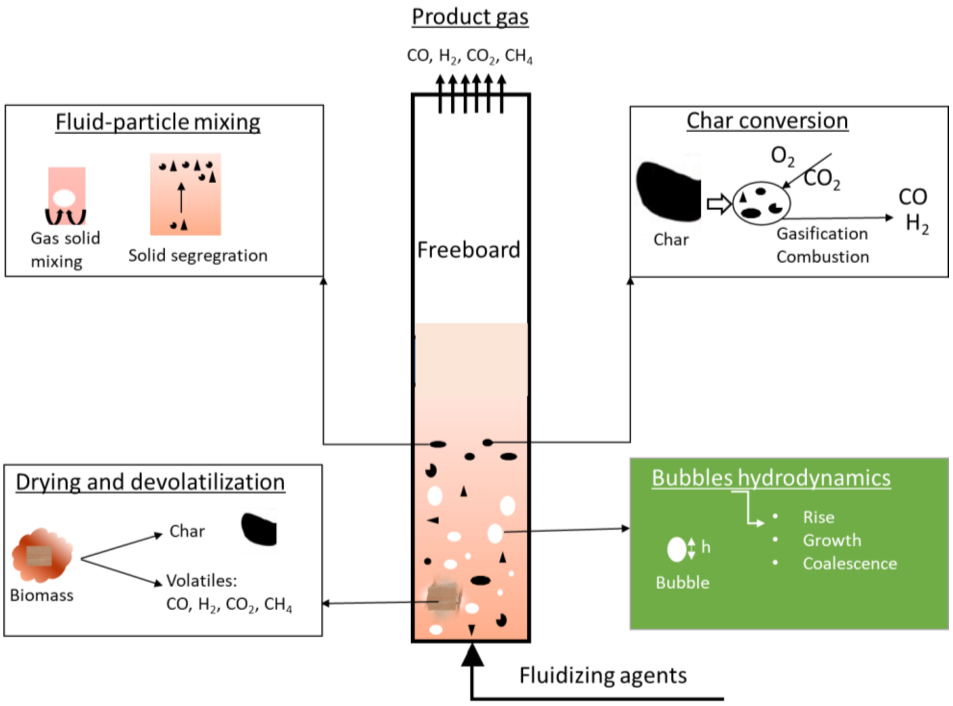

Figure 2-2. Particle scale mechanism in a BFB gasification reactor

Several experimental studies can be found in the literature for the study of biomass gasification. Kim et al. (Kim *et al.*, 2013) have studied biomass gasification in a pilot-scale BFB gasifier with air as the gasifying agent. Silica sand was used as a bed material and the experimental conditions were controlled by varying the biomass and the air feed rates. The biomass feed ranged from 25 kg/h to 55 kg/h and the air flow rate varied from 33-54 Nm^3/hr. The product gas composition increased from 14.5% to 16.5% for H_2, 13.8% to 16.8% for CO and 4% to 5.3% for CH_4 with a change in ER from 0.27 to 0.19. The H_2 concentration is relatively high compared to different other literature studies. The authors believed that the higher concentration of H_2 was due to the configuration of the gasifier that consisted of a longer freeboard region and had top fuel feeding. The syngas calorific value was above 4.7 MJ/Nm³, which is suitable for power generation using a syngas engine.

Campoy et al. (Campoy *et al.*, 2008) have studied the biomass gasification behaviour with air and air/steam as a gasifying agent in a BFB using wood pellets. Experiments were conducted at constant air flow rates with varying biomass and steam flow rates. As the steam addition increased, biomass throughput was decreased to maintain a sufficient temperature level in the reactor. In pure air gasification, the gas composition and the gas yield varied in between 18.2-15.8% of CO, 13.2-8.7% of H_2, 6-4.6% of CH_4 and 0.6-1.2 Nm³/kg of biomass respectively as the ER was changed from 0.19 to 0.35 (Campoy *et al.*, 2008). The addition of steam resulted in higher H_2 in the product gas, whereas the plant efficiency increased linearly with an increase in ER. However, the tar yield was increased at higher ERs, which is in contrast to the other literature findings. An increase in the tar content could be due to an increase in the biomass flow rate from 11.5 kg/h to 20.5 kg/h to adjust the steam to biomass ratio. The pilot plant was upgraded by adding an auxiliary electrical heating (Campoy *et al.*, 2009) and experiments were performed with O_2 enriched air-steam mixtures. The CO and H_2 contents increased to 25% and 27% respectively with a maximum LHV of 8 MJ/Nm³.

Meng et al. (Meng *et al.*, 2019) have investigated the effect of gasifying agents such as air, air-steam, oxygen-enriched air and oxygen-steam in a pilot-scale BFB gasifier. Experiments were performed with sawdust particles ranging from 150-350 µm and the bed material ranges from 180-250 µm. The H_2 content increased with an increase in ER from 0.2 to 0.3 for all the gasifying agents. There was a significant increase in the H_2, CO and CH_4 content in the product gas with an increase in the oxygen content from 21% to 99% in the gasifying agent. As a result of less nitrogen in the product gas, the LHV increased from 6.16 to 12.17 MJ/m³. Compared to using air as the gasifying agent, oxygen-enriched air increased the LHV due to lower dilution by N_2, the air-steam favoured higher H_2 production due to enhancing the forward WGS reaction and O_2-steam resulted in lower N_2 and higher H_2 in the product gas.

There are a considerable number of publications focusing on the different aspects of BFB gasifiers (Arena & Di Gregorio, 2014; Fremaux *et al.*, 2015; Hervy *et al.*, 2019; Karatas *et al.*, 2013; Makwana *et al.*, 2019; Nam *et al.*, 2018; Sarker *et al.*, 2015; Serrano *et al.*, 2016; Subramanian *et al.*, 2011; M. M. Yu *et al.*, 2015). However, it is difficult to compare the results directly since the operating conditions, reactor configuration and biomass properties differ from one reactor to another. Change of airflow to manipulate ER will alter the fluidization environments. Whereas, adjusting the biomass flow rate to manipulate ER reduces the temperature at the feeding area, which will lead to altered devolatilization conditions. The composition and the geometry of biomass are significantly different even with the same species due to the variation in age, geography, rainfall patterns, climate etc. BFB gasifiers exhibit some degree of segregation of the biomass particles in the bed, which is rarely discussed in the literature. The gas residence time and reactor configurations could significantly change the product gas composition via WGS and reforming reactions. It is difficult to compare the result recorded with different types of gasifiers such as autothermal vs allothermal gasifiers.

In a BEB gasification of biomass, inorganic components of the biomass cause the bed to agglomerates. This leads to defluidization of the bed and halts the operation of the gasifier. Inorganic components sinter to forms a coating on the surface of bed material grains which initiates the bed agglomeration. Different experts believe that the biomass should be converted into a slagging form to make a gasifier more flexible for different types of fuels. This eliminates the problems of agglomeration in the gasifier. Therefore, the concept of an entrained flow gasifier was developed and tested with different configurations. A little ash melting cannot be avoided completely during a biomass gasification process, which increases the importance of the EF gasifier, as the melted ash is slagged out of the gasifier (Van der Drift et al., 2004).

In an entrained flow gasifier, the fuel and the gasifying agent (oxygen, air/steam) are injected co-currently into the gasifier. EF biomass gasifier is essentially a continuous flow reactor operated at elevated temperature and pressure (around 1400°C and 20-70 bar (Basu, 2018). Biomass is pre-treated to a suitable size before entering into the gasifier.

Figure 2-3 shows a schematic diagram of an EF slagging gasifier. Originally designed for a coal and petroleum coke particle (Duchesne, 2012), entrained flow gasifiers are being investigated extensively for biomass gasification to meet the requirement of green energy targets. However, oxygen operated gasifiers are expensive as they require substantial amounts of compression and refrigeration work for oxygen separation from air (Bhattacharya *et al.*, 2012).

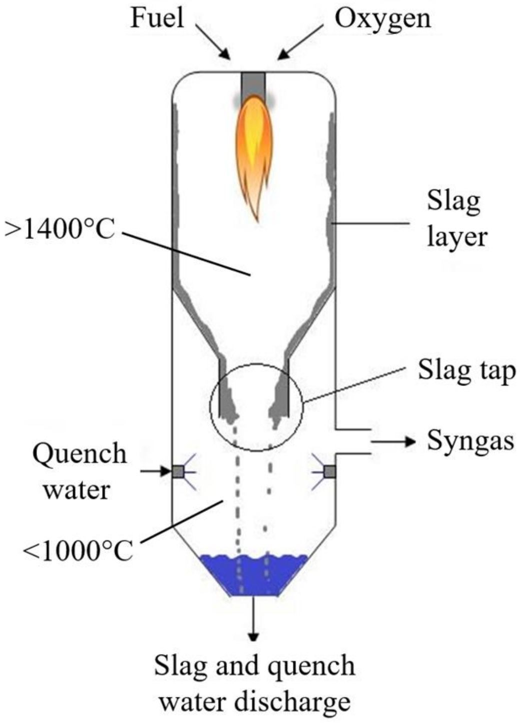

Figure 2-3. Entrained flow gasifier (Duchesne, 2012)

Syngas may consist of additional particulate matter (fly ash and unconverted char) along with nitrogen and sulphur compounds. Ash particles in the biomass form a silicate melt known as slag, which moves down along the reactor wall and flows out from the bottom of the reactor. It is also to be noted that the slag built upon the inner surface of the reactor is expected to protect the refractory lining of the reactor and reduce heat loss. On the other hand, plugging by slag can be an operational difficulty in some cases. The higher viscosity of the slag, the higher the plugging risks. One of the alternatives to achieve a proper slag flow is operating at a higher temperature. This increases oxygen demand significantly and reduces the process efficiency (Duchesne, 2012). The other option for proper slag flow is blending the fuels or adding a fluxing agent. Limestone and dolomite are feasible alternatives as fluxing agents because of their low costs and higher content of calcium and magnesium. Calcium and magnesium reduce the sticking probabilities of the slag to the reactor inner wall because of reduced slag viscosity (Duchesne, 2012).

Ku et al. (Ku *et al.*, 2014; Ku *et al.*, 2019) have investigated the effect of reactor temperature, excess air ratio/equivalence ratio (λ), gasifying medium, steam/carbon ratio, reactor structure and feedstock properties on the performance of the EF reactor. H_2 and CO productions increased with an increase in the reactor temperature. While increasing excess air ratio decreased both H_2 and CO productions and increasing the steam/carbon ratio increased the H_2 production but decreased the CO production (Ku *et al.*, 2014). The addition of O_2 gave higher CO production and carbon conversion, whereas excessive oxygen use gave a reduced combustible gas yield and cold gas efficiency (CGE). The addition of steam resulted in an increased amount of H_2, carbon conversion and LHV. Biomass having higher fixed carbon or volatile content and a lower moisture content gave a high combustible gas yield (Ku *et al.*, 2019)

Guo et al. (Guo *et al.*, 2020) have studied particle hydrodynamics, heat transfer and devolatilization kinetics by developing a Eulerian-Lagrangian (EL) CFD model in an OpenFOAM. Four different approaches were tested for the quantitative comparison. The spheroidal particle shape assumption with adjusted spheroidal surface area and the Kishore-Gu model proves to favour the drying and devolatilization process. However, the sphere and simplified non-sphere model predict 61% and 43% longer residence times, respectively, than the spheroid models, and the longer residence time seems to favour the char conversion process (Guo *et al.*, 2020).

Liang et al. (Liang *et al.*, 2020) have developed a CPFD simulation model for an EF gasification reactor for the Utah bituminous coal. The detailed particle information and residence time were studied. The rapid expansion from a tracer injector and fast reactions play an important role in forming the particle distribution zone in the gasifiers. The authors pointed out that due to the complexity of the EF gasification reactions and the computational power limitation, the models were often simplified to two-dimensional or semi three-dimensional models. There was also limited information available in the literature about the particle temperatures, carbon contents, and locations for the discrete particles (Liang *et al.*, 2020).

The advantages and disadvantages of the BFB and EF gasifiers are summarized in Table 2-2. Apart from the aforementioned gasifiers, there are also other types of gasifiers such as plasma reactors and rotary kiln reactors.

Table 2-2. Advantages and disadvantages for the different types of gasifiers (Molino *et al.*, 2016; L. Zhang *et al.*, 2010)

Advantages	Disadvantages
Fluidized bed	
Flexible feed rate and composition High ash fuels are acceptable Able to pressurize High volumetric capacity Easy temperature control	Operating temperature limited by ash clinkering/sintering High tar and fines content in the gas Possibility of high C content in fly ash
Entrained flow	
Flexible to feedstock Very low in tar and CO_2, CH_4	Extreme feedstock size reduction required Complex operational control Carbon loss with ash

2.3 Application of syngas

Syngas application was one of the major aspects of the biomass gasification process. As discussed in Chapter 1, research is more focused on the application of syngas in the production of transportation fuels and chemicals. Some major application in the domain of biofuels includes methanol synthesis, hydrogen production, biofuels via Fischer-Tropsch synthesis etc.

2.3.1 Methanol synthesis

Methanol, also known as methyl alcohol or wood spirits, is one of the important industrial chemicals that can be used directly as a transportation fuel, blended into conventional fuels or converted into further hydrocarbons (Rauch *et al.*, 2014). Methanol is an important ingredient for the production of formaldehyde, acetic acid, methyl tertiary butyl ether, and gasoline.

Methanol is produced from the hydrogenation of carbon oxides over a suitable catalyst, for example, copper oxide, chromium oxide or zinc oxide, etc. Methanol synthesis reactors require a specific ratio of $CO/CO_2:H_2$. It is difficult to obtain the desired ratio directly from a gasifier. The ratio needs to be shifted to a higher hydrogen content and this is usually done via a water gas shift reaction. Two moles of H_2 are needed to react with CO and three moles of H_2 are needed to react with CO_2 for methanol formation according to the reaction stoichiometric given in Table 2-3. The first two reactions are exothermic and give a net decrease in molar volume. Therefore, methanol generation is favoured by high pressure and low temperature. The generated heat during the production must be removed continuously to have a high catalyst activity and life. As the reaction between CO/CO_2 with H_2 gives other products such as formaldehyde, dimethyl ether, or higher alcohol, the selectivity of the catalyst is an important parameter for methanol production. Copper oxides, chromium oxides or zinc oxides-based catalysts are used in commercial methanol production plants.

Table 2-3. Reaction formulas for methanol synthesis

$CO + 2H_2 \rightleftharpoons CH_3OH$	-90.64 kJ/mol	R2.11
$CO_2 + 3H_2 \rightleftharpoons CH_3OH + H_2O$	-49.67 kJ/mol	R2.12
$CO_2 + H_2 \rightleftharpoons CO + H_2O$	+41 kJ/mol	R2.13

The primary reason for catalyst deactivation is the loss of active copper sites. The copper sites get physical blockage by large by-product molecules, poisoning by sulphur or halogens in the synthesis gas, which forms inactive copper salts and develops sintering from copper crystallites into larger crystals, thereby reducing the surface to volume ratio (Rauch *et al.*, 2014).

Methanol can be converted into other hydrocarbons for example to diesel, gasoline, olefins (propylene and ethylene), dimethyl ether under certain process conditions and in presence of a suitable catalyst (Rauch *et al.*, 2014).

2.3.2 Fischer Tropsch synthesis

Fischer Tropsch (FT) synthesis is based on the catalytic conversion of the syngas into a wide range of hydrocarbon products. N-paraffins and 1-olefins are the main products obtained from the FT synthesis. The overall reactions during a FT synthesis can be represented by the following chemical reactions.

Major reactions

Paraffins	$(2n+1)H_2 + nCO \rightarrow C_nH_{(2n+2)} + nH_2O$	R2.14
Olefins	$2nH_2 + nCO \rightarrow C_nH_{2n} + nH_2O$	R2.15
Water-gas shift reaction	$CO + H_2O \rightleftharpoons CO_2 + H_2$	R2.16

Side reactions

Alcohols	$2nH_2 + nCO \rightarrow C_nH_{2n+2}O + (n -1) H_2O$	R2.17
Boudouard reaction	$2CO \rightarrow C + CO_2$	R2.18

Catalyst modifications

Catalyst oxidation/reduction	$M_xO_y + yH_2 \rightleftharpoons yH_2O + xM$ $M_xO_y + yCO \rightleftharpoons yCO_2 + xM$	R2.19
Bulk carbide formation	$yC + xM \rightleftharpoons yM_xC_y$	R2.20

FT synthesis is a key conversion process in GtL that produces synthetic fuels and chemicals. This is a well-established conversion process at the industrial level though based on natural gas and coal. Research is focused on the utilization of this technique to convert syngas obtained from biomass. The fuels produced from FT synthesis are of high quality because of low aromaticity and zero sulphur contents. Products such as LPG, gasoline, jet fuel, diesel fuels can be obtained through FT synthesis (van der Laan, 1999). The Sasol FT plant in South Africa and the Shell GtL plant in Bintulu Malaysia are examples of commercial-scale plants based on the FT synthesis (De Klerk & Furimsky, 2010).

However, the FT synthesis involves a complex reaction mechanism due to a large number of intermediate reaction species. It includes three-phase operation, heat and mass transfer resistances, catalyst deactivation etc. There is no consensus about the exact reaction mechanism, however, carbide and CO-insertion mechanisms are identified as the most probable ones by different authors (Todic *et al.*, 2014). In addition, the reaction of CO and H_2 is highly selective (the ability to form a different product with a different catalyst) on the catalyst.

2.3.3 Hydrogen production

Hydrogen fuel is one of the promising future energy sources. H_2 production from a dual fluidized bed steam gasification with CO_2 adsorption together with suitable catalysts can reach up to 70 % on a volume basis (Soukup *et al.*, 2009). Hydrogen production via biomass gasification is more economical than natural gas reforming by steam (Lau *et al.*, 2002).

2.3.4 Mixed alcohol production

Depending upon the process conditions and catalysts, mixed alcohols are produced together with methanol. Mixed alcohols are important additives to gasoline to increase the octane number which reduces the emissions from a vehicle. Mixed alcohol enhances the resistance of the catalyst against sulphur poisoning which results in simpler gas cleaning facilities. Mixed alcohols can also be converted into higher quality fuels via dehydration and oligomerization (Rauch *et al.*, 2014). Generally, alkali-dopped oxides and sulphides (zinc/chromium oxides, molybdenum sulphides) are used as catalysts for mixed alcohol synthesis (Rauch *et al.*, 2014).

2.4 Modelling of biomass gasification

Modelling of biomass gasification involves a gas-solid multiphase interaction and is challenging due to the coupling of turbulent gas flow and particle motions together with inter-particle collisions. There are three modelling approaches present in the literature.

The modelling approaches include (i) thermodynamic equilibrium models, (ii) kinetic rate models and (iii) Artificial Neural Network (ANN) models (Gungor & Yildirim, 2013).

The equilibrium models give the maximum achievable yield from a gasification system. The equilibrium models are being used for preliminary studies, for example, to identify the most important process parameters. The infinite residence time allows the reactor to reach the chemical equilibrium states at a particular operating condition and the model is free from the reactor configuration. The assumptions such as infinite residence time, homogeneous conditions and uniform mixing over the reactor are never achieved. Therefore, different studies suggested to include a non-equilibrium factor in the models for improved and reliable predictions (Ghassemi & Shahsavan-Markadeh, 2014; Lim & Lee, 2014).

The kinetic models are capable of incorporating the residence time and the reactor dimensions and are considered as rigorous models. The models depend on the average mass and heat transfer coefficients. These models are used for reactor design, and for the development and improvement of the process efficiency.

The ANN models are the black-box models with higher prediction accuracy. However, it is hard to get the physical meaning from these models and the scale up and piloting abilities of the ANN models are restricted (Gungor & Yildirim, 2013).

CFD modelling of biomass gasification incorporates the principle of kinetic models as well as reactor hydrodynamics. The basic approaches to model gasification systems are Eulerian-Eulerian (EE) and Eulerian-Lagrangian (EL) approaches. Both the solid and gas phase is treated as continuous phases (interpenetrating continua) in the EE approach which are solved using the Navier-Stokes's equation. This approach is also known as a two-fluid model where each phase is differentiated by its volume fraction. The method has been widely used for modelling of gas-solid systems due to less demand for computer power. The EE approach lacks the discrete nature of solid particles and the detailed transient information of the two-phase interactions (Bin et al., 2009).

EL approach preserves the discrete nature of particles where each solid particle is modelled with Newton's law of motion in Lagrangian coordinates. The gas phase is treated as a continuous phase and is modelled with the Navier-Stokes's equations (Eulerian coordinate). This approach takes the consideration that the solid phase can exchange mass, momentum and energy with the fluid phase, i.e., strong coupling between the two phases. The trajectory of every particle is calculated at a specified interval. The EL approach gives high loading to a computer central processing unit due to the huge number of particles in the system and the requirement of the small-time steps for solving the particle collisions (Ku et al., 2015). The EL approach is computationally expensive and is limited to only 2×10^5 particles (Gidaspow et al., 2004).

MP-PIC modelling is developed from the EL approach, which reduces the computational costs related to the discrete modelling of the solid particles. Computational particles for MP-PIC modelling are a group of particles (called parcels) with similar properties such as size, density, residence time, velocity, etc. This eliminates the need for tracking the individual particles. The parcels are modelled in a discrete frame and the particle interactions are modelled in the Eulerian frame. Hence, the particles are solved both in the Eulerian and Lagrangian frames, correlated by an interpolation function (Bandara et al., 2017). The fluid particles are solved with a Eulerian approach. Barracuda virtual reactor is a commercial software based on MP-PIC modelling. The MP-PIC modelling is also known as computational particle fluid dynamics (CPFD) modelling. The strong coupling between fluid and particle-phase gives a high level of accuracy and fast computational time in Barracuda VR. The rapid development of the graphic process unit in computers has made the CPFD simulation capable of simulating the real process in a short time. The major advantage of CPFD is that it can downsize the billions of particles in a large commercial plant to millions of computational particles (Chen et al., 2013).

Different simulation tools are being used by different researchers for the simulation of the biomass gasification process, for example, OpenFOAM (Gupta *et al.*, 2020; Ku *et al.*, 2014), Ansys/Fluent (L. Yu *et al.*, 2007).

2.4.1 CPFD Model

Conventional CFD often struggles as the particle phase becomes denser, as in the case of the BFB gasifier (Snider *et al.*, 2011). CPFD approach is the latest reasonable version of solving the dense phased gas-solid flows. CPFD modelling solves the solid and fluid conservation equations in three-dimensional Cartesian coordinate. The mass and momentum equation of the fluid phase is expressed as the averaged forms of the detailed fluid-phase mass and momentum equations (Snider *et al.*, 2011). The following governing equations are based on the literature references (Cho *et al.*, 2020; Snider *et al.*, 2011; Snider *et al.*, 2010).

2.4.1.1 Governing equations

The gas phase mass and momentum conservation equations are given by the continuity and the Navier-Stokes equations represented by Equations 2.5 and 2.6 respectively.

$$\frac{\partial(\alpha_g \rho_g)}{\partial t} + \nabla \cdot (\alpha_g \rho_g \vec{u}_g) = \delta \dot{m}_p \qquad 2.5$$

$$\frac{\partial}{\partial t}(\alpha_g \rho_g \vec{u}_g) + \nabla \cdot (\alpha_g \rho_g \vec{u}_g \vec{u}_g) = -\nabla p + F + \alpha_g \rho_g g + \nabla \cdot (\alpha_g \tau_g) \qquad 2.6$$

α, ρ and $\vec{u}$ represents the volume fraction, density and velocity vector respectively. $\delta \dot{m}_p$ is the gas mass production rate per volume formed from the particle-gas chemical reaction. In the case of a cold flow model with no chemical reaction $\delta \dot{m}_p$ becomes zero. p is the mean flow gas pressure; g is the acceleration due to gravity. τ_g is the fluid phase stress tensor and F is the inter-phase momentum transfer rate per unit volume (particle to fluid phase).

For a Newtonian fluid, the gas phase stress tensor for each species, τ_g is given by:

$$\tau_{g,ij} = \mu \left[\left(\frac{\partial u_i}{\partial x_j} + \frac{\partial u_j}{\partial x_i} \right) - \frac{2}{3} \mu \delta_{ij} \frac{\partial u_k}{\partial x_k} \right] \qquad 2.7$$

where μ is the shear viscosity, which is the sum of the coefficient of laminar shear viscosity and turbulence viscosity as defined in the Smagorinsky turbulence model (Smagorinsky, 1963). The model is given in Equation 2.8 (Snider *et al.*, 2011).

$$\mu_t = C\,\rho_g \Delta^2 \left(\frac{\partial u_i}{\partial x_j} + \frac{\partial u_j}{\partial x_i}\right) \tag{2.8}$$

The Smagorinsky coefficient C has a default value of 0.01. Δ is the subgrid length given by Equation 2.9.

$$\Delta = (\delta x \delta y \delta z)^{1/3} \tag{2.9}$$

A fluid-phase transport equation is solved for each gas species. The calculation of the fluid phase properties is based on the mass fraction $Y_{g,i}$ of the gas species. $\delta \dot{m}_{i,c}$ is a chemical source term, which is the mass transferred between the gas species by the dissociation and the association of the chemical bond.

$$\frac{\partial}{\partial t}\left(\alpha_g\, \rho_g\, Y_{g,i}\right) + \nabla \cdot (\alpha_g\, \rho_g\, Y_{g,i}\vec{u}_g) = \nabla \cdot (\alpha_g\, \rho_g\, D_t \nabla Y_{g,i}) + \delta \dot{m}_{i,c} \tag{2.10}$$

D_t is the turbulent mass diffusivity and can be calculated in Equation 2.11. Sc is the Schmidt number in Equation 2.11. The standard value of the turbulent Schmidt number is 0.9 (Snider *et al.*, 2011).

$$\frac{\mu}{\rho_g D} = Sc \tag{2.11}$$

The energy conservation equation of the gas phase is:

$$\frac{\partial}{\partial t}\left(\alpha_g \rho_g h_g\right) + \nabla \cdot (\alpha_g \rho_g h_g \vec{u}_g) = \alpha_g \left(\frac{\partial P}{\partial t} + \vec{u}_g \cdot \nabla P\right) + \varphi - \nabla \cdot \left(\alpha_g \vec{q}\right) + \dot{Q} + S_h + \dot{q}_D + q_{wp} \tag{2.12}$$

where h is the enthalpy and q_{wp} is the radiative heat transfer between the thermal wall and the particle phase. The viscous dissipation (φ) and energy source per unit volume ($\dot{Q}$) are neglected in this work. S_h is the conservative energy exchange from the particle phase to the gas phase. $\dot{q}_D$ is the enthalpy diffusion term and $\vec{q}$ is the gas heat flux. The expressions for the $\vec{q}$ and $\dot{q}_D$ are given as:

$$\vec{q} = \lambda_g \nabla T_g \tag{2.13}$$

$$\dot{q}_D = \sum_{i=1}^{N} \nabla \cdot (h_i\, \alpha_g\, \rho_g\, D \nabla Y_{g,i}) \tag{2.14}$$

where λ is the thermal conductivity calculated as a sum of a molecular conductivity (λ_m) and an eddy-conductivity (λ_t) from Reynold's stress mixing theory. The eddy-conductivity is calculated from the turbulent Prandtl number correlation.

$$\mathrm{Pr}_t = \frac{\mathrm{C_p \mu_t}}{\mathrm{\lambda_t}} \tag{2.15}$$

The mass, momentum and energy conservation equations (Equations 2.5, 2.6 and 2.12) are solved for the gas mixture. The gas mixture properties are based on the mass fractions of the gas species calculated using Equation 2.10. The flow is considered as compressible and the gas phase temperature, pressure, enthalpy, density and mass fraction are correlated through the equation of state. CPFD uses the ideal gas equation of state. The partial pressure of a gas species is calculated as:

$$\mathrm{P}_i = \frac{\rho_g Y_{g,i} R T_g}{M_{w,i}} \tag{2.16}$$

and the mean flow gas pressure is given as:

$$\mathrm{P} = \sum_{\mathrm{i=1}}^{\mathrm{N}} \mathrm{P}_i \tag{2.17}$$

where R is the universal gas constant, T_g is the gas mixture temperature and $M_{w,i}$ is the molecular weight of a gas species i. The gas mixture enthalpy (h_g) is the sum of individual gas enthalpy (h_i), given by:

$$h_g = \sum_{\mathrm{i=1}}^{\mathrm{N}} Y_{g,i}\, h_i \tag{2.18}$$

$$h_i = \int_{T_o}^{T_g} C_{p,i}\, dT + \Delta h_{f,i} \tag{2.19}$$

where $\Delta h_{f,i}$ is the enthalpy of formation of species i at a reference temperature T_o. $C_{p,i}$ is the specific heat capacity of species i.

The gas-phase equations contain source terms, and the mass, momentum and energy are conserved between the phases. The gas chemistry does not change the total mass and enthalpy of the mixture; however, with the gas-solid reactions, mass, momentum, and energy are transferred to the gas phase by chemical conversion of solids to gas. This is known as the interphase momentum transfer rate per unit volume (F) in Equation 2.6.

The dynamics of the solid particles are calculated by solving a transport equation for the particle distribution function (PDF), f. The details of the transport equation can be obtained from the literature (Andrews & O'Rourke, 1996). PDF is a function of particle spatial position $\vec{x}_{\mathrm{p}}$, particle velocity $\vec{\mathrm{u}}_{\mathrm{p}}$, particle mass m_{p}, particle temperature T_p, and time t. Therefore, $f\left(\vec{x}_{\mathrm{p}}, \vec{\mathrm{u}}_{\mathrm{p}}, \mathrm{m}_{\mathrm{p}}, T_p, t\right) d\vec{\mathrm{u}}_{\mathrm{p}} dm_p dT_p$ is the average number of particles per unit volumes with masses in the interval $(m_p, m_p + dm_p)$, velocities in the interval $(\vec{\mathrm{u}}_{\mathrm{p}},\ \vec{\mathrm{u}}_{\mathrm{p}} +\ d\vec{\mathrm{u}}_{\mathrm{p}})$ and temperature in the interval $(T_p, T_p + dT_p)$.

The particle velocity and acceleration are given by:

$$\frac{\partial}{\partial \mathrm{t}}\left(\vec{x}_{\mathrm{p}}\right) = \vec{\mathrm{u}}_{\mathrm{p}} \qquad 2.20$$

$$\frac{\partial}{\partial \mathrm{t}}\left(\vec{\mathrm{u}}_{\mathrm{p}}\right) = \mathrm{D}_P\left(\vec{\mathrm{u}}_{\mathrm{g}} - \vec{\mathrm{u}}_{\mathrm{p}}\right) - \frac{\nabla \mathrm{P}}{\rho_{\mathrm{p}}} + \mathrm{g} - \frac{\nabla \tau_{\mathrm{p}}}{\rho_{\mathrm{p}} \alpha_{\mathrm{p}}} + \mathrm{F}_{\mathrm{p}} \qquad 2.21$$

The particle volume fraction in Equation 2.21 is given by:

$$\alpha_{\mathrm{p}} = \iiint \mathrm{f} \frac{\mathrm{m}_{\mathrm{p}}}{\rho_{\mathrm{p}}} \mathrm{dm}_{\mathrm{p}} \mathrm{d}\vec{\mathrm{u}}_{\mathrm{p}} \mathrm{d}T_p \qquad 2.22$$

where, D_P is the drag function which depends upon the particle size, position, velocity, and time. τ_{p} is the particle normal stress given by Equation 2.23. Particle interactions (particle to particle collisions) are modelled with the particle normal stress developed by Harris and Crighton (Harris & Crighton, 1994). The particle stress is derived from the particle volume fraction, which in turn is calculated from particle volumes mapped to the grid. Particle normal stress gives an approximation of the collective effects of all the neighbor particles of a particle. The CPFD method calculates the spatial gradients on a Eulerian grid and applies the gradient to discrete particles. The gradient in the particles accelerates the particle, which prevents the particle volume fraction from exceeding their close-pack volume faction. The particle pressure is a function of solid volume fraction and becomes zero when the solid volume fraction becomes zero (Snider *et al.*, 2011).

$$\tau_p = \frac{P_s \alpha_p{}^{\beta}}{\max[(\alpha_{cp} - \alpha_p),\ \omega(1 - \alpha_p)]} \qquad 2.23$$

Solid collisions depend upon the solid concentration and the solid velocity. Particle normal stress is exerted to a solid up to the point where the solid reaches the particle-mean velocity (Snider *et al.*, 2011). P_s is a constant (Pa), α_{cp} is the particle volume fraction at close packing, β is a constant (between 2 – 5) and ω is a very small number in the order of 10^{-8}.

The fluid mass source in Equation 2.5 is given by:

$$\delta \dot{m}_p = \iiint f \frac{dm_p}{dt} dm_p d\vec{u}_p dT_p \qquad 2.24$$

where the time-rate change of particle mass $\frac{dm_p}{dt}$ is the rate of change of the particle mass-producing gases through chemical reactions and is given by:

$$\frac{dm_p}{dt} = \frac{\alpha_g Mw_c}{\alpha_p \rho_p} m_p \frac{d[C(s)]}{dt} \qquad 2.25$$

The interphase momentum transfer (F) in Equation 2.6 is given by:

$$F = \iiint f \left[m_p \left\{ D_P(\vec{u}_g - \vec{u}_p) - \frac{\nabla P}{\rho_p} \right\} + \vec{u}_p \frac{dm_p}{dt} \right] dm_p d\vec{u}_p dT_p \qquad 2.26$$

The conservative energy exchange term S_h in Equation 2.12 from the particle phase to the gas phase is given by Equation 2.27 (Snider *et al.*, 2011).

$$S_h = \iiint f \left[m_p \left\{ D_P(\vec{u}_p - \vec{u}_g)^2 - C_V \frac{dP_p}{d_t} \right\} - \frac{dm_p}{dt} \left\{ h_p + \frac{1}{2}(\vec{u}_p - \vec{u}_g)^2 \right\} \right] dm_p d\vec{u}_p dT_p \qquad 2.27$$

where, h_p is the particle enthalpy and C_V is the specific heat of the particle. The lumped heat equation for the particle is:

$$C_V \frac{dT_p}{dt} = \frac{1}{m_p} \frac{\lambda_g Nu_{g,s}}{2r_p} A_s (T_g - T_p) \qquad 2.28$$

where $Nu_{g,s}$ is the Nusselt number for heat transfer from gas to the particle phase, m_p is the particle mass and r_p is the particle radius.

The radiative heat transfer between the thermal wall and the particle phase in the equation is given by:

$$q_{wp} = A_w F_{wp} \varepsilon_{wp} \sigma \left({T_w}^4 - {\overline{T}_p}^4 \right) \qquad 2.29$$

where A_w is the area of the thermal wall, T_w is the wall temperature, $\overline{T}_p$ is the average particle temperature in a cell, F_{wp} is a view factor, σ is the Stefan-Boltzmann constant and ε_{wp} is the emissivity between the wall and particles in the cell.

In multiphase simulations, drag models are very important for predicting hydrodynamics. The model calculates a force acting on a particle as a function of the particle and fluid properties and the flow conditions. For a system based on single particles, the drag force can be calculated by using:

$$\mathrm{F_p} = \mathrm{m_p D}\left(\vec{\mathrm{u}}_\mathrm{g} - \vec{\mathrm{u}}_\mathrm{p}\right) \qquad 2.30$$

where D is the drag function, which depends upon the fluid conditions such as drag coefficient ($\mathrm{C_d}$) and the Reynolds number (Re). The expressions for the drag function and the Reynolds are:

$$\mathrm{D} = \frac{3}{8} \frac{\mathrm{C_d} \rho_\mathrm{g} |\vec{\mathrm{u}}_\mathrm{g} - \vec{\mathrm{u}}_\mathrm{p}|}{\rho_\mathrm{p} \mathrm{r_p}} \qquad 2.31$$

$$\mathrm{Re} = \frac{2\, \rho_\mathrm{g} \mathrm{r_p} |\vec{\mathrm{u}}_\mathrm{g} - \vec{\mathrm{u}}_\mathrm{p}|}{\mu_\mathrm{g}} \qquad 2.32$$

The drag coefficient is defined as a function of Reynolds number and the details can be found in the literature (Patel *et al.*, 1993; Wen, 1966).

2.4.1.2 Numerical scheme

The gas-phase equations are solved with a numerical control volume approach. CPFD scheme solves the conservation equation by finite volume approach with staggered scaler and momentum nodes. The conservation equations are integrated over a control volume. The gas mixture velocity, density and pressure are coupled by a semi-implicit pressure equation derived from the gas mass conservation equation (Snider *et al.*, 2011). The fluid momentum, energy and pressure equations are solved with a conjugate gradient solver. The chemistry ordinary differential equations (ODE) are solved with a stiff, sparse ODE solver (Snider *et al.*, 2011).

In the MP-PIC scheme, particle properties are mapped to and from the Eulerian grid to get the grid properties for the particles. Fluid properties are mapped to discrete particle locations (Snider *et al.*, 2011). The particle volume fraction for a cell ξ is calculated as:

$$\alpha_{p\xi} = \frac{1}{V_\xi}\sum_{i=1}^{N_p}\frac{m_p}{\rho_p}\, n_p S_{p\xi} \qquad 2.33$$

where n_p is the number of the computational particles, $S_{p\xi}$ is the interpolation operator and N_p is the total number of computational particles. From the conservation of volume, the sum of the particle and the gas-solid fraction is unity, i.e., $\alpha_p + \alpha_g = 1$. The implicit form of the particle velocity equation is given by:

$$\mathrm{u}_p^{n-1} = \frac{\mathrm{u}_p^n + \Delta t\left[\mathrm{D}u_{g.p}^{n+1} - \frac{1}{\rho_p}\nabla p_p^{n+1} - \frac{1}{\rho_p\alpha_p}\nabla\tau_p^{n+1} - g\right]}{1 + \nabla t\cdot\mathrm{D}} \qquad 2.34$$

where $u_{g.p}^{n+1}$ is the interpolated fluid velocity at the particle location, ∇p_p^{n+1} is the interpolated pressure gradient at the particle location, $\nabla\tau_p^{n+1}$ is the interpolated particle stress gradient at the particle location (Thapa *et al.*, 2016). The new particle location for the next time step becomes:

$$\mathrm{x}_p^{n+1} = \mathrm{x}_p^n + \mathrm{u}_p^{n+1}\Delta t \qquad 2.35$$

The fluid momentum equation implicitly couples the fluid and the particles through interphase momentum transfer. The interphase momentum transfer per volume at cell ξ is (Thapa *et al.*, 2016):

$$\mathrm{F}_\xi^{n+1} = \frac{1}{V_\xi}\sum_{i=1}^{N_p} S_{p\xi}\left[D\left(u_{g.p}^{n+1} - u_p^{n+1}\right) - \frac{1}{\rho_p}\Delta u_p^{n+1} + \frac{1}{m_p}\frac{dm_p}{dt}u_p\right]\cdot n_p m_p \qquad 2.36$$

The time step for a transient model is an important parameter. The time step must be small enough to represent any rapidly changing variables of interest. If the time step is too big, an accumulation of errors will occur (G.-Q. Zhang *et al.*, 2000). To solve this problem, a varying time step can be utilized with the help of the Courant-Friedrichs-Lewy (CFL) number as shown in Equation 2.37.

$$\mathrm{CFL} = \frac{v\,\Delta t}{\Delta x_{cell}} \qquad 2.37$$

where v is velocity, Δt is time step and Δx_{cell} is cell size. The default values of minimum and maximum CFL in Barracuda VR are 0.8 and 1.5 respectively.

2.4.1.3 Reaction chemistry

Chemical reactions are an integral part of the many industrial applications and are closely coupled with the fluid-particles dynamics and the heat and mass transfer inside a reactor. For example, a heterogeneous reaction produces or consumes gases from solids affecting the total gas volume which changes the reactor hydrodynamics. Also, the reactor temperature affects the reaction rates and is thereby affecting the reactor heat and mass transfer and the hydrodynamics. There can be thousands of reactions in any industrial chemical process, and it is impossible to solve a large number of coupled reactions over a hundred seconds of simulation time. Thus, a common consensus is to postulate a limited set of reactions that describes the major conversion inside the reactor which makes the computational tracking easy (Snider *et al.*, 2011).

The reaction chemistry can be defined in two ways as follows:

- Volume average chemistry: The average properties of the solid phase in the chemical rate equations are calculated by interpolating discrete computational particle properties into the grid. The reaction rates are then calculated in each grid cells by solving an ODE. The total rate of change of solid carbon is proportional to the total number of particles. The time rate of change of mass of individual particles ($\frac{dm_p}{dt}$) is related to the total rate of change of molar concentration of solid carbon ($\frac{d[C(s)]}{dt}$) as follows (Snider *et al.*, 2011):

  $$\frac{dm_p}{dt} = \frac{\alpha_g M_c}{\rho_p \alpha_p}\, m_p \frac{d[C(s)]}{dt} \qquad 2.38$$

  where M_c is the molecular weight of carbon.
- Discrete particle chemistry: Every computational particle is assigned to a separate control volume for the reaction rate calculations. Discrete particle chemistry is only

applicable when a solid is either consumed or produced in a reaction. There will be no reactions in a computational cell unless a particle is present in the cell. The reaction rate is evaluated in terms of either mol/s or kmol/s. The temperature in the rate coefficient is the weighted between the individual particle temperature and the cell gas temperature. This results in higher accuracy at the cost of a bit slower computation. The complexity of handling millions of particles and calculating their rate equation is the challenge associated with discrete particle chemistry. However, depending upon the complexity and the number of particles in the system discrete particle chemistry is still recommended.

Devolatilization rate is given by Equation 2.39 (Wu *et al.*, 2010).

$$\frac{dm_p}{dt} = -A_v \, \mathrm{T} \exp\left(\frac{E_v}{T}\right)(m_p - m_{c,a}) \tag{2.39}$$

m_p is the particle mass and $m_{c,a}$ is the mass of char and ash in the particle. The activation energy (E_v) and the pre-exponential factor (A_v) are 3945.15 K^{-1} and 2.1×10^5 s^{-1} respectively (Wu *et al.*, 2010).

The composition of the volatiles is given by the pyrolysis gas composition presented in Table 2-4. Biomass was modelled as virtual elements consisting of fixed carbon, volatile matter, and ash.

Table 2-4. Pyrolysis gas compositions [molar fraction] (Zanzi et al., 2002)

Components	**Weight fraction (dry basis)**
Methane (CH_4)	0.1213
Carbon monoxide (CO)	0.6856
Carbon-dioxide (CO_2)	0.1764
Hydrogen (H_2)	0.0167

Kinetics equations were defined according to the mass action kinetics for both heterogeneous and homogeneous reactions. Five major global homogeneous and heterogeneous reactions were considered during the modelling process and are presented in Table 2-1. Rate coefficients are defined according to the Arrhenius equation:

$$k = Am_s e^{\frac{-E_a}{RT}} \tag{2.40}$$

where, A is the pre-exponential factor, E_a is the activation energy (same units as $R \cdot T$), R is the universal gas constant and T is the absolute gas temperature for homogeneous reactions and solid-gas film temperature for heterogeneous reactions. The solid-gas film temperature is calculated by weighing 50% of the particle temperature and 50% of the bulk gas temperature. $m_s = \alpha_p \rho_p$ is the solid mass of free carbon per unit cell volume (Snider *et al.*, 2011).

The reaction kinetics are taken from the different sources available in the literature. Table 2-5 gives the selected lists of reaction kinetics used for this current study. CPFD transforms the reaction rate equations into solvable ODEs and the solutions are developed as a jacobian matrix at each time and location (Snider *et al.*, 2011). Biomass was modelled as virtual elements consisting of fixed carbon, volatile matters, and ash.

Table 2-5. Reaction kinetics for air gasification

Reactions [2]	*Reaction rate: r (mol·m^{-3}·s^{-1})*
R 2.1 (Ku *et al.*, 2014)	$2.51 \times 10^{-3} m_s T \exp\left(\frac{-8996}{\mathrm{T}}\right)$ [O_2]
$R\ 2.2_f$ (Snider *et al.*, 2011)	$1.272\ m_s T\ exp\left(\frac{-22645}{\mathrm{T}}\right)$[$H_2O$]
$R\ 2.2_b$(Snider *et al.*, 2011)	$1.044 \times 10^{-4}\ m_s T^2\ exp\left(\frac{-6319}{\mathrm{T}} - 17.29\right)$[$H_2$][CO]
$R\ 2.3_f$ (Snider *et al.*, 2011)	$1.272\ m_s T\ exp\left(\frac{-22645}{\mathrm{T}}\right)$[$CO_2$]
$R\ 2.3_b$(Snider *et al.*, 2011)	$1.044 \times 10^{-4}\ m_s T^2\ exp\left(\frac{-2363}{\mathrm{T}} - 20.92\right)$[CO]^2
$R\ 2.4_f$ (Snider *et al.*, 2011)	$1.368\ \times 10^{-3}\ m_s T\ exp\left(\frac{-8078}{\mathrm{T}} - 7.087\right)$[$H_2$]
$R\ 2.4_b$(Snider *et al.*, 2011)	$0.151\ m_s T^{0.5}\ exp\left(\frac{-13578}{\mathrm{T}} - 0.372\right)$[$CH_4$]$^{0.5}$

---

[2] Reactions are given in Table 2-1. Only selected backward reaction kinetics are presented which are based on the literature

R 2.6 (Bates *et al.*, 2017)	$5.69 \times 10^{14} exp\left(\frac{-17610}{T}\right)[H_2][O_2]^{0\cdot5}$
R 2.7 (Xie *et al.*, 2013)	$5.62 \times 10^{12} exp\left(\frac{-16000}{T}\right)[CO][O_2]^{0\cdot5}$
R 2.8 (Bates *et al.*, 2017)	$5.0118 \times 10^{14} exp\left(\frac{-24357}{T}\right)[CH_4]^{0\cdot7}[O_2]^{0\cdot8}$
$R\ 2.9_f$(Snider *et al.*, 2011)	$7.68 \times 10^{10}\ exp\left(\frac{-36640}{T}\right)[CO]^{0\cdot5}[H_2O]$
$R\ 2.9_b$(Snider *et al.*, 2011)	$6.4 \times 10^{9}\ exp\left(\frac{-39260}{T}\right)[H_2]^{0\cdot5}[CO_2]$
$R\ 2.10_f$ (Thapa *et al.*, 2014)	$3 \times 10^{5}\ T\ exp\left(\frac{-15042}{T}\right)[CH_4][H_2O]$
$R\ 2.10_b$ (Thapa *et al.*, 2014)	$0.0265\ T\ exp\left(\frac{-32900}{T}\right)[CO][H_2]^2$

Multiple numerical approaches can be used in the case of EF gasifiers, however, other CFD tools neglect particle-particle interactions as the reactor operates at lower solid fractions. The particle-particle interactions play an important role around the fuel injector in an EF gasifier. Particle-particle interaction in the model can be altered by altering the close pack volume fraction and the maximum momentum redirection from particle collisions in the case of the CPFD modelling. In addition, the blended acceleration model (BAM) was activated as the particle mixture was composed of a broad range of particle sizes. BAM blocks unrealistic particle segregation by absorbing the sustained particle contact.

3 Materials and methods

Experiments were performed in the cold flow model of the BFB reactor and the pilot-scale BFB gasification reactor located at USN. A short overview of the cold flow model and the pilot-scale BFB gasifier is presented in this chapter.

3.1 Cold flow model of the BFB reactor

Figure 3-1 shows the laboratory scale cold flow model of the BFB reactor along with a simplified sketch. The experimental setup consists of pressure measurement sensors connected to a computer program, airflow supply and the fluidized bed. The pressure sensors measure the pressure within the bed for different airflow rates.

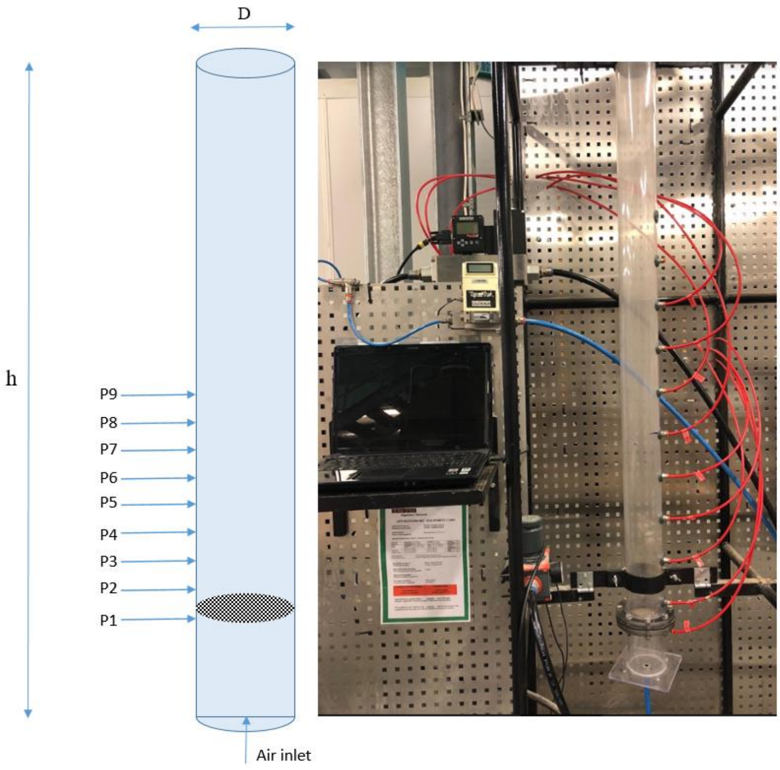

Figure 3-1. Cold flow model of a bubbling fluidized bed

LabVIEW is used to acquire the data measured by the pressure sensors at the wall of the column. Compressed air at ambient temperature is supplied from the bottom of the bed. The supplied air passes through a porous plate distributor for even distribution of airflow into the bed. The airflow rate is controlled with a digital air flow meter connected to the computer at the facility. The bed consists of a transparent plastic cylinder with a height (h) of 1.5 m and diameter (D) 84 mm. The second pressure sensor (P2) lies 35 mm above the air distributor and the distance between the sensors is 100 mm.

3.2 Fluidized bed gasification reactor at USN Porsgrunn

Experiments were performed in a pilot-scale fluidized bed gasification reactor located at the University of South-Eastern Norway, Porsgrunn. Figure 3-2 shows the isometric view of the BFB gasifier with auxiliary connections. Figure 3-3 shows the picture of the gasification reactor. The reactor is designed to operate in a bubbling fluidization regime and at atmospheric pressure conditions.

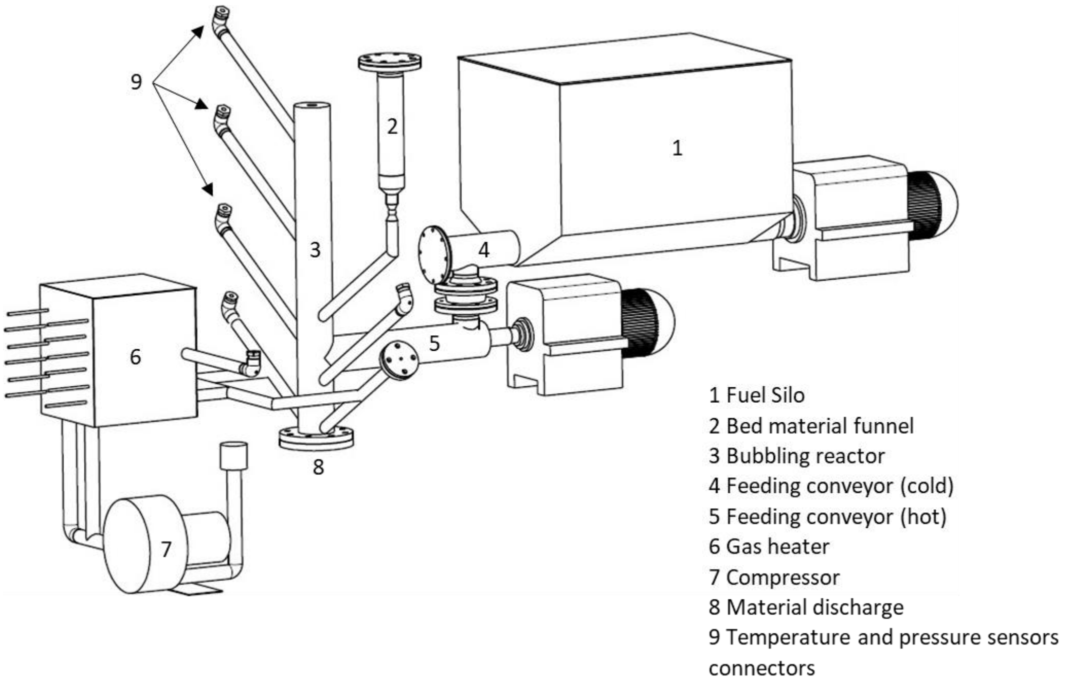

Figure 3-2. Isometric view of the BFB gasifier with auxiliary connections.

The setup consists of a reactor (3), biomass storage - silo (1), biomass feeding screws (4 and 5) and bed material funnel (2). Product gas from the reactor is combusted in a chimney (not shown in the figure). The setup is facilitated by three electrical heaters with 3kW each, one to heat the gasifying agent in the gas heater (6) and the other two are to heat up the reactor. The reactor has an inner diameter of 0.1 m, a height of 1 m and a wall thickness of 4 mm. The inner surface of the reactor is coated with refractory material, while the outer surface is insulated with thick fiberglass.

The gasifying air is supplied by a compressor and is preheated before entering the reactor. The airflow rate is measured by a BROOK air flowmeter and is controlled manually during the experiments. The air preheater heats the gasifying air to a temperature of around 450°C. Fuel is stored in a sealed silo and is conveyed to the reactor using two screw conveyors. The cold screw conveyor is connected to the hot screw conveyor with a non-conductive flange to avoid heat flow from the reactor to the silo. The flange acts as a biomass bridge to avoid any backward propagation of fire reaching the silo. Biomass feed rate is manipulated by changing the motor speed (>16% full conveyor capacity) or motor operating time (< 16% of full capacity) for the cold screw motor. The hot screw motor operates continuously during the reactor operation. Biomass is fed at a height of 0.25 m above the air distributor. Four pressure and temperature sensors are installed along the reactor and additional sensors are placed at the air preheater, the air inlet, the gas outlet, the silo, the screw conveyors and the reactor heaters. The pressure sensor measures the gauge pressure at the given position.

Figure 3-3. Fluidized bed gasification reactor at USN Porsgrunn

Data acquisition and parameter control are performed through a PLC controller, connected to a computer with a LabVIEW program. The default cut-off temperature for the reactor heater and air preheater is 1000°C and 600°C respectively. A constant nitrogen flow of 0.5 L/min is maintained through the silo during the experiments to avoid any gas movements from the reactor to the silo. An additional nitrogen supply line is kept in standby conditions to flush the reactor in case of any emergency shutdown. The facility has also sensors for the detection of H_2, CO and N_2 to identify any gas leakage. The produced gas is burnt in a ventilated chimney after the gas sampling line by adding some amounts of propane.

A gas-sampling line is located at the exit of the reactor, attached with a tar trap set up for online measurements of the product gas composition. A separate manual sampling valve is also available just before the tar trap setup. The produced gas was sampled using 0.025 dm^3 airtight syringes and the collected gas sample was analyzed in an SRI gas chromatography (GC) with a thermal conductivity detector (TCD). Figure 3-4 shows the GC that was used for the gas analysis.

Figure 3-4. SRI gas chromatography

The GC has a packed column of molecular sieve 13x for the detection of N_2, O_2, CO, and CH_4 and uses a gradient elution method. The GC has also a silica gel packed column for the detection of CO_2. The GC operates in the range of −15 to 120°C at 10 psi. The GC operates with helium as a carrier gas and the H_2 concentration was calculated by the difference method. Helium does not accurately predict the H_2 composition at lower concentrations. The accuracy of the calculated H_2 concentration was validated using nitrogen as the carrier gas. The GC uses the Peaksimple software for the visualization of the measured value.

Figure 3-5 shows the schematic diagram of the gasification reactor, where the exact location of the different sensors and the biomass feeding position are illustrated. The temperature and pressure sensors provide real-time measurements in the PLC system and are logged continuously. The PLC control system is used to control the biomass feeding, heating and the high temperature shutdown.

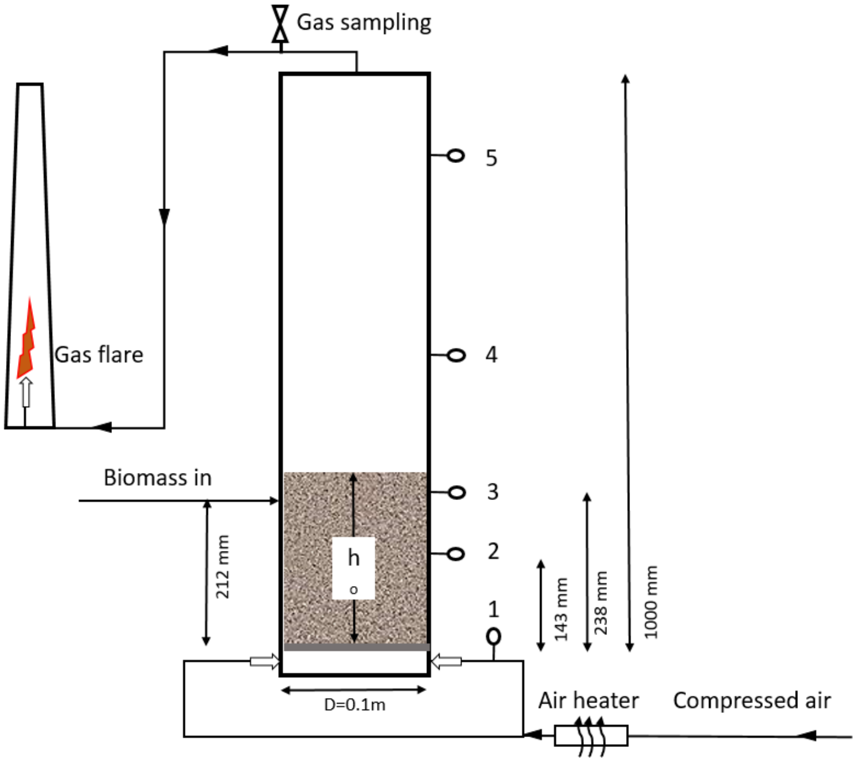

Figure 3-5. Schematic block diagram of the fluidized bed gasification reactor, points 1-5 indicates pressure and temperature sensor probe, h_o is the initial bed height.

Before the operation of the gasifier, the screw conveyor was calibrated for feed rate at different speeds for wood chips, wood pellets, and grass pellets. Sand with a density of 2650 kg/m^3 was used as a bed material for all the experiments. The reactor heaters and the air preheater were switched on while maintaining a sufficient air flow to keep the bed fluidizing. Once the reactor is heated up to around 300°C, some amount of biomass is combusted (limited supply of biomass at low flow rate/batch feeding) to heat up the reactor to the desired temperature at a faster rate.

During the experiments, the reactor heaters were switched on occasionally to maintain the desired reactor temperature. Manipulation of air preheater was also useful in setting up the reactor temperature. The bed pressure was constantly monitored to identify any formation of agglomerates inside the reactor. The bed height for all the experiments was less than the biomass feeding height, which gave the top biomass-feeding configuration.

Characterization of the biomass was performed to know the elemental composition of the biomass used for the experiments. Ultimate and proximate analyses were performed at the Eurofins testing facility and the results are presented in Table 3-1.

Table 3-1. Characterization of biomass

Material	**Wood pellets**	**Grass pellets**	**Wood chips**
Proximate analysis (wt.%, dry basis)			
Fixed Carbon	15.2	14.61	15.21
Volatiles	84.5	75.9	84.14
Ash	0.3	9.49	0.65
Moisture	7.9	8.4	11.1
Ultimate analysis (wt.%, dry basis)			
Ash	0.3	9.49	0.58
C	50.9	46.9	51.0
H	6.0	5.7	6.1
N	0.11	3.19	0.11
S	0.011	0.25	0.011
Cl	0.011	0.77	0.011
O (by difference)	42.6	33.7	42.2
Molecular formula [3]	$CH_{1.40}O_{0.63}$	$CH_{1.45}O_{0.54}$	$CH_{1.42}O_{0.62}$
LHV (MJ/kg, dry basis)	18.94	16.7	18.8
Bulk density (kg/m^3)	1139	985	625

---

[3] Calculated wrt ultimate analysis. Source: https://www.e-education.psu.edu/egee439/node/606

4 Results and discussion

In this chapter, some results from the published papers are presented along with non-published results. The results and discussion are presented according to the timeline of the papers prepared/published. The lists of the published and the submitted papers are given below:

Paper I. Timsina R., Thapa R.K., Moldestad B.M. and Eikeland M.S. (2019). Effect of particle size on flow behaviour in fluidized beds. *International Journal of Energy Production and Management*, 4(4), 287-297.

Paper II. Timsina R., Moldestad B., Eikeland M.S. and Thapa R.K. (2019). Simulation of air-biomass gasification in a bubbling fluidized bed using CPFD model. *Linköping University Electronic Press*, Issue no. 170, pp. 145-150.

Paper III. Timsina R., Thapa R.K., Moldestad B.M. and Eikeland M.S. (2020). Experiments and computational particle fluid dynamics simulations of biomass gasification in an air-blown fluidized bed gasifier. *International Journal of Energy Production and Management*, 5(2), 102-114.

Paper IV. Timsina R., Thapa R.K. and Eikeland M.S. (2019). Aspen Plus simulation of biomass gasification for different types of biomass. *Linköping University Electronic Press*, Issue no. 170, pp. 151-157.

Paper V. Timsina R., Thapa R.K., Moldestad B.M. and Eikeland M.S. (2020). Simulation of entrained flow gasification reactor with Multi-Phase Particle in Cell (MP-PIC) approach. *Linköping University Electronic Press*, Issue no. 176, pp. 428-434.

Paper VI. Timsina R., Thapa R.K., Moldestad B.M. and Eikeland M.S. (2021). Computational particle fluid dynamics simulation of biomass gasification in an entrained flow gasifier. *Chemical Engineering Science: X*, 12, 100112.

Paper VII. Timsina R., Thapa R.K., Moldestad B.M. and Eikeland M.S. (2021). Methanol synthesis from syngas: a process simulation. Presented at the *SIMS EUROSIM 2021*, September 21-23, Virtual Conference.

Paper VIII. Timsina R., Jaiswal R., Thapa R.K., Moldestad, B.M.E., Bhattarai A., Jecmenica M. and Eikeland, M.S. (2021). Experimental evaluation of wood and grass pellets in a bubbling fluidized bed gasifier. Submitted to *Chemical Science*.

4.1 Paper I: Experimental and CPFD simulation studies of a cold flow model of BFB reactor

Analysis of the fluidization characteristics such as mixing and segregation was achieved in these experiments. A simulation model was developed in Barracuda VR and the results obtained from the simulation model were validated against the experimental results. The effects of different particle sizes on fluidization behaviour were investigated during the cold flow model study. Experiments were done by mixing sand particles of a mean diameter of 293 µm (small particle) and 750 µm (large particle). Different sets of experiments were performed for different compositions of small and large particles. The minimum fluidization velocity decreases with the addition of small particles in the mixture. The experiment with 20% small particles and 80% large particles gives a reduction in minimum fluidization velocity of 60.8% compared to the minimum fluidization velocity with only large particles.

In most industrial applications, bed material consists of a wide range of particle size distributions. Theoretical calculation of minimum fluidization velocity is based on the average size of the bed materials and doesn't take into accounts of the particle size distribution. However, the simulation model accounts for the particles size distributions of the mixture. The screenshots of the reactor hydrodynamics with different compositions of small particles in the mixture are presented in Figure 4-1.

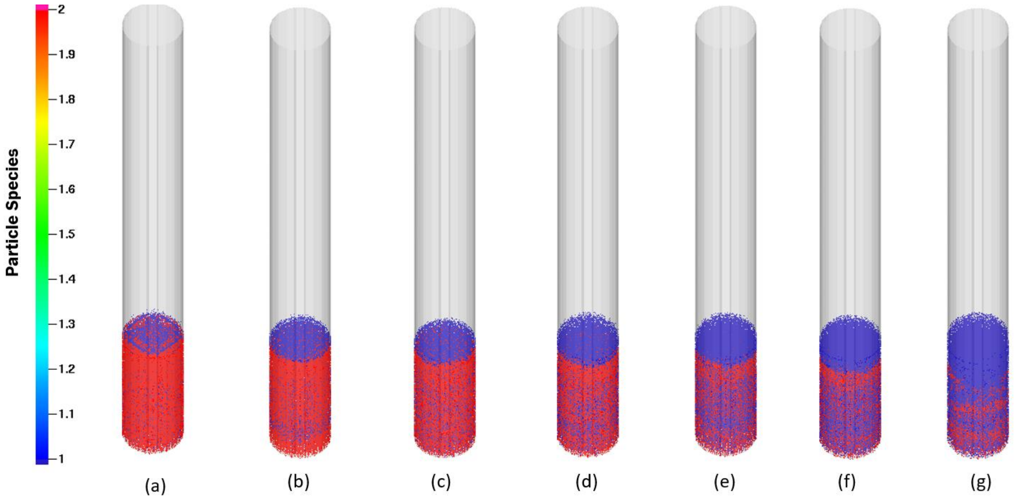

Figure 4-1. Particles distribution of the mixtures at bubbling regime (1- small particles, 2- large particles).

Figure 4-1 (a)-(f) show the particles distributions for the mixture with 10%-60% small particles and Figure 4-1 (g) shows the particle distributions of the mixture with 75% small particles and 25% large particles. The particle mixtures are well distributed with some degree of accumulation of small particles at the top of the bed for all the cases. Overall, it can be argued that there is a good mixing for the mixture with 10%-30% of small particles. The addition of 10-30% of small particles into the large particles can bring down the operating fluid velocity for the bubbling bed reactor. This makes the operation simple and decreases the required flow rate of air or steam or oxygen into the system. Thus, the reduction of the required amounts of gasifying agents to the reactor can significantly reduce the operating costs.

The Ergun drag model is appropriate for higher packing systems whereas the Wen-Yu drag model is suitable for dilute systems having gas volume fraction higher than 0.8. (Cho et al., 2020; Jayarathna et al., 2019; Patel et al., 1993). Therefore, different drag models were tested to predict the pressure drop as a function of superficial gas velocity. The experiment was performed at ambient conditions with air as a fluidizing agent. Figure 4-2 shows the comparison of the different drag models along with the experimental result.

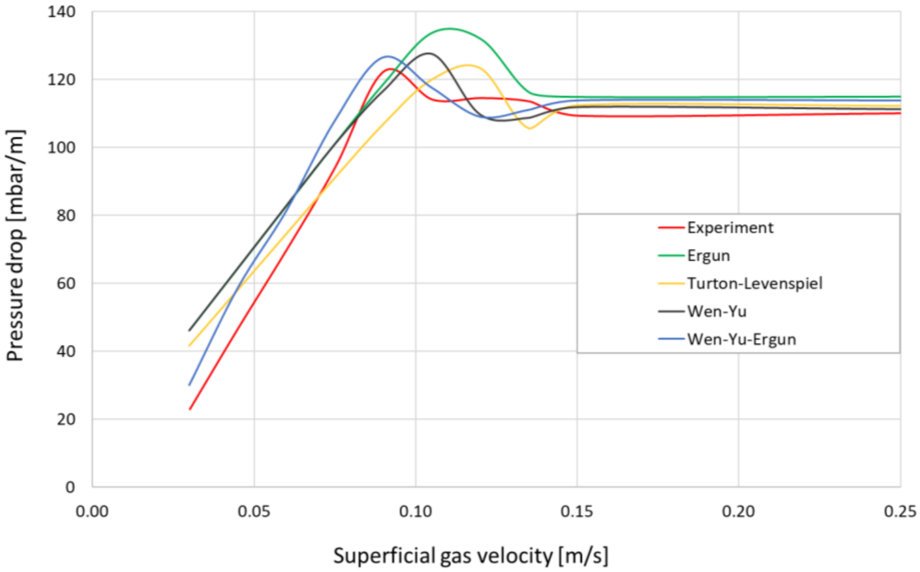

Figure 4-2. Pressure drops versus superficial gas velocities profiles (150-400 μm)

The figure depicts that the Wen-Yu-Ergun is best suited for these types of systems. The pressure drop varies more when the bed is in static conditions, due to the different drag coefficients for different drag models. The pressure drop is identical for all the models when the bed is in the bubbling regime.

Therefore, this study showed that a CFD model can be tuned properly to simulate a cold flow model of a BFB reactor. The experiments and simulations with mixtures of small and large particles showed some degree of particle segregation. Larger particles tend to settle down towards the bottom of the bed and the smaller particles tend to accumulate towards the upper half of the bed. It is difficult to have particles of the same size, which significantly affect the fluidization behaviour during the experiments. These results will help to understand the fluidization behaviours and characteristics such as mixing and segregation.

4.2 Paper II and III. Experimental and CPFD simulation studies for wood chips gasification

The papers contain the results from wood chips gasification in a pilot-scale BFB gasifier and the CPFD model developed for the same gasifier. Experiments were performed at temperatures between 700°C and 800°C to study the product gas composition. The product gas composition was monitored at regular intervals. Sand particles in the range of 100-425 µm (average diameter of 285 µm) were used as bed materials during the experiments. The initial bed height was 0.250 m. Table 4-1 shows the product gas composition for the different samples collected during the experiments. Experiments were performed at an ER of 0.13 for the wood chips (2.08 kg/hr biomass and superficial air velocity of 0.17 m/s). The variation of the sample composition is due to the inhomogeneity of the biomass feed and the variation in the reactor temperature. The average and the standard deviation of the gas composition are presented in the last two rows of Table 4-1.

Table 4-1. Product gas compositions from the gasification experiments

Components		H_2	O_2	N_2	CH_4	CO	CO_2 (By difference)
Sample (Volume %)	1	0.0496	0.0091	0.403	0.0739	0.2071	0.2372
	2	0.0683	0.0246	0.403	0.0691	0.1932	0.2206
	3	0.0793	0.0104	0.41	0.0642	0.1975	0.2186
	4	0.1332	0.0071	0.348	0.0778	0.2175	0.1963
	5	0.1497	0.0087	0.3519	0.0755	0.2207	0.1733
	6	0.1224	0.0094	0.3878	0.0681	0.2105	0.1817
Mean		**0.1004**	**0.0105**	**0.384**	**0.0715**	**0.2077**	**0.2046**
Standard deviation		0.04	0.006	0.027	0.005	0.01	0.024
SD (%)		39.8%	57.1%	7.0%	7.0%	4.8%	11.7%

The presence of oxygen in product gas could be due to the short residence time of the fluidizing agents (air). As the biomass is introduced at the top of the bubbling bed and the oxidizing agents have less contact time with the char present in the bed. Also, some air contamination was expected as the samples were taken out using syringes. The average temperature during these experiments was measured to be about 725°C. The gas yield, LHV, carbon conversion efficiency (CCE), CGE, and energy rate were found to be 2.5 Nm^3/hr, 6.3 MJ/m^3, 56.5%, 41.7%, and 15.75 MJ/hr respectively.

A CPFD model has been developed to simulate the air biomass gasification for the pilot-scale BFB gasifier. The details of the modelling setup and the system description are presented in Paper II and III. The results from the developed model were validated against the experimental results. The major focus was to optimize the flow behaviour and thermochemical behaviour inside the BFB gasification reactor.

Figure 4-3 shows the particle volume fraction, the particle temperature distribution and the mole fractions of CO, H_2 and CH_4 along with the height of the reactor. The gas compositions vary only in the freeboard region. Therefore, the char partial oxidation is less significant compared to the homogenous phase reactions. The increasing hydrogen concentration along the reactor indicates the dominance of the water gas shift and the methane reforming reaction.

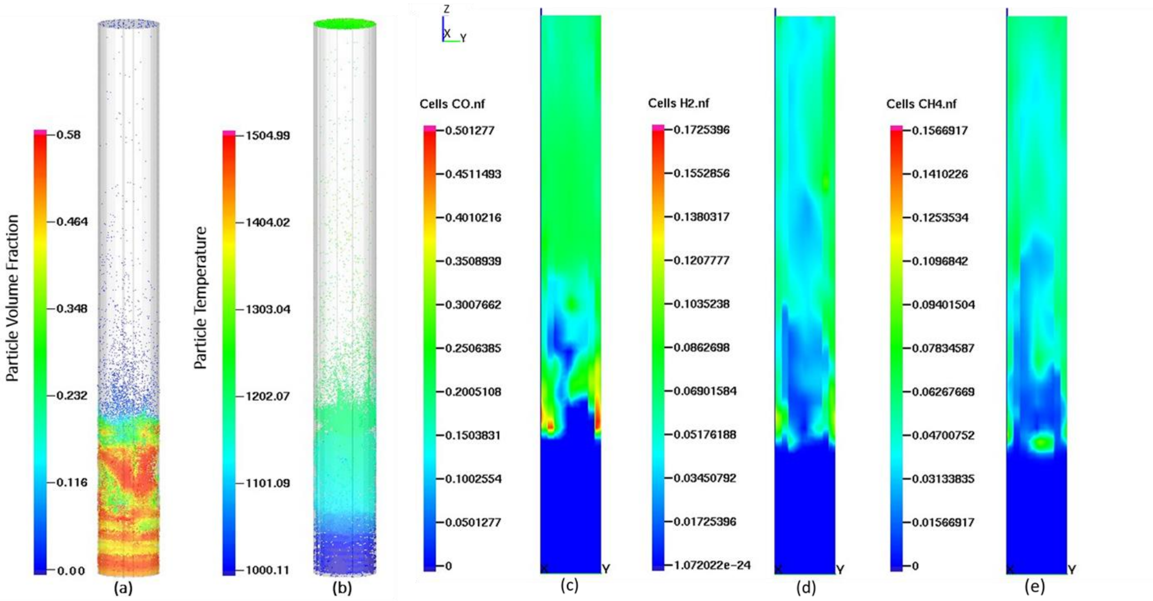

Figure 4-3. Bed hydrodynamics and chemistry at 200 s (a). Particle volume fraction (b). Particle temperature (K) (c)-(e). Gas composition along the reactor (mole fraction)

The operation of the optimized reactor would give uniform particle distribution and ensure operation in the bubbling fluidization regime. Figure 4-3 (a) shows that the reactor operates at the bubbling fluidization regime with the entrainment of few particles in the freeboard region. The solid volume fraction after the onset of the bubbling regime in the bed is reduced from the solid volume fraction of the static bed. Although the system was set to a temperature of 1000K, due to the exothermic nature of the reactions, the temperature rises to around 1200K inside the reactor. Therefore, these results show that the chemical transformations and the bed hydrodynamics are quite complex in a BFB reactor.

Therefore, these experiments and simulation results provide a good illustration of gasification behaviour for wood chips. The product gas consisted of CO, H_2 and CH_4 and has the potential to be used in direct energy applications such as heat and power generation. As the CCE was 56.5%, the author suggests further experiments for possible improvements and modifications.

4.3 Paper IV. Process simulation of biomass gasification

Paper IV presents the simulation results from the model developed in Aspen Plus for the biomass gasification process. Equilibrium models are primarily used to identify the most important process parameter/s. The equilibrium models give the maximum achievable yield from a system based on the minimization of Gibbs's free energy. Therefore, an equilibrium model was developed in Aspen Plus to study a biomass gasification process. The model was used to study the product gas composition at different steam to biomass ratios (STBR), temperatures and biomass feed loadings and for different biomass feedstocks. The detailed results from the developed model are presented in Paper IV.

Figure 4-4 shows the composition of H_2, CO, CO_2 and CH_4 from the simulation for different types of biomass. The H_2 composition is quite similar for all the biomass feeds. The CO concentration for wood residue, miscanthus and olive residue is similar, whereas it is significantly lower for the pig manure. The CO_2 concentration for the pig manure is 30% whereas the other feeds have CO_2 concentration below 25%. The carbon and hydrogen content in the feed are lowest for the pig manure. The C/O ratio is approximately 1:1 for pig manure and 1.2:1 for the other types of biomass.

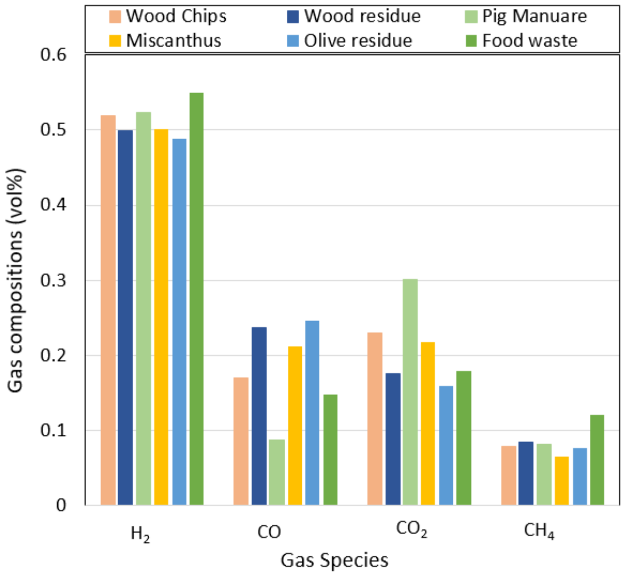

Figure 4-4. Gas compositions for different biomass feed (700°C)

The higher proportion of oxygen per carbon atom and the high concentration of ash (18.15%) compared to the other types of biomass could be the reason for high CO_2 and low CO in pig manure. The CH_4 concentration is around 8% for all the types of biomass except the food waste, which is around 12%.

The quality of syngas produced depends upon the reactor temperature. Figure 4-5 shows the variations of the product gas compositions at different temperatures.

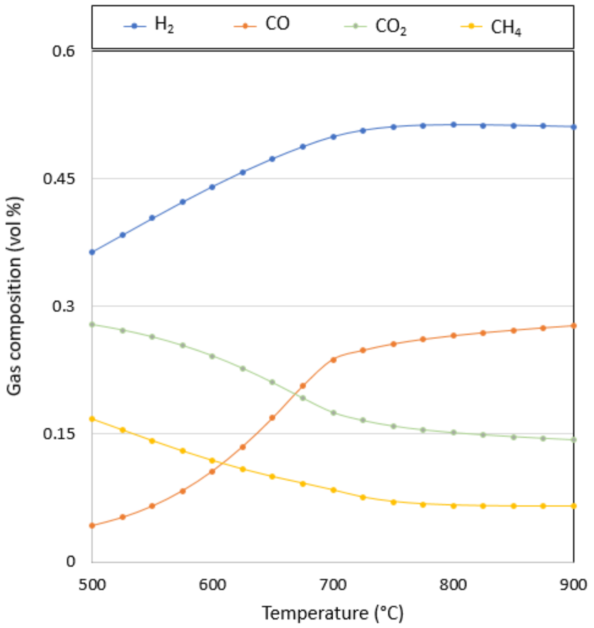

Figure 4-5. Gas composition for wood residue (STBR = 0.6)

The concentration of H_2 and CO increases initially with temperature and stabilizes after 700°C. The CO_2 and CH_4 concentration decreases with an increase in temperature and become steady after around 700°C.

The model was able to predict the gasifier's performance reasonably well in a relatively short time. The desired product gas composition can be obtained by selecting suitable biomass feedstocks and the operating conditions.

4.4 Paper V and VI. CPFD simulation of an EF gasifier

A CPFD model was developed to study the biomass gasification behaviour in an EF gasifier. The CPFD model was validated against the results published in the literature for the PEBG plant (Weiland *et al.*, 2013). The system description and the CPFD model development can be found in Paper VI. The major focus was to optimize the flow behaviour and thermochemical behaviour inside the EF gasification reactor.

As the reactor hydrodynamics is concerned, the reactor is desired to have a uniform mixing between the fuel particles and the fluidizing agent. Figure 4-6 shows the instantaneous particle distribution after 50 seconds. The particle scale information is captured by the Lagrangian tracking of solid particles.

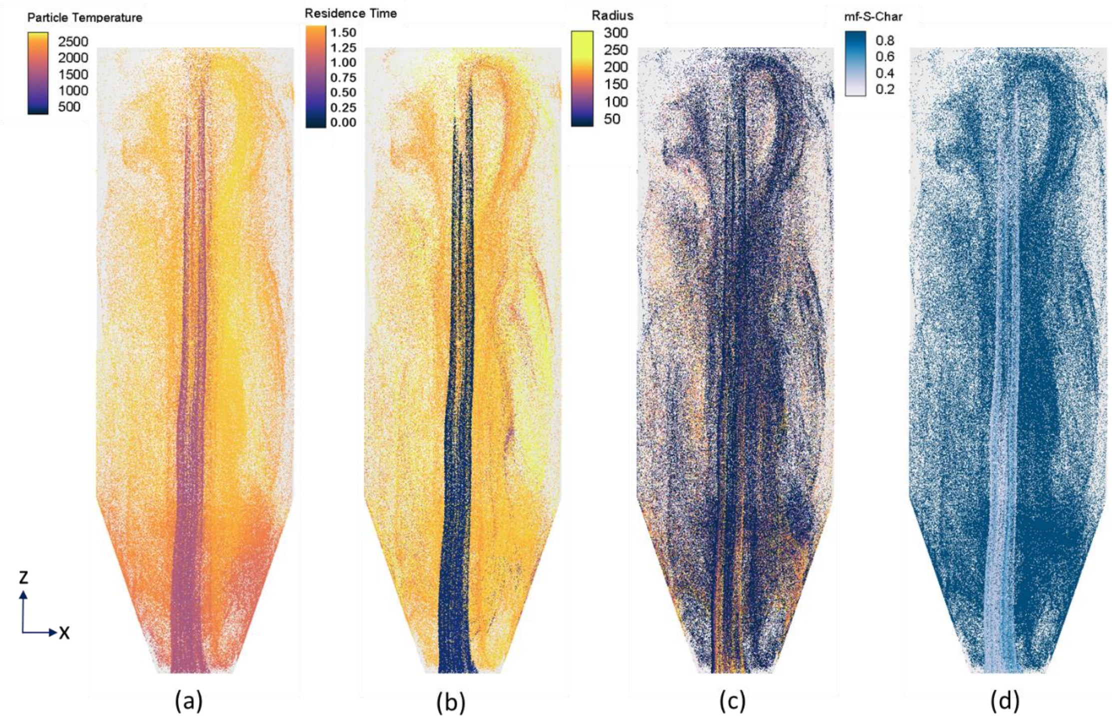

Figure 4-6. The instantaneous distributions of particles with respect to (a) temperature (K) (b), residence time (s) (c) particle radius (μm), and (d) char content (mass fraction) at 50.0 s

As depicted in Figure 4-6 (a), particle temperature in the central region is lower, with particles flowing downward. This is due to most particles following the central path where a significant number of reactions (endothermic) occurs compared to the peripheral region. This also leads to shorter residence time for the particles flowing through the central region, as shown in Figure 4-6 (b). Particles in the central region of the gasifier have the lowest residence time (high speed), whereas the particle towards the outer region has high residence time (low speed). The particle species with longer residence time are the particles that undergo recirculation, expansion along the radial direction. Figure 4-6 (c) shows the near-uniform distribution of the particle with respect to size. The particle temperature, as well as the residence time, is highly related to the carbon conversion of the particles. Figure 4-6 (d) shows the particle char content for the simulated gasifier. The char content is lower in the central region and higher in the other region. Even with the lower residence time, carbon conversion is higher in the central region, which indicates that the higher residence time may not always result in higher carbon conversion.

Detailed analysis of the char conversion, product gas composition (axial and in 3D), reactor temperature, equivalence ratio and fluid dynamics are presented in Paper VI.

As discussed in Chapter 2.4.1.3, chemistry is an integral part of an EF gasifier which is closely coupled with the fluid-particles dynamics and the heat and mass transfer inside a reactor. The major chemical reactions were computed for each computational cell at each computational time step giving a transient 3D behaviour. Figure 4-7 shows the radially averaged reaction rates along the gasifier depth.

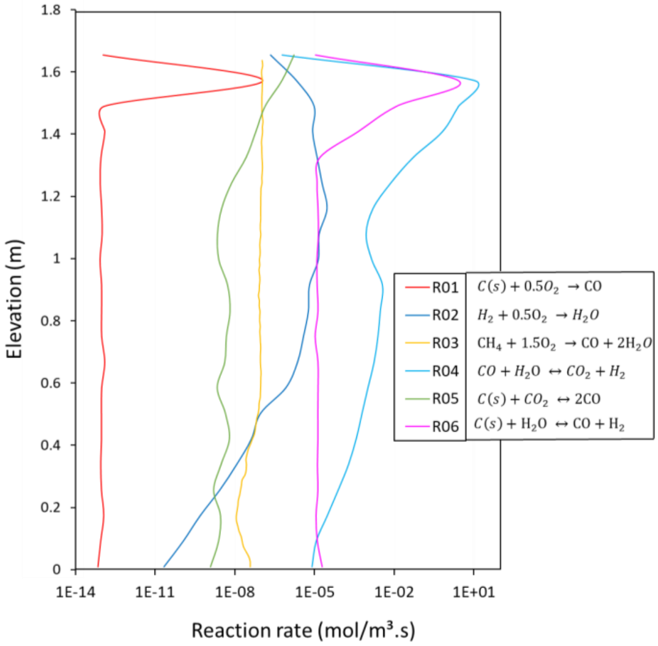

Figure 4-7. Chemical reaction rate versus elevation at t = 50s. Reaction rates are shown on a logarithmic scale.

The figure shows that the reaction rates for different reactions are in the range of several orders of magnitude. The endothermic nature of the water gas shift reaction favours the reaction towards the backward direction. The reaction rate extent of the WGS reaction determines the CO and CO_2 concentration along with the reactor depth. The reaction rate decreases significantly for R04 with increasing reactor depth due to the decrease in reactor temperature and the lower amounts of steam concentration. Production of steam is from the oxidation of H_2 (R02), which significantly decreases with the reactor depth. This also limits the reaction rate for R04. The reaction rate for the R03 reaction is slow throughout the reactor elevation since CH_4 is present at a low concentration compared to the other gases in the reactor. The dominant methane production source is the devolatilization step, whereas the methanation reaction is not considered during this study due to its slow reaction rate.

Char oxidation (R01) is significant in the high-temperature region and all available oxygen is consumed around the fuel injector region. The char-steam reaction (R06) is also significant in the reactor entrance region, due to the presence of H_2O in this region. The majority of steam production in this region is from the reaction R02. The produced steam is quickly consumed by the reaction R06 as the reactor depth increases.

The CPFD simulation gave comprehensive results for the reactor hydrodynamics and the chemistry inside an EF reactor. The results are a step forward for a better understanding and operation of an EF biomass gasifier. The CPFD software is being applied commercially for the entrained flow (coal) gasifiers. Commercially applied technology with lacking literature data creates a wider gap between academic and commercial applications. This paper tries to fill the gaps between academia and industries.

4.5 Paper VII. Process simulation for the conversion of syngas into methanol

An equilibrium model was developed in Aspen Plus to study the conversion of syngas into methanol. The model was used to optimize some of the operating parameters in a methanol synthesis plant (distillation column) and provides an overview of the overall conversion steps and efficiency. The details of the modelling setup and the system's unit operations are presented in Paper VII. Table 4-2 shows the principal reaction in a methanol synthesis plant.

Table 4-2. Reaction formulas for methanol synthesis

Reactions	Reaction heat(kJ/mol)
(a) $CO + 2H_2 \rightleftharpoons CH_3OH$	-90.64
(b) $CO_2 + 3H_2 \rightleftharpoons CH_3OH + H_2O$	-49.67
(c) $CO_2 + H_2 \rightleftharpoons CO + H_2O$	+41

In a methanol synthesis plant, optimal production is essential to achieve higher plant efficiency. Table 4-3 shows the mass balance for the simulated case. The table shows the yield of 2.33 tonnes of methanol per tonne of syngas ($CO+H_2$) supplied [*calculated as methanol_out/(CO_in + H_2_in)*]. Considering an operation of 8600 hr/year, the annual mass production of methanol is equal to 96492 tonnes. The conversion of CO, CO_2 and H_2 are 50.4%, 99.8% and 100% respectively and the results are similar to the study of Luyben (Luyben, 2010).

Table 4-3. Mass balance for the simulated case

Compound	In (t/hr)	Out (t/hr)
CO	2.8	1.39
CO_2	13.2	0.01
H_2	2.02	0
Methanol	0	11.22
H_2O	0	5.40

Several studies by different researchers show that methanol mainly originates from the CO_2 hydrogenation, and hardly from the CO hydrogenation (Kagan *et al.*, 1975; Nestler *et al.*, 2018). Therefore, conversion of CO to methanol principally occurs via the water gas shift reaction with subsequent CO_2 hydrogenation.

Figure 4-8 shows the purity of methanol for different molar reflux ratios. The purity of methanol increases with an increase in the molar reflux ratio, however the reboiler duty and cost increase linearly with an increase in reflux ratio. The purity of methanol synthesis increases steadily initially and exponentially for the higher methanol purity. Therefore, a tradeoff is required for the reflux ratio and the desired methanol purity in the column distillate.

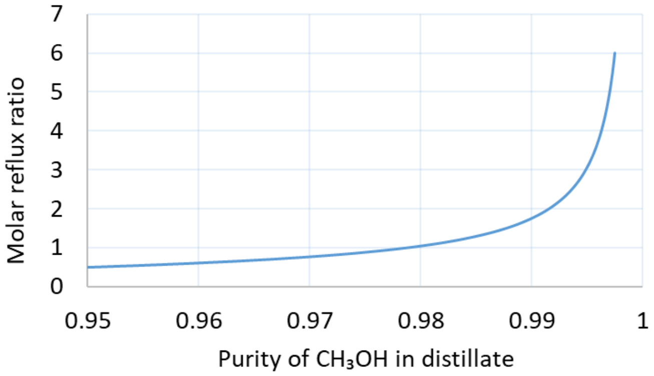

Figure 4-8. Molar reflux ratio vs methanol purity in distillate

Energy costs and heat exchanger capital costs decrease with an increase in the number of stages in the distillation tower, however, the total capital costs of the plant will increase. Therefore, optimal operating conditions is necessary for the desired output. A cooling duty of 23.62 GJ/hr was required for the given flowrate specifications with a reactor size of 5 m^3. The model can further be improved by adding a suitable catalyst in the reactor, selecting/optimizing the reaction kinetics as well as performing the sensitivity analysis for the synthesis reactor.

4.6 Paper VIII. Experimental studies of biomass gasification in a BFB gasifier: (submitted for publication)

Experiments were performed in the BFB gasification reactor present at USN. Wood pellets and grass pellets were used for the experiments to study the gasification behaviour at different equivalence ratios. The gasifier performance was calculated in terms of gas yield, LHV, CCE, CGE and the energy rate and the results are presented in Paper VIII. Commercially available wood pellets and grass pellets were used as feedstock for the experiments. The biomass feed rate was calibrated before the experiments for each type of biomass at different motor speeds. The properties of the different biomass are presented in Table 3-1. Calculation of ER for wood pellets is presented in Table 4-4. Product gas was sampled using 0.025 dm^3 airtight syringes and the collected gas sample was analyzed in the GC.

Table 4-4. Calculated ER for wood pellets, based on air flow rates and ultimate analysis

Wood pellets at 5.4 kg/hr feed rate			
Feed rate (kg/hr)	Stoichiometric air (kg/hr)	Actual air flow rate (kg/hr)	Equivalence ratio
5.4	32.67	7	0.214
		8	0.245
		9	0.275
		10	0.306
Wood pellets with a 7 kg/h air flow rate			
Feed rate (kg/hr)	Stoichiometric air (kg/hr)	Actual air flow rate (kg/hr)	Equivalence ratio
3.18	18.88	7	0.371
4.44	26.88		0.26
5.4	32.67		0.214

Electrical heaters can heat up the bed material to around 675°C with a reasonable heating rate. Thus, some amount of biomass was combusted to accelerate the bed heating to a higher temperature of 700°C to 800°C. The reactor temperature decreased considerably at ERs below 0.1 by turning off the electrical heaters. At higher ERs, it was possible to maintain the desired reactor temperature with an occasional electrical heat supply. The system pressures were constantly monitored to identify any blockage or formation of agglomerates in the bed. Normally, samples were extracted after about one hour of operation of the gasifier and at intervals of 10 minutes.

The product gas volume flow rate was calculated by balancing N_2 in the inlet and outlet gas flow rates. The accuracy of such measurement depends upon the precise measurement of the inlet air flow rate and the GC measurements. As the calculation of CCE and energy rates depends on the gas yield, any uncertainties associated with calculated product gas can also appear in those parameters. The total energy rate is an important parameter in thermal energy generation applications.

As compared to the wood chips, the gasification of wood pellets was relatively easy, and the feed flow rate was more continuous. Experiments were performed with sand as bed material. Sand has a density of 2650 kg/m^3 and particles sizes from 850-1000 μm. The initial bed height was 0.2 m. The gasification experiments were performed at temperatures between 800°C and 900°C. Fly out of some sand particles, ash, and fine carbon particles (char) during the experiments was observed because of uniform cross-sectional area and shallow bed. The primary objective was to see the effects of ER on the gasifier performance. Figure 4-9 and Figure 4-10 show the product gas composition at different equivalence ratios.

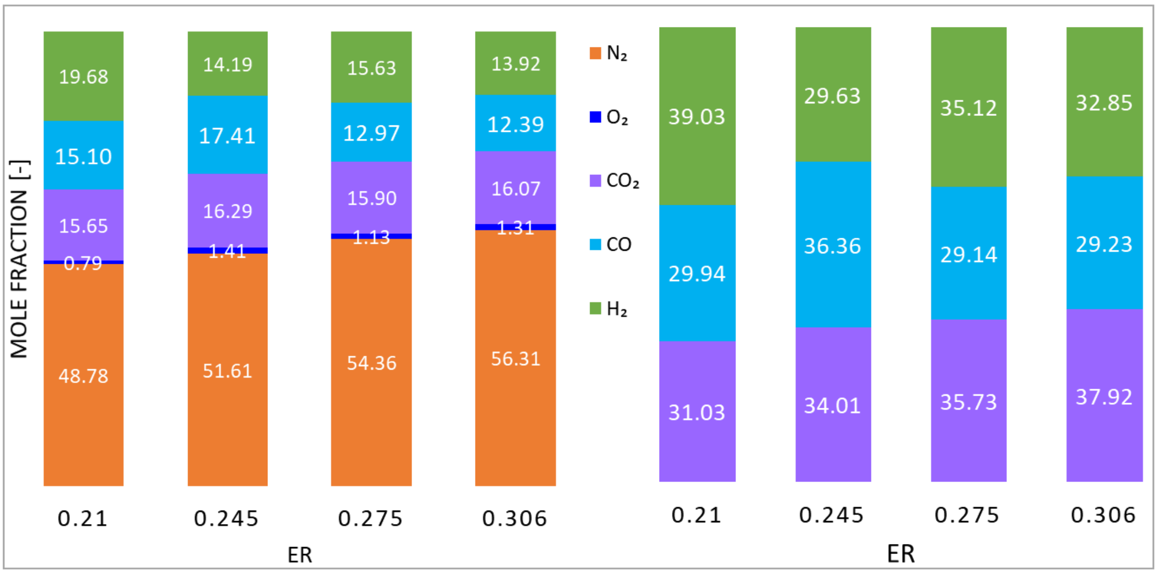

(a) (b)

Figure 4-9. Product gas composition at different ERs (at 5.4 kg/hr feed rate) for wood pellets. (a) with all the gas components (b) recalculated without N_2 and O_2

As seen from Figure 4-9 and Figure 4-10, an increase in the equivalence ratio gave an increase in the nitrogen content in the product gas. As depicted in Figure 4-9, the sum of CO and H_2 concentration decreased with an increase in ER. However, the CO and H_2 concentration for ER 0.245 deviates from the other ERs trends. This can be due to the measurement uncertainties in the sampling process and the variation in the reactor temperature. The reactor temperature fluctuated between ±20°C of the average reactor temperature during these experiments. Lower amounts of the sum of H_2 and CO at higher ERs can be due to the combined effect of gas phase reactions and the higher N_2 content in the product gas.

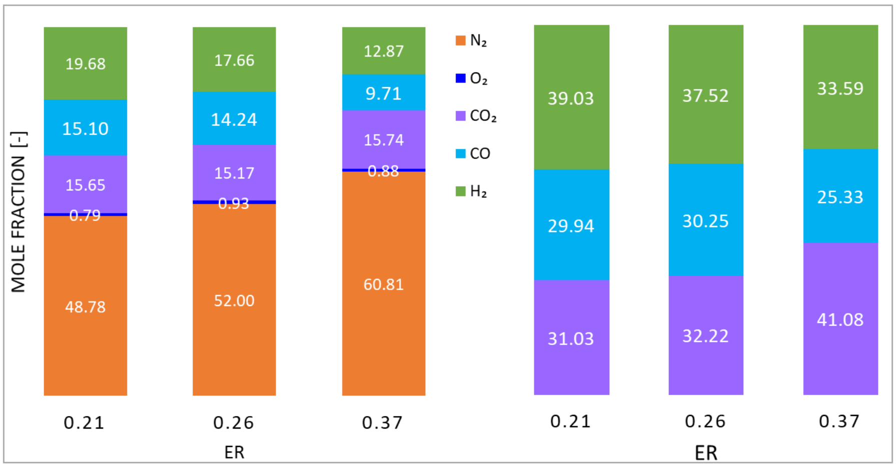

(a) (b)

Figure 4-10. Product gas composition at different ERs (at 7 kg/hr air flow rate) for wood pellets. (a) with all the gas components (b) recalculated without N_2 and O_2

The gasifier performance is calculated in terms of different parameters and presented in Table 4-5.

Table 4-5. Gasification performance indicators for wood pellets

ER	Product gas (Nm³/hr)	Gas yield (Nm³/Kg biomass)	LHV (MJ/Nm³)	CCE (%)	CGE (%)	Energy rate (MJ/hr)
at 5.4 kg/hr feed rate						
0.21	8.42	1.56	4.03	50.4	34.9	33.98
0.245	9.10	1.68	3.73	59.6	35.0	33.93
0.275	9.70	1.80	3.33	54.5	33.2	32.27
0.306	10.4	1.93	3.07	57.7	32.8	31.92
at 7 kg/hr air flow rate						
0.21	8.42	1.56	4.04	50.4	34.9	33.98
0.26	7.9	1.78	3.71	55.1	36.6	29.29
0.37	6.75	2.12	2.62	41.77	30.88	17.67

As a rule of thumb, the CO_2 concentration increases with an increase in ER which can be clearly seen from Figure 4-9 (b) Figure 4-10 (b). The leakage of air into the syringe during the sampling procedure may be the reason why small amounts of O_2 was present in the product gas. Mostly the reactor temperature was maintained around 850°C, which could be the reason why no methane was found in the product gas. However, this could also be due to the inability of the GC to measure methane at low concentrations. The higher biomass feeding, the higher will the pyrolysis rate be, which reduces the bed temperature significantly. A decrease in the reactor temperature alters the char conversion as well as lowers the LHV of the product gas. Therefore, the reactor temperature was monitored continuously throughout the experiments. Table 4-5 gives the performance indicator for the gasifier for wood pellets gasification.

A significant difference in the gas yield (+24%), LHV (-23.8%), CCE (+14.5%), CGE(-6%) and energy rate (-6%) can be seen with change in ER from 0.21 to 0.306. With an increase in the equivalence ratio, the gas yield increased, however, the LHV of the product gas decreased due to the dilution with nitrogen. The reduced CGE with an increase in ER is due to decreased LHV. CCE is increased with an increase in the ER, as the biomass has more oxygen to react with. However, for an ER of 0.37, the energy rate and the CCE are significantly lower compared to the other similar cases. This is due to the significant dilution of the product gas by nitrogen and the missing data for tar and char particle elutriation in the product gas stream.

Similar results were obtained for grass pellets as for wood pellets. However, the grass pellets have a considerably higher ash content compared to the wood and the melting point of the ash is lower. Therefore, the experiments with grass pellets were performed at temperature 750°C. During the experiments, the high ash content and the low ash melting temperature for grass pellets caused a number of failed attempts due to agglomerate formation. At higher ER, local hotspots initiated the formation of agglomerates due to high oxygen loading. The high ash content and the low ash melting temperature for grass pellets resulted in frequent agglomerates formation.

This study gave a clear overview of the gasification for the considered pellets in a BFB gasifier at the considered reactor temperature. The H_2, CO, CO_2, CH_4, and N_2 contents were 10.27%, 8.9%, 16.5%, 2.53%, and 60.9% respectively for the grass pellets at an ER of 0.195. The H_2, CO, CO_2, and N_2 contents were 13.92%, 12.4%, 16.1%, and 56.3% respectively for wood pellets at an ER of 0.306. Wood pellets gasification gave comparatively good product gas composition compared to the grass pellets. The results indicate that the product gas with these feedstocks is suitable for heat and power generation. Gasification of biomass with steam/oxygen or using a DFB gasifier is suggested to get high quality product gas suitable for biofuels/higher value chemicals synthesis.

5 Conclusions and future recommendations

Gasification has several benefits including the versatility of produced gas and high carbon conversion efficiency. The current work includes experimental work, CPFD and process simulations of biomass gasification. In addition, a process simulation of the conversion of syngas into methanol was performed.

Biomass gasification was the major focus of this study. Several experimental studies were performed in a cold flow model of a BFB reactor and a pilot-scale BFB gasifier. The reactor hydrodynamics, minimum fluidization velocity and the mixing behaviour of the bed were investigated using the cold flow model. Experiments using mixtures of small and large particles showed some degree of particle segregation. Larger particles tend to settle down towards the bottom and the smaller particles tend to accumulate towards the upper half of the bed. Gasification experiments were performed for different types of biomass at different air flow rates and biomass flow rates in a BFB gasifier. The product gas compositions and the gasifier performance (based on the mass balance of N_2 in the inlet and outlet gas) were measured and analyzed. The results gave a complete overview of the gasifier performance for the considered pellets and chips. The results from the gasifier indicated that the product gas was suitable for heat and power application. Increasing the ER gave an increased gas yield per kilogram of biomass, however, the LHV of the product gas decreased due to the dilution of the product gas with nitrogen.

CPFD models were developed for the cold flow model of the BFB reactor and the pilot-scale BFB gasifier. The biomass gasification behaviour was investigated at different operating parameters. The model development was based on the conservation of mass, momentum, and energy. The gas phase was modelled as a continuous phase and the solid particle as a dispersed phase, considering the interaction between the phases. The models were validated against the experimental data. A similar CPFD model was developed for biomass gasification in an EF gasifier. The model is validated against the results published in the literature.

The results from the model showed that bed hydrodynamics play a significant role in biomass conversion in a BFB gasifier. The bubbling behaviour of the bed influenced the heat and particle distribution, thus affecting the gasification behaviour. Therefore, the effect of ER and biomass feed on the performance of the gasifier was investigated in this study. For a case with birch wood, the CO concentration decreased from 25 to 13.2 mole %, whereas the CO_2 concentration increased from 17 to 19.5 mole % when the ER increased from 0.2 to 0.3.

The results from the CPFD simulation of the EF gasifier show that the char oxidation is significant in the high-temperature region, whereas the char-CO_2 reaction is prevalent throughout the reactor (along with depth). The endothermic nature of the water gas shift reaction favours the reaction towards the backward direction. The reaction rate extent of the WGS reaction determines the CO and CO_2 concentration along with the reactor depth. Simulations show the zones of high and low-temperature regions, suggesting different reaction zones such as a partial combustion zone near the fuel injector followed by a gasification zone.

A process simulation model was developed to study the BFB biomass gasification in Aspen Plus. The model was used to predict the gasifier performance for different operating conditions, i.e., temperature, steam to biomass ratio and biomass loadings. H_2/CO ratio increases with an increase in STBR for all the types of biomass, and the H_2/CO ratio was highest for pig manure and lowest for olive residue. Olive residue, wood residue and miscanthus gave the H_2/CO ratio of 1.5-2.1, which are more suitable for biofuel and higher value chemicals synthesis.

A process model was developed to study the conversion of syngas into methanol. The model was used to investigate the operating parameters in a methanol synthesis plant (distillation column) and gives an overview of the overall conversion steps and efficiency. Hydrogen recycles gave an increase of 50.4% in the production of methanol compared to the results without a H_2 recycle stream.

Research and development are continuous processes. This research was able to meet the objective of the given project. However, there are still challenges and bottlenecks in the thermal conversion technologies of biomass and the authors recommend the following for future works:

The gasifier performance indicates that the syngas is suitable for heat and power application. Gasification of biomass with steam/oxygen or using a DFB gasifier is suggested to get high quality product gas suitable for biofuels and higher value chemicals synthesis.

Tar in the product gas causes catalyst poisoning and clogging. Therefore, tar elemental analysis and tar yield should be studied more precisely to predict the biomass gasification behaviour accurately.

It is better to simulate a BFB gasifier in Barracuda VR with an industrial scale reactor. Barracuda VR is a good tool to simulate a large-scale system so that many particles can fit in each computational cell. Laboratory scaled gasifiers can be scaled up using appropriate scaling rules and can be simulated in Barracuda VR.

In the case of an entrained flow gasifier, impurities present in the biomass potentially develop accumulations and clogging in the quench water handling system. Thus, a proper investigation of the condensate contaminants is required to address this issue. The ash-slag behaviour is of great importance in these types of reactors and the influence of fuel type should be investigated before running the experiments. Simulation of the complete plant including the feeding system as well as the quench bath for gas cooling and the inclusion of tar and slag should not be left out in future studies.

The need for small fuel particle size in the EF gasifier adds up to the costs and energy demands. The total process efficiency could be increased by reducing the energy consumption during the milling process. Other pre-treatments alternatives such as torrefaction and pyrolysis should also be investigated. Therefore, a detailed techno-economic evaluation is needed to find the most efficient plant configuration.

Literature cited

Agu, C. E. (2019). *Bubbling Fluidized Bed Behaviour for Biomass Gasification.* (Doctor Philosophiae). University of South-Eastern Norway, Porsgrunn. Retrieved from http://hdl.handle.net/11250/2618843

Andrews, M. J., & O'Rourke, P. J. (1996). The multiphase particle-in-cell (MP-PIC) method for dense particulate flows. *International Journal of Multiphase Flow, 22*(2), 379-402. https://doi.org/10.1016/0301-9322(95)00072-0

Arena, U., & Di Gregorio, F. (2014). Gasification of a solid recovered fuel in a pilot scale fluidized bed reactor. *Fuel, 117*, 528-536. https://doi.org/10.1016/j.fuel.2013.09.044

Bandara, J. C. (2021). *Simulation and parameter optimization of fluidized-bed and biomass gasification.* (Doctor Philosophiae). University of South-Eastern Norway, Porsgrunn. Retrieved from https://hdl.handle.net/11250/2738320

Bandara, J. C., Eikeland, M. S., & Moldestad, B. M. (2017). *Analyzing the effects of particle density, size, size distribution and shape for minimum fluidization velocity with Eulerian-Lagrangian CFD simulation.* Paper presented at the Proceedings of the 58th Conference on Simulation and Modelling (SIMS 58), Reykjavik, Iceland. https://doi.org/10.3384/ecp1713860

Basu, P. (2018). *Biomass gasification, pyrolysis and torrefaction: practical design and theory* (Second ed.). London UK: Academic press (Elsevier).

Bates, R. B., Ghoniem, A. F., Jablonski, W. S., Carpenter, D. L., Altantzis, C., Garg, A., . . . Field, R. P. (2017). Steam‐air blown bubbling fluidized bed biomass gasification (BFBBG): Multi‐scale models and experimental validation. *AIChE Journal, 63*(5), 1543-1565. https://doi.org/10.1002/aic.15666

Bhattacharya, A., Bhattacharya, A., & Datta, A. (2012). Modeling of hydrogen production process from biomass using oxygen blown gasification. *International journal of hydrogen energy, 37*(24), 18782-18790. https://doi.org/10.1016/j.ijhydene.2012.09.131

Bin, C., Cong, W., Zhiwei, W., & Liejin, G. (2009). Investigation of gas-solid two-phase flow across circular cylinders with discrete vortex method. *Applied Thermal Engineering, 29*(8-9), 1457-1466. https://doi.org/10.1016/j.applthermaleng.2008.06.025

Campoy, M., Gomez-Barea, A., Vidal, F. B., & Ollero, P. (2009). Air–steam gasification of biomass in a fluidised bed: Process optimisation by enriched air. *Fuel Processing Technology, 90*(5), 677-685. https://doi.org/10.1016/j.fuproc.2008.12.007

Campoy, M., Gómez-Barea, A., Villanueva, A. L., & Ollero, P. (2008). Air− steam gasification of biomass in a fluidized bed under simulated autothermal and adiabatic conditions. *Industrial & engineering chemistry research, 47*(16), 5957-5965. https://doi.org/10.1021/ie800220t

Chen, C., Werther, J., Heinrich, S., Qi, H.-Y., & Hartge, E.-U. (2013). CPFD simulation of circulating fluidized bed risers. *Powder Technology, 235*, 238-247. https://doi.org/10.1016/j.powtec.2012.10.014

Cho, S., Park, C., Lee, J., Lyu, B., & Moon, I. (2020). Finding the best operating condition in a novel process for explosive waste incineration using fluidized bed reactors. *Computers & Chemical Engineering*, 107054. https://doi.org/10.1016/j.compchemeng.2020.107054

Chowdhury, H., & Loganathan, B. (2019). Third-generation biofuels from microalgae: a review. *Current Opinion in Green and Sustainable Chemistry, 20*, 39-44. https://doi.org/10.1016/j.cogsc.2019.09.003

De Klerk, A., & Furimsky, E. (2010). *Catalysis in the refining of Fischer-Tropsch syncrude*: Royal Society of Chemistry.

Demirbas, A. (2007). Progress and recent trends in biofuels. *Progress in energy and combustion science, 33*(1), 1-18. https://doi.org/10.1016/j.pecs.2006.06.001

Duchesne, M. A. (2012). *Slagging in entrained-flow gasifiers.* (Doctor Philosophiae). Université d'Ottawa/University of Ottawa, Retrieved from https://ruor.uottawa.ca/handle/10393/23353

Franco, C., Pinto, F., Gulyurtlu, I., & Cabrita, I. (2003). The study of reactions influencing the biomass steam gasification proces. *Fuel, 82*(7), 835-842. https://doi.org/10.1016/S0016-2361(02)00313-7

Fremaux, S., Beheshti, S.-M., Ghassemi, H., & Shahsavan-Markadeh, R. (2015). An experimental study on hydrogen-rich gas production via steam gasification of biomass in a research-scale fluidized bed. *Energy Conversion and Management, 91*, 427-432. https://doi.org/10.1016/j.enconman.2014.12.048

Gavrilović, L., Jørgensen, E. A., Pandey, U., Putta, K. R., Rout, K. R., Rytter, E., . . . Blekkan, E. A. (2021). Fischer-Tropsch synthesis over an alumina-supported cobalt catalyst in a fixed bed reactor–Effect of process parameters. *Catalysis Today, 369*, 150-157. https://doi.org/10.1016/j.cattod.2020.07.055

Ghassemi, H., & Shahsavan-Markadeh, R. (2014). Effects of various operational parameters on biomass gasification process; a modified equilibrium model. *Energy Conversion and Management, 79*, 18-24. https://doi.org/10.1016/j.enconman.2013.12.007

Gidaspow, D., Jung, J., & Singh, R. K. (2004). Hydrodynamics of fluidization using kinetic theory: an emerging paradigm: 2002 Flour-Daniel lecture. *Powder Technology, 148*(2-3), 123-141. https://doi.org/10.1016/j.powtec.2004.09.025

Gungor, A., & Yildirim, U. (2013). Two dimensional numerical computation of a circulating fluidized bed biomass gasifier. *Computers & Chemical Engineering, 48*, 234-250. https://doi.org/10.1016/j.compchemeng.2012.09.012

Guo, N. (2020). *Modelling of reacting multi-phase flow for biomass gasification.* (Doctor Philosophiae). Norwegian University of Science and Technology, Trondheim Norway. Retrieved from https://ntnuopen.ntnu.no/ntnu-xmlui/bitstream/handle/11250/2650837/Ning%20Guo_PhD.pdf

Guo, N., Llamas, Á. D. G., Li, T., Umeki, K., Gebart, R., & Løvås, T. (2020). Computational fluid dynamic simulations of thermochemical conversion of pulverized biomass in a dilute flow using spheroidal approximation. *Fuel, 271*, 117495. https://doi.org/0.1016/j.fuel.2020.117495

Gupta, S., Choudhary, S., Kumar, S., & De, S. (2020). Large eddy simulation of biomass gasification in a bubbling fluidized bed based on the multiphase particle-in-cell method. *Renewable energy, 163*, 1455-1466. https://doi.org/10.1016/j.renene.2020.07.127

Güell, B. M., Sandquist, J., & Sørum, L. (2013). Gasification of biomass to second generation biofuels: a review. *Journal of Energy Resources Technology, 135*(1), 014001-014009. https://doi.org/10.1115/1.4007660

Harris, S., & Crighton, D. (1994). Solitons, solitary waves, and voidage disturbances in gas-fluidized beds. *Journal of Fluid Mechanics, 266*, 243-276. https://doi.org/10.1017/S0022112094000996

Hervy, M., Remy, D., Dufour, A., & Mauviel, G. (2019). Air-blown gasification of Solid Recovered Fuels (SRFs) in lab-scale bubbling fluidized-bed: Influence of the operating conditions and of the SRF composition. *Energy Conversion and Management, 181*, 584-592. https://doi.org/10.1016/j.enconman.2018.12.052

Hofbauer, H., Reinhard, R., Klaus, B., Reinhard, K., & Christian, A. (2002). *Biomass CHP Plant Güssing–a success story*. Paper presented at the Expert meeting on pyrolysis and gasification of biomass and waste. https://pivotalirm.com/files/tech/017.pdf

IEA. (2019). Global Energy & CO_2 Status Report 2019. Retrieved from https://www.iea.org/reports/global-energy-co2-status-report-2019

Jayarathna, C. K., Balfe, M., Moldestad, B. M., & Tokheim, L.-A. (2019). Improved multi-stage cross-flow fluidized bed classifier. *Powder Technology, 342*, 621-629. https://doi.org/10.1016/j.powtec.2018.10.026

Kagan, Y. B., Liberov, L., Slivinskii, E., Loktev, S., Lin, G., Rozovskii, A. Y., & Bashkirov, A. (1975). Mechanism of methanol synthesis from carbon dioxide and hydrogen.[Tracer study of conversion over Cu--Zn--aluminium oxide SNM-1 catalyst]. *Dokl. Chem.(Engl. Transl.);(United States), 221*.

Karatas, H., Olgun, H., & Akgun, F. (2013). Experimental results of gasification of cotton stalk and hazelnut shell in a bubbling fluidized bed gasifier under air and steam atmospheres. *Fuel, 112*, 494-501. https://doi.org/10.1016/j.fuel.2013.04.025

Kaur, R., Gera, P., Jha, M. K., & Bhaskar, T. (2019). Thermochemical Route for Biohydrogen Production. In *Biohydrogen* (pp. 187-218): Elsevier.

Kim, Y. D., Yang, C. W., Kim, B. J., Kim, K. S., Lee, J. W., Moon, J. H., . . . Do Lee, U. (2013). Air-blown gasification of woody biomass in a bubbling fluidized bed gasifier. *Applied energy, 112*, 414-420. https://doi.org/10.1016/j.apenergy.2013.03.072

Kirnbauer, F., & Hofbauer, H. (2011). Investigations on bed material changes in a dual fluidized bed steam gasification plant in Gussing, Austria. *Energy & Fuels, 25*(8), 3793-3798. https://doi.org/10.1021/ef200746c

Ku, X., Li, T., & Løvås, T. (2015). CFD–DEM simulation of biomass gasification with steam in a fluidized bed reactor. *Chemical Engineering Science, 122*, 270-283. https://doi.org/10.1016/j.ces.2014.08.045

Ku, X., Li, T., & Løvås, T. (2014). Eulerian–lagrangian simulation of biomass gasification behavior in a high-temperature entrained-flow reactor. *Energy & Fuels, 28*(8), 5184-5196. https://doi.org/10.1021/ef5010557

Ku, X., Wang, J., Jin, H., & Lin, J. (2019). Effects of operating conditions and reactor structure on biomass entrained-flow gasification. *Renewable energy, 139*, 781-795. https://doi.org/10.1016/j.renene.2019.02.113

Köhler, J., Walz, R., Marscheder-Weidemann, F., & Thedieck, B. (2014). Lead markets in 2nd generation biofuels for aviation: A comparison of Germany, Brazil and the USA. *Environmental Innovation and Societal Transitions, 10*, 59-76. https://doi.org/10.1016/j.eist.2013.10.003

Larsson, A. (2014). *Fuel conversion in a dual fluidized bed gasifier-Experimental quantfication and impact on performance.* (Doctor Philosophiae). Chalmers University of Technology, Gothenberg, Sweden. Retrieved from http://publications.lib.chalmers.se/records/fulltext/203166/203166.pdf

Lau, F. S., Bowen, D. A., Dihu, R., Doong, S., Hughes, E. E., Remick, R., . . . Zabransky, R. (2002). *Techno-economic analysis of hydrogen production by gasification of biomass*. Retrieved from Des Plaines, Illinois United States: https://www.osti.gov/servlets/purl/816024

Li, J., & Zhang, J. (2017). Analytical study on char combustion of spheroidal particles under forced convection. *Powder Technology, 313*, 210-217. https://doi.org/10.1016/j.powtec.2017.02.054

Li, T., Wang, L., Ku, X., Güell, B. M., Løvås, T., & Shaddix, C. R. (2015). Experimental and modeling study of the effect of torrefaction on the rapid devolatilization of biomass. *Energy & Fuels, 29*(7), 4328-4338. https://doi.org/10.1021/acs.energyfuels.5b00348

Liang, Y., Guo, C. Y., Zhao, X., Qin, Q., Cheng, Y., & He, L. (2020). CPFD simulation on particle behaviour in an entrained-flow gasifier. *Clean Energy, 4*(1), 75-84. https://doi.org/10.1093/ce/zkz032

Lim, Y.-i., & Lee, U.-D. (2014). Quasi-equilibrium thermodynamic model with empirical equations for air–steam biomass gasification in fluidized-beds. *Fuel Processing Technology, 128*, 199-210. https://doi.org/10.1016/j.fuproc.2014.07.017

Lu, H., Ip, E., Scott, J., Foster, P., Vickers, M., & Baxter, L. L. (2010). Effects of particle shape and size on devolatilization of biomass particle. *Fuel, 89*(5), 1156-1168. https://doi.org/10.1016/j.fuel.2008.10.023

Luyben, W. L. (2010). Design and control of a methanol reactor/column process. *Industrial & engineering chemistry research, 49*(13), 6150-6163.

Makwana, J. P., Pandey, J., & Mishra, G. (2019). Improving the properties of producer gas using high temperature gasification of rice husk in a pilot scale fluidized bed gasifier (FBG). *Renewable energy, 130*, 943-951. https://doi.org/10.1016/j.renene.2018.07.011

Meng, F., Ma, Q., Wang, H., Liu, Y., & Wang, D. (2019). Effect of gasifying agents on sawdust gasification in a novel pilot scale bubbling fluidized bed system. *Fuel, 249*, 112-118. https://doi.org/10.1016/j.fuel.2019.03.107

Molino, A., Chianese, S., & Musmarra, D. (2016). Biomass gasification technology: The state of the art overview. *Journal of Energy Chemistry, 25*(1), 10-25. https://doi.org/10.1016/j.jechem.2015.11.005

Nam, H., Rodriguez-Alejandro, D. A., Adhikari, S., Brodbeck, C., Taylor, S., & Johnson, J. (2018). Experimental investigation of hardwood air gasification in a pilot scale bubbling fluidized bed reactor and CFD simulation of jet/grid and pressure conditions. *Energy Conversion and Management, 168*, 599-610. https://doi.org/10.1016/j.enconman.2018.05.003

Nestler, F., Krüger, M., Full, J., Hadrich, M. J., White, R. J., & Schaadt, A. (2018). Methanol synthesis–industrial challenges within a changing raw material landscape. *Chemie Ingenieur Technik, 90*(10), 1409-1418. https://doi.org/10.1002/cite.201800026

NMBU. (2020). Bio4Fuels. *Centre for environment-friendly energy research, The Research Council of Norway.* Retrieved from https://www.nmbu.no/en/services/centers/bio4fuels

Paisley, M., & Overend, R. (2002). *Verification of the Performance of Future Energy Resources' SilvaGas (R) Biomass Gasifier--Operating Experience in the Vermont Gasifier*. Paper presented at the Pittsburgh coal conference, Pittsburgh, Pennsylvania, USA. http://uicchemegroupa.wikispaces.com/file/view/verification+of+silvagas+process.pdf

Panahi, A., Levendis, Y. A., Vorobiev, N., & Schiemann, M. (2017). Direct observations on the combustion characteristics of Miscanthus and Beechwood biomass including fusion and spherodization. *Fuel Processing Technology, 166*, 41-49. https://doi.org/10.1016/j.fuproc.2017.05.029

Pandey, U., Runningen, A., Gavrilović, L., Jørgensen, E. A., Putta, K. R., Rout, K. R., . . . Hillestad, M. (2021). Modeling Fischer–Tropsch kinetics and product distribution over a cobalt catalyst. *AIChE Journal*, e17234. https://doi.org/10.1002/aic.17234

Patel, M., Pericleous, K., & Cross, M. (1993). Numerical modelling of circulating fluidized beds. *International Journal of Computational Fluid Dynamics, 1*(2), 161-176. https://doi.org/10.1080/10618569308904470

Pecha, M. B., Arbelaez, J. I. M., Garcia-Perez, M., Chejne, F., & Ciesielski, P. N. (2019). Progress in understanding the four dominant intra-particle phenomena of lignocellulose pyrolysis: chemical reactions, heat transfer, mass transfer, and phase change. *Green chemistry, 21*(11), 2868-2898. https://doi.org/10.1039/C9GC00585D

Qin, K. (2012). *Entrained flow gasification of biomass.* (Doctor Philosophiae). Technical University of Denmark, 2800 Kgs. Lyngby. Retrieved from https://orbit.dtu.dk/en/publications/entrained-flow-gasification-of-biomass

Qin, K., Lin, W., Fæster, S., Jensen, P. A., Wu, H., & Jensen, A. D. (2013). Characterization of residual particulates from biomass entrained flow gasification. *Energy & Fuels, 27*(1), 262-270. https://doi.org/10.1021/ef301432q

Rauch, R., Hrbek, J., & Hofbauer, H. (2014). Biomass gasification for synthesis gas production and applications of the syngas. *Wiley Interdisciplinary Reviews: Energy and Environment, 3*(4), 343-362. https://doi.org/10.1002/wene.97

Rautenbach, C. (2012). *An experimental and theoretical study of dense fluidized bed fluid dynamics.* (Doctor Philosophiae). Telemark University College, Porsgrunn. Retrieved from http://hdl.handle.net/11250/2437795

Rhodes, M. J. (1990). *Principles of powder technology* (First ed.). United States: Wiley.

Sarker, S., Bimbela, F., Sánchez, J. L., & Nielsen, H. K. (2015). Characterization and pilot scale fluidized bed gasification of herbaceous biomass: A case study on alfalfa pellets. *Energy Conversion and Management, 91*, 451-458. https://doi.org/10.1016/j.enconman.2014.12.034

Serrano, D., Kwapinska, M., Horvat, A., Sánchez-Delgado, S., & Leahy, J. J. (2016). Cynara cardunculus L. gasification in a bubbling fluidized bed: The effect of magnesite and olivine on product gas, tar and gasification performance. *Fuel, 173*, 247-259. https://doi.org/10.1016/j.fuel.2016.01.051

Smagorinsky, J. (1963). General circulation experiments with the primitive equations: I. The basic experiment. *Monthly weather review, 91*(3), 99-164. https://doi.org/10.1175/1520-0493(1963)091<0099:GCEWTP>2.3.CO;2

Smoot, L. D., & Smith, P. J. (1985). *Coal gasification and combustion* (1 ed.). New York: Plenum Press.

Snider, D. M., Clark, S. M., & O'Rourke, P. J. (2011). Eulerian–Lagrangian method for three-dimensional thermal reacting flow with application to coal gasifiers. *Chemical Engineering Science, 66*(6), 1285-1295. https://doi.org/10.1016/j.ces.2010.12.042

Snider, D. M., Guenther, C., Dalton, J., & Williams, K. (2010). *CPFD Eulerian-Lagrangian numerical scheme applied to the NETL bench-top chemical looping experiment.* Paper presented at the 1st International Conference on Chemical Looping, Solaize, France

Soukup, G., Pfeifer, C., Kreuzeder, A., & Hofbauer, H. (2009). In situ CO_2 capture in a dual fluidized bed biomass steam gasifier–bed material and fuel variation. *Chemical Engineering & Technology: Industrial Chemistry - Plant Equipment - Process Engineering - Biotechnology, 32*(3), 348-354. https://doi.org/10.1002/ceat.200800559

Subramanian, P., Sampathrajan, A., & Venkatachalam, P. (2011). Fluidized bed gasification of select granular biomaterials. *Bioresource technology, 102*(2), 1914-1920. https://doi.org/10.1016/j.biortech.2010.08.022

Tanger, P., Field, J. L., Jahn, C. E., DeFoort, M. W., & Leach, J. E. (2013). Biomass for thermochemical conversion: targets and challenges. *Frontiers in plant science, 4*, 218. https://doi.org/10.3389/fpls.2013.00218

Thapa, R. K. (2015). *Optimization of flow behavior in biomass gasification reactor.* (Doctor Philosophiae). Telemark University College, Porsgrunn Norway. Retrieved from http://hdl.handle.net/11250/2458253

Thapa, R. K., Frohner, A., Tondl, G., Pfeifer, C., & Halvorsen, B. (2016). Circulating fluidized bed combustion reactor: Computational Particle Fluid Dynamic model validation and gas feed position optimization. *Computers & Chemical Engineering, 92*, 180-188. https://doi.org/10.1016/j.compchemeng.2016.05.008

Thapa, R. K., Pfeifer, C., & Halvorsen, B. (2014). Modeling of reaction kinetics in bubbling fluidized bed biomass gasification reactor. *Int. J. Energy Environment, 5*, 35-44.

Todic, B., Ma, W., Jacobs, G., Davis, B. H., & Bukur, D. B. J. C. T. (2014). CO-insertion mechanism based kinetic model of the Fischer–Tropsch synthesis reaction over Re-promoted Co catalyst. *Catalysis Today, 228*, 32-39. https://doi.org/10.1016/j.cattod.2013.08.008

Van der Drift, A., Boerrigter, H., Coda, B., Cieplik, M., & Hemmes, K. (2004). *Entrained Flow Gasification of Biomass Ash Behaviour, Feeding Issues, System Analyses*. Retrieved from Petten, Netherlands: https://www.osti.gov/etdeweb/biblio/20479502

van der Laan, G. P. (1999). *Kinetics, selectivity and scale up of the Fischer-Tropsch synthesis.* (Doctor Philosophiae). University of Groningen, Netherland. Retrieved from http://www.adktroutguide.com/files/1999_Phd_Thesis_-_Kinetics_Selectivity_and_Scaleup_of_FT_Synthesis.pdf

Vassilev, S. V., Baxter, D., Andersen, L. K., & Vassileva, C. G. (2010). An overview of the chemical composition of biomass. *Fuel, 89*(5), 913-933. https://doi.org/10.1016/j.fuel.2009.10.022

Vassilev, S. V., Vassileva, C. G., & Vassilev, V. S. (2015). Advantages and disadvantages of composition and properties of biomass in comparison with coal: An overview. *Fuel, 158*, 330-350. https://doi.org/10.1016/j.fuel.2015.05.050

Voultsos, I., Katsourinis, D., Giannopoulos, D., & Founti, M. (2020). Integrating LCA with Process Modeling for the Energetic and Environmental Assessment of a CHP Biomass Gasification Plant: A Case Study in Thessaly, Greece. *Eng—Advances in Engineering, 1*(1), 2-30. https://doi.org/10.3390/eng1010002

Wang, Y., Ho, S.-H., Yen, H.-W., Nagarajan, D., Ren, N.-Q., Li, S., . . . Chang, J.-S. (2017). Current advances on fermentative biobutanol production using third generation feedstock. *Biotechnology advances, 35*(8), 1049-1059. https://doi.org/10.1016/j.biotechadv.2017.06.001

Weiland, F., Hedman, H., Marklund, M., Wiinikka, H., Öhrman, O., & Gebart, R. (2013). Pressurized oxygen blown entrained-flow gasification of wood powder. *Energy & Fuels, 27*(2), 932-941. https://doi.org/10.1021/ef301803s

Wen, C. (1966). *Mechanics of fluidization.* Paper presented at the Chemical Engineering Progress Symposium Series.

Wu, Y., Zhang, J., Smith, P. J., Zhang, H., Reid, C., Lv, J., & Yue, G. (2010). Three-dimensional simulation for an entrained flow coal slurry gasifier. *Energy & Fuels, 24*(2), 1156-1163. https://doi.org/10.1021/ef901085b

Xie, J., Zhong, W., Jin, B., Shao, Y., & Huang, Y. (2013). Eulerian–Lagrangian method for three-dimensional simulation of fluidized bed coal gasification. *Advanced Powder Technology, 24*(1), 382-392. https://doi.org/10.1016/j.apt.2012.09.001

Yu, L., Lu, J., Zhang, X., & Zhang, S. (2007). Numerical simulation of the bubbling fluidized bed coal gasification by the kinetic theory of granular flow (KTGF). *Fuel, 86*(5-6), 722-734. https://doi.org/10.1016/j.fuel.2006.09.008

Yu, M. M., Masnadi, M. S., Grace, J. R., Bi, X. T., Lim, C. J., & Li, Y. (2015). Co-gasification of biosolids with biomass: Thermogravimetric analysis and pilot scale study in a bubbling fluidized bed reactor. *Bioresource technology, 175*, 51-58. https://doi.org/10.1016/j.biortech.2014.10.045

Zanchi, G., Pena, N., & Bird, N. (2012). Is woody bioenergy carbon neutral? A comparative assessment of emissions from consumption of woody bioenergy and fossil fuel. *Gcb Bioenergy, 4*(6), 761-772. https://doi.org/10.1111/j.1757-1707.2011.01149.x

Zanzi, R., Sjöström, K., & Björnbom, E. (2002). Rapid pyrolysis of agricultural residues at high temperature. *Biomass and Bioenergy, 23*(5), 357-366. https://doi.org/10.1016/S0961-9534(02)00061-2

Zhang, G.-Q., Ernst, L. J., & de Saint Leger, O. (2000). *Benefiting from thermal and mechanical simulation in micro-electronics* (1st ed.). Netherlands: Springer.

Zhang, L., Xu, C. C., & Champagne, P. (2010). Overview of recent advances in thermo-chemical conversion of biomass. *Energy Conversion and Management, 51*(5), 969-982. https://doi.org/10.1016/j.enconman.2009.11.038

Zhang, X., Zhang, M., Zhang, H., Jiang, Z., Liu, C., & Cai, W. (2020). A review on energy, environment and economic assessment in remanufacturing based on life cycle assessment method. *Journal of Cleaner Production, 255*, 120160. https://doi.org/10.1016/j.jclepro.2020.120160

Appendix

Calculation of stoichiometric air flow rate for wood pellets:

The molecular formula is calculated from the ultimate analysis on a dry basis for the given biomass. The elemental mass percentage is divided by the molecular weight to determine the atomic value for each element. The obtained values were divided by the atomic number of carbons to normalize the molecule. So, for every carbon, you get 1.4 atoms of hydrogen, 0.63 atoms of oxygen etc.

Molecular formula: **$CH_{1.4}O_{0.63}$**

Stoichiometric combustion with air:

$$CH_{1.4}O_{0.63} + 1.035(O_2 + 3.76\ N_2) \rightarrow CO_2 + 0.7H_2O + 3.8926\ N_2$$

Fuel air ratio at the stoichiometric condition:

$$\begin{aligned} f_s &= \left.\frac{m_f}{m_a}\right|_{stoichiometric} \\ &= \frac{nM_f}{nM_a} \\ &= 0.1654 \end{aligned}$$

Further, the air-fuel ratio is given by *$1/f_s$ = 6.05*. Therefore, around *6.05* kg of air is needed for the complete combustion of 1 kg of wood pellets. Similarly, *6.78* and *6.15* kg of air is needed for complete combustion of 1 kg of grass pellets and wood chips respectively.

The ash fusibility temperature for the different types of biomass is presented in Table A01.

Table A01. Ash fusibility temperature for different types of biomass

	Wood pellets	Grass pellets	Wood chips
Shrinking starting temperature (°C)	1090	1090	1070
Deformation temperature (°C)	1460	1150	1420
Hemisphere temperature (°C)	1460	1180	1430
Flow temperature (°C)	1460	1190	1440

B. Scientific articles: published/submitted

Paper I

Effect of particle size on flow behaviour in fluidized beds

Ramesh Timsina, Rajan K. Thapa, Britt M. E. Moldestad and Marianne S. Eikeland

DOI: doi.org/10.2495/EQ-V4-N4-287-297

International Journal of Energy Production and Management, Volume 4 (2019), Issue 4, 287-297.

ISSN: 2056-3280 (online) and ISSN: 2056-3272 (print)

Short overview

The paper presents the effects of different particle sizes on fluidization behaviour in BFB gasifiers. Experiments were done by mixing sand particles of mean diameter 293µm (small particle) and 750 µm (large particle) at different volume ratios. A CPFD model was developed to compare the experimental data and explore the bed hydrodynamics (in cold conditions). The paper is published in an issue from the Wessex Institute of Technology (WIT Press).

R. Timsina, et al., Int. J. of Energy Prod. & Mgmt., Vol. 4, No. 4 (2019) 287-297

EFFECT OF PARTICLE SIZE ON FLOW BEHAVIOR IN FLUIDIZED BEDS

RAMESH TIMSINA, RAJAN K. THAPA, BRITT M. E. MOLDESTAD & MARIANNE S. EIKELAND
Department of Process, Energy and Environmental Technology, University of South-Eastern Norway,
Kjølnes Ring 56, 3901, Porsgrunn, Norway.

ABSTRACT

The fluidization behaviour depends on particle properties such as particle size, sphericity, density and the properties of the fluidizing agent. In this study, the effects of different particle sizes on fluidization behaviour were investigated. Experiments were done by mixing sand particles of mean diameter 293 μm (small particle) and 750 μm (large particle). The experiment with 20% small particles and 80% large particles gave a reduction in minimum fluidization velocity of 60.8% compared to the minimum fluidization velocity with only large particles. CPFD simulations were performed using the commercial software Barracuda®. There is a good agreement between the results from the experiments and the simulations. The minimum fluidization velocity is also calculated using different theoretical equations based on the average particle size for the mixture. The obtained experimental results were compared with the minimum fluidization velocity calculated using different equations available in the literature. There are significant differences in minimum fluidization velocities obtained from the different empirical equations. The pressure drop profiles for large and small particles follow the trends presented in the literature. The experimental minimum fluidization velocities were found to be 0.46 and 0.092 m/s for the large and small particles respectively.

Keywords: bubbling fluidized bed, fluidization, particle size.

1 INTRODUCTION

The fluidization technology is used in several industrial operations due to uniform heat and mass transfer. Industrial applications such as calcination and roasting of minerals, combustion, gasification, flue-gas desulphurization, chemical reactors use the fluidization technology. The technology involves complex multiphase flows, heat and mass transfer and several reactions within the bed.

Gasification of biomass is a thermochemical conversion process, which gives product gases such as CO, H_2, CO_2 and CH_4, together with tar and a solid residue consisting of ash and char [1]. Fluidized beds are commonly used for biomass gasification. The fluidized bed technology uses bed material to heat up the biomass particles to a temperature range of 700–900°C [2]. Even distribution of heat and mass transfer and excellent solid mixing make the fluidized bed gasification one of the attractive technologies for biomass gasification.

In a bubbling fluidized bed gasifier, the fluidizing agent such as air or steam is introduced from the bottom of the bed. The fluidizing agent keeps the bed in a fluid like state. The fluidized bed biomass reactors operate within the bubbling fluidization regime. The fluidization regime is very much dependent on particle size, particle size distribution, solid density (compactness of the substance) and the sphericity of particles (sphericity gives a rough estimation of a particle shape) and the properties of the fluidizing agent. It is important to investigate the effects of these parameters on the performance of a fluidized bed biomass gasification reactor.

Velocity measures the quantity of the fluidizing agents into the bed materials. When a fluid at low velocity is introduced into a bed of solid particles, fluid hardly percolates in between the space present between the solid particles. With an increase in the fluid velocity, a point is

© 2019 WIT Press, www.witpress.com
ISSN: 2056-3272 (paper format), ISSN: 2056-3280 (online), http://www.witpress.com/journals
DOI: 10.2495/EQ-V4-N4-287-297

achieved where all the solid particles are suspended by upward flowing fluid. The bed at this state is called the bed at minimum fluidization. The velocity with which the bed fluidizes is known as the minimum fluidization velocity. Any other velocity with which the bed fluidizes is called the fluidization velocity. The difference between the fluidization velocity and the minimum fluidization velocity is known as excess velocity.

Industrial fluidized beds use bed materials with size distributions. Bed hydrodynamics change significantly with small changes in particles size and particle size distributions. The average size of the mixture changes with change in particles size distribution of the mixture. A mixture of the same particle species with different average sizes gives the minimum fluidization velocity in between the minimum fluidization velocities of the two particles [3]. The mixing state of the binary systems in fluidized beds are classified as (a) complete mixing (b) complete segregation (c) partial mixing [4].

Jayarathna and Halvorsen [5] have studied the minimum fluidization velocity and bed expansion for mixtures of particles with different sizes. Spherical glass powders were used in their experiments, and it was found that the minimum fluidization velocity decreased with increase in the concentration of the small particles in the mixture.

Mixtures of different particle sizes show the phenomenon of particle segregation. Segregation reduces the heat and mass transfer and the expansion of the bed. Huilin *et al.* [6] investigated the mixing and segregation of particles in a fluidized bed. Simulations were performed to study the flow behaviour and segregation of particles in a mixture based on Eulerian–Eulerian approach and kinetic theory of granular flow for a binary mixture. Smaller particles tend to accumulate towards the top of the bed and larger particles tend to move towards the bottom of the bed [6].

The minimum fluidization velocity for the binary particles with large difference in sizes and densities were studied by Noda *et al.* [4]. Experiments were performed to develop an equation for predicting the minimum fluidization velocity for the binary systems such as wood chips, iron beads, soya bean with sands/glass beads.

Oliveira *et al.* [7] developed an experimental correlation for the minimum fluidization velocity for the binary mixture of sand and biomass. The bed hydrodynamics is directly related to the biomass shape and size. The different combinations of biomass and sand exhibits the state of complete mixing, complete segregation and partial mixing [7].

Perez *et al.* [8] studied minimum fluidization velocity for the mixture of sugarcane bagasse particles and the quartz sand. The minimum fluidization velocity increased with increase in the amounts of large particles (biomass) as well as increase in the size of the large particles. The developed correlation based on the experiments gives approximately accurate minimum fluidization velocities [8].

Ramakers *et al.* [9] have studied the minimum fluidization and the bed porosity for the mixture of wood particles and sand. The results showed the different results compared to the values obtained from the correlations from literature. The experimental results have a clear trend. For complete mixing of sand and the wood particles, a maximum of 10 weight % of wood particles should be used with superficial gas velocity of around 3–4 times the minimum fluidization velocity [9].

Paudel and Feng [10] developed a correlation based on the weight percentage for a mixture of biomass (corn cobs and walnut shells) and bed material (sand, glass beads and alumina). The results from the correlations were in good agreement with the experimental results [10].

The particles size and the proportion of the different species in the bed influences the complete mixing in the bed. Hence, the experiments and the simulations were performed to determine the minimum fluidization velocity for mixtures of small and large particles. The experiments were done by mixing sand particles with particle sizes of 150–400 µm (mean diameter 293 µm) and 600–850 µm (mean diameter 750 µm). Air was used as the fluidizing agent. The experimental minimum fluidization velocities were compared with the theoretical minimum fluidization velocities.

2 THEORETICAL BACKGROUND

Fluid flow rate gives the quantity of the fluidizing agents per unit time. When the fluid flow rate into the bed of solid particles with a range of particle sizes is increased, the smaller particles move towards the voids present in between the large particles. The large particle in the mixture tends to remain in stationary conditions up to certain airflow rate, at which the bed starts to fluidize. Further increase of air velocity into the bed gives segregation and settling of particles. The large particles tend to settle down towards the bottom of the bed and the smaller particles move towards the top of the bed [11]. Segregation is a non-desired phenomenon in a fluidized bed. Therefore, the study of particle size distribution in the fluidized bed is of great significance. Considering the fluidization behaviour of the particles, Geldart defined them into four different groups. Geldart's classification of particles is presented in Fig. 1. The abscissa represents the average size of the mixture (µm) in logarithmic scale and the ordinate represents the difference in density of the bed material and the gas density (g/cm^3).

Group C particles are a small fine cohesive particle with very high interparticle forces. Fluidization of group C particles gives rise to channelling or plugging of the bed. Group A particles are ideal for fluidization because of good solid mixing of particles at relatively low fluid velocity. The bubbles split and coalesce several times while passing through the bed during fluidization. Group B particles have good solid mixing and heat transfer between the biomass and bed materials. The bubbles grow and coalesce as they move upwards. Group D particles have a large diameter. It is difficult to fluidize group D particles as the bubbles coalesce rapidly along the bed and exhibit severe channelling, spouting and exploding behaviour [11]. Most of the fluidized bed gasifiers use Geldart B particles as a bed material, and therefore this study was focused on group B particles.

The different types of particles have different minimum fluidization velocity. Moreover, the fluidization characteristics of a bed depend on density, excess velocity and the particle

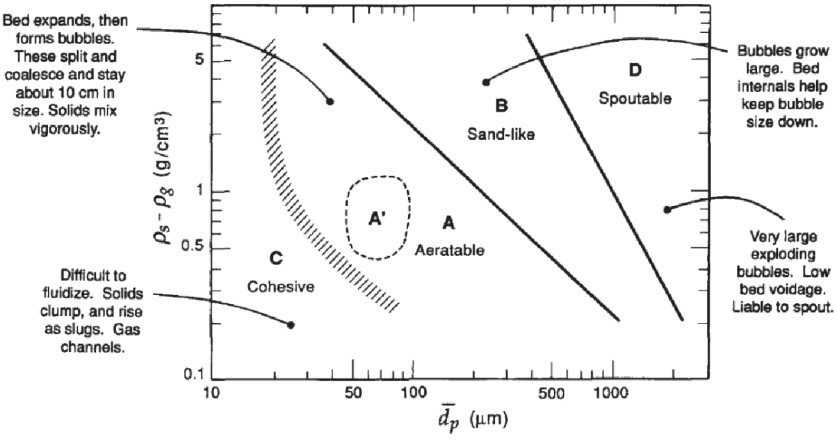

Figure 1: Particle behaviour when suspended by gas [12].

size distribution. Bulk density takes the account of voids present in the solid mixture, given by the ratio of weight of solids divided by the total volume occupied by solids and the voids. Bulk density changes with the change in particle size distribution. Ergun proposed the mathematical model to predict the fluid flow through a bed of solid particles. The model gives the minimum fluidization velocity of the bed material used in fluidized bed gasification reactor.

The pressure drop, ΔP, across the bed of height L, containing solids with a particles diameter d_p is given by Ergun equation [11].

$$\frac{\Delta P}{L} = \frac{150\mu}{\Phi_p{}^2 d_p{}^2}\frac{(1-\varepsilon)^2}{\varepsilon^3}U + \frac{1.75\rho_g}{\Phi_p d_p}\frac{(1-\varepsilon)}{\varepsilon^3}U^2 \tag{1}$$

where ΔP is the pressure drop due to the weight of the bed, U is the superficial gas velocity, μ is the dynamic fluid viscosity, Φ_p is the sphericity, ε is the voidage (space left in between the solid particles) of the bed and ρ_g is the gas density.

At minimum fluidization condition, all the solid particles are suspended in the bed. The drag force between the upward flowing gas and the bed materials is balanced by the weight of the particles at minimum fluidization.

$$\underbrace{\begin{pmatrix}\text{Pressure}\\ \text{drop}\\ \text{across bed}\end{pmatrix}\begin{pmatrix}\text{crosssectional}\\ \text{area}\\ \text{of bed}\end{pmatrix}}_{\text{Drag force}} = \underbrace{\begin{pmatrix}\textit{volume}\\ \textit{of}\\ \textit{bed}\end{pmatrix}\begin{pmatrix}\textit{fraction}\\ \textit{consisting}\\ \textit{of solids}\end{pmatrix}\begin{pmatrix}\textit{specific}\\ \textit{weight}\\ \textit{of solids}\end{pmatrix}}_{\text{Particle weights}} \tag{2}$$

For positive ΔP [11, 13],

$$\Delta P\, A_t = A_t\, L_{mf}\left(1-\varepsilon_{\mathrm{mf}}\right)\left[\left(\rho_s-\rho_g\right)\frac{g}{g_c}\right] \tag{3}$$

Here, A_t is the cross-sectional area of the bed, L_{mf} is the height of the bed at minimum fluidization conditions, ε_{mf} is the voidage at minimum fluidization, ρ_s is the density of bed materials, g is the acceleration due to gravity and g_c is the force-weight conversion factor. The force-weight factor can be ignored for flow with gases unless the bed is deep at high pressure [11].

Or

$$\frac{\Delta P}{L_{mf}} = \left(1-\varepsilon_{\mathrm{mf}}\right)\left(\rho_s-\rho_g\right)g \tag{4}$$

The superficial gas velocity U_{mf} at minimum fluidization conditions can be calculated by combing the eqn (1) and eqn (4). The solution for $U_{mf} > 0$ [14] gives:

$$U_{\mathrm{mf}} = \frac{\left\{-150\mu\left(1-\varepsilon_{\mathrm{mf}}\right)+\sqrt{\left[150\mu\left(1-\varepsilon_{\mathrm{mf}}\right)\right]^2+7\rho_g\varepsilon_{\mathrm{mf}}{}^3\Phi_p{}^3 d_p{}^3\left(\rho_s-\rho_g\right)g}\right\}}{3.5\rho_g\Phi_p d_p} \tag{5}$$

Further, eqns (1) and (4) can be simplified in the form of Reynolds and Archimedes number at minimum fluidization condition as follows [11].

$$\underbrace{\frac{1.75}{\Phi_p \varepsilon_{mf}^3} \mathrm{Re}_{p,mf}^2}_{\text{Inertial part}} + \underbrace{\frac{150(1-\varepsilon_{mf})}{\Phi_p^2 \varepsilon_{mf}^3} \mathrm{Re}_{p,mf}}_{\text{Viscous part}} - \mathrm{Ar} = 0 \tag{6}$$

where $\mathrm{Re}_{p,mf} = d_p U_{mf} \rho g/\mu$ and $\mathrm{Ar} = \rho_g d_p^3 g(\rho_s - \rho_g)/\mu^2$. The first term represents the inertial part and the second term represents the viscous part in eqn (6). Further, eqn (6) can be written as:

$$K_1 \mathrm{Re}_{p,mf}^2 + K_2 \mathrm{Re}_{p,mf} - \mathrm{Ar} = 0 \tag{7}$$

Where

$$K_1 = \frac{1.75}{\Phi_p \varepsilon_{mf}^3} \text{ and } K_2 = \frac{150(1-\varepsilon_{mf})}{\Phi_p^2 \varepsilon_{mf}^3}$$

The voidage and the sphericity are the critical factors to determine the minimum fluidization velocity. The voidage at minimum fluidization is strongly dependent on the particle sphericity. The Ergun equation calculates the pressure-drop based on the voidage and the sphericity of the fixed bed. This does not give the exact pressure drop at transient fluidization conditions. There are different empirical correlations developed by different researchers to predict the minimum fluidization velocity for different operating conditions. Some of the correlations are presented in Table 1.

In general, the inertial part in Ergun's equation is neglected for small particles with $\mathrm{Re}_{p,mf} < 20$ [11]. This simplifies the eqn (5) to:

$$U_{mf} = \frac{d_p^2 (\rho_s - \rho_g) g}{150\mu} \frac{\Phi_p^2 \varepsilon_{mf}^3}{1-\varepsilon_{mf}} \tag{8}$$

3 EXPERIMENTAL

The experiments were done in a laboratory scale bubbling fluidized bed available at the University of South-Eastern Norway. The experimental set-up along with a

Table 1: Empirical equations for minimum fluidization velocity by different authors.

Author	**Equation**
Wen and Yu [15]	$U_{mf} = \frac{\mu_g}{\rho_g d_p}\left(\sqrt{33.7^2 + 0.0408\,Ar} - 33.7\right)$
Richardson *et al.* [11, 16]	$U_{mf} = \frac{\mu_g}{\rho_g d_p}\left(\sqrt{25.7^2 + 0.0365\,Ar} - 25.7\right)$
Doichev and Akhmakov [17]	$U_{mf} = \frac{\mu_g}{\rho_g d_p}\left(1.08 \times 10^{-3}\,Ar^{0.947}\right)$
Barbosa *et al.* [18]	$\mathrm{Re}_{mf} = 1.9 \times 10^{-3}\,Ar^{0.87}, U_{mf} = \frac{Re_{mf}\mu}{\rho_g d_p}$

simplified sketch are presented in Figure 2. The experimental setup consists of pressure measurement sensors connected to a computer program, airflow supply and the fluidized bed. The pressure sensors measure the pressure within the bed for different airflow rates. LabVIEW is used to acquire the data measured by the pressure sensors at the wall of the column. Compressed air at ambient temperature is supplied from the bottom of the bed. The supplied air passes through a porous plate distributor for even distribution of airflow into the bed. The airflow rate is controlled by the pressure reduction valve and is measured by a digital flow meter. The bed consists of a transparent plastic cylinder with height (h) 1.5 m and diameter (D) 84 mm. The second pressure sensor (P2) lies 35 mm above the air distributor and the distance between the sensors is 100 mm.

The experiments were carried out with the different proportions of large and small particles. Sand particles with different mean diameters were used for the experiments. The small particles were in the range of 150–400 μm and the large particles were in the range of 600–850 μm. The various parameters used for the experiments are presented in Table 2.

The bed volume for each of the experiments was 1200 ml. The composition of the small particles in the experimental sample were 0% (pure large particles), 10%, 20%, 30%, 40%, 50%, 60%, 75%, and 100%. The solid volume fraction was calculated based on the weight of a known volume of sand. The particles were mixed thoroughly before pouring into the bed column. The air flow rate was gradually increased until the bed reached the fluidization state. The minimum fluidization velocity was calculated using the empirical correlations shown in Table 1. The voidage at minimum fluidization conditions was taken as the solid void fraction at fixed bed condition for all the theoretical calculations. All of the obtained experimental values for the minimum fluidization velocity satisfied the conditions of $Re_{p,mf} < 20$. The theoretical minimum fluidization velocities based on only the viscous term of eqn (4) is also calculated.

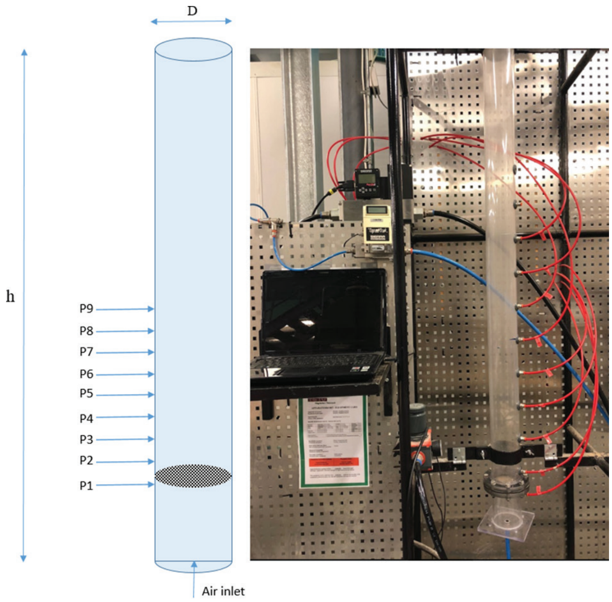

Figure 2: Experimental setup for bubbling fluidized bed.

Table 2: Various experimental parameters.

Particle density	2650 kg/m^3
Air density	1.225 kg /m^3
Air viscosity	1.8 × 10-5 Pa.S
Solid void fraction	0.49 – 0.50
Superficial gas velocity	0.03 – 0.6 m/s

4 COMPUTATIONAL MODEL

Computational fluid dynamics (CFD) are used to model the systems handling the fluid flow. Conventional CFD is a well-accepted technique for single-phase systems. Multiphase CFD models use either an Eulerian–Eulerian, or Eulerian–Lagrangian approach. The Eulerian–Eulerian approach models the solid and gas phase separately with Navier–Stokes equation. The discrete particle phase is not considered in Eulerian modelling and are solved with the kinetic theory of granular flow. In the Eulerian–Lagrangian approach, fluid is treated as a continuous phase and the particles as a discrete phase. The solid particles are approximated with Newton's law of motion. This gives high loading to CPU during simulations and is often limited to 2D or quasi-3D and in the order of 10^4 number of particles [19]. The MP PIC modelling is based on the Eulerian approach for fluid particles and Lagrangian approach for the solid particles. Barracuda® is a software package based on the MP PIC modelling, which is known as the Computational Particle Fluid Dynamics (CPFD) approach.

A simulation model was developed to compare the minimum fluidization velocity obtained from the experiment. The operating parameters for the simulation models are same as that of the experimental study. The results from the simulation modelling are validated against the experimental results to give an acceptable result for the minimum fluidization velocity for the mixture.

5 RESULTS AND DISCUSSIONS

The pressure drop profiles with respect to superficial gas velocity for large and small particles are presented in Figure 3. The presented figure shows the pressure drop profile and the minimum fluidization velocity for the large and the small particles.

The minimum fluidization velocity is 0.46 m/s for the large particles. The pressure drop at the minimum fluidization condition is 116 mbar/m for the large particles. The minimum fluidization velocity is 0.092 m/s for the small particles. The pressure drop at the minimum fluidization condition is 122 mbar/m for the small particles. The pressure drop profile for both particles follows the similar trends presented in the literature by Kunni *et al.* [11].

The obtained results from the experiments were validated using a simulation model based on CPFD approach in Barracuda. Figure 4 shows the comparison of the pressure drop along the bed for a particle with mean diameter 293 μm.

There is some deviation of the pressure drop for the static bed (before the minimum fluidization velocity). The minimum fluidization velocity from the simulation model is 0.09 m/s and 0.092 m/s from the experiment. The results from the simulations have a good agreement with the results from the experiments. Further the experiments and the simulations were done for each of the mixtures of large and small particles as described above and the minimum fluidization velocity of the mixture were calculated.

The minimum fluidization velocity of the mixtures with different composition of small and large particles was investigated in this study. Figure 5 gives the minimum fluidization velocity for the mixture of different proportion of small and large particle.

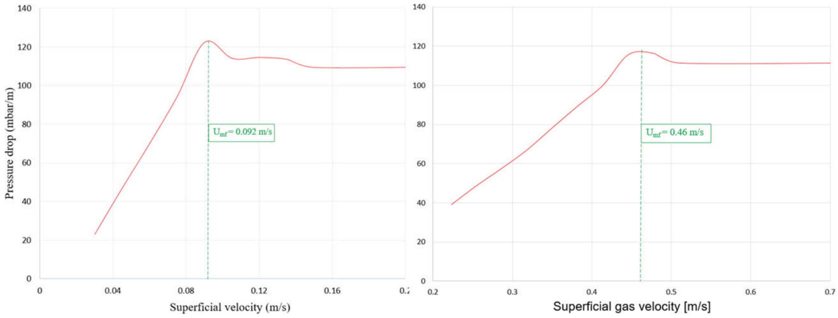

Figure 3: Pressure gradient profile for a): small particles (d_p = 293 μm) b): large particles (d_p = 750 μm).

The minimum fluidization velocity decreases with the addition of small particles in the mixture. The experiment with 20% small particles and 80% large particles gives a reduction in minimum fluidization velocity of 60.8% compared to the minimum fluidization velocity with only large particles. The addition of small particles can bring down the operating air velocity of fluidized bed biomass gasifiers. Biomass gasification reactors are usually operated in the bubbling regime. Higher air velocity provides high amounts of oxygen to the reactor, which can be undesirable. This is because the gasification is a thermochemical process that should be operated with limited supply of oxygen and excess supply of oxygen can convert the gasification process into combustion.

The simulation results agree well with the experimental results. Different drag models available in Barracuda are used in the simulations. It was found that the Wen-Yu-Ergun model gives the best prediction for the mixtures with up to 40% small particles. The Wen-Yu model agree with the experimental results with 50% small and 50% large particles. The mixtures with 60% and 75% small particles are well predicted by using the Ergun drag model. The different drag models also affect the value of the minimum fluidization velocity.

The theoretical minimum fluidization velocities calculated using equations presented in Table 1 deviates significantly from the measured minimum fluidization velocity. The theoretical minimum fluidization velocities were calculated based on the mean particle size for the

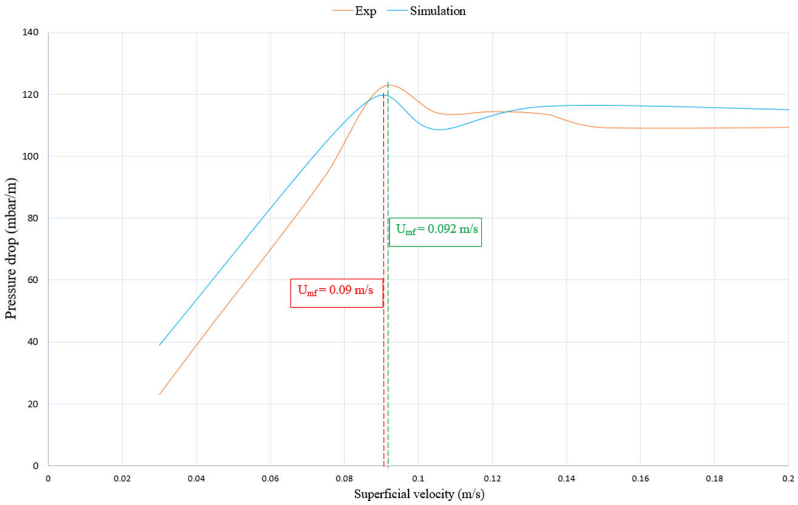

Figure 4: Pressure drop for small particles (d_p = 293 μm) (experiment and simulation).

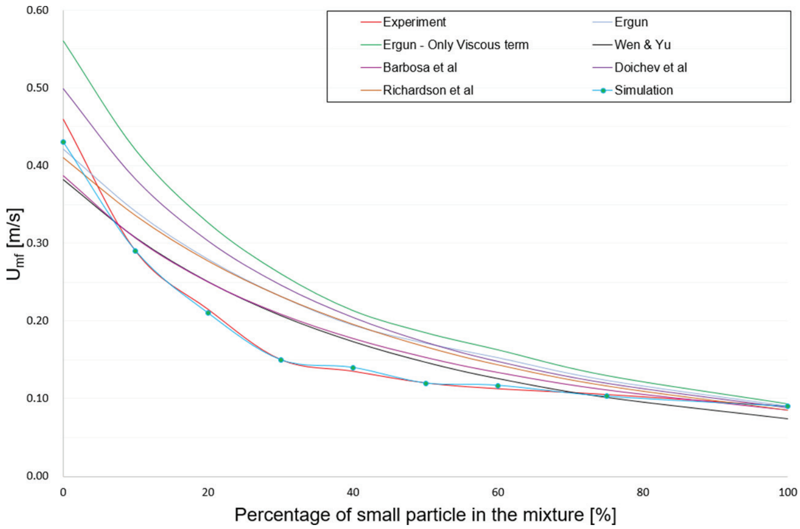

Figure 5: Minimum fluidization velocity.

mixture. For example, the minimum fluidization velocity based on Ergun equation deviates from the experimental result by 0%–35%. There is a deviation of 0%–28% with the Wen and Yu relationship compared to the experimental results. The Doichev *et al.* equation gives a deviation of 0%–41%. There are significant differences in minimum fluidization velocity based on different correlations for the mixtures with less than 40% of the small particle. This is mainly due to that the calculation of minimum fluidization velocity is based on the average particle diameter of the mixture. The calculated minimum fluidization velocity considering only the viscous term of the mixture gives a deviation of 3%–45%. The deviation increases with the increase of the proportion of the large particles in the mixture.

In the experiments sand with a wide range of particle sizes are used. The particle size distributions are not considered when calculating the theoretical minimum fluidization velocity from the different correlations, whereas the simulation model accounts of the particles size distributions of the mixture. The screenshot of the simulations of different compositions of small particles in the mixture is presented in the Figure 6.

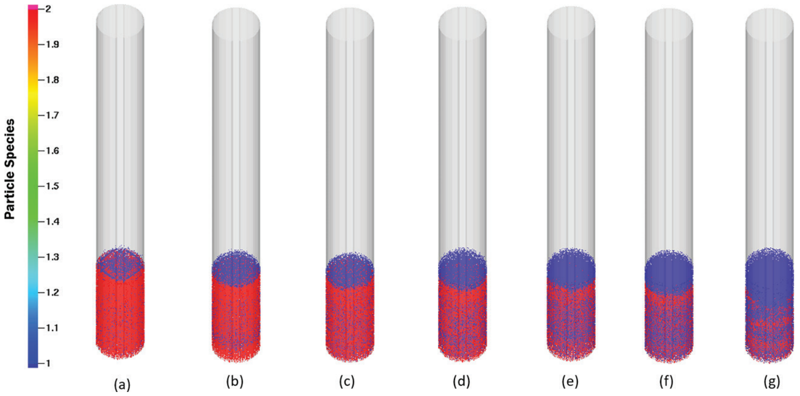

Figure 6. Particles distribution of the mixtures at bubbling regime (1- small particles, 2- large particles)

Figure 6 (a)-(f) show the particles distributions for the mixture with 10%–60% small particles and Figure 6 (g) shows the particle distributions of the mixture with 75% small particles and 25% large particles. The particle mixtures are well distributed with a degree of accumulation of small particles at the top of the bed for all the cases. Overall, it can be argued that there is a good mixing for the mixture with 10%–30% of small particles. The addition of 10–30% of small particles into the large particles can bring down the operating fluid velocity for the bubbling bed reactor. This makes the operation simple and decreases the required flow rate of air or steam into the system. The stability of the gasification process is a major challenge particularly involving the use of steam as a fluidizing agent. Steam at high temperature and pressure is challenging to handle and may cause loss of property and lives. Thus, the reduction of the required amounts of steam flow rate to the gasification process can reduce the issues related to the high requirement of fluidizing agent.

6 CONCLUSION

The experiments and the simulations were performed with two different sized sand particles. The minimum fluidization velocity for large and small particles as well as for the mixture of small and large particles were calculated. The theoretical minimum fluidization velocities for different particle mixtures are also calculated using different correlations for the drag function. The experimental minimum fluidization velocity is 0.46 m/s and 0.092 m/s for the large and small particles respectively. The theoretical minimum fluidization velocity calculated based on the different equation lies close to the experimental value for the small particles. There is a significant difference in minimum fluidization velocity for the mixture with different proportion of small and large particles based on the empirical relationships. The Doichev *et al.* equation gives a deviation of 0–41% in the calculation of the minimum fluidization velocity compared to the experimental results. The deviation increases with the decrease of small particles in the mixture.

The experiment with 20% small particles and 80% large particles gives a reduction in minimum fluidization velocity of 60.8% compared to the minimum fluidization velocity with 100% large particles. Using this mixture can reduce the operating velocity of a fluidized bed biomass gasifier significantly. The experiments and simulations with mixtures of small and large particles showed some degree of particle segregation. Larger particles tend to settle down towards the bottom of the bed and the smaller particles tend to accumulate towards the upper half of the bed. There is good mixing for the mixture with 10%–30% of small particles at a fluid velocity close to the minimum fluidization velocity. Future work includes a development of a drag model that satisfies the experimental results for all the compositions of the small and the large particles in the mixture. The deviations of the theoretical correlations are due to the fact that the correlations do not account for the particle size distribution of the mixture.

ACKNOWLEDGEMENTS

The author would like to thank the University of South-Eastern Norway for providing all the necessary arrangements for the experimental work.

REFERENCES

[1] Bandara, J.C., Moldestad, B.M. & Eikeland, M.S., Analysing the effect of temperature for steam fluidized-bed gasification of biomass with MP-PIC simulation. *Journal homepage: www. IJEE. IEEFoundation. org*, **9(6)**, pp. 529–542, 2018.

[2] Franco, C., Pinto, F., Gulyurtlu, I. & Cabrita, I., The study of reactions influencing the biomass steam gasification process☆. *Fuel*, **82(7)**, pp. 835–842, 2003. https://doi.org/10.1016/s0016-2361(02)00313-7

[3] Rowe, P. & Nienow, A.W., Minimum fluidisation velocity of multi-component particle mixtures. *Chemical Engineering Science*, **30(11)**, pp. 1365–1369, 1975. https://doi.org/10.1016/0009-2509(75)85066-4

[4] Noda, K., Uchida, S., Makino, T. & Kamo, H., Minimum fluidization velocity of binary mixture of particles with large size ratio. *Powder Technology*, **46(2–3)**, pp. 149–154. https://doi.org/10.1016/0032-5910(86)80021-3

[5] Jayarathna, C. & Halvorsen, B., Experimental and computational study of particle minimum fluidization velocity and bed expansion in a bubbling fluidized bed. in *SIMS*. 2009.

[6] Huilin, L., Yunhua, Z., Ding, J., Gidaspow, D. & Wei, L., Investigation of mixing/segregation of mixture particles in gas–solid fluidized beds. *Chemical Engineering Science*, **62(1–2)**, p. 301–317, 2007. https://doi.org/10.1016/j.ces.2006.08.031

[7] Oliveira, T., Cardoso, C. & Ataíde, C., Bubbling fluidization of biomass and sand binary mixtures: Minimum fluidization velocity and particle segregation. *Chemical Engineering and Processing: Process Intensification*, **72**, pp. 113–121, 2013. https://doi.org/10.1016/j.cep.2013.06.010

[8] Pérez, N.P., Pedroso, D.T., Machin, E.B., Antunes, J.S., Ramos, R.A.V. & Silveira, J.L., Fluid dynamic study of mixtures of sugarcane bagasse and sand particles: Minimum fluidization velocity. *Biomass and Bioenergy*, **107**, pp. 135–149, 2017. https://doi.org/10.1016/j.biombioe.2017.08.015

[9] Ramakers, B.J., De Ridder, R. & Kerkhof, P.J., Fluidization behavior of wood/sand mixtures. *Maderas. Ciencia y tecnologia*, **6(2)**, pp. 145–153, 2004. https://doi.org/10.4067/s0718-221x2004000200005

[10] Paudel, B. & Feng, Z.G., Prediction of minimum fluidization velocity for binary mixtures of biomass and inert particles. *Powder Technology*, **237**, pp. 134–140, 2013. https://doi.org/10.1016/j.powtec.2013.01.031

[11] Kunii, D. & Levenspiel, O., High-Velocity Fluidization. *Fluidization Engineering*, 193–210, Elsevier, 2013. https://doi.org/10.1016/b978-0-08-050664-7.50014-7

[12] Kunii, D. & Levenspiel, O., Circulating fluidized-bed reactors. *Chemical Engineering Science*, **52(15)**, pp. 2471–2482, 1997. https://doi.org/10.1016/s0009-2509(97)00066-3

[13] Cocco, R., Karri, S.R. & Knowlton, T., Introduction to fluidization. *Chem. Eng. Prog*, **110(11)**, pp. 21–29, 2014.

[14] Niven, R.K., Physical insight into the Ergun and Wen & Yu equations for fluid flow in packed and fluidised beds. *Chemical Engineering Science*, **57(3)**, pp. 527–534, 2002. https://doi.org/10.1016/s0009-2509(01)00371-2

[15] Wen, C. & Yu, Y., A generalized method for predicting the minimum fluidization velocity. *AIChE Journal*, **12(3)**, pp. 610–612, 1966. https://doi.org/10.1002/aic.690120343

[16] Richardson, J. & M.d.S. Jerónimo, Velocity-voidage relations for sedimentation and fluidisation. *Chemical Engineering Science*, **34(12)**, pp. 1419–1422, 1979. https://doi.org/10.1016/0009-2509(79)85167-2

[17] Doichev, K. & Akhmakov, N., Fluidisation of polydisperse systems. *Chemical Engineering Science*, **34(11)**, pp. 1357–1359, 1979. https://doi.org/10.1016/0009-2509(79)80032-9

[18] Lin, C.L., Wey, M.Y. & You, S.D., The effect of particle size distribution on minimum fluidization velocity at high temperature. *Powder Technology*, **126(3)**, pp. 297–301, 2002. https://doi.org/10.1016/s0032-5910(02)00074-8

[19] Ku, X., Li, T. & Løvås, T., CFD–DEM simulation of biomass gasification with steam in a fluidized bed reactor. *Chemical Engineering Science*, **122**, pp. 270–283, 2015. https://doi.org/10.1016/j.ces.2014.08.045

Paper II

Simulation of air-biomass gasification in a bubbling fluidized bed using CPFD model

Ramesh Timsina, Britt Moldestad, Rajan K. Thapa and Marianne S. Eikeland

DOI: doi.org/10.3384/ecp20170145

Published in the Linköping Electronic Conference Proceedings, SIMS 60, 145-150.

ISSN: 1650-3686 (print), 1650-3740 (online)

Short overview

The paper presents the results from a CPFD model developed in Barracuda to simulate a gasification process in an atmospheric BFB gasifier. The model is validated against the experimental results for the gasification experiments. It was presented at the 60th Conference on Simulation and Modelling (SIMS 60) held at Västerås, Sweden from 12th to 16th August 2019. The paper is published in the conference proceedings.

Simulation of air-biomass gasification in a bubbling fluidized bed using CPFD model

Ramesh Timsina Britt Moldestad Marianne S. Eikeland Rajan K. Thapa
Department of Process Energy and Environmental Technology University of South-Eastern Norway,
{ramesh.timsina, britt.moldestad, marianne.eikeland, rajan.k.thapa}@usn.no

Abstract

Biomass is a renewable energy source. Biomass gasification process produces producer gas, which can be further used for power generation or as raw materials for the production of secondary fuels. Experiment on the air gasification of biomass in a bubbling fluidized bed reactor was performed in a pilot-scale reactor located at the University of South-Eastern Norway (USN). A kinetics-based simulation model was developed based on MultiPhase Particle-In-Cell MP-PIC approach, using commercial software Barracuda®, and the results were compared with the experimental data. The average volume percentage of carbon monoxide, hydrogen, methane and nitrogen were found to be around 20%, 10%, 7% and 38% respectively in the experiment. The simulation results agree well for carbon monoxide, hydrogen and methane, but there is a difference in nitrogen volume percentage compared to the experimental results. The oxygen concentration during the experiment was around 1% suggesting a good performance of the gasifier. The char partial oxidation is less significant compared to the homogenous phase reactions. This shows that devolatilization reaction and the homogenous phase reactions dominate the char gasification reaction.

Keywords: air-biomass gasification, bubbling fluidized bed, CPFD

1 Introduction

Due to the rapid increase in the consumption of conventional fossil fuels, the global temperature is rising quite fast. One of the alternatives to counteract the increase in temperature is the use of renewable energy sources. Biomass gasification is one of the renewable energy production technologies and includes thermochemical conversion of carbonaceous fuels mainly into syngas (a mixture of CO and H_2) with the application of gasifying medium such as air, steam, and oxygen. Among the different biomass gasification technologies, fluidized bed reactors are commonly used. The fluidized bed technology uses bed material such as sand, or olivine to heat up the biomass particles at a temperature range of 700-900°C (Franco *et al.*, 2003). The gasification temperature is comparatively low, and this inhibits the agglomeration and sintering of the ash, which prevents causing serious problems during the operation of the gasifier. In addition, even distribution of heat and mass transfer, and excellent solid mixing make the fluidized bed reactor one of the attractive technologies for biomass gasification.

The product of gasification can be used for power generation in a gas engine, methanol synthesis or as the raw materials for production of secondary fuels, such as biodiesel, bio-ethanol and methanol (Bandara *et al.*, 2018). The operation of the fluidized bed gasification involves multiphase flow, various chemical reactions and heat transfer. It is a big challenge to investigate the effects of different parameters from the experimental study only, because of the requirements to build different setup configurations and procedures. Instead, modeling and simulations give better ideas for a wide range of design and operational parameters.

Modelling and simulation of such complex systems are needed for a good understanding of the process, designing and optimization. Computational fluid dynamics (CFD) are used to model the systems handling the fluid flow. Conventional CFD is a well-accepted technique for single-phase systems. Multiphase CFD models use either a Eulerian-Eulerian, or Eulerian-Lagrangian approach. The Eulerian-Eulerian approach models the solid and gas phase separately with the Navier-Stokes equation. The discrete particle phase is not considered in Eulerian modelling and is solved with the kinetic theory of granular flow. In the Eulerian-Lagrangian approach, fluid is treated as a continuous phase and the particles as a discrete phase. The solid particles are approximated with Newton's law of motion. This gives high loading to CPU during simulations and is often limited to 2D or quasi-3D and in the order of 10^4 number of particles (Ku *et al.*, 2015). The MP PIC modelling is based on the Eulerian approach for fluid particles and Lagrangian approach for the solid particles. Barracuda® is a software package based on the MP PIC modelling, which is known as the Computational Particle Fluid Dynamics (CPFD) approach.

Air is commonly used as the gasifying agent, which gives product gases with a Higher Heating Value (HHV) of 4-7 MJ/Nm^3. The low HHV is due to the dilution of

DOI: 10.3384/ecp20170145

the produced gas by nitrogen. Oxygen/steam blown biomass gasification produces gas with HHV of 10-18 MJ/Nm^3 (Schuster *et al.*, 2001; Li *et al.*, 2004). However, there will be an additional cost to produce oxygen/steam. There are many CFD models reported in the literature on steam gasification of biomass. CPFD modelling was chosen in this study because of its reliability and shorter simulation time. However, no previous work was found for the modelling of air gasification of biomass in a bubbling fluidized reactor using CPFD approach.

1.1 Previous works

Schuster et al. and Li et al. have studied the gasification of biomass based on the thermodynamic equilibrium model. Such models deviate significantly from the experimental results compared to the kinetics-based models (Schuster *et al.*, 2001, Li *et al.*, 2004).

Xie et al. have developed a model based on the MP-PIC approach for coal gasification in a fluidized bed reactor. Flow patterns, particle species profile, gas compositions, distributions of reaction rates were studied during their study (Xie *et al.*, 2013). The obtained results from the simulation model agree well with the experimental data.

Most of the biomass gasification simulations based on the MP-PIC approach have been applied with steam as the gasifying agent. Loha et al. have studied the flow pattern, gas composition and pressure distribution for different temperature and steam to biomass ratio in a laboratory scale bubbling fluidized bed gasifier. The gasification of rice husk during the experiment agreed well with the simulation based on the reaction kinetics of the gasification process (Loha *et al.*, 2014).

Further, the MP-PIC modelling has been applied to simulate the dual circulating bubbling fluidized bed (DCBFG) gasifier. Liu et al. studied the gasification of almond prunings in a dual fluidized bed gasifier. The model showed that the H_2 production, as well as CO production, was increased with increase in gasifier temperature and steam to biomass ratio (Liu *et al.*, 2016). Thapa et al. have developed a model for biomass gasification in DCBFG based on the MP-PIC approach. The published result agrees well with the experimental data obtained from the biomass gasification plant in Güssing, Austria (Thapa *et al.*, 2014).

In the present works, a simulation model for a bubbling fluidized bed gasifier has been developed in barracuda, and the results have been compared with the experimental data. The objective of this paper is to develop a model for air-gasification of biomass and validate the model against the experimental results.

2 Methods

2.1 Experimental Setup

The gasification rig installed at the University of South-Eastern Norway (USN) is a bubbling fluidized bed reactor with a fuel capacity of 20kW. Figure 1 and Figure 2 show the block diagram and the picture of the gasification rig at USN.

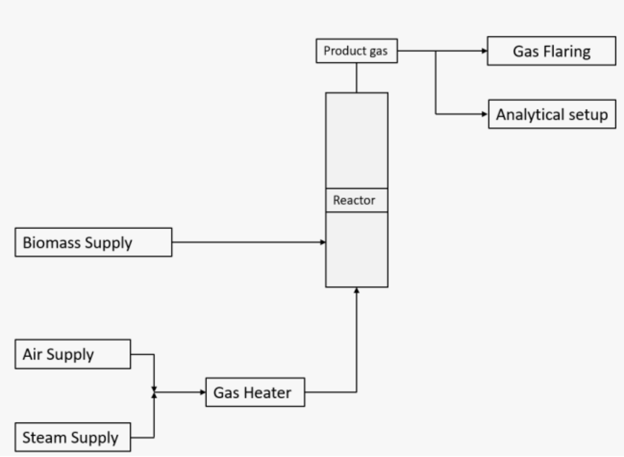

Figure 1. Block diagram of biomass gasification reactor at USN

The gasifier consists of a preheater (A), which heats up the fluidizing agents (air or steam) to about 450°C. The screw conveyors (B1 and B2), transfer the biomass from the fuel silo (C) to the reactor (D). Biomass is added into the silo before starting the experiments. The system is purged with nitrogen during the idle conditions of the reactor. The reactor is installed with pressure and temperature sensors at different locations to monitor the pressure and the temperature of the reactor. The product gas leaves from the top of the reactor for the gas analysis (F) and the flaring (E). The different parameters were controlled/changed/monitored during the experiment with the help of a computer program available at the experimental facility.

Figure 2. Picture of the bubbling bed reactor at USN

There are two screw conveyors as shown in Figure 3. The cold screw conveyor supplies the biomass from fuel silo to hot conveyor and the hot conveyor introduces the biomass into the reactor bed. The conveyors are perpendicular to each other.

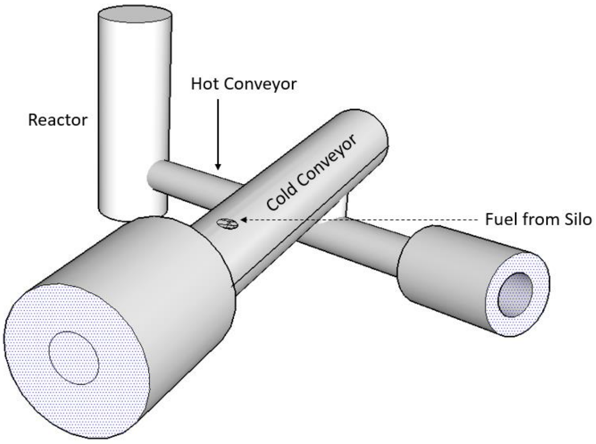

Figure 3. Cold and hot conveyor

The reason for separating the two-screw conveyer is to avoid the combustion of wood chips during the transportation process. The reactor is insulated to reduce heat loss during the experiments. The reactor is 100 mm in diameter and 1000 mm in height.

Sand with an average particle diameter of 285µm was used as bed materials during the experiments. Wood chips with approximately 0.5 cm average diameter was used for the experiments. The reactor was heated initially to about 700°C before the introduction of the biomass into the reactor for gasification experiments. Gas collected on syringe were analyzed on SRI 8610C gas chromatograph.

2.2 CPFD Simulation setup

A simulation model was developed by using Barracuda VR17 software. Wen-Yu drag model was used with 60% momentum loss after the particle collision. The reactor was designed as an open cylinder with a diameter of 100 mm and a height of 1000mm.

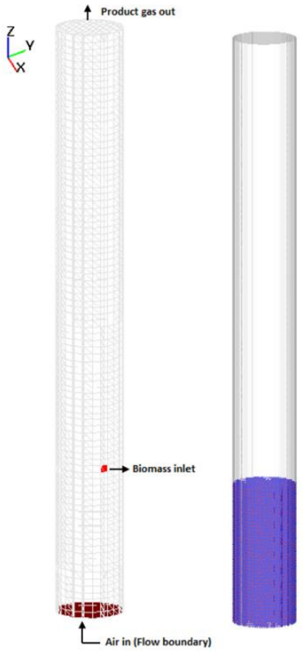

Figure 4. (a) Boundary conditions (b) Initial bed material

Figure 4 shows the boundary conditions and the initial height of bed material used for the simulation. The developed geometry was divided into 7128 computational cells.

Table 3 shows the properties of the bed material, and the gasifying agent used for the simulation process. The exit of particles from the reactor was set to zero by default, and the pressure boundary at the top of the reactor ensures the out flow of the product gas from the

Table 1. Reaction kinetics for air gasification

Reaction	Rate Kinetics
Char partial combustion (Xie *et al.*, 2013) $2C + O_2 \leftrightarrow 2CO$	$r = 4.34\times10^{7}\ m_s\theta_f \exp\left(\frac{-13590}{T}\right)[O_2]$
CO oxidation (Xie *et al.*, 2013) $CO + 0.5O_2 \leftrightarrow CO_2$	$r = 5.62\times10^{12} \exp\left(\frac{-16000}{T}\right)[CO][O_2]^{0.5}$
H_2 oxidation (Bates *et al.*, 2017) $H_2 + 0.5O_2 \leftrightarrow H_2O$	$r = 5.69\times10^{11} \exp\left(\frac{-17610}{T}\right)[H_2][O_2]^{0.5}$
CH_4 oxidation (Xie *et al.*, 2013) $CH_4 + 2O_2 \leftrightarrow CO_2 + 2H_2O$	$r = 3.552\times10^{11}\ T^{-1} \exp\left(\frac{-15700}{T}\right)[CH_4][O_2]$
Water gas shift reaction (Xie *et al.*, 2013) $CO + H_2O \leftrightarrow CO_2 + H_2$	$r = 7.68\times10^{10}\ T \exp\left(\frac{-36640}{T}\right)[CO]^{0.5}[H_2O]$
Methane reforming (Solli *et al.*, 2018) $CH_4 + H_2O \leftrightarrow CO + 3H_2$	$r = 3.00\times10^{5} \exp\left(\frac{-15042}{T}\right)[CH_4][H_2O]$

reactor. The air supply into the bed was kept constant during the experiments and the simulation process. Air at 1000K was supplied during the simulation to reduce the simulation time. During the experiments, preheating of air was done before introducing into the reactor bed. The reaction rate kinetics are presented in Table 1 based on the Arrhenius reaction rate model. The properties of the wood chips used in the simulation model are presented in Table 2 (Doherty *et al.*, 2013)

Table 2. Properties of wood chips

Proximate analysis (dry basis, wt. %)	
Volatile matter	80
Fixed carbon	18.84
Ash	1.16
Moisture	*20*

Table 3. Initial conditions

Items	*Parameters*
Bed material	285 µm average diameter, 0.54 volume fraction, density 2650 kg/m^3, 200 mm initial bed height
Gasifying fluid	Air, 0.2 m/s, 1000K, 101325Pa

3 Results and discussions

Experiments were done with wood chips and air in the bubbling fluidized reactor. The gas composition from the simulation is presented in Figure 5. The gas composition is irregular because of different physical and chemical transformation occurring inside the reactor, whereas the average gas compositions seems to be stable throughout the simulation.

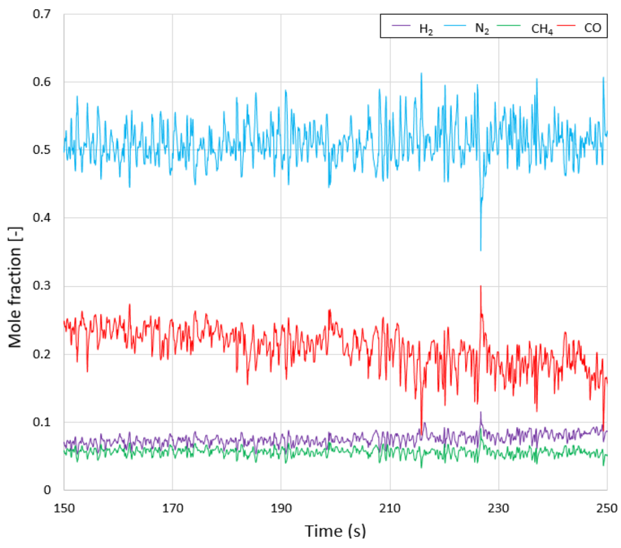

Figure 5. Gas composition for the simulation model

In the beginning, the hydrogen concentration in the product gas is due to the devolatilization of the biomass in the hot bed. Water vapor that is produced during methane oxidation favors the water gas shift reaction which slightly increases the hydrogen production with time. Further, the average gas composition from the simulation results are compared with the experimental results and is presented in Figure 6.

The simulation model predicts well the fraction of the different gas components and there is a good agreement between experimental and computational results regarding the hydrogen, carbon monoxide and methane concentration.

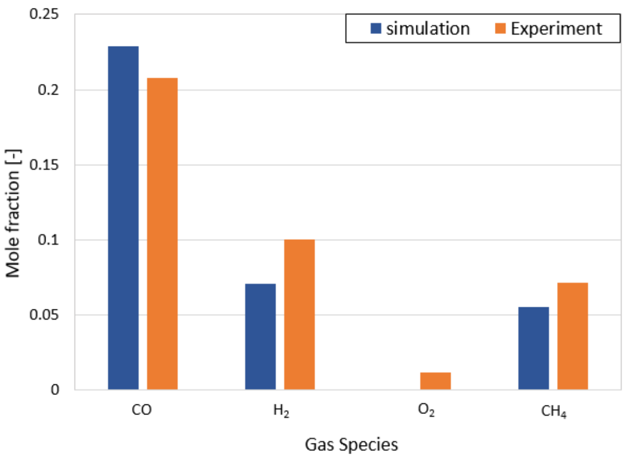

Figure 6. Comparison of average gas species

There are several reactions occurring during the gasification process. The major chemical reactions are modelled using the six major reactions presented in Table 1. The other minor chemical reactions are not included in the barracuda simulations, as they require a lot of computer capacity and time. The average oxygen concentration during the simulation was found to be zero whereas oxygen concentration during the experiment was around 1% of the total volume composition. This may be due to the sampling procedure, as the samples were taken in a syringe for the gas analysis. This shows that the CPFD model gives a comprehensive result.

The product gas compositions during the simulation were monitored at the different heights along the reactor. Figure 7 shows the mole fractions of carbon monoxide, hydrogen and the methane along the height of the reactor. There are not any distinct variations up to the biomass feeding position. The char partial oxidation is less significant compared to the homogenous phase reactions. Devolatilization as well as chemical transformations of biomass inside the bed give different gas compositions. The increasing hydrogen concentration along the reactor indicates the dominance of the water gas shift reaction and the methane reforming reaction.

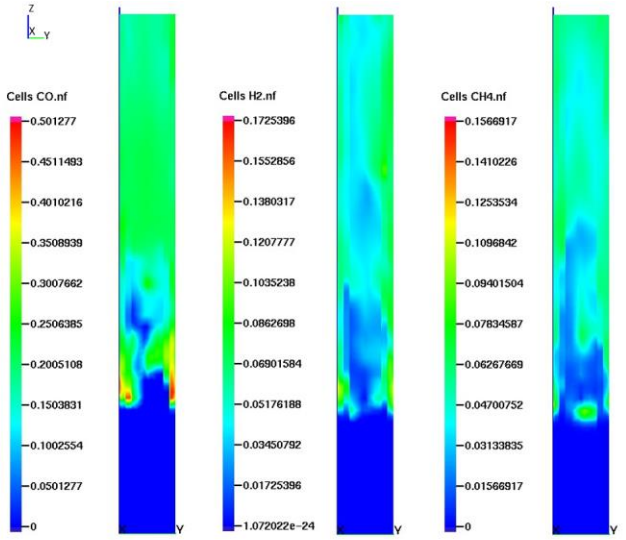

Figure 7. Gas composition along the reactor (Mole fraction)

This shows that the chemical transformations as well as the bed hydrodynamics is quite complex in a bubbling fluidized bed reactor. The operation of the optimized reactor would give uniform particle distribution and ensure operation in the bubbling fluidization regime. Figure 8 shows the particle volume fraction and the particle temperature distribution along the reactor height.

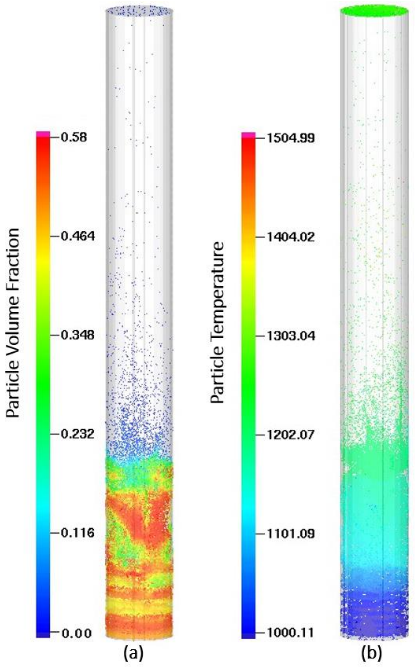

Figure 8. Simulation bed hydrodynamics at 200 s (a). Particle volume fraction (b). Particle temperature

Figure 8 (a) shows that the reactor operates at the bubbling fluidization regime with entrainment of few particles in the freeboard region. The solid volume fraction after the onset of the bubbling regime in the bed is reduced from the solid volume fraction of the static bed. Although the system was set to a temperature of 1000K, due to the exothermic nature of the reactions, the temperature rises up to around 1200K inside the reactor.

4 Conclusions

Air gasification of biomass in bubbling fluidized bed reactor was performed in a pilot-scale reactor at USN. A kinetic-based CPFD simulation model was used to simulate the gasification of biomass using Barracuda. The experimental setup as well as the simulation model were operated in the bubbling fluidizing regime. The results from the simulation were compared with the experimental data. The average volume percentage of carbon monoxide, hydrogen and methane were found to be around 20%, 10%, and 7% respectively during the experiment. There is a good agreement between experimental and computational results regarding the hydrogen, carbon monoxide and methane concentration. Oxygen concentration during the experiment was around 1%. The small amount of oxygen during the experiment may be due to manual sampling process used for gas sampling. The char partial oxidation is less significant compared to the homogenous phase reactions during the gasification process.

Acknowledgements

The authors would like to thank the University of South-Eastern Norway (USN) for providing the facilities for the experiments and the Barracuda VR for the simulation.

References

J. C. Bandara, B. ME. Moldestad and M. S. Eikeland. Analysing the effect of temperature for steam fluidized-bed gasification of biomass with MP-PIC simulation. *International Journal of Energy and Environment*, 9(6): 529-542, 2018.

R. B. Bates et al., Steam-air blown bubbling fluidized bed biomass gasification (BFBBG): Multi-scale models and experimental validation. *AIChE Journal*, 63(5): 1543-1565, 2017. doi:10.1002/aic.15666.

W. Doherty, A. Reynolds and D. Kennedy. Aspen plus simulation of biomass gasification in a steam blown dual fluidized bed. 2013.

C. Franco, F. Pinto, I. Gulyurtlu and I. Cabrita. The study of reactions influencing the biomass steam gasification process. *Fuel* 82(7): 835-842, 2003. doi:10.1016/S0016-2361(02)00313-7.

X. Ku, T. Li and T. Løvås. CFD–DEM simulation of biomass gasification with steam in a fluidized bed reactor. *Chemical Engineering Science*, 122: 270-283, 2015. doi:10.1016/j.ces.2014.08.045.

X. Li et al., "Biomass gasification in a circulating fluidized bed. *Biomass and Bioenergy*, 26(2): 171-193, 2004. doi:10.1016/S0961-9534(03)00084-9

H. Liu, R. J. Cattolica and R. Seiser. CFD studies on biomass gasification in a pilot-scale dual fluidized-bed system. *International Journal of Hydrogen Energy*, 41(28): 11974-11989, 2016. doi:10.1016/j.ijhydene.2016.04.205

C. Loha, H. Chattopadhyay and P. K. Chatterjee. Three dimensional kinetic modeling of fluidized bed biomass gasification. *Chemical Engineering Science*, 109: 53-64, 2014. doi:10.1016/j.ces.2014.01.017

G. Schuster, G. Löffler, K. Weigl and H. Hofbauer. Biomass steam gasification–an extensive parametric modeling study. *Bioresource technology*, 77(1): 71-79, 2001. doi:10.1016/S0960-8524(00)00115-2

K.-A. Solli, R. K. Thapa and B. ME. Moldestad. Screening of kinetic rate equations for gasification simulation models. Proceedings of The 9th EUROSIM Congress on Modelling and Simulation, EUROSIM 2016.

R. Thapa, C. Pfeifer and B. M. Halvorsen. Modeling of reaction kinetics in bubbling fluidized bed biomass gasification reactor. *Int. J. Energy Environment*, 5: 35-44, 2014.

J. Xie, W. Zhong, B. Jin, Y. Shao and Y. Huang. Eulerian–Lagrangian method for three-dimensional simulation of fluidized bed coal gasification. *Advanced Powder Technology*, 24(1): 382-392, 2013. doi:10.1016/j.apt.2012.09.001

Paper III

Experiments and computational particle fluid dynamics simulations of biomass gasification in an air-blown fluidized bed gasifier

Ramesh Timsina, Rajan K. Thapa, Britt M. E. Moldestad and Marianne S. Eikeland

DOI: doi.org/10.2495/EQ-V5-N2-102-114

International Journal of Energy Production and Management, Volume 5, (2020), Issue 2, 102-114.

ISSN: 2056-3280 (online) and ISSN: 2056-3272 (print)

Short overview

The paper presents the results from the gasification experiments in a pilot-scale BFB gasifier. A CPFD model was developed in Barracuda to simulate the gasification process and validated against the experimental results. The effects of different biomass feed, Air to Biomass Ratio (ABR) were studied. It was presented at the Energy Production and Management conference (EPM 2020) held online from 16th – 18th June 2020. The paper is published in an issue from the Wessex Institute of Technology (WIT Press).

R. Timsina, et al., Int. J. of Energy Prod. & Mgmt., Vol. 5, No. 2 (2020) 102-114

EXPERIMENTS AND COMPUTATIONAL PARTICLE FLUID DYNAMICS SIMULATIONS OF BIOMASS GASIFICATION IN AN AIR-BLOWN FLUIDIZED BED GASIFIER

RAMESH TIMSINA, RAJAN K. THAPA, BRITT M.E. MOLDESTAD & MARIANNE S. EIKELAND
Department of Process, Energy and Environmental Technology, University of South-Eastern Norway, Porsgrunn, Norway

ABSTRACT

Experiments were performed in a pilot-scale bubbling fluidized bed gasification reactor with air as a fluidizing agent. Birch wood chips and sand particles were used as biomass and bed materials. Average molar product gas composition was 0.214 of CO, 0.212 of CO_2, 0.103 of H_2, 0.074 of CH_4 and 0.397 of N_2. A kinetics-based model was developed for the gasification process and simulated using commercial software Barracuda®. The model is validated against the measured gas compositions. The validated model was used to study the product gas compositions for olive waste and straw pellets. The effects of equivalence ratio (ER) on the product gas composition for birch wood was also studied in one of the simulations. Birch wood gave the highest (20.5 mole %) CO production rate and lowest (9.0 mole %) H_2 production rate. The product gas flow rate was 1.96 Nm^3 per kg of biomass and the lower heating value of the product gas was 6.65 MJ/Nm^3. The CO concentration decreased from 25 to 13.2 mole %, whereas CO_2 concentration increased from 17 to 19.5 mole % when increasing ER from 0.2 to 0.3. The CO and H_2 concentrations for the olive waste were 8.1 and 56.1 mole %. The CO and H_2 concentrations for the straw pellets were 6 and 73.4 mole %.

Keywords: air-blown, biomass gasification, bubbling bed, CPFD, MP-PIC approach.

1 INTRODUCTION

European Union has an energy policy to achieve 20% share of the renewable energy in total energy consumption, a reduction of 20% greenhouse gas emissions and 20% improvements in the efficiency of biomass-based conversion technologies by 2020 (EU 20-20-20). The policy shows the great importance of the renewable energy [1]. Among the renewable energy sources, biomass has a huge potential to fulfil the future energy demands in the world. Biomass is not only geographically distributed with abundant availability [2] but also mitigates climate change.

Among the different alternatives to convert the biomass into biofuels, biomass gasification is one of the attractive routes. Biomass gasification is the partial oxidation of the carbonaceous fuels (biomass) into syngas (a mixture of mainly CO and H_2) in the presence of air, oxygen and/or steam [3]. The gasification process converts biomasses such as wood chips, agricultural waste, etc. into high-energy product gas. The products of the gasification are used to produce the second-generation biofuels and chemicals. The product gas can also be used to produce electricity and heat in a heat and power plant. The produced biofuels can be integrated into the existing infrastructure [4]. The gasification technology can be integrated into existing conventional power plants to increase the efficiency [5].

Fluidized bed reactors are commonly used for biomass gasification due to the uniform gas–solid mixing. The uniform mixing gives the homogeneous reactor temperature. Although gas cleaning is required after the gasifier, fluidized bed gasification reactor has the potential for scaling up the gasification system at relatively low costs. The gasification temperature is comparatively low (700–900°C), which avoids the issue of agglomeration and sintering of

© 2020 WIT Press, www.witpress.com
ISSN: 2056-3272 (paper format), ISSN: 2056-3280 (online), http://www.witpress.com/journals
DOI: 10.2495/EQ-V5-N2-102-114

the ash. Fluidized beds have high efficiency, are relatively simple to control and have a wide range of operating conditions compared to other thermal conversion technologies [3].

There are different steps in bubbling fluidized bed biomass gasification. Biomass undergoes pyrolysis/devolatilization, partial oxidation, char gasification, tar conversion and water gas shift reaction during the gasification process. The processes depend strongly on the fuel properties, the gasifying agent, the bed material and operational properties such as temperature, pressure and biomass feed rate. These are the key parameters for optimal design and operation of the biomass gasification reactor.

Due to experimental setup limitations, it is difficult to study the effect of the different parameters on the biomass gasification. The problems can be minimized by using a validated computational model. Modelling and simulation of biomass gasification in a bubbling fluidized bed reactor is complex as it involves solid−gas and solid−solid interactions along with the chemical transformation in the reactor [6]. Kinetics-based models are complex and are based on the conservation of mass, momentum and energy of the involved particles. However, during the past few decades, there has been a significant progress in this field. Bubbling fluidized bed gasifiers involve multiphase flow along with various chemical and physical transformations and heat and mass transfer.

Modelling of multiphase flow systems are challenging due to the coupling of turbulent gas flow and particle motions together with inter-particle collisions. The basic approaches for modelling of the gas–solid multiphase system are Eulerian–Eulerian and Eulerian–Lagrangian. In the Eulerian–Eulerian approach, conservation laws and the turbulence of both solid and fluid particles are solved with Navier–Stokes equation considering them as a continuous phase. The main disadvantage of this method is the lack of detailed transient information of the two-phase interactions [7]. In the Eulerian–Lagrangian approach, fluid particles are treated as the continuous phase and the solid particles are treated as a discrete phase. The fluid particles are solved by Navier–Stokes equations and the solid particles are solved with the Newton's equation of motion. There is strong coupling between the two phases. Eulerian–Lagrangian approach gives high loading to a computer central processing unit due to the huge number of particles in the system and the requirement of the small time step for solving the particle collisions [6].

MP-PIC modelling is developed from the Eulerian–Lagrangian approach, which reduces the computational costs related to the discrete modelling of the solid particles. Computational particles for MP-PIC modelling is a group of particles (called parcels) with similar properties such as size, density, residence time, velocity, etc. This eliminates the need for tracking of the individual particles. The parcels are modelled in a discrete frame and the particle interactions are modelled in Eulerian frame. Hence, the particles are solved both in Eulerian and Lagrangian frame, correlated by an interpolation functions [8]. The fluid particles are solved with an Eulerian approach. Barracuda VR is a commercial software based on the MP-PIC modelling, also known as the computational particle fluid dynamics (CPFD). The strong coupling between fluid and particle phase gives a high level of accuracy and fast computational time in Barracuda. The rapid development of the graphic process unit in computers has made the CPFD simulation capable of simulating the real process in short time.

Guo *et al.* [9] have carried out experiments with wood powder (particle size of less than 250 μm) with air as a gasifying medium. An autothermal gasifier was used to study the gasification temperature, gas yield, gas composition, heating value and gasification efficiency for different equivalence ratio (ER) and biomass particle sizes. The gas temperature and H_2 production increased with increase in ER. The gas yield, heating value and gasification efficiency increased with a decrease in biomass particle size [9]. Lv *et al.* [10] also showed that smaller particles are favourable to obtain higher gas yield and heating value of the product gas. Introduction of the steam in air gasification of biomass improved the gas quality [10]. The current study involves the gasification of birch wood chips with particle sizes in the range of 1–15 mm, which reduces the cost related to the preparation of the feedstocks.

Li *et al.* [11] have studied the air-blown biomass gasification in a circulating fluidized bed reactor. Results from the developed equilibrium model based on Gibbs free energy deviates due to the limitations of the reaction kinetics in the model. The model was tuned by adjusting the amounts of unconverted carbon and methane. The tuned model gave the product gas compositions, cold gas efficiency and the heating value of the product gas close to the experiment [11]. The simulation results agreed well with the experimental results using the reaction kinetics involved in air gasification of biomass in this study.

There are many CFD/CPFD models reported in the literature for steam gasification of biomass and coal [12–15]. However, no previous work was found for the modelling of air gasification of biomass in a bubbling fluidized bed reactor using CPFD approach. Simulations were performed using Barracuda VR 17.4.1 version. The main objective of the simulations is to study the effect of ER and the biomass feed on the performance of the gasifier.

2 EXPERIMENTAL SETUP

The experiments were carried out in a bubbling fluidized bed gasification reactor with a fuel capacity of 20 kW located at the University of South-Eastern Norway. The reactor used for the experiment is presented in Fig. 1. The reactor consists of a stainless steel cylindrical reactor (D) with 100 mm internal diameter, height of 1 m above the air distributor and wall thickness of 4 mm. An electric heating coil is attached to the outer surface of the reactor. The inner surface of the reactor is coated with refractory material, whereas the outer surface is insulated with thick fiberglass. Before starting the experiments, the fuel silo (C) is filled with biomass and sealed properly. The fuel is supplied through two-screw conveyors B_1 and B_2. The schematic block diagram of the screw conveyors can be found in [16].

Figure 1: Experimental setup for bubbling fluidized bed.

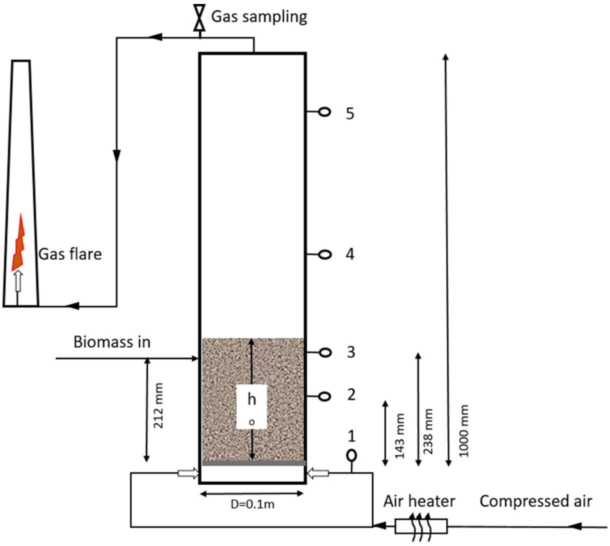

Figure 2: Schematic block diagram of the bubbling fluidized bed gasification reactor: points 1–5 indicate pressure and temperature sensor probe and h_o is the initial bed height.

Fig. 2 shows the schematic diagram of the gasification reactor, where the exact location of the different sensors and the biomass feeding position are illustrated. The temperature and pressure sensors are located at five different positions along the height of the reactor. The temperature and pressure sensors provide the real-time measurements in a computer program available at the experimental facility. The pressure sensor measures the gauge pressure at the given position. The air flow rate is measured by BROOK air flowmeter with an operating range of 0.48–4.7 kg/h. There is a gas sampling location (F) just outside of the reactor. The product gas passes through the gas transmission line for combustion into the flare (E). There is an air heater (A) that heats up the gasifying air to a temperature around 450°C. The heated air is introduced into the bed just below the gas distributor plate.

Experiments were performed using birch wood chips of an irregular shape and with length ranges from 1 to 15 mm. The proximate analysis of the chips is presented in Table 1. Sand with an average particle diameter of 285 μm was used as bed material during the experiments. The initial bed height was 250 mm. The diameter of the sand particles was in the range of 100–425 μm. The composition of the pyrolysis gases (volatiles) from the different biomasses is presented in Table 1.

Table 1: Proximate analysis and pyrolysis gas compositions for different biomass.

Proximate analysis [26–27]				**Pyrolysis gas compositions (molar fraction) [18, 28]**			
	Ash	*FC*	*VM*	CH_4	CO	CO_2	H_2
Birch wood	1.16	18.84	80	12.13	68.56	17.64	1.67
Straw pellets	9.8	11.2	79	8.00	48.4	4.7	38.9
Olive waste	7.17	25.48	67.35	18.3	47.8	12.3	21.6

3 COMPUTATIONAL MODEL

A CPFD model was developed using the Barracuda software to simulate the gasification process. The reactor was modelled as an open cylinder. A cylinder with inner diameter of 0.1 m and height of 1 m was drawn using the CAD software and the drawing was imported into Barracuda. The total number of cells were specified before generating the grid on the imported geometry. The grids act as control volumes, where the Barracuda solver solves the governing equations. The computational grid, initial bed conditions and boundary conditions are presented in Fig. 3.

A mesh with 3577 real computational cells was used. The properties of components in the product gas, air and sand particles were imported from the available database in Barracuda. The Wen-Yu drag model was used with 60% momentum loss after the particle collision. The blended acceleration model was activated as the particle mixtures have different sizes and densities. The normal and tangential coefficients of the particle–wall interaction were set to a default value of 0.3 and 0.99, respectively. Normal and tangential coefficients give the fraction of the normal and tangential components of the particle momentum, which is retained by the particle after collision with the wall. Particles moving towards a region of the close packed bed will be rerouted randomly based on particle normal stress function and the particle incident angle. Maximum momentum redirection from the collision was set to 40% of the original value.

Volatiles matter, char and ash composition of the biomass feed were specified according to Table 1 on a dry basis. The char volume in the bed was assumed 9% of the total bed volume during the simulation modelling. The initial and boundary conditions are presented in Table 2. The silica particle diameter in the range of 100–425 μm with an average diameter of 285 μm was specified in the particle initial conditions. The formation of the tar and the higher hydrocarbons were neglected during this work.

The inflow of biomass is done by applying ‘Particle feed: On’ in the boundary conditions for the biomass. A pressure boundary was added at the top of the reactor to assist the outflow of the product gas. ‘No particle exit’ option was enabled in the pressure boundary condition to prevent the particles from passing through the pressure boundary. The reactor was set to a temperature of 1000 K initially as it takes considerable time to heat up the particles to the

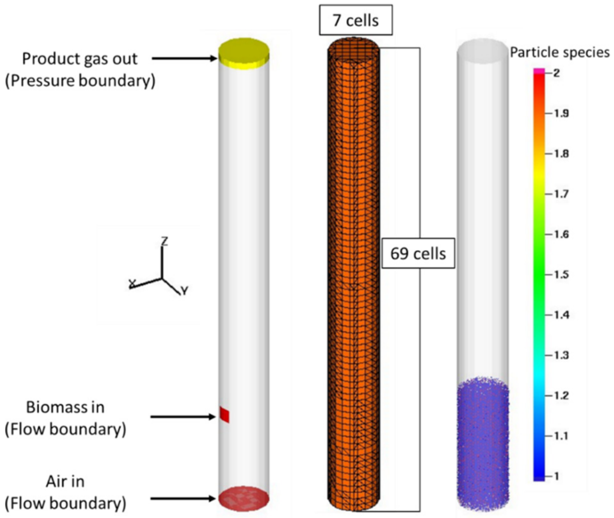

Figure 3: Schematic illustration of the barracuda model, (a) Boundary conditions, (b) Computational grid, (c) Initial particle in the bed (1-sand, 2- char).

Table 2: Initial and boundary conditions.

Initial conditions		
Fluid: air	Particle: silica	Particle: char
• 1000 K and 101325 Pa	• 1000 K and 101325 Pa • Particle size: 100–425 μm • 0.49 volume fraction • Density 2650 kg/m^3 • 250 mm initial height fill	• 1000 K and 101325 Pa • Particle size: 500 μm spherical • 0.05 volume fraction • Density 300 kg/m^3 • 250 mm initial height fill
Boundary conditions		
Air	Biomass	Product gas
• 1000 K and 101325 Pa • 0.17 m/s	• 500 K and 101325 Pa • Particle feed ON • 2.08 kg/hr	• 101325 Pa • No particle exit

reactor temperature. The particle flow should be assisted by a fluid stream and the fluid volume flow can be adjusted by adjusting the slip velocity. Arrhenius reaction rate model was used for the reaction kinetics in the model. The reaction kinetics is presented in Table 3. The

Table 3: Reaction kinetics for air gasification [17–22].

Char partial oxidation	$2C + O_2 \leftrightarrow 2CO$	$4.34\times10^{7} m_s T \exp\left(\frac{-13590}{T}\right)[O_2]$
Char oxidation	$C + O_2 \leftrightarrow CO_2$	$5.7\times10^{12} m_s \exp\left(\frac{-4595}{T}\right)[O_2]^{0.78}$
CO_2 gasification	$C + CO_2 \leftrightarrow 2CO$	$1.12\times10^{8} m_s P^{0.31} \theta_f \exp\left(\frac{-29518}{T}\right)[CO_4]$
H_2 oxidation	$H_2 + 0.5O_2 \leftrightarrow H_2O$	$5.69\times10^{11} \exp\left(\frac{-17610}{T}\right)[H_2][O_2]^{0.5}$
CO oxidation	$CO + 0.5O_2 \leftrightarrow CO_2$	$5.62\times10^{12} \exp\left(\frac{-16000}{T}\right)[CO][O_2]^{0.5}$
CH_4 oxidation	$CH_4 + 1.5O_2 \leftrightarrow CO + 2H_2O$	$5.0118\times10^{11} \exp\left(\frac{-24357}{T}\right)[CH_4]^{0.7}[O_2]^{0.8}$
Water gas shift	$CO + H_2O \leftrightarrow CO_2 + H_2$	$7.68\times10^{10} T \exp\left(\frac{-36640}{T}\right)[CO]^{0.5}[H_2O]$
Methane reforming	$CH_4 + H_2O \leftrightarrow CO + 3H_2$	$3\times10^{5} \exp\left(\frac{-15042}{T}\right)[CH_4][H_2O]$

constants of the reaction rate kinetics for the major reactions were taken from the different sources available in the literature.

4 RESULTS AND DISCUSSIONS

4.1 Experimental results

The results of the temperature and the pressure measurements at the reactor wall (Sensor 3 in Fig. 2) of the bubbling bed during the experiment are presented in Fig. 4. The figure shows the temperature and pressure reading after 220 min from the start of the experiment.

The temperature and the pressure inside the gasification reactor are fluctuating because of different physical and chemical transformation. The temperature seems to be fluctuating more compared to the pressure in the reactor. This is mainly because of the irregular feeding of biomass through the screw conveyor. Irregular feeding of biomass changes the ER, thereby changing the reaction mechanism. High amount of biomass favours the partial oxidation, whereas low amount of biomass favours the complete oxidation, thereby increasing the reactor temperature. Uniform feeding is still challenging for systems handling wood chips in biomass gasification [23].

4.2 Simulation model validation

The average gas compositions from the simulation were compared with the experimental results, which are presented in Fig. 5. There is a good agreement between the experiments and the simulation results. The developed model was used to study the gasification process.

4.3 Simulation results

Simulations were performed for 100 s, and the gas composition, gas temperature and gas flow rates were monitored. The average gas composition was taken as the time average composition for the final 50 s of the simulations. Fig. 6 shows the bed hydrodynamics in the gasifier after 100 s of simulation time. Fig. 6a shows that the reactor operates at the bubbling

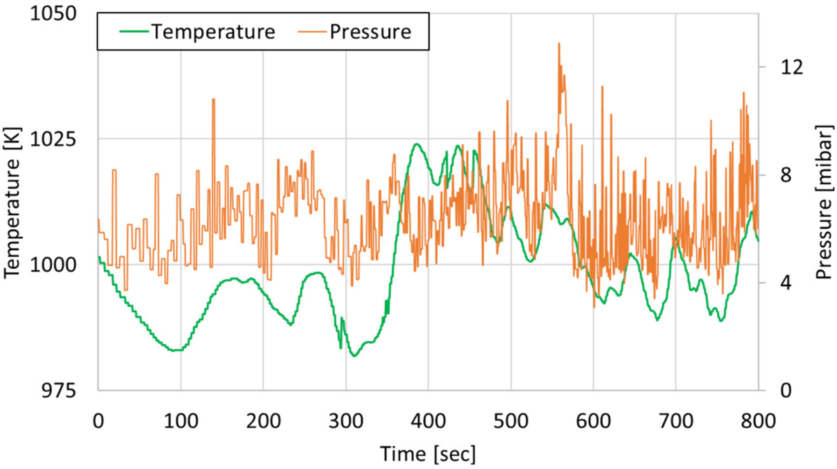

Figure 4: Temperature and pressure inside the reactor.

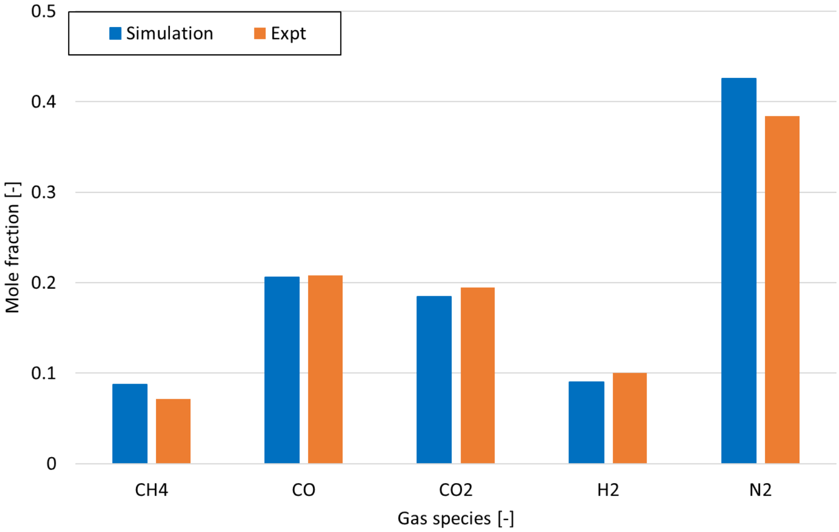

Figure 5: Average gas species for the experiment and the simulation.

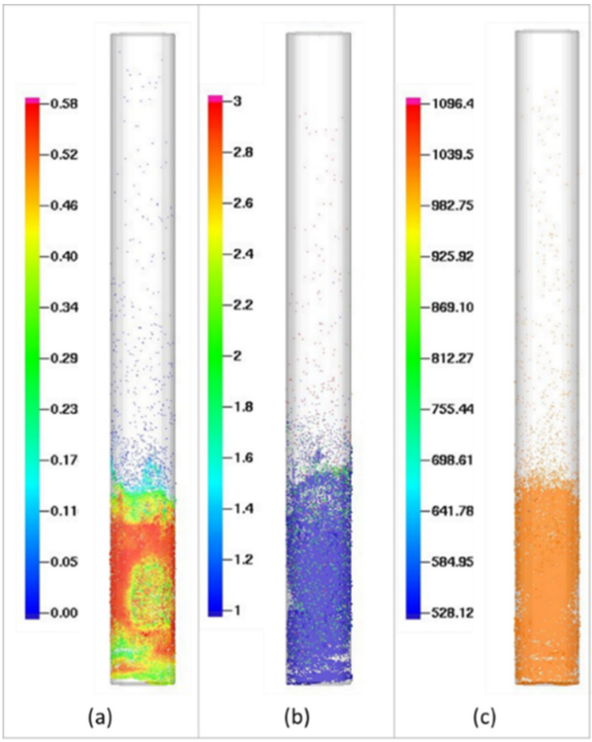

Figure 6: Bed hydrodynamics at 100 s: (a) particle volume fractions, (b) particle species distribution (1: sand, 2: char and 3: biomass) and (c) particle temperature (K).

fluidization region with a few particles entrained in the freeboard region. The entrained particles in the freeboard region are mainly biomass particles and char because these particles have a low density compared to sand. Fig. 6b shows the distribution of the different particle species in the bubbling fluidized bed. Blue particles depict the bed materials, green particles depicts the char inside the bed and the red particles depict the biomass particles. Fig. 6c shows the particle temperature distribution. Uniform particles temperature depicts the uniform mixing of the biomass and the sand particles. The reactor was continuously heated to supply the heat required for the gasification process, which slightly increases the reactor temperature with time.

The model was used to compare the product gas composition for different types of biomass as stated in Table 1. Fig. 7 shows the average product gas composition on a molar basis for olive waste, straw pellets and birch wood at 1000 K.

Birch wood have the lowest hydrogen production and highest carbon monoxide production because of the low amounts of hydrogen and high amounts of CO in the pyrolysis gas composition. CO_2 and CH_4 production for straw pellets is very small compared to other biomasses. Along with the different combination of ER and biomass, the desired output product gas composition can be achieved.

Simulations were performed for different ER to see the product gas composition. ER is used to indicate the amounts of oxidizer in the reactor.

ER was adjusted with adjusting the biomass inflow into the reactor model, as the change in airflow would change the bed hydrodynamics and the particle/gas residence time. The stoichiometric air to fuel ratio was taken as 5.5 for the birch wood used during the experiments.

Fig. 8 depicts the product gas composition for the different ER at 1000 K for birch wood. The CO concentration decreased from 25 to 13.2 mole %, whereas the CO_2 concentration increased from 17 to 19.5 mole % with change in ER from 0.15 to 0.3. With same increase in ER, the nitrogen concentration increased by 38.5%. With increasing ER, the process shifts towards combustion, as the amount of air (oxygen) increases. Fig. 8 shows the increase in CO_2 concentration with increasing ER. The H_2 and CH_4 concentration decreases slightly for the given range of ER.

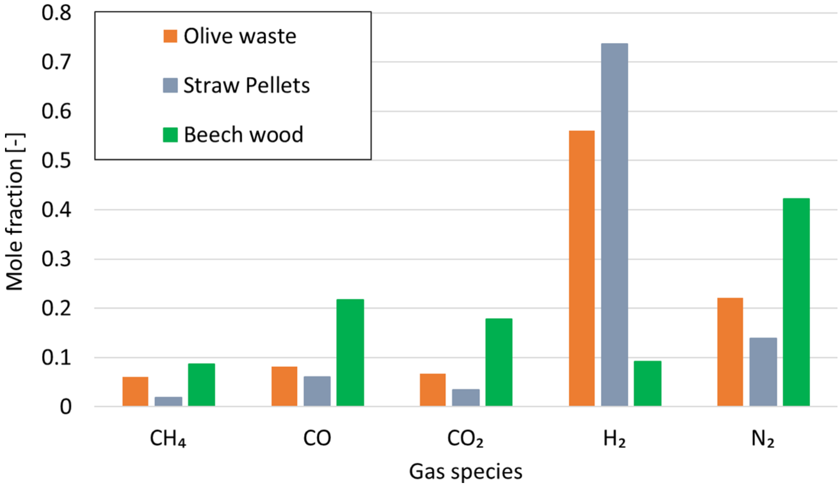

Figure 7: Product gas composition for different types of biomass.

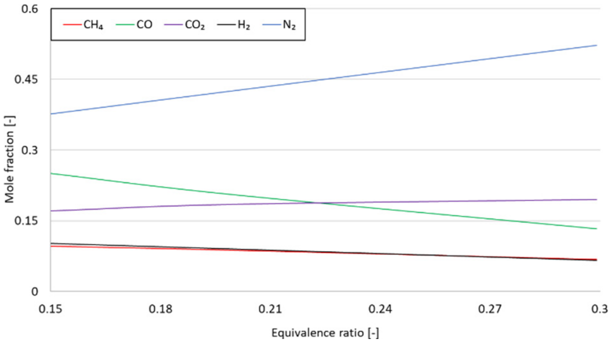

Figure 8: Product gas composition for different equivalence ratio.

The product gases were monitored during the simulation. Fig. 9 shows the composition of the product gas for birch wood over the simulation time.

The system reaches a steady state after around 15 s of simulation time. Fig. 9a shows the gas composition with respect to simulation time. The CO_2 production increased abruptly after 2 s. The high fraction of CO_2 just after the start up represents the combustion process because of the excess oxygen present inside the reactor. Production of CO, H_2 and CH_4 started gradually after 5 s of simulation time illustrates that the combustion process is gradually shifted towards gasification. The gas production rate at steady state fluctuates around its mean value because of the different physical and chemical transformations occurring inside the reactor. Fluctuations in the production of the gases are similar to the temperature fluctuations during the experiment as depicted in Fig. 4. Any industrial process is critical during the start-up and shut down process. It can be seen from Fig. 9b that the temperature rises up to 1406 K just after the start up. This indicates that a gasification reactor should be able to withstand high temperatures.

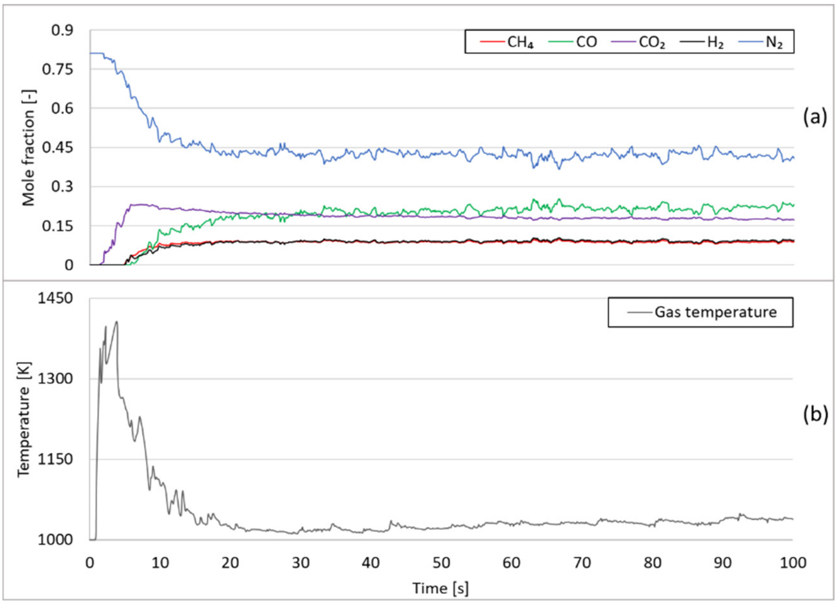

Figure 9: Product gas properties with respect to time: (a) mole fraction and (b) temperature.

The average mass production rate of the product gas was found to be 0.0013 kg/s. As the product gas was produced at a high temperature, the ideal gas law was applied to calculate the gas production rate at normal temperature and pressure conditions (25°C and 1 atm). The product gas flow rate was calculated as 1.96 Nm^3/kg of biomass. The volume production was found to be 0.144 $Nm^3/s/m^2$. The average gas compositions on the volume basis were 0.088 of CH_4, 0.207 of CO, 0.186 of CO_2, 0.091 of H_2 and 0.428 of N_2, respectively. The lower heating value of the product gas was calculated as 6.65 MJ/Nm^3.

5 CONCLUSION

Experiments were performed in a pilot-scale bubbling fluidized bed gasification reactor at the University of South-Eastern Norway. Birch wood chips were used for the experiments with air as a fluidizing agent. A model based on MP-PIC approach was developed and simulated using Barracuda®. The average gas composition from the model was validated against the experimental results. The effect of ER and biomass feed on the performance of the gasifier was studied in this work. Gas composition, gas flow rate and lower heating value of the product gas were calculated for birch wood. The product gas composition varied with change in the biomass feed. The gasification process shifts towards the combustion process with the increase of the ER. For a case with birch wood, the CO concentration decreased from 25 to 13.2 mole %, whereas the CO_2 concentration increased from 17 to 19.5 mole % when the ER increased from 0.2 to 0.3. During the start-up of the simulation, the gas temperature rises up to 1406 K implying that combustion is taken place. The process shifts gradually towards gasification with time. The gas temperature lies close to 1000 K during the steady-state operation. The simulation results give a good understanding of the air gasification of biomass in a bubbling fluidized bed gasification reactor. Along with the different experimental observation, the simulation works overcome the different issues related to biomass gasification using air as a fluidizing agent.

REFERENCES

[1] Hernández, J.J., Aranda-Almansa, G. & Bula, A., Gasification of biomass wastes in an entrained flow gasifier: Effect of the particle size and the residence time. *Fuel Processing Technology*, **91(6)**, pp. 681–692, 2010. https://doi.org/10.1016/j.fuproc.2010.01.018

[2] Haryanto, A., Fernando, S.D., Pordesimo, L.O. & Adhikari, S., Upgrading of syngas derived from biomass gasification: A thermodynamic analysis. *Biomass and bioenergy*, **33(5)**, pp. 882–889, 2009. https://doi.org/10.1016/j.biombioe.2009.01.010

[3] Bandara, J.C, Moldestad, B.M.E., & Eikeland, M.S., Analysing the effect of temperature for steam fluidized-bed gasification of biomass with MP-PIC simulation, **9**(6), pp. 529–542, 2018.

[4] Güell, B.M., Sandquist, J. & Sørum, L., Gasification of biomass to second generation biofuels: a review. *Journal of Energy Resources Technology*, **135(1)**, p. 014001, 2013. https://doi.org/10.1115/1.4007660

[5] Bridgwater, A., The technical and economic feasibility of biomass gasification for power generation. *Fuel*, **74(5)**, pp. 631–653, 1995. https://doi.org/10.1016/0016-2361(95)00001-L

[6] Agu, C.E., Pfeifer, C., Eikeland, M., Tokheim, L.A. & Moldestad, B.M., Detailed One-Dimensional Model for Steam-Biomass Gasification in a Bubbling Fluidized Bed. *Energy & Fuels*, **33(8)**, pp. 7385–7397, 2019. https://doi.org/10.1021/acs.energyfuels.9b01340

[7] Bin, C., Cong, W., Zhiwei, W., & Liejin, G., Investigation of gas-solid two-phase flow across circular cylinders with discrete vortex method. *Applied Thermal Engineering*, **29(8–9)**, pp. 1457–1466, 2009. https://doi.org/10.1016/j.applthermaleng.2008.06.025

[8] Bandara, J.C., Eikeland, M.S., & Moldestad, B.M.E., Analyzing the effects of particle density, size, size distribution and shape for minimum fluidization velocity with Eulerian-Lagrangian CFD simulation. *Proceedings of the 58th SIMS Conference*, pp. 60–65, 2017. https://doi.org/10.3384/ecp1713860

[9] Guo, X., Xiao, B., Liu, S., Hu, Z., Luo, S., & He, M., An experimental study on air gasification of biomass micron fuel (BMF) in a cyclone gasifier. *International Journal of Hydrogen Energy*, **34(3)**, pp. 1265–1269, 2009. https://doi.org/10.1016/j.ijhydene.2008.11.107

[10] Lv, P.M., Xiong, Z.H., Chang, J., Wu, C.Z., Chen, Y. & Zhu, J.X., An experimental study on biomass air–steam gasification in a fluidized bed. *Bioresource technology*, **95(1)**, pp. 95–101, 2004. https://doi.org/10.1016/j.biortech.2004.02.003

[11] Li, X.T., Grace, J.R., Lim, C.J., Watkinson, A.P., Chen, H.P. & Kim, J.R., Biomass gasification in a circulating fluidized bed. *Biomass and bioenergy*, **26(2)**, pp. 171–193, 2004. https://doi.org/10.1016/S0961-9534(03)00084-9

[12] Dupont, C., Boissonnet, G., Seiler, J.M., Gauthier, P. & Schweich, D., Study about the kinetic processes of biomass steam gasification. *Fuel*, **86(1–2)**, pp. 32–40, 2007. https://doi.org/10.1016/j.fuel.2006.06.011

[13] Watkinson, A., Lucas, J. & Lim, C., A prediction of performance of commercial coal gasifiers. *Fuel*, **70(4)**, pp. 519–527, 1991. https://doi.org/10.1016/0016-2361(91)90030-E

[14] Li, X., Grace, J.R., Watkinson, A.P., Lim, C.J. & Ergüdenler, A., Equilibrium modeling of gasification: a free energy minimization approach and its application to a circulating fluidized bed coal gasifier. *Fuel*, **80(2)**, pp. 195–207, 2001. https://doi.org/10.1016/S0016-2361(00)00074-0

[15] Yan, H.M., Heidenreich, C. & Zhang, D.K., Mathematical modelling of a bubbling fluidised-bed coal gasifier and the significance of 'net flow'. *Fuel*, **77(9–10)**, pp. 1067–1079, 1998. https://doi.org/10.1016/S0016-2361(98)00003-9

[16] Timsina, R., Moldestad, B., Eikeland, M.S. & Thapa R.K. Simulation of air-biomass gasification in a bubbling fluidized bed using CPFD model. *Proceedings of the 60th SIMS Conference,* pp. 145–150, 2020. https://doi.org/10.3384/ecp20170145

[17] Snider, D.M., Clark, S.M. & O'Rourke, P.J., Eulerian–Lagrangian method for three-dimensional thermal reacting flow with application to coal gasifiers. *Chemical engineering science*, **66(6)**, pp. 1285–1295, 2011. https://doi.org/10.1016/j.ces.2010.12.042

[18] Sreejith, C., Muraleedharan, C. & Arun, P., Air–steam gasification of biomass in fluidized bed with CO2 absorption: A kinetic model for performance prediction. *Fuel processing technology*, **130**, pp. 197–207, 2015. https://doi.org/10.1016/j.fuproc.2014.09.040

[19] Thapa, R., Pfeifer, C. & Halvorsen, B.M., Modeling of reaction kinetics in bubbling fluidized bed biomass gasification reactor. *Int. J. Energy Environment*, **5,** pp. 35–44.

[20] Bates, R.B., Ghoniem, A.F., Jablonski, W.S., Carpenter, D.L., Altantzis, C., Garg, A., Barton, J.L., Chen R. & Field, R.P., Steam-air blown bubbling fluidized bed biomass gasification (BFBBG): Multi-scale models and experimental validation. *AIChE Journal*, **63(5)**, pp. 1543–1565, 2017. https://doi.org/10.1002/aic.15666

[21] Xie, J., Zhong, W., Jin, B., Shao, Y., and Huang, Y., Eulerian–Lagrangian method for three-dimensional simulation of fluidized bed coal gasification. *Advanced Powder Technology*, **24(1)**, pp. 382–392, 2013. https://doi.org/10.1016/j.apt.2012.09.001

[22] Solli, K.-A., Thapa, R.K., and Moldestad, B.M.E., Screening of Kinetic Rate Equations for Gasification Simulation Models. *Proceedings of The 9th EUROSIM Congress on Modelling and Simulation, EUROSIM 2016, The 57th SIMS Conference on Simulation and Modelling SIMS 2016*, **142**, pp. 105–112, 2018. https://doi.org/10.3384/ecp17142105

[23] Svoboda, K., Pohořelý, M., Hartman, M., & Martinec, J., Pretreatment and feeding of biomass for pressurized entrained flow gasification. *Fuel processing technology*, **90(5)**, pp. 629–635, 2009. https://doi.org/10.1016/j.fuproc.2008.12.005

Paper IV

Aspen Plus simulation of biomass gasification for different types of biomass

Ramesh Timsina, Rajan K. Thapa and Marianne S. Eikeland

DOI: doi.org/10.3384/ecp20170151

Published in the Linköping Electronic Conference Proceedings, SIMS 60, 151-157.

ISSN: 1650-3686 (print), 1650-3740 (online)

Short overview

The paper presents a simulation study of the biomass gasification process using a thermodynamic equilibrium model in Aspen Plus. Reaction kinetics is unknown, and the products of gasification are estimated based on the minimization of Gibb’s free energy. The model was used to study the product gas composition for different feedstocks, at different temperatures and biomass feed loadings. It was presented at the 60th Conference on Simulation and Modelling (SIMS 60) held at Västerås, Sweden from 12th to 16th August 2019. The paper is published in the conference proceedings.

Aspen Plus simulation of biomass gasification for different types of biomass

Ramesh Timsina Rajan K. Thapa Marianne S. Eikeland

Department of Process Energy and Environmental Technology University of South-Eastern Norway,
{ramesh.timsina, rajan.k.thapa, marianne.eikeland}@usn.no

Abstract

A steady-state Aspen Plus model was developed for biomass gasification in a fluidized bed reactor. A combination of different Aspen Plus unit operations was used to model the gasification process. The model was used to predict the gasifier performance for different operating conditions like temperature, Steam to Biomass Ratio (STBR) and biomass loadings. Further, the gas compositions were compared for different types of biomass feed. The gasification reactor is based on Gibbs minimization with restricted equilibrium approach. Hydrogen production was around 50% for all the biomasses while CO production varies from 8% (Pig manure) to 24.5% (Olive residue) at 700°C. H_2/CO ratio increases with an increase in STBR for all the biomass and the ratio was the highest for the pig manure and lowest for the olive residue. Olive residue, wood residue and miscanthus gave the H_2/CO ratio of 1.5-2.1, which are more suitable as a feedstock in Fischer-Tropsch synthesis depending upon the operating temperature, a catalyst used and other operating conditions. For the wood residue, an increase in temperature increases the H_2 and CO production whereas CO_2 and CH_4 concentration decreases and becomes stable after 700°C. H_2 concentration increased from 46 % to 54 % and CO concentration decreases from 30% to 20% with an increase in STBR from 0.6 to 1 for the wood residue.

Keywords: Aspen plus, biomass, biomass gasification, H_2/CO ratio

1. Introduction

Due to the increasing energy demand, and the rising global temperature, research is focused towards the alternative energy sources such as wind energy, solar energy and the energy from biomass. Biomass sources such as Municipal Solid Waste (MSW), food wastes, wood wastes, rice husks, sugarcane bagasse and poultry wastes can be utilized to produce product gases (a mixture of CO, H_2 and CH_4) through biomass gasification. Biomass gasification is a thermochemical conversion of carbonaceous materials, mainly into syngas (a mixture of CO and H_2), with the application of gasifying medium such as air, steam, and oxygen.

Among the different types of biomass gasification technologies, fluidized bed gasification is an attractive technology because of the even distribution of heat and mass transfer and excellent solid mixing. The fluidized bed gasification technology uses bed material to heat up the biomass particles in the temperature range of 700-900°C (Franco *et al.*, 2003). The syngas can be converted into liquid fuels by Fischer-Tropsch (FT) synthesis, which is also known as Gas-To-Liquid (GTL) process (Riedel *et al.*, 1999). Biomass gasification also enables energy recovery from the waste. The main challenge for the successful operation of the biomass-based energy production technologies is low carbon concentration in the biomass and the low efficiency of the biomass gasification technology.

The conversion of biomass into syngas gases through gasification especially depends upon the biomass characteristics. The amounts of the fixed carbon, volatiles, moisture, ash and the calorific value determines the output product gas composition (McKendry, 2002).

The biomass is dried and devolatilized during the gasification process. Devolatilization is an endothermic process where the hot bed material supplies the required amount of heat. For simplicity, the process of devolatilization can be modelled using 1.

$$C_xH_yO_z = aCH_4 + bCO + dCO_2 + eH_2 + fC_xH_y + gC + hH_2O \quad (1)$$

The amount of ash and the other minor components produced during the gasification process can be neglected. The conversion of biomass depends upon the pressure, temperature and heat and mass transfer. The next step is the char gasification. Char reacts with fluidizing agents, as well as CO_2 and H_2 produced during the devolatilization of the biomass. Char reactivity and its amounts affect the product gas compositions (Thapa and Halvorsen, 2014).

Figure 1 shows the potential reaction pathways for the biomass gasification process. Biomass undergoes pyrolysis to produces gases (such as CO, H_2, CH_4, and H_2O), liquids (tar, oil), phenols, acids and the solid char. The char reacts with the gasifying medium, which further reacts with the gases produced during the pyrolysis process to give the product gas.

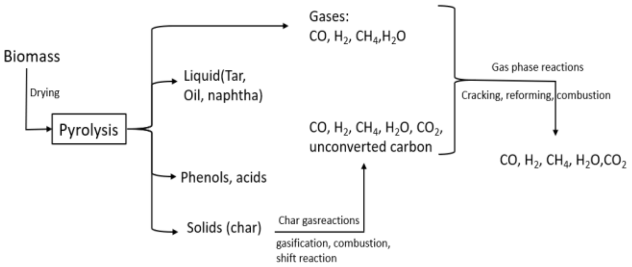

Figure 1. Potential reaction pathways for gasification

1.1 1.1 Previous works

Gagliano et al. have developed an equilibrium-based model in Aspen Plus for predicting the chemical composition of product gas for different types of biomass with different moisture contents. There is a good agreement of the gas compositions between simulation results and the experimental results for pellets and rubber wood (Gagliano *et al.*, 2017).

Doherty et al. have developed a model which represents an industrial scale plant in Gussing Austria. The model is based on restricted equilibrium in RGibbs reactor and simulations were performed for various gasification temperature, moisture content of biomass, STBR, air-fuel ratio, air temperature and steam temperature. The simulation results for syngas compositions, cold gas efficiency and heating values agree well with the experimental data (Doherty *et al.*, 2013).

Nikoo and Mahinpey simulated biomass gasification in a fluidized bed reactor. The model was validated with the experimental results from the lab-scale fluidized bed reactor. Effects of the different parameters such as temperature, equivalence ratio, STBR and biomass particle size were studied during their simulations (Nikoo and Mahinpey, 2008).

Liu et al. studied the simulation of biomass gasification based on the Gibbs equilibrium. The validated model was used to study the effects of gasification temperature, pressure and equivalence ratio. The optimal equivalence ratio was approximately 0.3 with optimal gasification efficiency of 85.92% (Liu *et al.*, 2016).

Suwatthikul et al. have carried out the sensitivity analysis for gasification temperature, equivalence ratio and the STBR. A validated Aspen plus model gave an optimal operating temperature of 911°C, equivalence ratio of 0.18 and STBR of 1.78 to achieve energy self-sufficient conditions for steam gasification in a fluidized bed reactor. Suwatthikul et al. achieved a maximum carbon conversion efficiency of 91.03% (Suwatthikul *et al.*, 2017).

Product gases from the gasification process have to be cleaned further and adjusted accordingly for suitable application to the GTL process. Fuels from GTL process have low emissions of CO, nitrogen oxides, hydrocarbons and particulate matters. The Fischer Tropsch synthesis can be considered as hydrogenation of CO to produce higher hydrocarbons compounds known as synthetic fuels (Kim *et al.*, 2009). For the industrial application of syngas in Fischer-Tropsch synthesis, it is desired to have hydrogen to carbon monoxide ratio (H_2/CO) of 1.5 - 2.1 (Tristantini *et al.*, 2007).

Modelling and simulation of biomass gasification give a good understanding of the process, designing and optimization for a wide range of design configuration and operational parameters. The developed models can be used to study the biomass gasification process. Aspen Plus® is a commercial software package to simulate an industrial process. Although there is not included inbuilt library model to simulate fluidized bed biomass gasification in Aspen Plus, different unit operations

Table 1. Ultimate and Proximate analysis of different biomass feedstock

Feedstocks	*Moisture*	*Proximate analysis (wt. %, dry)*			*Ultimate analysis (wt. %, dry)*					
		FC	*VM*	*Ash*	*C*	*H*	*O*	*N*	*S*	*Cl*
Wood chips (Doherty *et al.*, 2013)	20	18.84	80	1.16	51.19	6.08	41.3	0.2	0.02	0.05
Wood residue (Fremaux *et al.*, 2015)	5.01	17.83	81.81	0.36	50.26	6.72	42.66	0.16	0.2	0
Pig manure (Xiao *et al.*, 2010)	21.61	16.07	65.78	18.15	36.45	4.89	37.89	4.52	0.88	0
Miscanthus (Kok and Özgür 2013)	2	16.33	82.14	1.53	45.52	5.93	48.32	0.13	0.1	0
Olive residue (Masiá *et al.*, 2007)	10.63	25.48	67.35	7.17	54.18	5.37	31.7	1.28	0.21	0.13
Food waste(Begum *et al.*, 2013)	29.3	20.69	72.4	6.91	56.65	8.76	23.54	3.95	0.19	0

were combined to represent the biomass gasification as close as possible. This paper presents the simulation for different types of biomass presented in Table 1.

2. Modeling of biomass gasification

A model for bubbling fluidized bed biomass gasification with steam as a fluidizing agent is developed in Aspen Plus®. The model predicts the performance of a fluidized bed gasifier for the different types of biomass. The gasification process is dissociated into different representative units modelled by the different blocks in Aspen Plus. These models offer a convenient way to give information about the gasifier in a short time. These models are either based on kinetics rates or the state of thermodynamic equilibrium in a Gibbs reactor. The developed model is based on the restricted equilibrium in a Gibbs reactor model. Aspen plus flowsheet of the reactor is presented in Figure 2.

The flowsheet was developed from the available unit operation blocks, material streams and the energy stream. Different conventional components were chosen from the database along with two non-conventional components for the biomass and the ash modeling. Non-conventional components were defined according to the ultimate and proximate analysis for the biomass. Table 1 gives the ultimate and proximate analysis of the different biomass feedstocks.

The process consists of different stages such as biomass decomposition (DECOMP), pyrolysis (PYRO), gasification (GASIFIER), combustion (COMB) and different separation units (cyclone and separator). MIXNCPSD stream class was used as both conventional and non-conventional solids were present in the model with particle size distribution. Peng-Robinson equation of state with Boston-Mathias (PR-BM) alpha function was used to calculate the thermodynamic properties. Applications of PR-BM includes refineries, gas-processing, and petrochemical applications like crude oil conversion and gas plants. All the inputs to the feed (flow rate, composition, thermodynamic state) and the unit operation block (thermodynamic conditions, chemical reaction etc) were taken from the experimental study performed by Fremaux et. al. (Fremaux *et al.*, 2015). The assumptions made during the modelling of the gasification process in Aspen Plus are as follows:

- Isothermal and Steady state process.
- The pressure drop across the block is zero.
- Tar formation is not considered.
- The system is in steady state and isothermal.
- Char contains only carbon.
- Modelling of ash is not considered

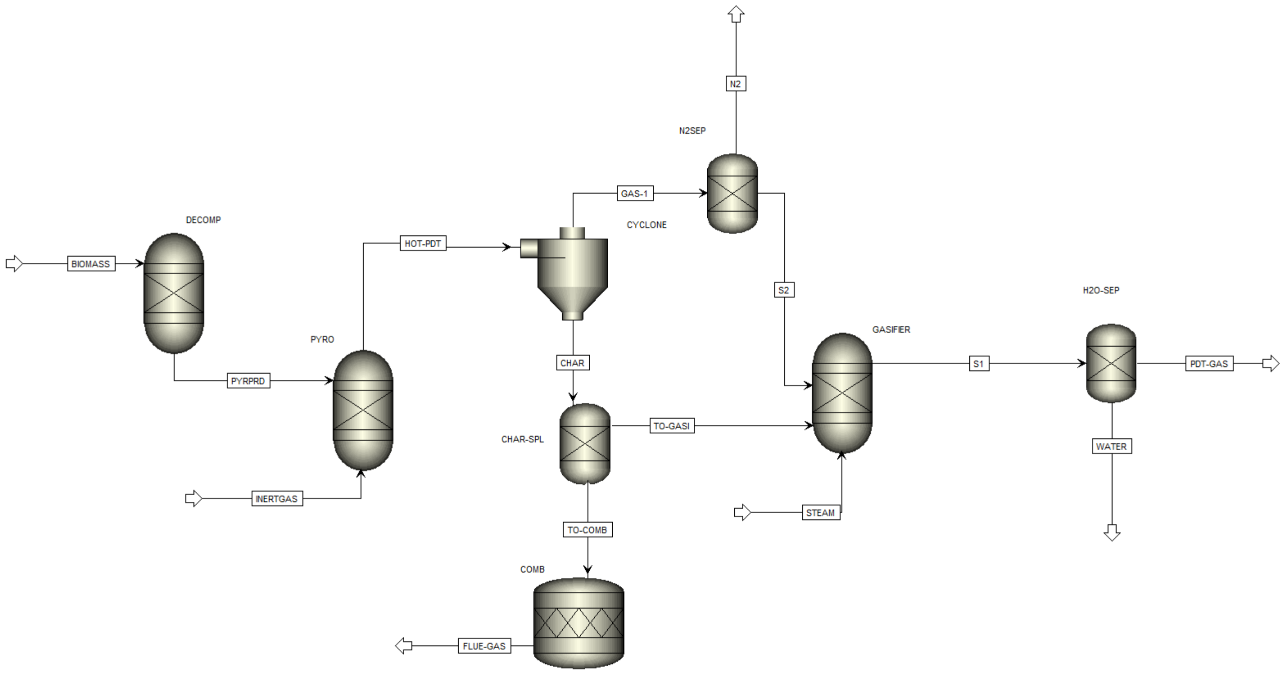

Figure 2. Aspen plus flowsheet for biomass gasification

Figure 2 shows the flow sheet in Aspen Plus. Biomass was decomposed into its constituting elements such as H_2O, ASH, C, H, N, Cl, S, O based on the ultimate analysis. A calculator module was used to calculate the yield components of the biomass feed in the DECOMP reactor. The decomposed biomass product enters a yield reactor, simulated as a pyrolysis step in gasification. The PYRO reactor was set to operate at 500°C and the inert gas (N_2) was used to assist the pyrolysis step (Visconti *et al.*, 2015). The products from the pyrolysis were separated by using a cyclone. The char produced after the pyrolysis was taken into another yield reactor (GASIFIER), simulated as a gasification reactor.

Around 5% of the char was combusted in RStoic reactor. The generated energy can be used as a supplement heat for the gasifier. In addition to char, gaseous product (nitrogen-free) from the pyrolysis process and the steam is added into the gasifier.

The calculation in the RGibbs gasifier was based on the restricted equilibrium with zero temperature approach for each of the reaction. The zero-approach option in RGibbs calculates the chemical equilibrium constant for the specified reaction at the reactor operating temperature. The equilibrium state of the reactor is also dependent upon the load per area of the reactor. Low load gives the state close to the equilibrium whereas higher load gives the non-equilibrium state within the reactor. High load is preferred to achieve a high conversion rate and low equipment costs. The overview of the temperature and the pressure in the different reactors is presented in Table 2.

Table 2. Thermodynamic state of different reactor

Reactor	*Thermodynamic state*	
	Temperature (°C)	*Pressure (bar)*
DECOMP	500	1
PYRO	500	1
COMB	800	1
GASIFIER	700	1

Table 3 shows the lists of chemical reactions specified during this simulation study with their change in Gibbs energies respectively.

Table 3. Reactions involved in gasification (Suwatthikul *et al.*, 2017)

Reactions		ΔH (kJ/mol)
$C + O_2 \rightarrow CO_2$	(2)	-394
$C + 0.5O_2 \rightarrow CO$	(3)	-111
$CO + 0.5O_2 \rightarrow CO_2$	(4)	-283
$C + CO_2 \rightarrow 2CO$	(5)	+172
$C + H_2O \rightarrow CO + H_2$	(6)	+131
$C + 2H_2 \rightarrow CH_4$	(7)	-74.8
$CO + H_2O \rightarrow H_2 + CO_2$	(8)	-41.2
$CO + 3H_2 \rightarrow CH_4 + H_2O$	(9)	-206
$H_2 + S \rightarrow H_2S$	(10)	-20.2
$N_2 + 2H_2 \rightarrow NH_3$	(11)	-92.2
$H_2 + Cl_2 \rightarrow 2HCl$	(12)	-184.6

The product from the gasifier undergoes water separation to give the output product composition on a dry volume basis.

3. Results and Discussions

Simulation results of the wood residue feedstock were compared with the experimental results published by Fremaux et al. Figure 3 shows the composition of the different gases. Hydrogen and carbon dioxide production increases with an increase in Steam to Biomass Ratio (STBR) while the carbon monoxide production decreases with increase in STBR. Methane concentration is almost constant for the given range of STBR.

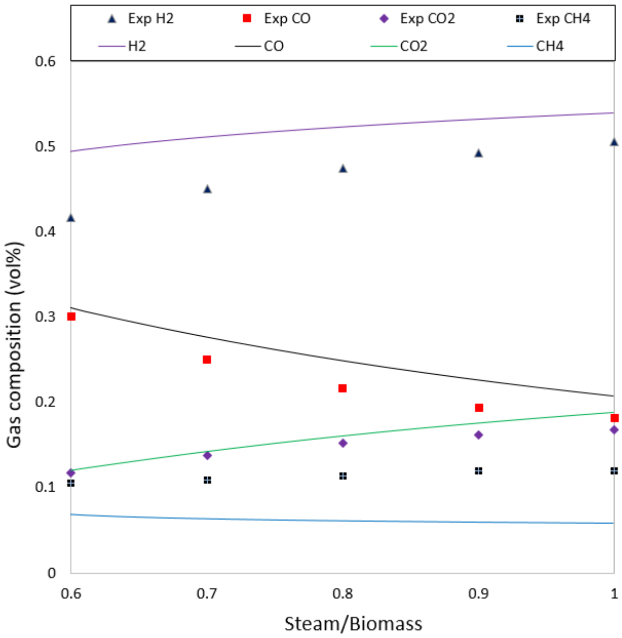

Figure 3. Gas composition for wood residue

The model predicts well the fraction of the different gas components, and there is a good agreement between experimental and computational results regarding carbon monoxide and carbon dioxide concentration. There is little difference in the hydrogen concentration, as the model doesn't represent the true phenomenological behavior of biomass gasification during the experiments.

Figure 4 shows the composition of hydrogen, carbon monoxide, carbon dioxide and methane from the simulation for different biomass. Hydrogen composition is quite similar for all the biomass feed.

Carbon monoxide concentration for wood residue, miscanthus and olive residue is similar, whereas the lowest for the pig manure. Carbon dioxide concentration for pig manure feed is 30% whereas other feed has CO_2 concentration below 25%. The carbon and hydrogen concentration are lowest for the pig manure. The C/O ratio is approximately 1:1 for pig manure and 1.2:1 for the other biomass.

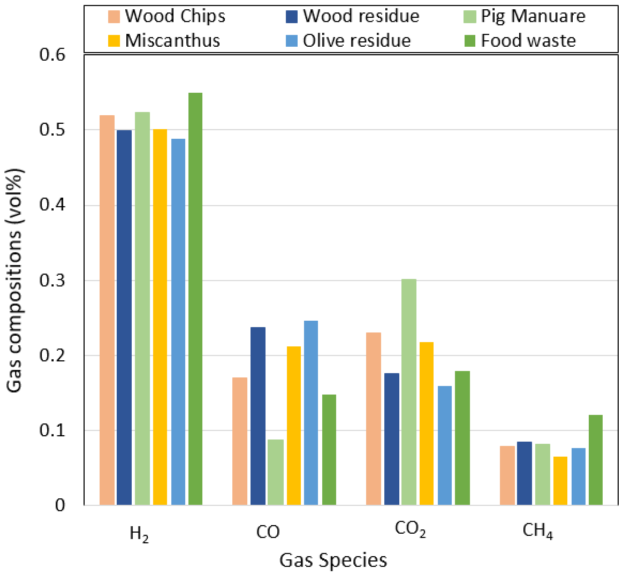

Figure 4. Gas compositions for different biomass feed (700°C)

The higher proportion of oxygen per carbon atom could be the reason for high CO_2 and low CO in pig manure. The main reason for high CO_2 and low CO is due to the high concentration of ash (18.15%) in pig manure compared to the other biomass. Methane concentration is around 8% for all the biomass except the food waste, which is around 12%.

The end use of the product gas depends upon the quality of the gas produced during gasification. One of the qualities of the product gas required for feedstock for GTL synthesis is the H_2/CO ratio. H_2/CO was calculated for all the biomass feed for different STBR. Figure 5 shows the H_2/CO ratio for STBR in the range of 0.5-1.

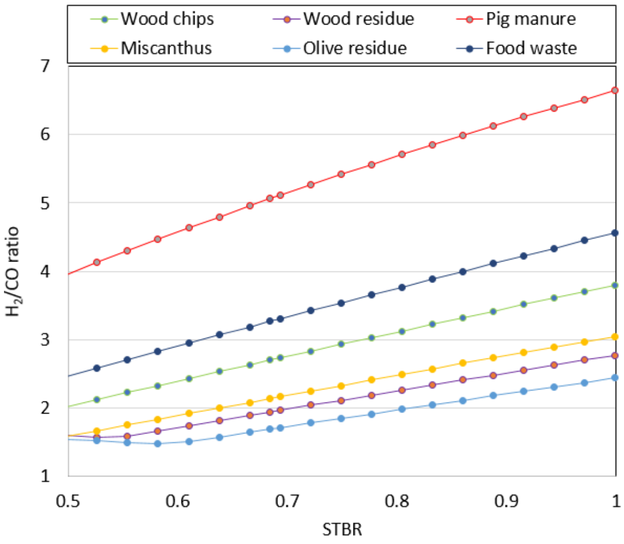

Figure 5. H_2/CO ratio for different biomass feed (700°C)

H_2/CO ratio is highest for the pig manure because of the high amounts of moisture and higher C/O ratio compared to other biomasses. Food waste also has a higher H_2/CO ratio because of its high moisture content. According to Tristantini et al., the optimal H_2/CO ratio is 1.5-2.1. This is achievable from the olive residue, wood residue, miscanthus in the STBR range of 0.5 to around 0.75. Syngas from wood chips is more suitable in FT synthesis at lower STBR. FT synthesis not only depends on the H_2/CO ratio, but also temperature, catalyst used and the system. Thus, the suitable H_2/CO ratio can be chosen depending upon the plant requirements.

The quality of syngas produced depends upon the reactor temperature. Figure 6 shows the variations of the product gas compositions at different temperatures.

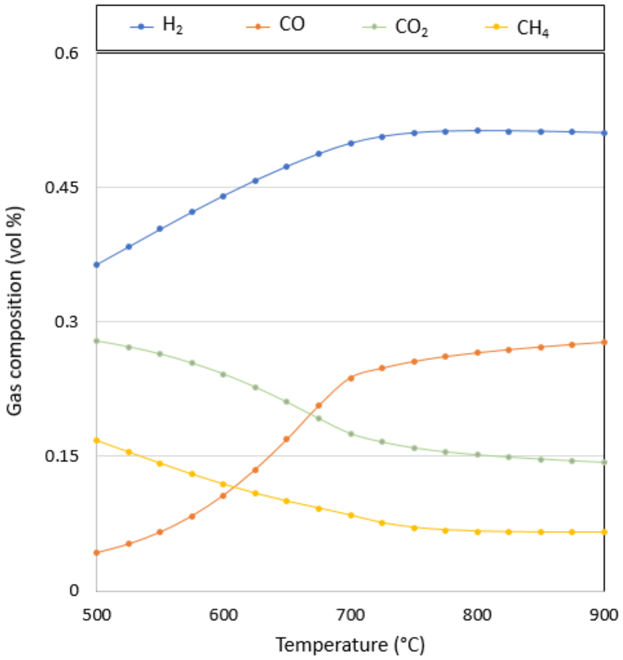

Figure 6. Gas composition for wood residue (STBR = 0.6)

Hydrogen and carbon monoxide concentration increases initially and stabilizes after 700°C. Carbon dioxide and methane concentration decrease with increase in temperature and becomes steady after around 700°C. H_2/CO ratio also becomes steady at around 1.8 after 700°C., The gas compositions were analyzed for different biomass feed. Figure 7 shows the product gas compositions for different biomass loadings.

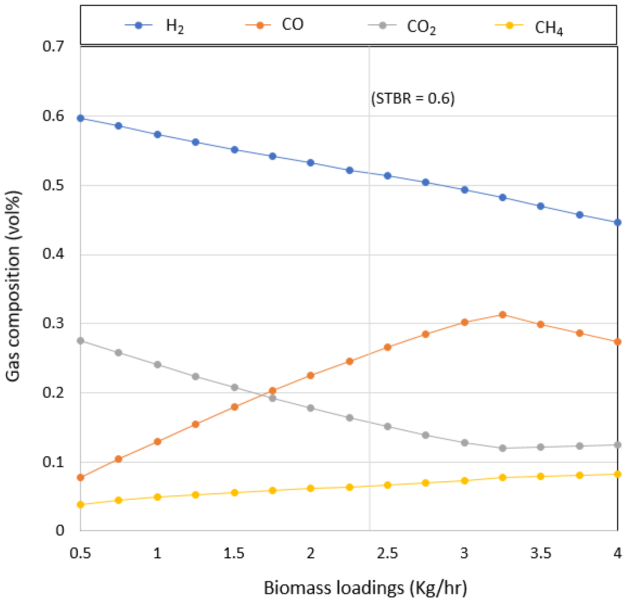

Figure 7. Gas composition for wood residue (700°C)

Hydrogen concentration decreases with an increase in biomass feed whereas CO concentration increases for biomass feed up to 3.25 kg/hr. CO_2 concentration decreases and then becomes stable after biomass loading of 3.25 kg/hr. Methane concentration remains similar for all the feed rate. Increase in biomass feed favors the forward reactions (2)-(7). Further, CO_2 produced during the reactions (2) and (4) reacts with carbon from the biomass to produce CO and the carbon partial oxidation produces CO. Thus, CO concentration increases with increase in biomass feed. The H_2 produced from the reaction (6) and (8) reacts with carbon (7) to produces CH_4. Hence, there is a decrease in H_2 concentration with an increase in biomass feed rate.

4. Conclusions

A steady-state Aspen Plus model was developed for biomass gasification in a fluidized bed. Simulations results were validated against the experimental data for a research scale fluidized-bed reactor. The model was used to predict the gasifier performance for different operating conditions and parameters like temperature, STBR and biomass loadings. The gas compositions were compared for different biomass feed. Hydrogen production was around 50% for all the biomasses while CO production varies from 8% (Pig manure) to 24.5% (Olive residue) at 700°C. H_2/CO ratio increases with an increase in STBR for all the biomass and H_2/CO ratio was highest for pig manure and lowest for olive residue. Olive residue, wood residue and miscanthus gave the H_2/CO ratio of 1.5-2.1, which are more suitable as a feedstock in Fischer-Tropsch synthesis depending upon the operating temperature, a catalyst used and other operating conditions. For wood residue, an increase in temperature increases the H_2 and CO production, whereas CO_2 and CH_4 concentration decreases and becomes stable after 700°C. H_2 concentration increased from 46 % to 54 % and CO concentration decreases from 30% to 20% with an increase in STBR from 0.6 to 1 for wood residue. The experimental results may vary from the simulation modeling, as the decomposition of biomass feed doesn’t represent the true phenomenological behavior during the gasification process. Suitable syngas composition for GTL synthesis can be obtained by selecting suitable biomass at desirable operating conditions of the gasifier.

Acknowledgements

The authors would like to thank the University of South-Eastern Norway (USN) for providing the necessary software for the simulation works.

Abbreviations

∇H - Enthalpy change
C - Carbon
H/H_2 - Hydrogen
FC - Fixed Carbon
VM - Volatile Matter
N -Nitrogen
Cl - Chlorine
GTL – Gas-to-Liquid
MSW - Municipal Solid Waste
STBR - Steam to Biomass Ratio
$C_xH_yO_z$ - Biomass elemental composition
C_xH_y - Higher hydrocarbons (C_2+)

CO - Carbon monoxide
O - Oxygen
CO_2 - Carbon dioxide
CH_4 - Methane
H_2O - Steam (water)
S - Sulphur
kg/hr- Kilogram per hour

References

S. Begum, M. G. Rasul, D. Akbar, and N. Ramzan. Performance analysis of an integrated fixed bed gasifier model for different biomass feedstocks. *Energies*, 6(12): 6508-6524, 2013. doi:10.3390/en6126508

W. Doherty, A. Reynolds, and D. Kennedy. Aspen plus simulation of biomass gasification in a steam blown dual fluidised bed. 2013.

C. Franco, F. Pinto, I. Gulyurtlu, and I. Cabrita. The study of reactions influencing the biomass steam gasification process. *Fuel*, 82(7): 835-842, 2003. doi:10.1016/S0016-2361(02)00313-7

S. Fremaux, S. M. Beheshti, H. Ghassemi, and R. S. Markadeh. An experimental study on hydrogen-rich gas production via steam gasification of biomass in a research-scale fluidized bed. *Energy Conversion and Management*, 91: 427-432, 2015. doi:10.1016/j.enconman.2014.12.048

A. Gagliano, F. Nocera, M. Bruno, and G. Cardillo. Development of an equilibrium-based model of gasification of biomass by Aspen Plus. Energy Proceedings, 111:1010-1019, 2017. doi:10.1016/j.egypro.2017.03.264

Y. H. Kim, K. W. Jun, H. Joo, C. Han, and I. K. Song. A simulation study on gas-to-liquid (natural gas to Fisher–Tropsch synthetic fuel) process optimization.

Chemical Engineering Journal, 155(1-2): 427-432, 2009. doi:10.1016/j.cej.2009.08.018

M. V. Kok and E. Özgür. Thermal analysis and kinetics of biomass samples. *Fuel Processing Technology*, 106: 739-743, 2013. doi:10.1016/j.fuproc.2012.10.010

L. Liu, Y. Huang and C. Liu. Prediction of rice husk gasification on fluidized bed gasifier based on ASPEN Plus. *Bioresources*, 11(1): 2744-2755, 2016.

A. T. Masiá, B. Buhre, R. P. Gupta and T. F. Wall. Characterising ash of biomass and waste. *Fuel Processing Technology*, 88(11-12): 1071-1081, 2007. doi:10.1016/j.fuproc.2007.06.011

P. McKendry. Energy production from biomass (part 1): overview of biomass. *Bioresource technology*, 83(1): 37-46, 2002. doi:10.1016/S0960-8524(01)00118-3

M. B. Nikoo and N. Mahinpey. Simulation of biomass gasification in fluidized bed reactor using ASPEN PLUS. *Biomass and Bioenergy* 32(12): 1245-1254, 2008. doi:10.1016/j.biombioe.2008.02.020

T. Riedel et al., Comparative study of Fischer–Tropsch synthesis with H2/CO and H2/CO2 syngas using Fe-and Co-based catalysts. *Applied Catalysis A: General*, 186(1-2): 201-213, 1999. doi: 10.1016/S0926-860X(99)00173-8

A. Suwatthikul, S. Limprachaya, P. Kittisupakorn and I. M. Mujtaba. Simulation of steam gasification in a fluidized bed reactor with energy self-sufficient condition. *Energies*, 10(3): 314, 2017. doi:10.3390/en10030314

R. Thapa and B. Halvorsen. Stepwise analysis of reactions and reacting flow in a dual fluidized bed gasification reactor. *Adv. Fluid Mech*, 82(12): 37-48, 2014.

D. Tristantini, S. Lögdberg, B. Gevert, Ø. Borg and A. Holmen. The effect of synthesis gas composition on the Fischer–Tropsch synthesis over Co/γ-Al2O3 and Co–Re/γ-Al2O3 catalysts. *Fuel Processing Technology*, 88(7): 643-649, 2007. doi:10.1016/j.fuproc.2007.01.012

A. Visconti, M. Miccio and D. Juchelková. An aspen plus tool for simulation of lignocellulosic biomass pyrolysis via equilibrium and ranking of the main process variables." *International Journal of Mathematical Models and Methods in Applied Sciences*, 9: 71-86, 2015.

X. Xiao et al., Catalytic steam gasification of biomass in fluidized bed at low temperature: conversion from livestock manure compost to hydrogen-rich syngas. *Biomass and Bioenergy*, 34(10): 1505-1512, 2010. doi:10.1016/j.biombioe.2010.05.001

Paper V

Simulation of entrained flow gasification reactor with Multi Phase Particle in Cell (MP-PIC) approach

Ramesh Timsina, Rajan K. Thapa, Britt M. E. Moldestad and Marianne S. Eikeland

DOI: doi.org/10.3384/ecp20176428

Published in the Linköping Electronic Conference Proceedings, SIMS 61, 428-434.

ISSN: 1650-3686 (print), 1650-3740 (online)

Short overview

The paper contains results from a developed model in Barracuda for the simulation of an EF gasifier. The model is validated against experimental gas compositions reported in the literature. The model was used to study the flow behaviour as well as the distribution of product gases and temperature inside the reactor. It was presented at the 61st Conference on Simulation and Modelling (SIMS 61) held online from 22nd to 24th September 2020. The paper is published in the conference proceedings.

Simulation of entrained flow gasification reactor with Multi Phase Particle in Cell (MP-PIC) approach

Ramesh Timsina Rajan K. Thapa Britt M. E. Moldestad Marianne S. Eikeland

Department of Process, Energy and Environmental Technology, University of South-Eastern Norway, Porsgrunn,
{ramesh.timsina, rajan.k.thapa, britt.moldestad, marianne.eikeland}@usn.no

Abstract

Entrained flow gasification is a promising technology for conversion of biomass into valuable fuels and chemicals. Residues and byproduct formed during a gasification process possess a significant challenge prior to the production of synthetic fuel (biofuel). Present work focuses on the simulation of an entrained flow gasification reactor in Barracuda, which is based on the Computational Particle Fluid Dynamics (CPFD) modelling. The model is validated against experimental gas compositions reported in the literature. The model was used to study the flow behavior as well as the distribution of product gases and temperature inside the reactor. Simulations showed zones of high and low-temperature regions suggesting different reactions zones such as a partial combustion zone near a fuel injector followed by a gasification zone. The flow behavior inside the reactor shows zones of recirculation, spreading and the fast flowing zone. Results from the product gas distributions inside a reactor supports the reason behind the zones with different temperature.

Keywords: entrained flow, biomass gasification, CPFD, MP-PIC approach

1 Introduction

World economy primarily depends upon the use of fuels, dominated by the use of fossil fuels compared to the use of renewable fuels. Fossil fuels has a share of 81% in the total energy consumption (Dudley, 2018). Due to the negative impact of the use of the fossil fuels, clean and efficient energy sources are getting prioritized in the energies and climate policies across the globe (Solorio and Jörgens, 2020). Biomass energy is a carbon-neutral fuel due to its sustainable life cycle. Besides this, low amounts of N_2 and S in biomass generates low emissions of NOx and SOx. Biomass has been one of the economic and efficient energy sources for the humankind for many years. Biomass energy covers about 14% of the global energy demands and plays an important role in replacing the fossil fuel (Bandara et al., 2018). Biomass gasification is a key technology for the conversion of biomass into syngas, a mixture of CO and H_2. The produced syngas can be used as a source for the production of bio fuels, valuable chemicals as well as for the heat and power generation.

Nearly 25% of the global emission in 2016 were generated by transport sector, out of which air- and road transportation accounts for 86% (Guo, 2020). Fossils fuels primarily drive the transport sector. Among the different alternatives, second generation biofuels via gasification and catalytic conversion is a promising technology. Integration of biofuels from biomass does not require major infrastructure modification, which makes it very relevant to conservative industries such as aviation and marine (Guo, 2020).

Due to the high content of volatile matters, thermal gasification often encounters technical challenges related to tar formation. This problem can be overcome by operating at high temperatures (> 1100°C), which promotes tar-reforming reactions (Llamas et al., 2020). Entrained flow (EF) biomass gasification reactors meet this requirements and typically operate at high temperatures (1300-1500°C) and high pressure (25-30 bar) (Molino et al., 2016).

EF gasification reactors can operate both in a slagging and non-slagging mode. Slagging mode EF biomass gasifiers are more flexible due the ability to melt the ash formed during the operation. Also, the EF gasifiers have high carbon conversion efficiency as compared to the fluidized bed gasifiers (Weiland et al., 2013).

In addition, solid fuel particles have typically very short residence time (2-3 sec) (Qin, 2012). Therefore, smaller particles of typically around a few hundred microns are needed to achieve good heat transfer and mixing (Guo, 2020). Pre-treatment of biomass particles to achieve particle size of a few hundred microns of feedstocks requires a high amounts of energy. Also, the less reactive products, i.e. soot and char, formed during the devolatilization steps limits the complete conversion of fuel. Therefore, it is crucial to model EF reactors accurately to the increase the overall efficiency.

Figure 1 depicts the different processes occurring inside a gasifier. The main chemical reactions for the biomass gasification process are listed below (R1-R7). Heat is supplied to the reactor during the primary pyrolysis/devolatilization, which gives the volatiles and char. Volatiles consists of non-condensable gases such as CO, CO_2, CH_4, H_2 and condensable tar.

DOI: 10.3384/ecp20176428

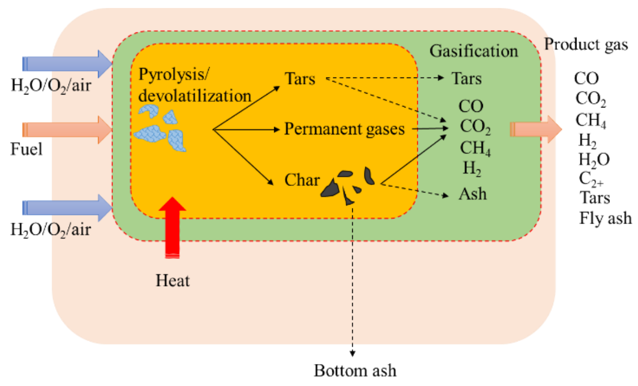

Figure 1. Process occurring in a gasifier: pyrolysis/devolatilization of fuel and gasification/reformation of the resulting gases and char

After initial decomposition, a variety of gas-solid and gas-gas reactions take place. Tars formed during the EF gasification cracks into light hydrocarbons such as CH_4, C_{2+}. Liu et al. have demonstrated that the reaction rate of char gasification is relatively high at a temperature range of 1273-1673K (Liu et al., 2006).

The hydrodynamics and the reactions are quite complex, which limits the optimization of a gasifier performance. It is difficult to study the hydrodynamics and reactions from the experimental tests. Simulation using computational fluid dynamics is becoming an important tool to study these parameters. During this study, a CPFD model is developed for the Pressurized Entrained Flow Biomass Gasification plant (PEBG) operated by Weiland et al. (2013).

1.1 Previous works

Wu et al. (2010) have studied EF coal slurry gasifiers. A three-dimensional numerical model based on the probability density function was developed and the simulation results agree well with the industrial data. Chen et al. (2012) have developed a numerical methods for the prediction of the coal gasification in an EF gasifier. The model particularly focused on the influence of the injection pattern and provide an accurate prediction for syngas formation. Abani and Ghoniem (2013) have developed a model for coal-fed EF gasifiers using large-eddy simulations and Reynolds-averaged Navier Stokes models. The model shows that the unsteady mixing is critical for the estimation of the product gas and carbon conversion. Kumar and Ghoniem (2013) have developed a multiscale model for EF gasifiers to investigate the effects of particle grinding size on carbon conversion. Fine grinding accelerated the char conversion under diffusion-control conditions, whereas there is not noticeable effects under kinetic-control operation.

Due to the complexity of the EF gasification reaction and the limitation of the computational power, the above mentioned model were often simplified to two dimensional or semi three dimensional. Most of the simulations were based on the steady state simulations. There were also limited information about the particle temperatures, carbon content and locations for the discrete particles (Liang et al., 2020).

Liang et al. (2020) have developed a CPFD simulation model for an EF gasification reactor. The detailed particle information and residence time were studied. The rapid expansion from a tracer injector and fast reactions plays an important role in forming the particle distribution zone in the gasifiers.

Thus, further understanding of the reactor hydrodynamics and the transient behavior of the reactor is crucial. This paper will gives information about the transient behavior and the reactor hydrodynamics.

2 Numerical model

There are two distinct approaches in modelling of gas-solid flows in an EF reactor: Eulerian-Eulerian (EE) and Eulerian-Lagrangian (EL) approach. EE modelling defines the gas and solid phases as continuous phases (interpenetrating continua). It lacks the detailed transient information of the two-phase interactions and does not accounts the particle size distribution of the slid phase. The EL approach models the solid phase as discrete elements and the motion of the individual particles is tracked by using Newton's law of motion. The fluid-particle, particle-particle, and particle-wall interaction as well as the particle size distribution is taken into account (Thapa et al., 2014). Thus, EL modelling requires a high computer power to calculate these interactions.

Multi-Phase Particle-In-Cell (MP-PIC) modelling was developed by considering a computational particle as a group of particles (called parcels) with the same size, density, residence time, velocity etc. Parcels are modelled in the discrete frame and the particle interaction are modelled in the Eulerian frame. Fluid particles are solved with an Eulerian set of equations. This reduces the computational costs for discrete modelling of the solid particles.

The main governing equations for CPFD simulations are based on MP-PIC approach and are described by Snider et al. (Snider, 2001; Snider and Banerjee, 2010).

Biomass undergoes devolatilization after the introduction into the reactor. Biomass is then decomposed into char particles and gases at the reactor temperature in the absence of oxygen. Equation 1 defines the global reaction for the devolatilization process (Authier and Lédé, 2013).

$$Wood \xrightarrow{heat} H_2, CO, CO_2, CH_4, chars(s), tars \qquad (1)$$

The minor elements such as sulphur and nitrogen are neglected and all the tar formed during the process converts into CO, CO_2 and CH_4. The heavier hydrocarbons such as C_2H_2, C_2H_4 were neglected to make the model as simple as possible. The devolatilization rate is defined as (Wu et al., 2010):

$$\frac{dm_p}{dt} = -A_v \, \mathrm{T} \exp\left(\frac{E_v}{T}\right)(m_p - m_{c,a}) \qquad (2)$$

Where, m_p is the particle mass and $m_{c,a}$ is the mass of char and ash in the particle. The activation energy (E_v) and the pre-exponential factor (A_v) are 3945.15 K^{-1} and 2.1×10^5 s^{-1}respectively (Wu et al., 2010).

Char and ash are the main components of the particles after the devolatilization process. Char reacts with the gases present inside the reactor (heterogeneous reactions). The main reaction involving char gasification are as follows:

$$2C + O_2 \rightarrow 2CO \qquad (R1)$$

$$C + CO_2 \rightarrow 2CO \qquad (R2)$$

The reaction rate for the heterogeneous reactions is determined by the intrinsic reaction rate and the diffusion rate. The expression for the intrinsic reaction rate and the diffusion rate can be found in the study of Wu et al. (2010). Further, char reactivity plays an important role in determining the reaction rate of these equations. The reactivity of char is given by:

$$r_m = -\frac{1}{m_c}\frac{dm_c}{dt} = \frac{1}{(1-x_c)}\frac{dx_c}{dt} \qquad (3)$$

Where m_c and x_c are the mass of carbon contained in the sample and its conversion rate at time t (Gómez-Barea and Leckner, 2010).

A series of homogeneous reaction occurs inside the reactor. Five major global reaction were considered for this study.

$$CO + 0.5O_2 \rightarrow CO_2 \qquad (R3)$$

$$H_2 + 0.5O_2 \rightarrow H_2O \qquad (R4)$$

$$CH_4 + 1.5\,O_2 \rightarrow CO + 2H_2O \qquad (R5)$$

$$CO + H_2O \rightarrow CO_2 + H_2 \qquad (R6)$$

$$CH_4 + H_2O \rightarrow CO + 3H_2 \qquad (R7)$$

The reaction rates for these reactions are listed in Table 1.

Table 1. Reaction rate kinetics (Timsina et al., 2020)

Reactions	*Reaction rate (mol.m^{-3}.s^{-1})*
R1	$4.34\times10^7 m_s \mathrm{T}\exp\left(\frac{-13590}{\mathrm{T}}\right)[O_2]$
R2	$1.12\times10^8 m_s P^{0.31}\theta_f \exp\left(\frac{-29518}{\mathrm{T}}\right)[CO_4]$
R3	$5.62\times10^{12}\exp\left(\frac{-16000}{\mathrm{T}}\right)[CO][O_2]^{0.5}$
R4	$5.69\times10^{11}\exp\left(\frac{-17610}{\mathrm{T}}\right)[H_2][O_2]^{0.5}$
R5	$5.0118\times10^{11}\exp\left(\frac{-24357}{\mathrm{T}}\right)[CH_4]^{0.7}[O_2]^{0.8}$
R6	$7.68\times10^{10}\mathrm{T}\exp\left(\frac{-36640}{\mathrm{T}}\right)[CO]^{0.5}[H_2O]$
R7	$3\times10^5\exp\left(\frac{-15042}{\mathrm{T}}\right)[CH_4][H_2O]$

The temperature for the heterogeneous reactions were taken as a weighted average with 75% particle temperature and 25% gas temperature.

Barracuda includes the model for both gas-solids and gas-wall heat transfer as well as radiation model. It also has different built-in drag models (Software, 2016).

3 Computational model

The EF reactor simulated in this work is the same reactor constructed and operated by Weiland et al. (2013). The reactor diameter is 0.52m and the height is 1.67m as shown in Figure 2.

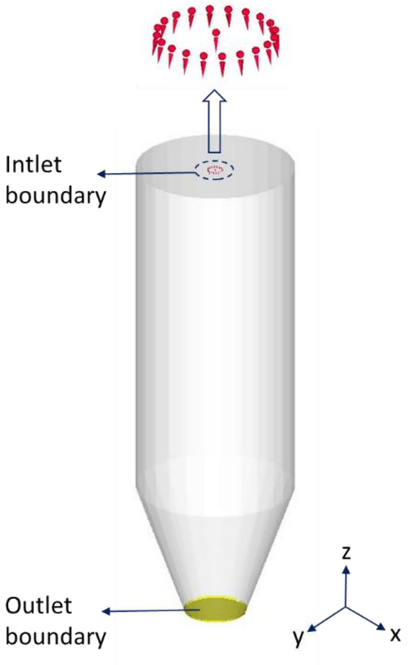

Figure 2. Schematic diagram of the CPFD model and its boundary conditions

A simulation model was developed in the Barracuda VR software. The reactor was modelled as an open cylinder with a conical shaped outlet at the bottom. The Wen-Yu-Ergun drag model was used for this work. A burner was modelled as an injector at the top center of the reactor. Other sets of injectors (20) were place concentrically outside of the fuel entrance burner. Oxygen required for gasification was supplied through these injector boundary parameters. The operating conditions of the reactor are shown in Table 2. Table 3 gives the properties of the biomass used during their study.

A total of 87300 real cells were generated using the inbuilt mesh generator available in Barracuda. In the CPFD simulations, the number of computational particles is controlled by a parameter called the number density (Software, 2016). Number density was set to 125000 to achieve a smoother and healthier particle feed for the system. This gives the particle to cell ratio of about 10:1.

Table 2. Experimental test conditions performed by Weiland et al. (2013)

Particle size, µm	100
Fuel feeding rate, kg/h	40
Total N_2 inlet, kg/h	14.4
O_2 inlet, kg/h	26.6
O_2 equivalence ratio	0.44
System pressure, bar	1.94

Injection boundary conditions were used to define the inflow of fuel and gasifying agents along with nitrogen into the reactor. Accuracy of the injection boundary is not affected by the mesh sizes of the geometry. The angle of expansion of the injection boundary was set to 20° but it is significantly dependent upon the gas behavior inside the reactor. A pressure boundary was defined at the bottom of the reactor to allow the outflow of the gas and the solid particles.

Table 3. Properties of the soft stem wood used by Weiland et al. (2013)

Proximate analysis (wt. %, dry)	
Fixed carbon	15.1
Volatile matter	84.5
Ash	0.4
Ultimate analysis (wt. %, dry)	
C	50.90
H	6.30
O	42.4
N	0.10
S	0.006
Cl	0.02

4 Results

The developed model was simulated for 50 seconds. The average gas composition were taken as the time average over final 20 seconds of simulations. The obtained results were compared with the results from an experiment performed by Weiland et al. (2013)[1].

The average molar composition of the produced gas on nitrogen free dry basis is 0.457 of CO, 0.275 of H_2, 0.226 of CO_2 and 0.038 of CH_4. Table 4 shows that the simulation results agree well with the experimental results. The mole percentage of CH_4 in the experiment also includes the mole percentage of C_2H_2 (0.3) and C_2H_4 (0.1).

Table 4. Comparison between the simulation and experimental results (mole percentage on nitrogen free dry basis)

	Product gas species			
	CH_4	CO	CO_2	H_2
Simulation	3.8	45.7	22.6	27.5
Experiment	2.7	48.5	21.1	27.8

As the EF gasification reactors operate at a high temperature, it was desired to monitor the reactor temperature. The gas temperature distribution inside the reactor is presented in Figure 3.

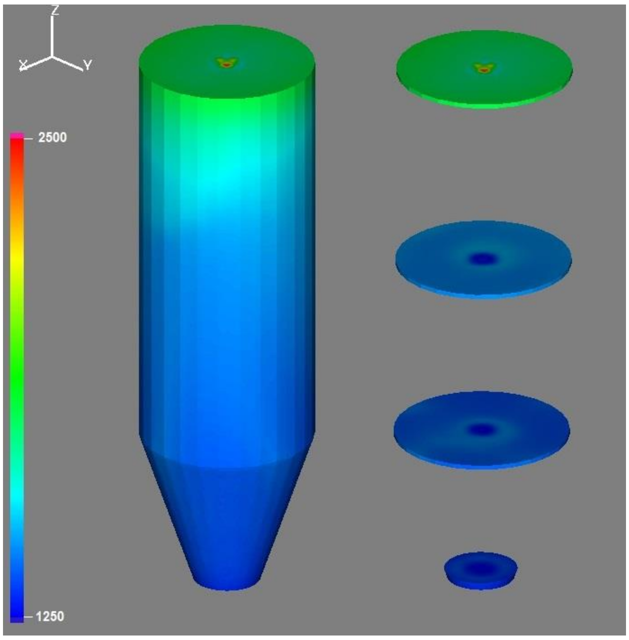

Figure 3. Gas temperature (K) distribution inside the reactor

It can be seen from Figure 3 that the temperature around the fuel injector is comparatively higher than in the rest of the reactor. Often the reactor injector up to the burners are purged with nitrogen to avoid the burning of biomass before the burner (Weiland et al., 2013). The reactor temperature at different cross sections (right) shows that the temperature distribution becomes uniform with an increase in the reactor depth.

The product gas composition was monitored along the height of the reactor. Figure 4 shows the mole fractions of CO, H_2 and CO_2 along the height of the reactor. There is a high concentration of CO and H_2 along the center of the reactor. From the distribution of the CO, it can be seen that there are dead spots at the top corner of the reactor. This gives rise to the uneven distribution of the gas components and the temperature inside the reactor. The gas distribution is similar along the radial direction except for in the top region (high temperature region as can be seen from Figure 3).

---

[1] Results are taken from the experiment on 14 February.

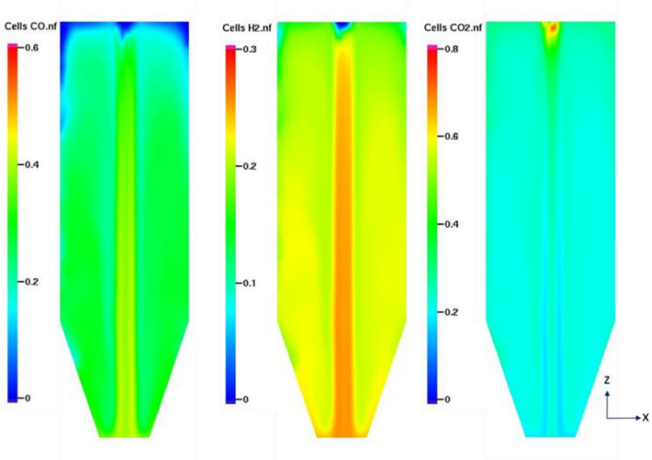

Figure 4. Gas composition along the reactor (mole fraction at t = 30 sec)

The high temperature close to the fuel burner (fuel injector) gives rise to high concentration of CO_2 and low concentration of CO and H_2. As the mixture of biomass and the pyrolysis gas move down, several chemical and physical transformation of the biomass occurs resulting in the product gas composition as shown in the Figure 4.

Therefore, it is important to know the fluid velocity and direction inside the reactor. Figure 5 shows the instantaneous fluid velocity distribution. It can be seen from the figure that recirculation of gas occurs near the wall of the reactor. The gas velocity in the central region gradually increases as it flows downward in the gasifier. The rapid gas expansion as well as recirculation is due to the expansion effects of the injection nozzles. Due to the jet velocity along the axial direction, expansion in radial direction is high compared to the axial direction. This is in agreement with the published result by Liang et al. (2020), where the reactor has three distinct flowing zones, i.e. the recirculation zone, the spreading zone and the fast flowing zone. The flow direction is random except in the middle of the reactor. This behavior has a great influence on the particle flow as well as the overall conversion efficiency of the process.

A summary of the results from the experiment can be obtained from the published article by Weiland et al. (2013). The article also compares the results from the different gasification technologies. A gasification process with higher concentration of CH_4 in the product gas is more suitable for power generation as well as for Substitute Natural Gas (SNG) production.

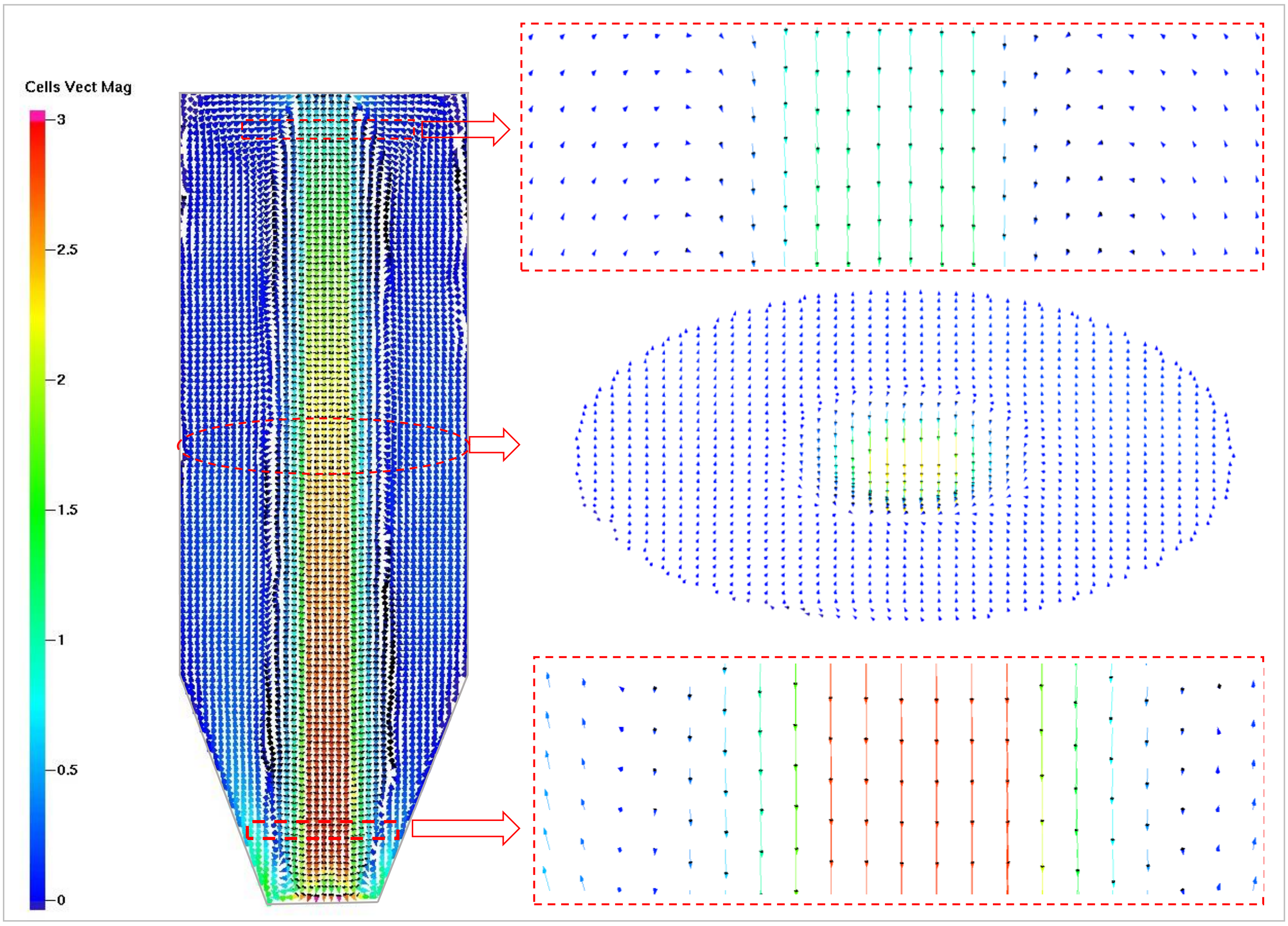

Figure 5. Gas speed distribution at t = 30 sec.

The H_2/CO ratio is an important parameter for the conversion of syngas into synthetic fuels. The ratio of H_2/CO will vary depending upon the synthesis route. For example, the low temperature Fischer-Tropsch synthesis (FT Synthesis) requires H_2/CO ratio in the range of 1.7 - 2.15 depending upon the catalyst, while the ratio is approximately 1.05 for FT synthesis at higher temperature (Weiland et al., 2013). Therefore, syngas requires shifting towards high H_2 content prior to the fuel synthesis irrespective of the gasification technology.

Higher operating temperature for the EF reactor reduces the amounts of tar and heavier hydrocarbons in the product gas compared to the other gasification technologies. This potentially reduces the cost for the extensive syngas cleaning prior to fuel synthesis. However, the gasification pressure needs to be high enough to make the conversion process economically feasible. The convective and radiative losses from the reactor also plays an important role for the thermal efficiency of the plants. Dry biomass powder was gasified during the experiments in PEBG gasifier.

However, Brown et al. (1986) have shown that the premixing of the coal with steam or coal with moisture gave high concentration of H_2, but lower CO/ CO_2 ratio decreases the carbon conversion. This could be due to the reduced gasification temperature.

Therefore, it is important to characterize (pros and cons) different alternatives before selecting a suitable conversion technology for the conversion of the biomass into biofuels via gasification. The difficulty of understanding the hydrodynamics as well as the reaction chemistry during an experiment can be studied by developing a simulation model. A CPFD model can give a detail insight of the reaction operating conditions, which in turn help a lot for the optimization and design of the EF reactor.

5 Conclusion

A CPFD simulation model was developed in Barracuda using the MP-PIC modelling approach. The model was used to simulate a pressurized entrained flow biomass gasification reactor operated by Weiland et al. (2013). The composition of the product gases obtained from the model agree well with the experimental results. The average molar composition of the produced gas on nitrogen free dry basis is 0.457 of CO, 0.275 of H_2, 0.226 of CO_2 and 0.038 of CH_4. An accurate prediction of the reactor performance is a challenging task, which is investigated in this study. A simple CFD model is presented in this work, which needs testing in different conditions and the authors believe that the model will be of use in the development and design of the entrained flow biomass reactor.

The gas expansion played a significant role for the particle speed and direction inside a reactor. Certain groups of particles in the center of the reactor has higher velocity and lower residence time. Other groups of the particles are recirculated giving a different flow direction and velocity. The CO_2 concentration is highest and the CO and H_2 concentration is lowest at the fuel injector.

Selection of suitable technology for the production of syngas prior to the synthetic fuel production depends upon different criteria such as biomass feed, desired syngas quality, capacity and costs. Entrained flow reactors are best suited for a feed with small particles at large capacity, at high temperatures and high pressures. Entrained flow reactors give cleaner syngas compared to fluidized and fixed bed reactors, which potentially reduces the cost for the extensive syngas cleaning prior to fuel synthesis.

Acknowledgements

The authors would like to thank the University of South-Eastern Norway (USN) for providing the Barracuda VR simulation tool.

Abbreviations

CPFD	Computational Particle Fluid Dynamics
EF	Entrained flow
EE	Eulerian-Eulerian
EL	Eulerian-Lagrangian
FT Synthesis	Fischer-Tropsch synthesis
MP-PIC	Multi-Phase Particle-In-Cell
PEBG	Pressurized Entrained Flow Biomass Gasification plant
SNG	Substitute Natural Gas

References

N. Abani and A. F. Ghoniem. Large eddy simulations of coal gasification in an entrained flow gasifier. *Fuel* 104: 664-680, 2013. doi.org/10.1016/j.fuel.2012.06.006.

O. Authier and J. Lédé. The image furnace for studying thermal reactions involving solids. Application to wood pyrolysis and gasification, and vapours catalytic cracking. *Fuel* 107: 555-569, 2013. doi.org/10.1016/j.fuel.2013.01.041.

J. C. Bandara, B. ME. Moldestad and M. S. Eikeland. Analysing the effect of temperature for steam fluidized-bed gasification of biomass with MP-PIC simulation. *International Journal of Energy and Environment* 9(6): 529-542, 2018.

Blaine W. Brown, L. Douglas Smoot and Paul O. Hedman. Effect of coal type on entrained gasification. *Fuel* 65(5): 673-678. 1986. doi.org/10.1016/0016-2361(86)90363-7.

C-J. Chen, H. Chen-I., and W-H. Chen. Numerical investigation on performance of coal gasification under various injection patterns in an entrained flow gasifier. *Applied energy* 100: 218-228. 2012. doi.org/10.1016/j.apenergy.2012.05.013.

B. Dudley. BP statistical review of world energy. *BP Statistical Review*, London, UK, accessed June 30 2020: 2018.

A. Gómez-Barea and B. Leckner. Modeling of biomass gasification in fluidized bed. *Progress in Energy and Combustion Science* 36(4): 444-509. 2010. doi.org/10.1016/j.pecs.2009.12.002.

N. Guo. Modelling of reacting multi-phase flow for biomass gasification. *Doctoral theses at NTNU* 1-224. 2020.

M. Kumar and A. F. Ghoniem. Application of a validated gasification model to determine the impact of coal particle grinding size on carbon conversion. *Fuel* 108: 565-577. 2013. doi.org/10.1016/j.fuel.2013.02.009.

Y. Liang, C.Y. Guo, X. Zhao, Q. Qin, Y. Cheng, and L. He. CPFD simulation on particle behaviour in an entrained-flow gasifier. *Clean Energy* 4(1): 75-84. 2020. doi.org/10.1093/ce/zkz032.

H. Liu, C. Luo, S. Kato, S. Uemiya, M. Kaneko andT. Kojima. Kinetics of CO_2/Char gasification at elevated temperatures: Part I: Experimental results. *Fuel Processing Technology* 87(9): 775-781. 2006. doi.org/10.1016/j.fuproc.2006.02.006.

Á. D. G. Llamas, N. Guo, T. Li, R. Gebart, T. Løvås, and K. Umeki. Morphology and volume fraction of biomass particles in a jet flow during devolatilization. *Fuel* 278: 118241. 2020. doi.org/10.1016/j.fuel.2020.118241.

A. Molino, S. Chianese, and D. Musmarra. Biomass gasification technology: The state of the art overview. *Journal of Energy Chemistry* 25(1): 10-25. 2016. doi.org/10.1016/j.jechem.2015.11.005.

K. Qin, A. D. Jensen, P. A. Jensen and W. Lin. Entrained Flow Gasification of Biomass. *Technical University of Denmark, Department of Chemical Engineering*. 1-224. 2012.

D. M. Snider. An incompressible three-dimensional multiphase particle-in-cell model for dense particle flows. *Journal of computational physics* 170(2): 523-549. 2001. doi.org/10.1006/jcph.2001.6747.

D. M. Snider and S. Banerjee. Heterogeneous gas chemistry in the CPFD Eulerian–Lagrangian numerical scheme (ozone decomposition). *Powder Technology* 199(1): 100-106. 2010. doi.org/10.1016/j.powtec.2009.04.023.

C. Software. Barracuda Virtual Reactor User Manual. *CPFD Software LLC*. Albuquerque. 2016

I. Solorio and H. Jörgens. Contested energy transition? Europeanization and authority turns in EU renewable energy policy. *Journal of European Integration* 42(1): 77-93. 2020. doi.org/10.1080/07036337.2019.1708342.

R. Thapa, C. Pfeifer and B. M. Halvorsen. Modeling of reaction kinetics in bubbling fluidized bed biomass gasification reactor. *Int. J. Energy Environment* 5: 35-44, 2014.

R. Timsina, R. K. Thapa, B. M. E. Moldestad and M. Eikeland. Experiments and computational particle fluid dynamics simulations of biomass gasification in an air-blown fluidized bed gasifier. *Int. J. of Energy Prod. & Mgmt.* 5(2): 102-114. 2020. doi.org/10.2495/EQ-V5-N2-102-114.

F. Weiland, H. Hedman, M. Marklund, H. Wiinikka, O. Öhrman, and R. Gebart. Pressurized oxygen blown entrained-flow gasification of wood powder. *Energy & Fuels* 27(2): 932-941. 2013. doi.org/10.1021/ef301803s.

Y. Wu, J. Zhang, P. J. Smith, H. Zhang, C. Reid, J. Lv, and G. Yue. Three-dimensional simulation for an entrained flow coal slurry gasifier. *Energy & Fuels* 24(2): 1156-1163. 2010. doi.org/10.1021/ef901085b.

Paper VI

Computational particle fluid dynamics simulation of biomass gasification in an entrained flow gasifier

Ramesh Timsina, Rajan K. Thapa, Britt M. E. Moldestad and Marianne S. Eikeland

DOI: doi.org/10.1016/j.cesx.2021.100112

Chemical Engineering Science: X, Volume 12, November 2021, 100112. ISSN: 2690-1400

Short overview

The paper contains results obtained from the developed CPFD model in Barracuda for the simulation of the PEBG plant. The model is validated against experimental gas compositions, flowrate, and reactor temperature reported in the literature. The major focus was to optimize the flow behaviour and thermochemical behaviour inside the reactor. The paper is published in Chemical Engineering Science: X.

Chemical Engineering Science: X 12 (2021) 100112

Contents lists available at ScienceDirect

Chemical Engineering Science: X

journal homepage: www.elsevier.com/locate/cesx

Computational particle fluid dynamics simulation of biomass gasification in an entrained flow gasifier

Ramesh Timsina *, Rajan K Thapa, Britt M.E. Moldestad, Marianne S. Eikeland

Department of Process, Energy and Environmental Technology, University of South-Eastern Norway, Kjølnes Ring 56, 3918 Porsgrunn, Norway

ARTICLE INFO

Article history:
Received 16 April 2021
Received in revised form 13 August 2021
Accepted 19 August 2021

Keywords:
Entrained flow
Biomass gasification
MP-PIC
CPFD
Clean energy

ABSTRACT

Entrained flow gasification is an established technology for coal and petroleum coke particles. The technology is being investigated extensively for biomass gasification to meet the requirement of the green energy targets. A three-dimensional computational particle fluid dynamics (CPFD) model is developed to simulate an Entrained Flow (EF) gasification reactor. The model is validated against experimental gas composition and process temperature reported from an experiment published in the literature. The interdependence between reactor hydrodynamics, thermal and reaction chemistry is demonstrated and described for an EF reactor. Simulations show zones of high and low temperatures suggesting different reaction zones, such as a partial combustion zone near the fuel injector followed by a gasification zone. Particles in the central region show high carbon conversion compared to the particles in the other zones. Char- O_2 and char-H_2O are significant in the gasifier entrance region, whereas the char-CO_2 reaction is prevalent throughout the reactor elevation. The optimal gasification performance (higher mole fraction of CO and H_2) is in the range of equivalence ratio 0.3 to 0.44.

© 2021 The Author(s). Published by Elsevier Ltd. This is an open access article under the CC BY license (http://creativecommons.org/licenses/by/4.0/).

1. Introduction

The world's energy consumption is ever-increasing, and the need for this energy to be environmentally friendly produced is increasingly important. Both on national and international levels, efforts are made to limit greenhouse gas emissions (IEA, 2019). For example, the European Union (EU) has set a target of 60% emission reduction to achieve carbon neutrality by 2050 (Voultsos et al., 2020). Bioenergy shared approximately 12.5% of the global energy demand in 2019, out of which 7.5 % is coming from the traditional biomass usage (Renewables 2020 - Global status report, 2020). Therefore, biomass is an important resource to replace the current consumption of fossil fuels (Bandara et al., 2018). Biomass gasification is a thermochemical conversion of carbonaceous fuels with the application of gasifying mediums such as air, steam, and oxygen. Gasification of biomass gives non-condensable gases such as carbon monoxide (CO), carbon dioxide (CO_2), hydrogen (H_2), methane (CH_4), higher molecular hydrocarbons (ethane, etc.), condensable vapors (tars) and solid residue (unconverted char and ash). Gasification and Integrated Gasification Combined Cycle (IGCC) is a promising option to improve the power generation efficiency from biomass. Lower emission of greenhouse gases, NO_X, and SO_X pollutants and low level of particulate emissions and market flexibility makes biomass gasification technology better as compared to conventional coal-fired power plants (Long et al., 2020).

Entrained Flow (EF) biomass gasifier is essentially a continuous flow reactor operated at elevated temperature (around 1400 °C) and pressure (20–70 bar) (Basu, 2018). Fuel, as well as the gasifying agent, are introduced concurrently into the reactor. Fuel particles typically have a very short residence time of 2–3 sec (Qin, 2012). Therefore, smaller particles of around a few hundred microns are needed to achieve a good heat transfer and mixing between the fuel particles and the gasifying agent (Guo, 2020). EF gasification has been an established technology for the coal and petroleum coke particles since 1950 (Duchesne, 2012), and the technology is being investigated extensively for biomass gasification to meet the requirements for reduced greenhouse gas emissions.

Several complex physical and chemical transformations occur over time and space in an EF gasifier. Particle movement and fluid flow play an important role in reactor hydrodynamics. The solid–gas flow in an EF reactor is characterized by a turbulent flow. Under ideal conditions, the residence time of the biomass particles lies within a few seconds giving a conversion efficiency as high as 99%. Reactor hydrodynamics, particle–particle collisions, char conversion, and fluid-particle mixing have a great impact on the gasification behavior of the EF gasifier. The conversion of biomass

---

* Corresponding author at: 50A, Vallermyrvegen, 3917 Porsgrunn, Norway.
E-mail addresses: ramesh.timsina@usn.no, timsinarames@gmail.com (R. Timsina).

https://doi.org/10.1016/j.cesx.2021.100112
2590-1400/© 2021 The Author(s). Published by Elsevier Ltd.
This is an open access article under the CC BY license (http://creativecommons.org/licenses/by/4.0/).

Nomenclature

Symbols	Description Unit
Δ	subgrid length [–]
A_v	pre-exponential factor [s^{-1}]
C_d	drag coefficient [–]
C_p	specific heat capacity (constant pressure) [J $K^{-1}kg^{-1}$]
C_V	specific heat capacity (constant volume) [J $K^{-1}kg^{-1}$]
C_s	Smagorinsky coefficient [–]
D_p	drag function [s^{-1}]
D_t	turbulent mass diffusivity [kg/(s.m^2)]
$\delta\dot{m}$	mass production rate [kg/s]
$\delta\dot{m}_{i,c}$	mass production rate from gas-phase reaction [kg/s]
E_v	activation energy [K^{-1}]
F	interphase momentum exchange rate per volume [N/m^3]
f	particle distribution function (PDF) [–]
g	acceleration due to gravity [m/s^2]
h	Enthalpy [J]
m	Mass [Kg]
$Nu_{g,s}$	Nusselt number [–]
P	Pressure [Pa]
Pr	Prandtl number [–]
P_s	constant [$Kgm^{-1}s^{-2}$]
$\dot{Q}$	energy source per volume [J/m^3]
$\vec{q}$	gas heat flux [J/m^3]
$\dot{q}_D$	enthalpy diffusion rate [J/m^3]
r	particle radius [m]
Re	Reynolds number [–]
S_h	conservative energy exchange [J]
Sc	Schmidt number [–]
T	Temperature [K]
t	time [s]
u	velocity [m/s]
$\vec{u}$	velocity (vector) [m/s]
v	velocity [m/s]
$Y_{g,i}$	mass fraction of each fluid species [–]

Greek letters

β	constant [–]
ε	constant [–]
ρ	density [Kg/m^3]
λ	thermal conductivity [J/(s.m.K)]
τ	stress [N^2/m^2]
μ	viscosity [kg/(m.s)]
φ	viscous dissipation [J]
α	volume fraction [–]
$k-\varepsilon$	k -epsilon [–]

Subscripts

g	gas phase
p	particle phase
i	species

depends upon the characteristics of the biomass, pressure, temperature, heat, and mass transfer inside a reactor. The characteristics of biomass include its shape and size and the amounts of fixed carbon, volatiles, moisture, ash, and calorific value. The char reactivity and the amount of char affect the product gas compositions (Bikane et al., 2020; Thapa & Halvorsen, 2014. Traditionally established monitoring systems (thermocouples, gas chromatography, etc.) are usually too slow to respond to a sudden change in process condition and could challenge the plant security (Sepman et al., 2017).

As the gasifier operates at high temperatures, the problems related to ash and tar formation during biomass gasification are minimal, giving high-quality syngas (CO, H_2). Reformation of tars into light hydrocarbons such as CH_4, C_2+, etc. occurs at a temperature above 1100 °C (Llamas et al., 2020). EF gasifiers are designed to work in slagging mode, where the variation in the ash melting point is less problematic as long as the operating temperature exceeds the slag fluid temperature. EF gasifiers have fuel flexibility because of their slagging mode operation. EF gasifiers have high carbon conversion efficiency as compared to fluidized bed gasifiers (Weiland et al., 2013).

The challenges associated with EF gasifiers are energy efficiency, heat recovery from the product gas, the durability of the systems, short residence time, fouling (slagging behavior), and installation costs. Pretreatment of the particles to a suitable size requires a significant amount of energy and costs. The suitable choice of milling techniques or fuel treatment (torrefaction or pyrolysis) can increase the total process efficiency (Weiland et al., 2013). Less reactive products such as soot and char formed during the gasification process limit the complete conversion of biomass. For an EF gasifier to be cost-competitive, especially industrial-scale applications, understanding various aspects of entrained flow gasification is imperative. Therefore, modeling and simulation of such systems have become necessary for a better understanding of the gasification process in a short time frame with a low cost.

The hydrodynamics and the reaction kinetics are quite complex in an EF reactor. Simulation using computational fluid dynamics is becoming an important tool to study these parameters. The current study focuses on the numerical simulation of the gas–solid flow with heat transfer and the chemical reactions inside an EF reactor. To achieve this goal, a CPFD model is developed for the Pressurized Entrained Flow Biomass Gasification plant (PEBG) designed, developed, and operated by Weiland et al. at the Energy Technology Centre (ETC) in Piteå, Sweden (Weiland et al., 2013). The CPFD numerical scheme incorporates the Multi Phase Particle-In-Cell (MP-PIC) modeling approach (Andrews & O'Rourke, 1996; Snider et al., 2011).

1.1. CFD modeling of EF gasifiers

Biomass gasification in an EF reactor involves different thermodynamic domains and complex reactions. Experimental optimization of the EF gasifiers is difficult and challenging (i.e., optimization of geometry, feeding positions, etc.). Therefore, simulation tools are becoming imperative and valuable tools for the study and for the process optimization towards the desired downstream applications. Computational Fluid Dynamics (CFD) models of such systems in plant scale have become practical due to the development of computer power and efficient numerical algorithms. CFD models are capable of simulating the effects of different operational parameters such as pressure, temperature, equivalence ratio, etc. (Chiesa et al., 2005; Gungor & Yildirim, 2013). The effect of different biomass feedstock, particle sizes, geometry, etc., can be evaluated with respect to the product gas compositions and LHV.

Modeling of multiphase flow systems in an EF is challenging due to the coupling of turbulent gas flow and particle motions.

Other challenges include the difficulties in modeling the momentum exchange between the phases, interparticle forces such as van der Waals forces, electrostatic forces, inter-particle collisions, and the difference in size, shape, and densities of the particles in the solid phase. In addition to these, the gasification of biomass possesses challenges related to the thermal model, devolatilization model, heterogeneous reactions, etc. (Bandara et al., 2018; Timsina et al., 2020).

The basic approaches to model gas–solid multiphase systems are the Eulerian-Eulerian (EE), and the Eulerian-Lagrangian (EL) approaches. The details of these approaches can be found in the literature (Thapa, 2015). The CPFD methodology follows the MP-PIC modeling approaches. MP-PIC approach is based on the EL approach, which introduces the concept of computational particles (parcels), where particles with similar properties such as size, density, residence time, velocity, etc., are grouped into a computational particle. Parcels are modeled in a discrete frame and the particle interactions are calculated on the Eulerian frame. The inter-particle stresses are calculated by an isotropic solid stress function and then interpolated back to the individual particles (Bandara et al., 2018). The fluid phase is solved with an Eulerian approach. The CPFD platform is developed from the MP-PIC modeling approach. The strong coupling between the fluid and the particle phases gives a high level of accuracy and fast computational time in CPFD modeling. MP-PIC employs a simple particle-'pressure' model that prevents particle from becoming closely packed and eliminates the need to track the collision of the particles directly (Mu et al., 2020; Verma & Padding, 2020). Intel(R) Core (TM) i7-8700 K CPU @ 3.70 GHz processor and Barracuda VR® 20.0.0 version were used to simulate the developed model.

The CPFD model has been successfully applied for reactors operating with a dilute flow of solid particles, where the gas–solid behavior is similar to that in an EF reactor. For example, risers of the circulating fluidized bed (Shi et al., 2015; Wang et al., 2015), downer of the circulating fluidized bed (Yingya Wu et al., 2020), downer reactor (Abbasi et al., 2013), downflow reactor (Lanza et al., 2016), cement calciners (Nakhaei et al., 2021; Nakhaei et al., 2018; Nakhaei et al., 2019) and pneumatic conveying system (Ariyaratne et al., 2017) has been modeled in CPFD platform. Besides, Liang et al. (Liang et al., 2020) have developed a CPFD model for an EF gasification reactor, and their results are discussed in Section 1.2.

The number of grid elements in a modeled geometry is important since it affects both the accuracy and the time it takes to simulate a process. A bulk flow region can be modeled with a coarse grid; however, a finer grid gives better results in areas with high gradients of temperature, pressure, concentrations, etc. The software package uses grid resolution only in Cartesian coordinates and it is possible to define a finer grid at a particular region. It is important to note that the grid generation should be performed carefully to capture every small part as it may affect the bed hydrodynamics significantly. The grid resolution was changed accordingly until the convergence of the simulation results with a reasonable simulation time was achieved. The effects of grid size on cell averaged particle properties are presented in Fig. 1. Coarse grid misrepresents the particle structure, whereas the finer grids lead to high computational costs.

1.2. Previous works

A number of studies have developed a CFD model (based on EL modeling) for EF reactors because of the wide applicability and versatility. However, most of the authors have modeled the EF reactor based on coal gasification (Abani & Ghoniem, 2013; Chen et al., 2012; Eluk et al., 2017; Kumar & Ghoniem, 2013; Yuxin Wu et al., 2010; Ye & Ryu, 2015). This section provides a brief overview of the recent previous works performed on the CFD simulation of an EF biomass gasification reactor.

The effect of reactor temperature, excess air ratio, steam/carbon ratio, gasifying medium, reactor structure, and feedstock properties are reported in (Ku et al., 2014; Ku et al., 2019). Ku et al. have shown a positive effect on both the H_2 and CO productions, increasing the reactor temperature. Increasing the excess air ratio decreased both H_2 and CO production, and increasing the steam/carbon ratio increases the H_2 production but decreases the CO production (Ku et al., 2014). The introduction of O_2 improved CO production and carbon conversion, whereas an excessive use of O_2 gave a reduced combustible gas yield and Cold Gas Efficiency (CGE). H_2 production, carbon conversion, and lower heating value rose after steam addition. Biomasses with a higher fixed carbon or volatile content and a lower moisture content gave a high combustible gas yield (Ku et al., 2019).

Gao et al. (Gao et al., 2018; Gao et al., 2016) have investigated the relative error of the developed model with the experimental results. A finite rate/eddy dissipation model was applied to calculate the reaction rates for homogeneous phase reactions and an intrinsic reaction rate model was used with user-defined functions (UDFs) to calculate char reaction rates. The relative error for LHV, gas production, CGE, and carbon conversion efficiency are within the ranges of 1–13%, 1–8%, 1–12%, and 1–11%, respectively (Gao et al., 2016). The relative errors between the simulated and experimental gasification performances were in the ranges of 9.6–23.3% (gas heating value), 1.2–5.9% (gas production), and 9.8–16.6 (carbon conversion efficiency) (Gao et al., 2018). The authors have also proposed/developed the reaction rate kinetics for char-CO_2 and char-O_2 reactions.

Guo et al. (Guo et al., 2020) have developed an EL CFD model in OpenFOAM to study particle hydrodynamics, heat transfer, and devolatilization kinetics. A total of four different approaches were tested for the quantitative comparison analyses. The spheroidal particle shape assumption with adjusted spheroidal surface area and the Kishore-Gu model proves to favor the drying and devolatilization process. However, the sphere and simplified non-sphere model predict 61% and 43% longer residence times, respec-

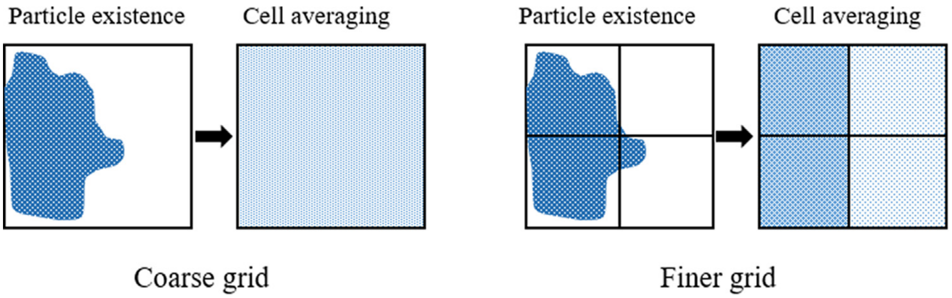

Fig. 1. Effect of grid size for cell averaged particle properties. The demonstration shows that cell averaging affects the particle concentration after cell averaging.

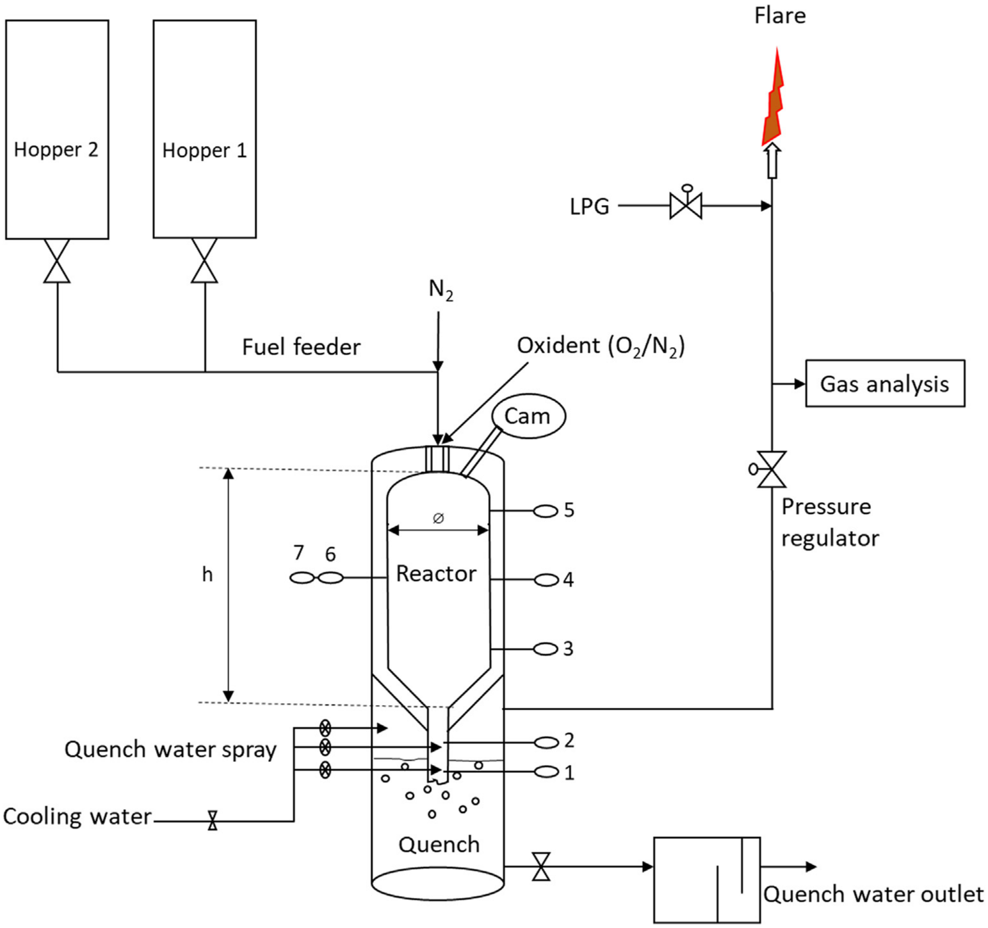

Fig. 2. Schematic process flow diagram of the PEBG plant adapted from (Weiland et al., 2013). Numbers (1–7) represent the thermocouples to monitor the temperature and pressure. The height (h) and the inner diameter (∅) are 1.67 m and 0.52 m, respectively.

tively, than the spheroid models, and the longer residence time seems to favor the char conversion process (Guo et al., 2020).

Liang et al. (Liang et al., 2020) have developed a CPFD simulation model for an EF gasification reactor for the Utah Bituminous coal. The detailed particle information and residence time were studied. The rapid expansion from a tracer injector and fast reactions play an important role in forming the particle distribution zone in the gasifiers. The authors pointed out that due to the complexity of the EF gasification reactions and the computational power limitation, the models were often simplified to two-dimensional or semi three-dimensional models. There was also limited information available in the literature about the particle temperatures, carbon contents, and locations for the discrete particles (Liang et al., 2020).

In view of these paper, this study aimed at giving detailed information about particle hydrodynamics, the temperature distribution inside the reactor, gas composition, reaction rates, and kinetics. This gives a better understanding of the reactor hydrodynamics and the transient behavior of the reactor, which is crucial at the industrial scale investments. To the best of the author's knowledge, no previous studies of reaction rate kinetics for EF reactors are available in the literature.

2. Experimental and CPFD model setup

The experimental studies were performed by Weiland et al. (Weiland et al., 2013). Fig. 2 shows the experimental setup located at the Energy Technology Centre (ETC) in Piteå, Sweden. The reactor diameter and height are 52 cm and 167 cm, respectively. The reactor has a conical-shaped outlet followed by a water sprayed quench bath for gas cooling and particle separation. Biomass stored in the hopper is fed at the top of the reactor along with O_2 and N_2. A quench bath maintains the system temperature and cools down the product gas out from the reactor. The details of the reactor can be found in the study of Weiland et al. (Weiland et al., 2013). The operating conditions of the reactor and the feed definition are shown in Table 1. For safety reasons, the gasifier was operated at pressure ≤ 2 bar.

The proximate and the ultimate analysis of the stem wood powder are shown in Table 2.

A CPFD model was developed in Barracuda to simulate biomass gasification in an EF reactor. A three-dimensional geometric model (cylinder with conical outlet) developed in AutoCAD was imported into the model. The geometry was meshed using the built-in mesh

Table 1
The experimental test conditions operated by Weiland et al. (Weiland et al., 2013).

Fuel feeding rate (kg/h)	40
Total N_2 inlet (kg/h)	15.1
O_2 inlet (kg/h)	27
O_2 inlet concentration	89
Oxygen equivalence ratio	0.49
System pressure (bar)	1.95
Desired process temperature (°C)	1200

Table 2
Ultimate and proximate analysis of the biomass.

Proximate analysis (wt.%, wet basis)		*Ultimate analysis (wt.%, dry basis)*	
Fixed Carbon	14.4	Ash	0.4
Volatiles	80.5	C	50.9
Moisture	4.7	H	6.3
Ash	0.4	N	0.10
		S	0.006
		Cl	0.02
		O (calculated)	42.4

Table 3
Particle phase model parameters and their values.

Fluid drag model	Wen-Yu
Close pack volume fraction	0.2
Maximum momentum redirection from collision	40%
Normal to wall momentum retention	0.15
Tangent to wall momentum retention	0.85
Pressure constant in the particle stress model	1
Initial time step	0.0001 s

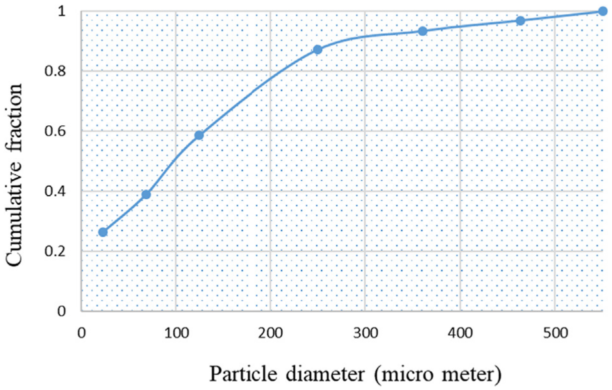

Fig. 3. Particle size distribution.

generator with a uniform grid option. A total of 193,167 computational cells were chosen for the current study. The model is validated against the experimental gas composition reported by Weiland et al. (Weiland et al., 2013). The Wen-Yu drag model was selected and the particle model parameters used in the model are presented in Table 3.

Modeling of an EF reactor commonly neglects particle–particle interactions as the reactor operates at lower solid fractions. However, particle–particle interactions play an important role around the fuel injector. Particle-particle interaction in the model can be altered by altering the close pack volume fraction and the maximum momentum redirection from particle collisions. In addition, the Blended Acceleration Model (BAM) was activated as the particle mixture was composed of a broad range of particle sizes (25–550 μm). BAM blocks the unrealistic particle segregation by absorbing the sustained particle contact (Bandara et al., 2021). The particle size distribution of the biomass feed is illustrated in Fig. 3.

The boundary conditions and the computational mesh of the developed model are shown in Fig. 4. Biomass and the fluidizing agent were implemented as an injection boundary. In the model, particle inflow should be assisted by a fluid stream and the flow can be manipulated by changing the 'slip velocity' option. However, an injection boundary was chosen for the introduction of particles into the reactor because it does not need the assistance of a fluid stream. The red triangles with spheres at the top represent the injection points. Totally 20 injection points along the circle and one at the middle were defined in the model.

Two flux planes were defined at the entrance and the reactor's exit to monitor the flow into and out of the reactor. Also, seven intermediate planes were defined to monitor the flow rate and the gas composition at approximately 20 cm apart. A pressure boundary (yellow plane) was defined at the bottom of the reactor to allow outflow of the product gas and the solid materials. The CPFD platform includes the model for both gas-solids and gas-wall heat transfer as well as the radiation between a thermal wall and particle-phase only. The user can choose a drag model from the available built-in drag models or can create a drag model of user choice.

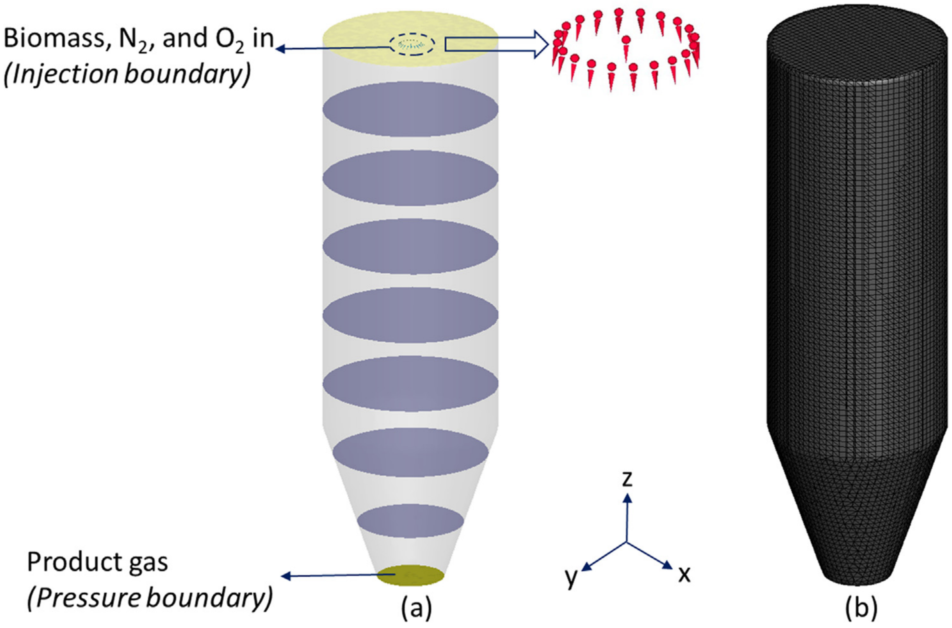

Fig. 4. (a) – Boundary conditions, (b) – computational grid. The planes in the left figure show the data capturing planes. The three-dimensional geometry was imported in the CPFD model and mesh was generated using an in-built mesh generator.

Chemical reactions are an integral part of many industrial applications and are closely coupled with the fluid-particles dynamics and the heat and mass transfer inside a reactor. The reactor temperature affects the reaction rates and thereby affecting the reactor heat transfer and the reactor hydrodynamics. Heterogeneous reactions produce or consume gases from solids affecting the total gas volume, which changes the reactor hydrodynamics. There can be thousands of reactions in any industrial chemical process and it is impossible to solve a large number of coupled reactions over a hundred seconds of simulation time. Thus, a common consensus is to postulate a limited set of reactions describing the major conversion inside the reactor, which makes computational tracking easy (Snider et al., 2011).

Devolatilization of the biomass is the first step in a biomass gasification process. Biomass particles are subjected to fast heating rates with short residence times. The devolatilization kinetic parameters are taken from the study of Guo et al. (Guo et al., 2020) as follows:

$$\frac{dm_{devol}}{dt} = -A\exp\left(-\frac{E}{T_p}\right)m_{devol} \tag{1}$$

Where, m_{devol} is the remaining volatile in the particle (kg) and t is time (s), A is a pre-exponential factor ($18.9 \times 10^3\ s^{-1}$), E is the activation energy ($2562.4\ K^{-1}$) and T_p is the particle temperature (K). In order to simplify the model, the formation of tar and other higher molecular hydrocarbons was neglected. Based on the literature data, volatiles count as 80% on a dry basis, and the remaining is char and ash after the devolatilization. The major reactions together with the kinetics are presented in Table 4. As the chemistry module was implemented as volume average chemistry, the temperature for the heterogeneous reactions was taken as a weighted average with 50% of the average particle temperature and 50% of the cell's gas temperature. The particles for the EF reactor are small enough, which does not add much uncertainty due to this assumption. m_s is the mass of carbon which gives the approximate amount of char components.

$$m_s = M_{wC} \times [C(s)]$$

M_{wC} is the molecular weight of carbon, and $[C(s)]$ is the molar concentration of solid carbon.

The time step for a transient model is an important parameter. It is important that the time step is small enough to represent any rapidly changing variables of interest. However, if the time step is too big, an accumulation of errors will occur (Zhang et al., 2000). To solve this problem, a varying time step can be utilized with the help of the Courant-Friedrichs-Lewy (CFL) number:

$$\mathrm{CFL} = \frac{v\Delta t}{\Delta x_{cell}} \tag{2}$$

$v$is velocity, Δt is time step and Δx_{cell} is cell size. The default minimum and maximum values of CFL in the model are 0.8 and 1.5, respectively, which gives stability for the numerical solver.

2.1. Governing equations

The gas phase mass and momentum conservation equations are given by the continuity and the Navier-Stokes equations represented by Equations (3) and (4) respectively.

$$\frac{\partial\left(\alpha_g\rho_g\right)}{\partial t} + \nabla\cdot\left(\alpha_g\rho_g\vec{u}_g\right) = \delta\dot{m}_p \tag{3}$$

$$\frac{\partial}{\partial t}\left(\alpha_g\rho_g\vec{u}_g\right) + \nabla\cdot\left(\alpha_g\rho_g\vec{u}_g\vec{u}_g\right) = -\nabla p + F + \alpha_g\rho_g g + \nabla\cdot\left(\alpha_g\tau_g\right) \tag{4}$$

where α, ρ and $\vec{u}$ represent the volume fraction, density, and velocity vector respectively. $\delta\dot{m}_p$ is the gas mass production rate per volume formed from the particle-gas chemical reaction. In the case of the cold flow model with no chemical reaction, $\delta\dot{m}_p$ becomes zero. P is the mean flow gas pressure, g is the acceleration due to gravity, τ_g is the fluid phase stress tensor and F is the inter-phase momentum transfer rate per unit volume (particle to fluid phase).

For a Newtonian fluid, the gas phase stress tensor for each species, τ_g is given by:

$$\tau_{g,ij} = \mu\left[\left(\frac{\partial u_i}{\partial x_j} + \frac{\partial u_j}{\partial x_i}\right) - \frac{2}{3}\mu\delta_{ij}\frac{\partial u_k}{\partial x_k}\right] \tag{5}$$

where μ is the shear viscosity, which is the sum of the laminar shear viscosity and the turbulence viscosity defined in the Smagorinsky turbulence model (Smagorinsky, 1963). The model is given in Equation (6) (Snider et al., 2011).

$$\mu_t = C_s\rho_g\Delta^2\left(\frac{\partial u_i}{\partial x_j} + \frac{\partial u_j}{\partial x_i}\right) \tag{6}$$

The Smagorinsky coefficient $C_s$has a default value of 0.01. Δ and is the subgrid length and is given by:

$$\Delta = (\delta x\delta y\delta z)^{1/3} \tag{7}$$

A fluid-phase transport equation is solved for each gas species. The calculation of the fluid phase properties is based on the mass fraction $Y_{g,i}$ of the gas species making up the fluid mixture. $\delta\dot{m}_{i,c}$ is a chemical source term, which is the mass transferred between the gas species by the dissociation and the association of the chemical bond.

$$\frac{\partial}{\partial t}\left(\alpha_g\rho_g Y_{g,i}\right) + \nabla\cdot\left(\alpha_g\rho_g Y_{g,i}\vec{u}_g\right) = \nabla\cdot\left(\alpha_g\rho_g D_t\nabla Y_{g,i}\right) + \delta\dot{m}_{i,c} \tag{8}$$

D_t is the turbulent mass diffusivity and can be calculated from Equation (9). Sc is the Schmidt number in Equation (9). The standard value of the turbulent Schmidt number is 0.9 (Snider et al., 2011).

$$\mu/(\rho_g D_t) = \mathrm{Sc} \tag{9}$$

Table 4
Reactions and kinetics.

Reaction	Reaction rate: r (mol.m-^{3}.s^{-1})	Reference
$C(s) + 0.5O_2 \rightarrow CO$	$2.51 \times 10^{-3} m_s T\exp(\frac{-8996}{T})[O_2]$	(Ku et al., 2014)
$H_2 + 0.5O_2 \rightarrow H_2O$	$5.69 \times 10^{14} exp(\frac{-17610}{T})[H_2][O_2]^{0.5}$	(Bates et al., 2017)
$CH_4 + 1.5O_2 \rightarrow CO + 2H_2O$	$5.01 \times 10^{14} exp(\frac{-24357}{T})[CH_4]^{0.}\square[O_2]^{0.8}$	(Bates et al., 2017)
$CO + H_2O \rightarrow CO_2 + H_2$	$7.68 \times 10^{10} exp(\frac{-36640}{T})[CO]^{0.5}[H_2O]$	(Snider et al., 2011)
$C(s) + CO_2 \rightarrow 2CO$	$1.272 m_s T exp(\frac{-22645}{T})[CO_2]$	(Snider et al., 2011)
$C(s) + H_2O \rightarrow CO + H_2$	$1.272 m_s T exp(\frac{-22645}{T})[H_2O]$	(Snider et al., 2011)

The energy conservation equation of the gas phase is:

$$\frac{\partial}{\partial t}\left(\alpha_g\rho_g h_g\right) + \nabla\cdot\left(\alpha_g\rho_g h_g\vec{u}_g\right) = \alpha_g\left(\frac{\partial P}{\partial t} + \vec{u}_g\cdot\nabla P\right) + \varphi - \nabla\cdot\left(\alpha_g\vec{q}\right) + \dot{Q} + S_h + \dot{q}_D + q_{wp} \tag{10}$$

where h is the enthalpy and q_{wp} is the radiative heat transfer between the thermal wall and the particle phase. The viscous dissipation (φ) and the energy source per unit volume ($\dot{Q}$) are neglected in this work. S_h is the conservative energy exchange from the particle phase to the gas phase. $\dot{q}_D$ is the enthalpy diffusion term and $\vec{q}$ is the gas heat flux. The expressions for the $\vec{q}$ and $\dot{q}_D$ are given as:

$$\vec{q} = \lambda_g\nabla T_g \tag{11}$$

$$\dot{q}_D = \sum_{i=1}^{N}\nabla\cdot\left(h_i\alpha_g\rho_g D\nabla Y_{g,i}\right) \tag{12}$$

where λ is the thermal conductivity calculated as a sum of a molecular conductivity (λ_m) and an eddy-conductivity (λ_t) from Reynolds stress mixing theory. The eddy-conductivity is calculated from the turbulent Prandtl number correlation.

$$Pr_t = \left(C_p\mu_t\right)/\lambda_t \tag{13}$$

The mass, momentum, and energy conservation equations are solved for the gas mixtures. The gas mixture properties are based on the mass fractions of the gas species calculated using Equation (8). The flow is considered compressible and the gas phase temperature, pressure, enthalpy, density, and mass fraction are correlated through the equation of state. CPFD uses the ideal gas equation of state.

The gas mixture enthalpy (h_g) is the sum of individual gas enthalpy (h_i), given by:

$$h_g = \sum_{i=1}^{N} Y_{g,i}h_i \tag{14}$$

$$h_i = \int_{T_o}^{T_g} C_{p,i}dT + \Delta h_{f,i} \tag{15}$$

where $\Delta h_{f,i}$ is the enthalpy of formation of species i at the reference temperature T_o. $C_{p,i}$ is the specific heat capacity of species i.

The gas-phase equations contain a source term and the mass, momentum, and energy are conserved between the phases. The gas chemistry does not change the mixture's total mass and enthalpy; however, with the gas–solid reactions, mass, momentum, and energy are transferred to the gas phase by chemical conversion of solids to gas. This is known as the interphase momentum transfer rate per unit volume (F) in Equation (4).

The dynamics of the solid particles are calculated by solving a transport equation for the Particle Distribution Function (PDF), f. The details of the transport equation can be obtained from the literature (Andrews & O'Rourke, 1996; Thapa et al., 2016). PDF is a function of particle spatial position $\vec{x}_p$, particle velocity $\vec{u}_p$, particle mass m_p, particle temperature T_p, and time t. Therefore, $f\left(\vec{x}_p, \vec{u}_p, m_p, T_p, t\right)d\vec{u}_p dm_p dT_p$ is the average number of particles per unit volumes with masses in the interval $(m_p, m_p + dm_p)$, velocities in the interval $(\vec{u}_p, \vec{u}_p + d\vec{u}_p)$ and temperature in the interval $(T_p, T_p + dT_p)$.

The particle velocity and acceleration are given by:

$$\frac{\partial}{\partial t}\left(\vec{x}_p\right) = \vec{u}_p \tag{16}$$

$$\frac{\partial}{\partial t}\left(\vec{u}_p\right) = D_P\left(\vec{u}_g - \vec{u}_p\right) - \frac{\nabla P}{\rho_p} + g - \frac{\nabla\tau_p}{\rho_p\alpha_p} + F_p \tag{17}$$

The particle volume fraction in Equation (17) is given by:

$$\alpha_p = \iiint f\frac{m_p}{\rho_p}dm_p d\vec{u}_p dT_p \tag{18}$$

where, D_P is the drag function which depends upon the particle size, position, velocity, and time. τ_p is the particle normal stress given by Equation (19). Particle interactions (particle to particle collisions) are modeled with the particle normal stress developed by Harris and Crighton (Harris & Crighton, 1994). The particle stress is derived from the particle volume fraction, which in turn is calculated from particle volumes mapped to the grid. Particle normal stress gives an approximation of the collective effects of all the neighbor particles of a particle. The CPFD method calculates the spatial gradients on an Eulerian grid and applies the gradient to discrete particles. The gradient in the particles accelerates the particle, which prevents the particle volume fraction from exceeding their close-pack volume faction. The particle pressure is a function of solid volume fraction and becomes zero when the solid volume fraction becomes zero (Snider et al., 2011).

$$\tau_p = \frac{P_s\alpha_p{}^{\beta}}{\max\left[\left(\alpha_{cp} - \alpha_p\right), \varepsilon\left(1 - \alpha_p\right)\right]} \tag{19}$$

Solid collisions depend upon the solid concentration and the solid velocity. Particle normal stress is exerted to a solid up to the point where the solid reaches the particle-mean velocity (Snider et al., 2011). P_s is a constant (Pa), α_{cp} is the particle volume fraction at close packing, β is a constant (between 2 and 5) and ε is a very small number in the order of 10^{-8}.

The fluid mass source in Equation (3) is given by:

$$\delta\dot{m}_p = \iiint f\frac{dm_p}{dt}dm_p d\vec{u}_p dT_p \tag{20}$$

where the time-rate change of particle mass dm_p/dt is the rate of change of the particle mass-producing gases through chemical reactions and is given by:

$$\frac{dm_p}{dt} = \frac{\alpha_g Mw_c}{\alpha_p\rho_p}m_p\frac{d[C(s)]}{dt} \tag{21}$$

The interphase momentum transfer (F) in Equation (4) is given by:

$$F = \iiint f\left[m_p\left\{D_P\left(\vec{u}_g - \vec{u}_p\right) - \frac{\nabla P}{\rho_p}\right\} + \vec{u}_p\frac{dm_p}{dt}\right]dm_p d\vec{u}_p dT_p \tag{22}$$

The conservative energy exchange term S_h in Equation (10) from the particle phase to the gas phase is given by (Snider et al., 2011):

$$S_h = \iiint f\left[m_p\left\{D_P\left(\vec{u}_p - \vec{u}_g\right)^2 - C_V\frac{dP_p}{d_t}\right\} - \frac{dm_p}{dt}\left\{h_p + \frac{1}{2}\left(\vec{u}_p - \vec{u}_g\right)^2\right\}\right]dm_p d\vec{u}_p dT_p \tag{23}$$

where, h_p is the particle enthalpy and C_V is the specific heat of the particle. The lumped heat equation for the particle is:

$$C_V\frac{dT_p}{dt} = \frac{1}{m_p}\frac{\lambda_g Nu_{g,s}}{2r_p}A_s\left(T_g - T_p\right) \tag{24}$$

where $Nu_{g,s}$ is the Nusselt number for heat transfer from gas to the particle phase, m_p is the particle mass and r_p is the particle radius.

The radiative heat transfer between the thermal wall and the particle phase in the equation is given by:

$$q_{wp} = A_w F_{wp} \varepsilon_{wp} \sigma \left(T_w{}^4 - \bar{T}_p{}^4 \right) \quad (25)$$

where A_w is the area of the thermal wall, T_w is the wall temperature, $\bar{T}_p$ is the average particle temperature in a cell, F_{wp} is a view factor, σ is the Stefan-Boltzmann constant and ε_{wp} is the emissivity between the wall and particles in the cell.

In multiphase simulations, drag models are very important for predicting hydrodynamics. The model calculates a force acting on a particle as a function of the particle and fluid properties and the flow conditions. The details of the drag force and its expressions together with the numerical scheme for the CPFD approach are presented in the supplementary material.

3. Results and discussion

A pilot-scale EF gasifier is simulated with a CPFD scheme for the particle dynamics. The computation is three-dimensional non-isothermal with heterogeneous and homogeneous gasification chemistry. The gasification process itself is a complex process involving interactions between the solid flow, gas flow, and the chemical reactions in a thermal environment. Simulations were carried out for 100 s and the gas compositions, temperature, residence time, chemical kinetics, and mass flow rate were monitored. The average gas compositions were taken as the time average of the final 20 s of simulation. A detailed description of the simulation results at the initial reactor temperature of 1200℃ is presented in Section 3.1.

3.1. Simulation results at 1200 °C reactor temperature

Validation of a CFD model is an important aspect during the study of the simulation results. Table 5 shows the comparison between the experimental and simulation results. The mole percentage of CH_4 in the experiment also includes the mole percentage of C_2H_2 (0.3) and C_2H_4 (0.1). The simulation results agree reasonably well with the experimental data.

As the reactor hydrodynamics is concerned, the reactor is desired to have a uniform mixing between the fuel particles and the fluidizing agent. Fig. 5 shows the instantaneous particle distribution after 50 s. Particle scale information is captured by the Lagrangian tracking of solid particles. As depicted in Fig. 5 (a), particle temperature in the central region is lower, with particles flowing downward. This is due to most particles following the central path where a significant number of reactions (endothermic) occurs compared to the peripheral region. This also leads to the shorter residence time for the particles flowing through the central region, as shown in Fig. 5 (b). Particles in the central region of the gasifier have the lowest residence time (high speed), whereas the particle towards the outer region has high residence time (low speed). The particle species with longer residence time are the particles that undergo recirculation, expansion along the radial direction. Fig. 5 (c) shows the particle radius, which shows the near-uniform distribution of the particle with respect to size. The particle temperature, as well as the residence time, is highly related to the carbon conversion of the particles. Fig. 5 (d) shows the particle carbon content (mass fraction) for the simulated gasifier. Particle carbon content is lower in the central region and higher in the other region. Even with the lower residence time, carbon conversion is higher in the central region, which indicates that the higher residence time may not always result in higher carbon conversion.

Particle carbon content determines the char conversion for the process. Char conversion depends on the reactor conditions as well as the residence time of the fuel particle. Therefore, it is important to analyze the residence time of the solid particles inside the gasifier. Fig. 6 (a) shows the average residence time for all the particles. After the reactor reaches the steady state, the residence time stabilizes around the median value. The different values for the residence time are due to the fact that all the particles do not follow the same path inside the reactor. Some particles circulate back into the top peripheral corner giving the largest residence time, while particles following a straight(ish) path have a lower residence time.

As depicted in Fig. 6 (b), most of the particles (48.1%) have a residence time of 1.38–1.48 s. The rightmost column gives the distribution of the particles having a residence time greater than 1.68 s. The highest residence time recorded was 3 s at the start of the simulation process. It took around 10 s of simulation time to reach near steady-state conditions as the biomass and the fuel is fed to a heated standstill reactor at time t = 0 s.

However, the carbon conversion depends upon different factors such as the reactant gas distribution inside the gasifier, fluid velocity, mixing, etc. Particles in the central region have a higher probability of easy access to gasifying agents such as oxygen. The conversion of the char inside the gasifier is affected by the fluid velocity and direction inside the reactor. Fig. 7 shows the instantaneous fluid velocity distribution.

As depicted in the figure, recirculation of mostly occurs around the wall of the reactor. Whereas, in the central region the fluid velocity increases gradually with descending gasifier elevation. The recirculation and rapid gas expansion are due to the expansion mechanism of the injection nozzles. The expansion in a radial direction is high compared to the axial direction due to the high jet velocity along the axial direction. This agrees well with the results published by Liang et al. (Liang et al., 2020), where the reactor consists of a zone of recirculation, spreading, and fast-flowing. The flow vector is nearly random throughout the reactor with exception in the middle of the reactor. This behavior of the entrained flow reactor has a great influence on the particle mixing and the overall conversion efficiency of the reactor. Further, the gas composition, reactor temperature, and reaction kinetics are analyzed during this study.

It is important to monitor the gas composition and the fluid temperature along the reactor. Fig. 8 gives the calculated parameters along with the height of the reactor. The cut-planes are at 0.2, 0.4, 0.6, 0.8, 1.0, 1.2, 1.4, 1.6 m from the bottom of the reactor. The figure shows the instantaneous mole fraction of CO, H_2, and CO_2 and the average fluid temperature (K) at t = 50 s. As shown in Fig. 8 (d), the average fluid temperature of the reactor gave a radial profile at the outlet, which shows that homogeneous mixing in the

Table 5
Comparison between the simulation and experimental results.

		CH_4	CO	CO_2	H_2	Syngas mass flow, dry basis (kg/h)
Simulation	mol %[1]	3.8	45.7	22.6	27.5	76.3
	mol/kg fuel[2]	3.7	25.5	8.0	213.1	
Experiment	mol %	2.7	48.5	21.1	27.8	74.6
	mol/kg fuel	2.42	26.5	7.1	210.6	

[1] Dry, N_2 free basis.
[2] Back calculated by the authors for this article as no such calculations are present in the referred article.

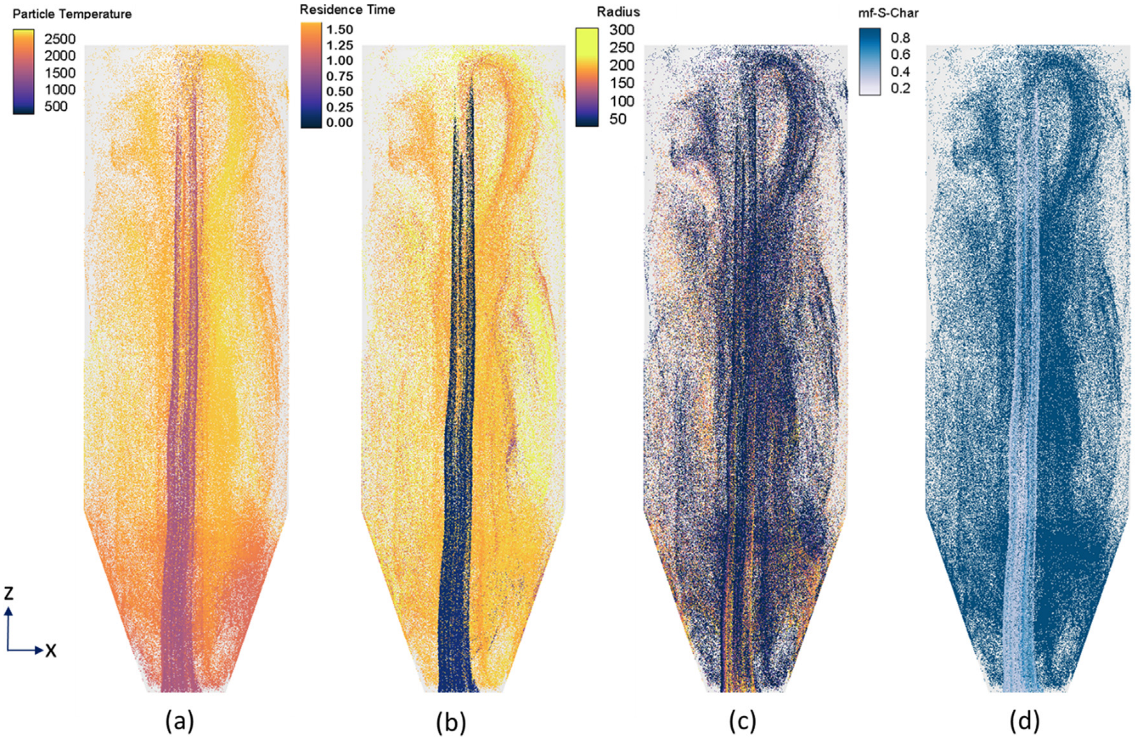

Fig. 5. The instantaneous distributions of particles with respect to (a) temperature (b), residence time (c) particle radius, and (d) carbon content at 50.0 s.

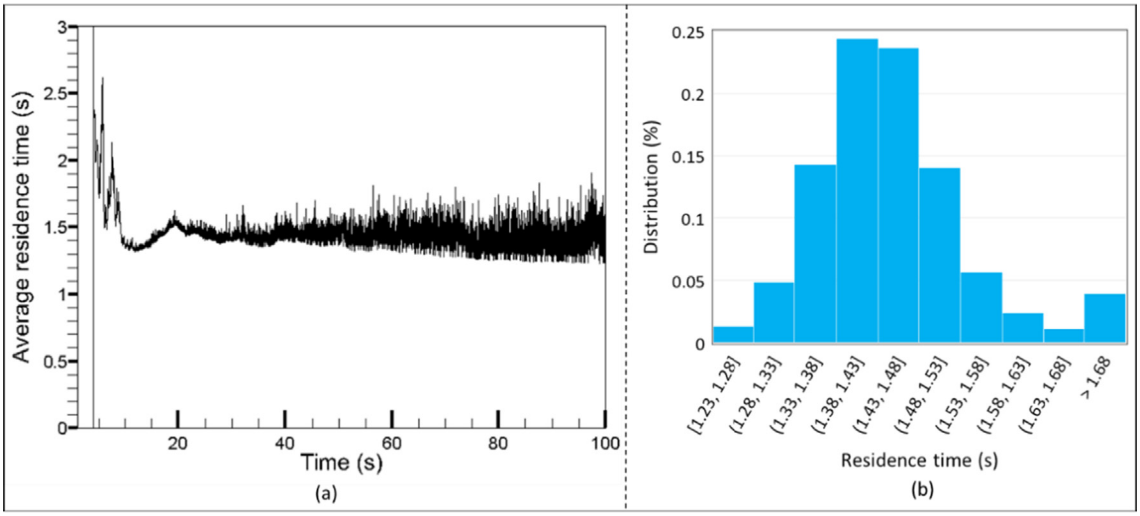

Fig. 6. (a) Average residence time for all particle species (b) Distribution percentage of the residence time in an interval of 0.05 s.

EF reactor is not achieved even at the exit areas. This is due to the fact that the majority of the particles are flowing through the central path where the majority of chemical reaction takes place and they take heat from the surroundings. Therefore, the central radial path has a lower temperature as compared to other regions in the radial direction.

The figures show the illustrative three-dimensional view of the gasifier during its operation. The bottom plane of the reactor gives the product gas from the reactor. The numerical values of the gas compositions and the reactor temperature are presented in Fig. 9. The gas compositions and the temperature are radially averaged at t = 50 s. Fig. 9 (b) shows the highest fluid temperature at the reactor injection burner. Analyzing the product gas composition and the temperature profile, combustion prevails around the burner region of the gasifier. Combustion supplies the necessary thermal heat for the other endothermic gasification reactions and the devolatilization of the biomass. There are no significant amounts of oxygen in the reactor. The oxygen concentration is 89 mol% in the injection burner and is completely consumed as it leaves the burner. Combustion in this region is the major reason for the peak fluid temperature.

As the chemical and thermal behavior are coupled together, a change in one affects the changes in the other one. Heat is supplied from walls as well as from the gas feed. Chemical transformation such as breaking chemical bonds gives sensible thermal energy, which changes the temperature. Gasification and combustion con-

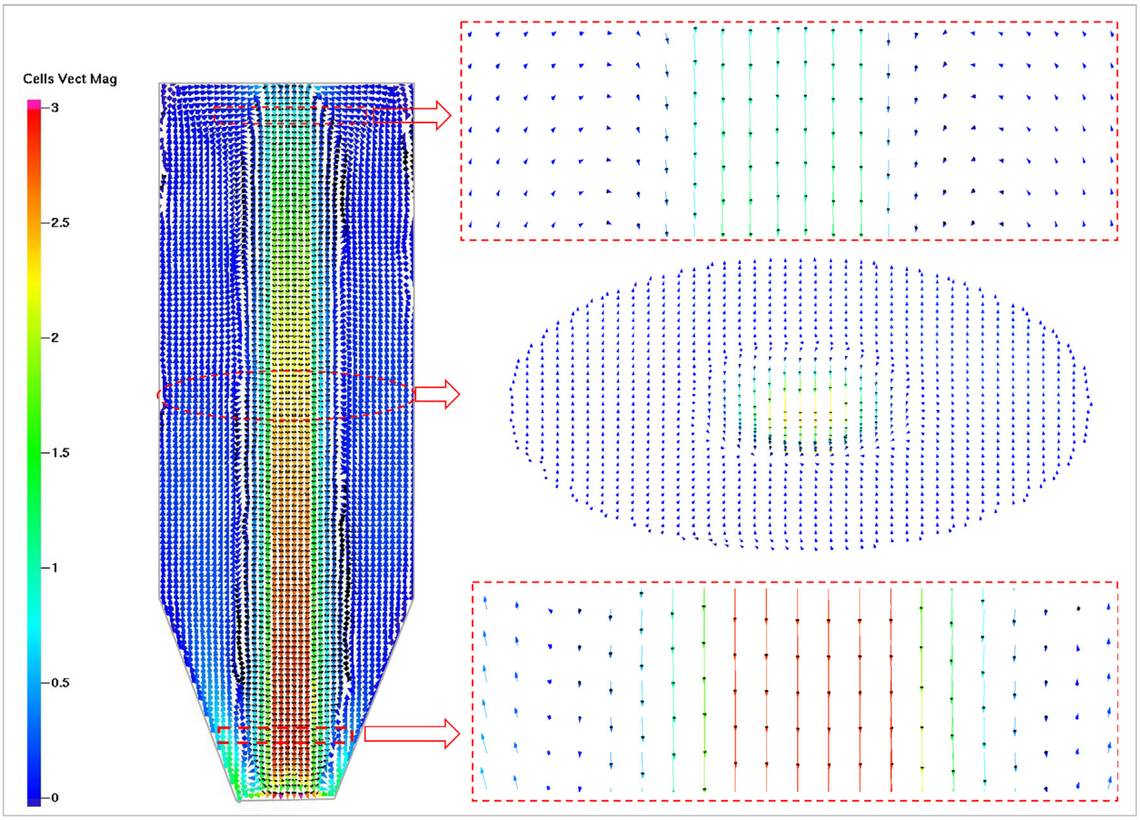

Fig. 7. Gas speed distribution at t = 50 sec.

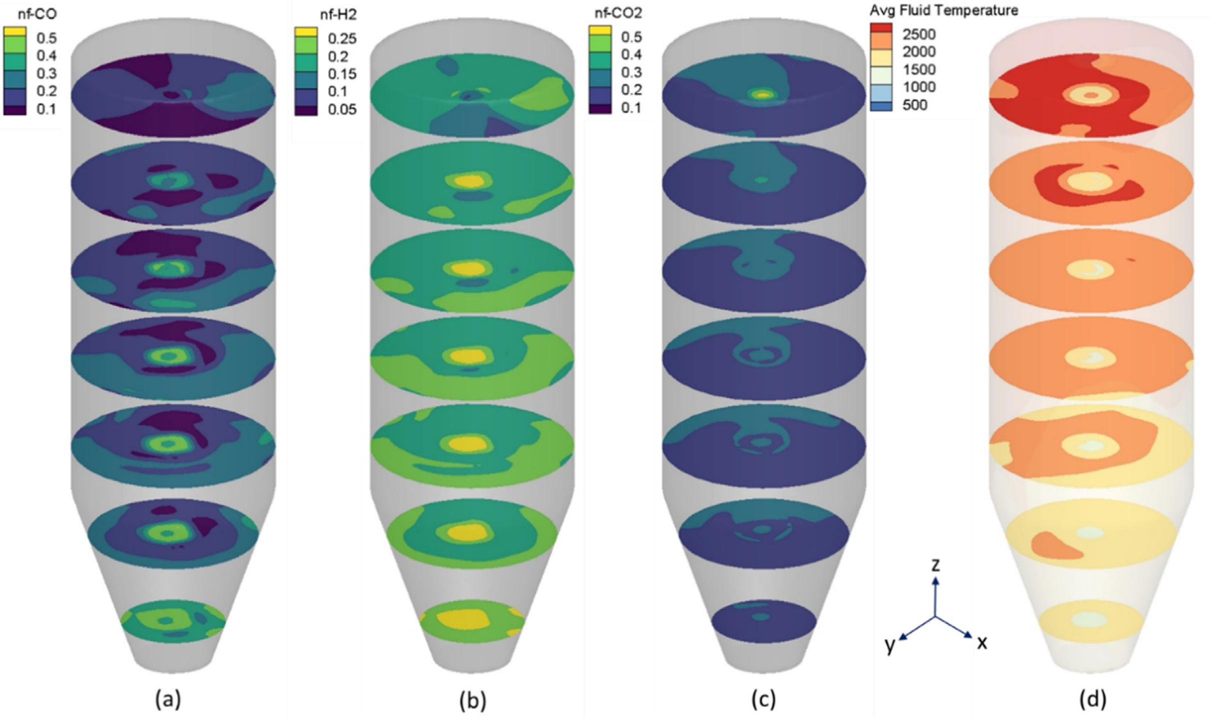

Fig. 8. Gasifier parameters at different levels in the reactor: Instantaneous mole fraction for gas species: - (a) CO, (b) H_2, (c) CO_2 and (d) time average fluid temperature.

sume and produce sensible heat respectively. Char gasification requires an optimal gas–solid contact; however, the conversion is sophisticated by the local variation in gas and temperature, depicted in Fig. 5 (a).

Chemistry affects the reactor dynamics by changing the gas composition and the reactor temperature. The above listed six chemical reactions were computed for each computational cell at each computational time step giving a transient 3D reactor behav-

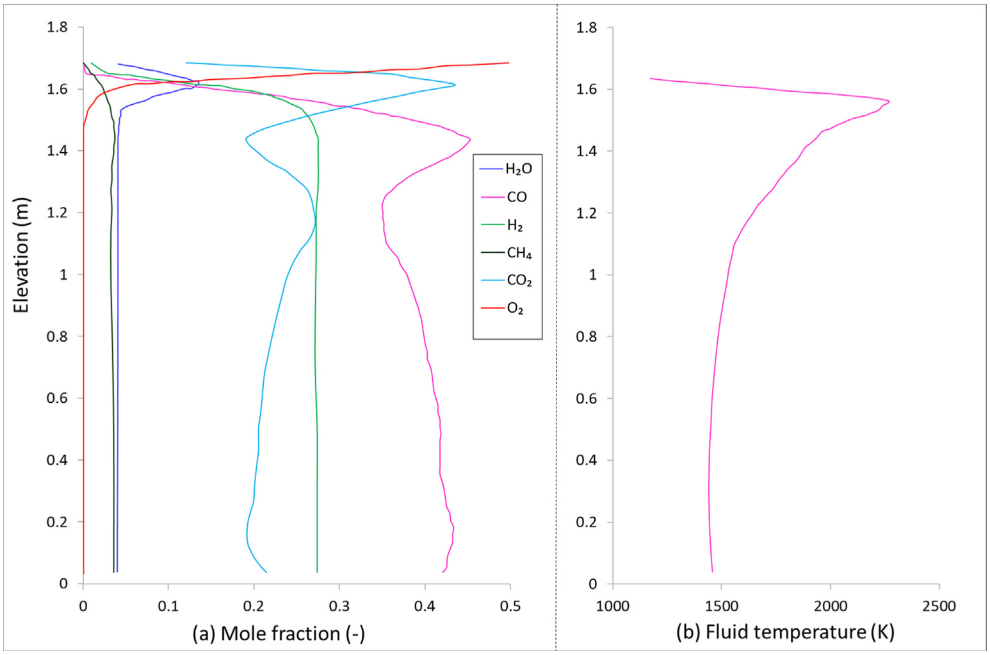

Fig. 9. (a), gas compositions (mole fraction) (b), fluid temperature versus elevation. Gas species and the fluid temperature are radially averaged.

ior. Fig. 10 shows the radially averaged reaction rates along with the gasifier depth. The figure shows that the reaction rates for different reactions are in the range of several orders of magnitude. As seen from Fig. 9 (a), CO is the dominant gas species throughout the reactor. As the reactor temperature is high around the fuel injector and the endothermic nature of the water gas shift reaction favors the forward reaction, the production of CO_2 is high in that region. The reaction rate decreases significantly for R04 with increasing reactor depth due to the decrease in reactor temperature and the small amounts of steam concentration as shown in Fig. 9 (a). Production of steam is from the oxidation of H_2 (R02), which significantly decreases with the reactor depth. This also limits the reaction rate for R04. The reaction rate for the R03 reaction is slow throughout the reactor elevation due to the fact that the CH_4 is present at a low concentration compared to the other gases in the reactor. The dominant methane production source is the devolatilization step, whereas the methanation reaction is not considered during this study due to its slow reaction rate.

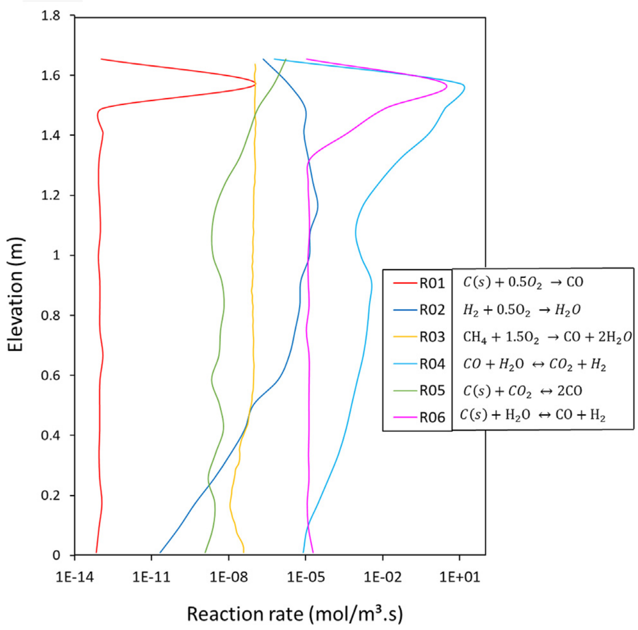

Fig. 10. Chemical reaction rate versus elevation at t = 50 s. Reaction rates are shown on a logarithmic scale.

Char oxidation (R01) is significant in the high-temperature region and all available oxygen is consumed around the fuel injector region. This gives the sufficiently low reaction below the fuel injector region. The char-steam reaction (R06) is also significant in the reactor entrance region, due to the presence of H_2O in this region. The majority of steam production in this region is from the reaction R02. The produced steam is quickly consumed by the reaction R06, as depicted by the mole fraction of H_2O in Fig. 9 (a).

The average mass production rate of the product gas was found to be 0.022 kg/s. As the product gas was produced at a high temperature, the ideal gas law was applied to calculate the gas production rate at normal temperature and pressure conditions (25 °C and 1 atm). The ratio of product gas to biomass was calculated as 3.61 Nm^3/kg of biomass. The average gas fractions on a volume basis were 0.038 of CH_4, 0.457 of CO, 0.226 of CO_2, and 0.275 of H_2. The lower heating value of the product gas is calculated as 7.8 MJ/kg. The carbon conversion efficiency was calculated as 99.1 % based on the amount of carbon converted into product gases using the formula $[(1 - m_{char})/(m_{biomass} \cdot \%C)] \cdot 100\%$. The lower heating values for the product gas components are taken from the literature (Waldheim & Nilsson, 2001). The CGE of the gasifier is calculated as 61.3% using equation (26):

$$CGE = \frac{\dot{m}_{gas}(kg/s) \cdot LHV_{gas}(MJ/kg)}{\dot{m}_{fuel}(kg/s) \cdot LHV_{gas}(MJ/kg)} \tag{26}$$

3.2. Effect of temperature

The effect of reactor temperature on the product gas was analyzed for the initial reactor temperature of 1000℃, 1100℃, 1200℃, and 1300℃. The time taken to reach the near steady-state condition decreased with an increase in reactor temperature.

The time taken to reach close to the steady-state increased from around 8 s to around 13 s as the reactor temperature increased from 1000℃ to 1300℃. Changes in the reactor temperature change the reaction rate and the time to reach the equilibrium/steady state. The product gas composition is the average value obtained from the reactor output.

Fig. 11 shows the product gas composition at four different reactor temperatures. With an increase in reactor temperature, the concentration of CO and H_2 increased slightly, whereas the concentration of CO_2 and CH_4 decreased slightly. Increasing the reactor temperature gave changes in the product gas composition, as illustrated in the figure. The predicted gas compositions are consistent with the experimental results of coal gasification published by Lee et al. (Lee et al., 1996). Therefore, it is crucial to study the reactor parameters to optimize reactor performance.

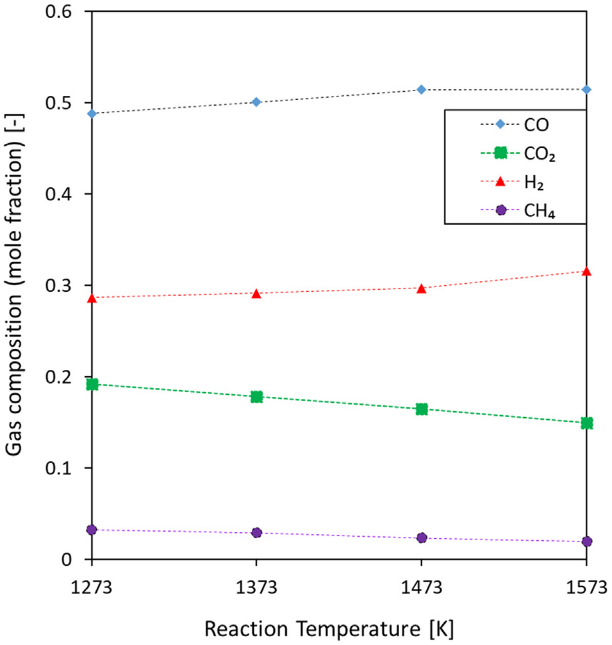

Fig. 11. Product gas composition at four different reactor temperatures (dry basis).

3.3. Effect of equivalence ratio

The effect of the oxygen equivalence ratio was simulated and analyzed for the developed model. The change in the oxygen supply changes the chemistry inside the reactor, which in turn affects the hydrodynamics inside the reactor. The variation of equivalence ratio (λ) is presented in Fig. 12. The product gas in the figure is presented on a dry, N_2 free basis.

The optimal gasification performance (higher mole fraction of CO and H_2) is in the range of equivalence ratio 0.3 to 0.44. An increase in the equivalence ratio above 0.6 gave oxygen in the product gas particularly due to short residence time for these types of gasifiers. The char in the product gas is consumed almost 100% for the equivalence ratio greater than 0.3. The higher the equivalence ratio the higher the reaction rates for combustion reaction thereby increasing the process temperature. For more parametric variations and variations of process conditions, interested readers are advised to read the results published by Weiland et al (Weiland et al., 2015).

4. Conclusion

This study investigated the biomass gasification behaviors in an entrained flow reactor by developing a simulation model based on the MP-PIC approach. The model is validated against the results from an experiment published in the literature. The results suggest the suitability of the model for multiphase systems such as EF reactors. The gasifier performance is quantified based on the results obtained from the model. The model gave a good prediction of the gasifier behavior and its chemistry, which can be used to optimize entrained flow reactors. The main focus was to evaluate the product gas composition, the reaction kinetics, and the flow behavior inside the gasifier. Simulations showed that the CPFD is an excellent tool to predict the gasification behavior inside an entrained flow reactor. The overall efficiency (or CGE) of industrial-scale entrained flow reactors is expected to be higher than for the pilot-scale reactor due to the lower ratio of thermal heat losses to fuel input.

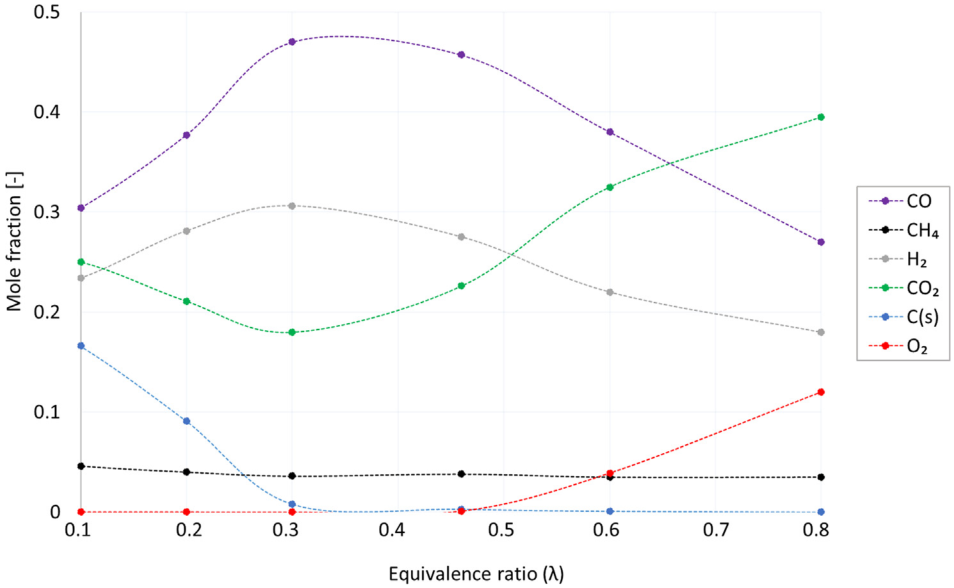

Fig. 12. product gas composition at a different equivalence ratio (dry basis).

Char oxidation is significant in the high-temperature region, whereas the char-CO_2 reaction is prevalent throughout the reactor depth. The endothermic nature of the water gas shift reaction favors the high production of CO_2 in high-temperature regions and its reaction rate decreased significantly with reactor depth. Simulations show the zones of high and low-temperature regions, suggesting different reaction zones such as a partial combustion zone near the fuel injector followed by a gasification zone. Change in the operational temperature from 1000℃ to 1300℃ gave an increase of 12.45% of CO and 17.5% of H_2 and a decrease of 34.55% of CH_4 and 17.15% of CO_2 on a dry nitrogen-free basis. At a lower equivalence ratio, some amounts of char were present in the product gas whereas, at a higher equivalence ratio, O_2 was present in the product gas. However, there are some uncertainties in these results. Simulation of the complete system including the feeding system as well as the quench bath for gas cooling and the inclusion of tar and slag, will overcome the uncertainties to a certain extent in this study.

CRediT authorship contribution statement

Ramesh Timsina: Conceptualization, Writing – original draft, Validation. **Rajan K Thapa:** Software, Investigation, Supervision. **Britt M.E. Moldestad:** Supervision, Writing – review & editing. **Marianne S. Eikeland:** Supervision, Writing – review & editing.

Declaration of Competing Interest

The authors declare that they have no known competing financial interests or personal relationships that could have appeared to influence the work reported in this paper.

Acknowledgments

The authors would like to thank the University of South-Eastern Norway for providing the CFD package and the computer resources for the simulation. We would like to acknowledge the research center for environmental-friendly energy research (FME) Bio4fuels [Project number: 257622] for supporting this work. This research did not receive any specific grant from a funding agency in the public, commercial, or non -profit sectors.

Appendix A. Supplementary data

Supplementary data to this article can be found online at https://doi.org/10.1016/j.cesx.2021.100112.

References

Abani, N., Ghoniem, A.F., 2013. Large eddy simulations of coal gasification in an entrained flow gasifier. Fuel 104, 664–680. https://doi.org/10.1016/j.fuel.2012.06.006.

Abbasi, A., Islam, M.A., Ege, P.E., de Lasa, H.I., 2013. CPFD flow pattern simulation in downer reactors. AIChE J. 59 (5), 1635–1647. https://doi.org/10.1002/aic.13956.

Andrews, M.J., O'Rourke, P.J., 1996. The multiphase particle-in-cell (MP-PIC) method for dense particulate flows. Int. J. Multiph. Flow 22 (2), 379–402. https://doi.org/10.1016/0301-9322(95)00072-0.

Ariyaratne, W.H., Ratnayake, C., Melaaen, M.C., 2017. Application of the MP-PIC method for predicting pneumatic conveying characteristics of dilute phase flows. Powder Technol. 310, 318–328. https://doi.org/10.1016/j.powtec.2017.01.048.

Bandara, J.C., Moldestad, B.M., Eikeland, M.S., 2018. Analysing the effect of temperature for steam fluidized-bed gasification of biomass with MP-PIC simulation. Int. J. Energy Environ. 9 (6), 529–542.

Bandara, J.C., Thapa, R., Nielsen, H.K., Moldestad, B.M.E., Eikeland, M.S., 2021. Circulating fluidized bed reactors–part 01: analyzing the effect of particle modelling parameters in computational particle fluid dynamic (CPFD) simulation with experimental validation. Part. Sci. Technol. 39 (2), 223–236. https://doi.org/10.1080/02726351.2019.1697773.

Basu, P., 2018. Biomass gasification, pyrolysis and torrefaction: practical design and theory (Second ed.). London UK: Academic press (Elsevier).

Bates, R.B., Ghoniem, A.F., Jablonski, W.S., Carpenter, D.L., Altantzis, C., Garg, A., Barton, J.L., Chen, R., Field, R.P., 2017. Steam-air blown bubbling fluidized bed biomass gasification (BFBBG): Multi-scale models and experimental validation. AIChE J. 63 (5), 1543–1565. https://doi.org/10.1002/aic.v63.510.1002/aic.15666.

Bikane, K., Yu, J., Long, X., Paterson, N., Millan, M., 2020. Linking char reactivity to structural and morphological evolution during high pressure pyrolysis of Morupule coal. Chemical Engineering Science: X 8, 100072. https://doi.org/10.1016/j.cesx.2020.100072.

Chen, C.-J., Hung, C.-I., Chen, W.-H., 2012. Numerical investigation on performance of coal gasification under various injection patterns in an entrained flow gasifier. Appl. Energy 100, 218–228. https://doi.org/10.1016/j.apenergy.2012.05.013.

Chiesa, M., Mathiesen, V., Melheim, J.A., Halvorsen, B., 2005. Numerical simulation of particulate flow by the Eulerian-Lagrangian and the Eulerian-Eulerian approach with application to a fluidized bed. Comput. Chem. Eng. 29 (2), 291–304. https://doi.org/10.1016/j.compchemeng.2004.09.002.

Duchesne, M. A., 2012. Slagging in entrained-flow gasifiers. (Doctor Philosophiae). Université d'Ottawa/University of Ottawa. Retrieved from https://ruor.uottawa.ca/handle/10393/23353.

Eluk, T., Levy, A., Korytnyi, E., Bar-Kohany, T., 2017. Transition mechanism between combustion regions in swirling entrained flow downer reactors. Energy Fuels 31 (2), 1927–1934. https://doi.org/10.1021/acs.energyfuels.6b02225.

Gao, X., Zhang, Y., Bao, F., Li, B., Zhao, Y., Ke, C., Jiang, B., 2018. CFD modeling of sawdust gasification in a lab-scale entrained flow reactor based on char intrinsic kinetics. Part 1: Model development. Chemical Engineering and Processing-Process Intensification. 125, 280–289. https://doi.org/10.1016/j.cep.2018.02.017.

Gao, X., Zhang, Y., Li, B., Yu, X., 2016. Model development for biomass gasification in an entrained flow gasifier using intrinsic reaction rate submodel. Energy Convers. Manage. 108, 120–131. https://doi.org/10.1016/j.enconman.2015.10.070.

Gungor, A., Yildirim, U., 2013. Two dimensional numerical computation of a circulating fluidized bed biomass gasifier. Comput. Chem. Eng. 48, 234–250. https://doi.org/10.1016/j.compchemeng.2012.09.012.

Guo, N., 2020. Modelling of reacting multi-phase flow for biomass gasification. Doctor Philosophiae. Norwegian University of Science and Technology.

Guo, N., García Llamas, Á.D., Li, T., Umeki, K., Gebart, R., Løvås, T., 2020. Computational fluid dynamic simulations of thermochemical conversion of pulverized biomass in a dilute flow using spheroidal approximation. Fuel 271, 117495. https://doi.org/10.1016/j.fuel.2020.117495.

Harris, S., Crighton, D., 1994. Solitons, solitary waves, and voidage disturbances in gas-fluidized beds. J. Fluid Mech. 266, 243–276. https://doi.org/10.1017/S0022112094000996.

IEA., 2019. Global Energy & CO2 Status Report 2019. https://www.iea.org/reports/global-energy-co2-status-report-2019. (accessed 28 March 2021)

Ku, X., Li, T., Løvås, T., 2014. Eulerian–lagrangian simulation of biomass gasification behavior in a high-temperature entrained-flow reactor. Energy Fuels 28 (8), 5184–5196. https://doi.org/10.1021/ef5010557.

Ku, X., Wang, J., Jin, H., Lin, J., 2019. Effects of operating conditions and reactor structure on biomass entrained-flow gasification. Renewable Energy 139, 781–795. https://doi.org/10.1016/j.renene.2019.02.113.

Kumar, M., Ghoniem, A.F., 2013. Application of a validated gasification model to determine the impact of coal particle grinding size on carbon conversion. Fuel 108, 565–577. https://doi.org/10.1016/j.fuel.2013.02.009.

Lanza, A., Islam, M.A., de Lasa, H., 2016. CPFD modeling and experimental validation of gas–solid flow in a down flow reactor. Comput. Chem. Eng. 90, 79–93. https://doi.org/10.1016/j.compchemeng.2016.04.007.

Lee, J.G., Kim, J.H., Lee, H.J., Park, T.J., Kim, S.D., 1996. Characteristics of entrained flow coal gasification in a drop tube reactor. Fuel 75 (9), 1035–1042. https://doi.org/10.1016/0016-2361(96)00084-1.

Liang, Y., Guo, C.Y., Zhao, X., Qin, Q., Cheng, Y., He, L., 2020. CPFD simulation on particle behaviour in an entrained-flow gasifier. Clean Energy. 4 (1), 75–84. https://doi.org/10.1093/ce/zkz032.

García Llamas, Á.D., Guo, N., Li, T., Gebart, R., Løvås, T., Umeki, K., 2020. Morphology and volume fraction of biomass particles in a jet flow during devolatilization. Fuel 278, 118241. https://doi.org/10.1016/j.fuel.2020.118241.

Long, X., Spiegl, N., Berrueco, C., Paterson, N., Millan, M., 2020. Fluidised bed oxy-fuel gasification of coal: Interactions between volatiles and char at varying pressures and fuel feed rates. Chemical Engineering Science: X. 8,. https://doi.org/10.1016/j.cesx.2020.100068 100068.

Mu, L., Buist, K.A., Kuipers, J.A.M., Deen, N.G., 2020. Scaling method of CFD-DEM simulations for gas-solid flows in risers. Chemical Engineering Science: X. 6, 100054. https://doi.org/10.1016/j.cesx.2019.100054.

Nakhaei, M., Grévain, D., Jensen, L.S., Glarborg, P., Dam–Johansen, K., Wu, H., 2021. NO emission from cement calciners firing coal and petcoke: A CPFD study. Applications in Energy and Combustion Science. 5, 100023. https://doi.org/10.1016/j.jaecs.2021.100023.

Nakhaei, M., Hessel, C.E., Wu, H., Grévain, D., Zakrzewski, S., Jensen, L.S., Glarborg, P., Dam-Johansen, K., 2018. Experimental and CPFD study of gas–solid flow in a cold pilot calciner. Powder Technol. 340, 99–115. https://doi.org/10.1016/j.powtec.2018.09.008.

Nakhaei, M., Wu, H., Grévain, D., Jensen, L.S., Glarborg, P., Dam–Johansen, K., 2019. CPFD simulation of petcoke and SRF co–firing in a full–scale cement calciner. Fuel Process. Technol. 196, 106153. https://doi.org/10.1016/j.fuproc.2019.106153.

Qin, K. (2012). Entrained flow gasification of biomass. (Doctor Philosophiae). Technical University of Denmark. Retrieved from https://hdl.handle.net/11250/2650837.

Ren21., 2020. Renewables 2020 - Global status report. Retrieved from https://www.ren21.net/wp-content/uploads/2019/05/gsr_2020_full_report_en.pdf. (accessed 08 April 2021)

Sepman, A., Yngve, Ö., Zhechao, Q., Henrik, W., Florian, M.S., 2017. Real-time in situ multi-parameter TDLAS sensing in the reactor core of an entrained-flow biomass gasifier. Proc. Combust. Inst. 36 (3), 4541–4548. https://doi.org/10.1016/j.proci.2016.07.011.

Shi, X., Sun, R., Lan, X., Liu, F., Zhang, Y., Gao, J., 2015. CPFD simulation of solids residence time and back-mixing in CFB risers. Powder Technol. 271, 16–25. https://doi.org/10.1016/j.powtec.2014.11.011.

Smagorinsky, J., 1963. General circulation experiments with the primitive equations: I. The basic experiment. Monthly weather review. 91(3), 99-164. 10.1175/1520-0493(1963)091<0099:GCEWTP>2.3.CO;2.

Snider, D.M., Clark, S.M., O'Rourke, P.J., 2011. Eulerian-Lagrangian method for three-dimensional thermal reacting flow with application to coal gasifiers. Chem. Eng. Sci. 66 (6), 1285–1295. https://doi.org/10.1016/j.ces.2010.12.042.

Thapa, R.K., 2015. Optimization of flow behavior in biomass gasification reactor. Doctor Philosophiae. Telemark University College, Norway.

Thapa, R.K., Frohner, A., Tondl, G., Pfeifer, C., Halvorsen, B., 2016. Circulating fluidized bed combustion reactor: Computational Particle Fluid Dynamic model validation and gas feed position optimization. Comput. Chem. Eng. 92, 180–188. https://doi.org/10.1016/j.compchemeng.2016.05.008.

Thapa, R.K., Halvorsen, B.M., 2014. Heat transfer optimization in a fluidized bed biomass gasification reactor. Heat Transfer XIII: Simulation and Experiments in Heat and Mass Transfer. 83, 169. https://doi.org/10.2495/HT140161.

Timsina, R., Thapa, R.K., Moldestad, B.M., Eikeland, M.S., 2020. Experiments and computational particle fluid dynamics simulations of biomass gasification in an air-blown fluidized bed gasifier. International Journal of Energy Production and Management. 5 (2), 102–114. https://doi.org/10.2495/EQ-V5-N2-102-114.

Verma, V., Padding, J.T., 2020. A novel approach to MP-PIC: Continuum particle model for dense particle flows in fluidized beds. Chemical Engineering Science: X. 6,. https://doi.org/10.1016/j.cesx.2019.100053 100053.

Voultsos, I., Katsourinis, D., Giannopoulos, D., Founti, M., 2020. Integrating LCA with Process Modeling for the Energetic and Environmental Assessment of a CHP Biomass Gasification Plant: A Case Study in Thessaly, Greece. Eng—Advances. Engineering. 1 (1), 2–30. https://doi.org/10.3390/eng1010002.

Waldheim, L., Nilsson, T., 2001. Heating value of gases from biomass gasification. Retrieved from http://gasificationofbiomass.org/app/webroot/files/file/publications/HeatingValue.pdf.

Wang, Q., Niemi, T., Peltola, J., Kallio, S., Yang, H., Lu, J., Wei, L., 2015. Particle size distribution in CPFD modeling of gas–solid flows in a CFB riser. Particuology. 21, 107–117. https://doi.org/10.1016/j.partic.2014.06.009.

Weiland, F., Hedman, H., Marklund, M., Wiinikka, H., Öhrman, O., Gebart, R., 2013. Pressurized oxygen blown entrained-flow gasification of wood powder. Energy Fuels 27 (2), 932–941. https://doi.org/10.1021/ef301803s.

Weiland, F., Wiinikka, H., Hedman, H., Wennebro, J., Pettersson, E., Gebart, R., 2015. Influence of process parameters on the performance of an oxygen blown entrained flow biomass gasifier. Fuel 153, 510–519. https://doi.org/10.1016/j.fuel.2015.03.041.

Wu, Y., Shi, X., Liu, Y., Wang, C., Gao, J., Lan, X., 2020. 3D CPFD simulations of gas-solids flow in a CFB downer with cluster-based drag model. Powder Technol. 361, 400–413. https://doi.org/10.1016/j.powtec.2019.07.044.

Wu, Y., Zhang, J., Smith, P.J., Zhang, H., Reid, C., Lv, J., Yue, G., 2010. Three-dimensional simulation for an entrained flow coal slurry gasifier. Energy Fuels 24 (2), 1156–1163. https://doi.org/10.1021/ef901085b.

Ye, I., Ryu, C., 2015. Numerical modeling of slag flow and heat transfer on the wall of an entrained coal gasifier. Fuel 150, 64–74. https://doi.org/10.1016/j.fuel.2015.01.111.

Zhang, G.-Q., Ernst, L.J., de Saint Leger, O., 2000. Benefiting from thermal and mechanical simulation in micro-electronics. Springer, Netherlands.

Paper VII

Methanol synthesis from syngas: a process simulation

Ramesh Timsina, Rajan K. Thapa, Britt M. E. Moldestad and Marianne S. Eikeland

DOI: doi.org/10.3384/ecp21185444

Published in the Linköping Electronic Conference Proceedings, SIMS EUROSIM 2021, 444 - 449. ISSN: 1650-3686 (print), 1650-3740 (online)

Short overview

The paper contains a process model developed in Aspen Plus to study the conversion of syngas into methanol. The model was used to optimize some of the operating parameters in a methanol synthesis plant (distillation column) and provides an overview of the overall conversion steps and efficiency. The paper was presented at the SIMS EUROSIM Conference on Modelling and Simulation (SIMS EUROSIM 2021) held online from 21st to 23rd September 2021.

Methanol synthesis from syngas: a process simulation

Ramesh Timsina* Rajan k. Thapa Britt M.E. Moldestad Marianne S. Eikeland

Department of Process, Energy and Environmental Technology, University of South-Eastern Norway, Porsgrunn
{ramesh.timsina, rajan.k.thapa, britt.moldestad, marianne.eikeland}@usn.no
*Corresponding author: ramesh.timsina@usn.no

Abstract

Methanol is one of the major candidates to take over the petroleum based liquid transportation fuel. Methanol synthesis from syngas is proposed in this paper. The Aspen Plus simulation software was used to simulate the conversion process from syngas into methanol. A CSTR reactor with defined reaction kinetics was taken at 40 bar and 270°C to simulate the methanol synthesis. Hydrogen recycles gave an increase of 50.4% in the production of methanol as compared to the results without a H_2 recycle stream. The conversion of CO, CO_2 and H_2 are 50.4%, 99.8% and 100% respectively for the case with the H_2 recycle. Considering an operation of 8600 hr/year, the annual mass production of methanol is equal to 96492 tonnes for a feed rate of 154972 t/year. A distillation column is used to separate the methanol from water. Simulations were performed to calculate the minimum number of stages for the different recovery ratios of methanol in distillate and the required molar reflux ratio versus the purity of methanol in the distillate. The column temperature and the composition profile were analyzed for the column. The model provides the insights of the methanol synthesis plants for a specific quality and the quantity of methanol production.

Keywords: *methanol synthesis, Aspen Plus, process simulation, CO_2 mitigation, Distillation.*

Abbreviations: *CSTR - Continuous Stirred Tank Reactor, GHG - Green House Gas, STM - Syngas to Methanol, TPC - Thermo-Photo Catalyst,*

1 Introduction

The increasing environmental problems due to the excessive use of fossil fuels have led to implementing laws and agreements to limit global Green House Gas (GHG) emissions. Several countries agreed to the objective of the Paris Climate Change Conference (COP21), i.e. to limit the rise of global temperature less than 2°C by 2035 as compared to the preindustrial era (Dessens *et al.*, 2016). Thus, biomass is one of the promising alternatives for the replacement of fossil fuels based liquid transportation fuels in the near future. As compared to the other renewable energy sources, biomass can be converted into added-value products similar to that of fossil fuels and power (Puig-Gamero *et al.*, 2018).

Lignocellulosic biomass and biomass waste can be converted into value-added chemicals and biofuels via thermochemical or biochemical conversion. The biochemical route is complex and more expensive than thermochemical conversion (Sikarwar *et al.*, 2017). Among the different thermochemical conversion technologies, gasification is considered the cost-effective and efficient technology for lignocellulosic biomass (Sikarwar *et al.*, 2017). The lower emission of GHGs is due to the low-oxidation environment and lower amount of sulfur and nitrogen present in the biomass (Kumari & Mohanty, 2020; Pauls *et al.*, 2016). Gasification of biomass gives a product gas mainly consisting of syngas (CO, H_2). However, the gas also contains CH_4, CO_2, H_2O, N_2 and impurities such as tars, NH_3, H_2S.

After gas cleaning and conditioning, the syngas obtained from biomass gasification can be used to produce biofuels and chemicals such as methanol.

Methanol is one of the important industrial chemicals that can be used directly as a fuel or can be blended into conventional fuels. Methanol is an important ingredient for the production of formaldehyde, acetic acid, methyl tertiary butyl ether, and gasoline.

China is the leading producer of methanol, approximately 50% of the global production and a total of 43 million tons was produced in 2016 (Yang et al., 2018). However, methanol production is mainly based on natural gas and coal. Olah et al. (Olah, 2005) proposed a 'methanol economy' as a realistic technique compared to the widely mentioned 'hydrogen economy' due to the suitability of the existing liquid fuel infrastructure (with a little modification) and higher safety compared to a hydrogen vehicle.

The current study gives insights into a methanol synthesis plant, its production scale. A study of the distillation column was done in greater detail. The column temperature and composition profile are presented. The relation between the minimum number of stages for the different recovery ratios of methanol in distillate and the required molar reflux ratio versus the purity of methanol in the distillate are presented in the paper.

2 Methanol synthesis from syngas and carbon dioxide

As the synthesis gas stream usually contains some amounts of CO_2, methanol can be produced via direct hydrogenation of CO and CO_2. Table 1 shows the reactions concerning the methanol synthesis and their reaction heats. Reaction (c) is the reverse water gas shift reaction which is mildly endothermic as opposed to reactions (a) and (b). Therefore, a significant amount of cooling duty is required for these types of reactors. The thermodynamics of the conversion limits the overall conversion and thus recycling of the unreacted gas is required to achieve higher conversion. Therefore, cooling duty and recycling capacity determines the successful operation of such reactors.

The mixture of CO and H_2 can also react to produce other hydrocarbons such as methane, ethanol, or higher hydrocarbons. Therefore, the selectivity and efficiency of the catalyst play an important role in the conversion efficiency of these types of reactors.

The methanol synthesis reactor requires a specific ratio of $CO/CO_2:H_2$, and it is hard to obtain the desired ratio directly from a gasifier. The ratio needs to be shifted to a higher hydrogen content and is usually done via a water gas shift reaction. Two moles of H_2 are needed to react with CO and three moles of H_2 are needed to react with CO_2 for methanol formation according to the reaction stoichiometric given in Table 1.

Table 1. Reaction formulas for methanol synthesis

Reactions	*Reaction heat (kJ/mol)*
(a) $CO + 2H_2 \rightleftharpoons CH_3OH$	-90.64
(b) $CO_2 + 3H_2 \rightleftharpoons CH_3OH + H_2O$	-49.67
(c) $CO_2 + H_2 \rightleftharpoons CO + H_2O$	+41

2.1 Previous works

Different literature studies on methanol production are based on different feedstock such as natural gas (Al-Sobhi & Elkamel, 2015; Kralj & Glavič, 2009), synthesis gas (Lange, 2001), CO_2 hydrogenation (Van-Dal & Bouallou, 2013) and coal (Li *et al.*, 2018).

Methanol synthesis has been a wide research topic over the years. Methanol synthesis from syngas was first suggested by Paul Sabatier in 1905 and the first industrial scale plant came into operation in 1923 by Badische Anilin-und-Soda-Fabrik (BASF). The technology has been studied extensively during the 1970's Arab Oil Embargo, as an alternative to fossil-based petroleum (Wu-Hsun 1994).

Inlet temperature, reactor pressure and temperature, reactor types, catalysts system and process configurations have been the most investigated parameters. Hoseiny et al. (Hoseiny *et al.*, 2016) and Manenti et al. (Manenti *et al.*, 2011) have investigated

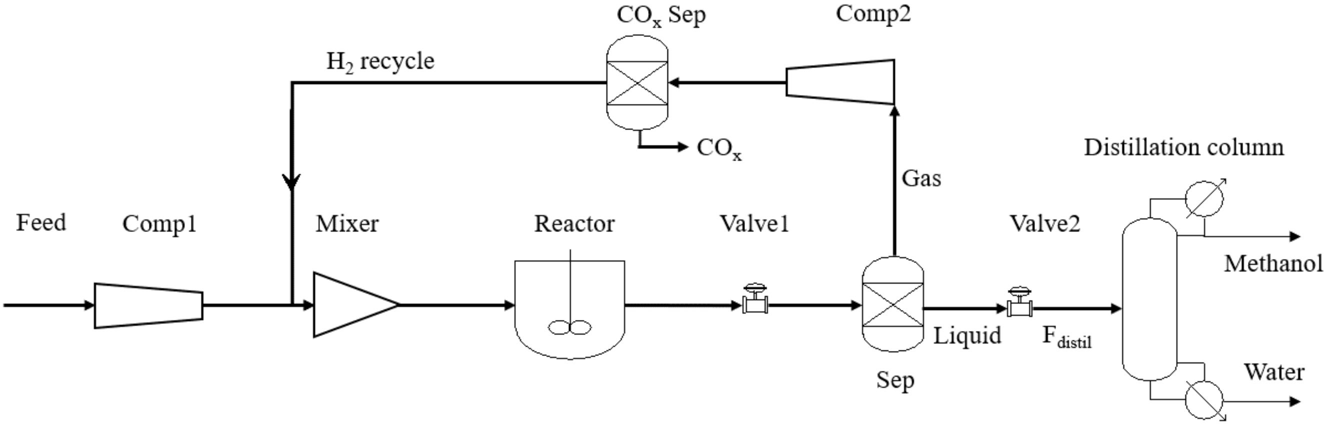

Figure 1. Schematic diagram for Aspen Plus model. Comp: Compressor, Sep: Separator, CO_x: Carbon oxides

the influence of feed temperature and reactor pressure in the methanol synthesis.

Cui and Kær (Cui & Kær, 2020) have studied the three different types of reactors i.e., adiabatic, water-cooled and gas-cooled reactor to investigate the traditional syngas to methanol (STM) process. The water-cooled reactor showed efficient heat removal, low hot-spot temperature and a relatively wide range of inlet temperature for control. The adiabatic reactor and the gas-cooled reactor demonstrated a relatively low and medium performance and low to medium capital costs (Cui & Kær, 2020).

Wu et al (Wu *et al.*, 2019) have developed a novel thermo-photo catalyst (TPC) for methanol production from syngas over Cu/Zn/Al catalyst. The authors demonstrated that the yield of methanol from TPC was 2.8 times higher than that from the thermal catalyst. TPC proved to be superior as compared to the thermal catalyst for the STM process.

Luyben (Luyben, 2010) has developed an economically feasible design for methanol production with three gas recycle streams to produce high quality methanol from syngas. Luyben showed a tradeoff between reactor pressure and feed compressor energy, reactor size and recycle flow rate, venting rate and reactant losses and flash pressure and flash compression energy (Luyben, 2010).

3 Materials and methods

Aspen Plus V11 was used to simulate the conversion of syngas into methanol. The process model developed in Aspen Plus is presented in Figure 1. The 'RK-Aspen' physical properties model was used for all the unit operations except the distillation column. Van Laar equations were used in the distillation column for the calculation of liquid activity coefficients. Different components as present in Table 4 were also defined in the physical property's environment. Table 4 also gives the mass flow rate for the different gases present in the feedstock and the molar ratio of $CO:CO_2:H_2$ is 1:3:10. A total of 11 moles is required to react completely with 1 mole of CO and 3 moles of CO_2, however, 10 moles of H_2 were taken due to the presence of the H_2 recycle path. The following assumptions were considered for the simulation process.

1. All gases were ideal.
2. Pressure and temperature were uniform inside the reactor.
3. The process was steady and isothermal.
4. The synthesis gas is pure and is supplied at a specified molar flow rate.

The standard operating condition for the methanol synthesis reactor are in pressure and temperature in the range of 50-100 atm and 220-280°C respectively (Ortiz *et al.*, 2013). The blocks used to simulate the methanol synthesis are summarized in Table 2.

Table 2. Block description used for methanol synthesis

Name	*Type, description*
Comp	Compressor: Both compressors compress the gases into 40 bars.
Reactor	RCSTR: Rigorous continuous stirred tank reactor with rate-controlled reactions based on known kinetics.
Sep	Separator: Separates liquids and gases.
CO_x Sep	Separator: Separates CO_x from H_2.
Distillation column	RadFrac: Rigorous 2 or 3- phase fractionation for single columns.

The pure syngas feed was compressed and heated up to the reactor operating pressure and temperature. Exothermic gas phase reactions were defined in the reactor for the synthesis of the methanol. The defined reactions in the reactor are presented in Table 1 and the reaction kinetics were taken from the study of Luyben (Luyben, 2010). The product from the reactor is depressurized to separate the non-converted gases from the liquid. The liquid enters into the distillation column to give methanol in the distillate and water in the bottom.

Table 3. The thermodynamic state of different units/flows

	Thermodynamic state	
	Temperature(°C)	Pressure (bar)
Feed	50	1
Comp1	-	40
Reactor	270	40
Valve1	-	10
Sep	60	10
Comp2	-	40
CO_x Sep	270	40
Valve2	-	1.5
F_{distil}	60	1.5

The conversion of hydrogen at this stage (without a recycle stream) is only about 50%, therefore a recycle stream is chosen to increase the hydrogen conversion. The separated gas is compressed to separate CO_x in another separator. H_2 separated from the CO_x separator enters the mixer before the reactor as a recycle feed. The overview of the temperature and pressure in the different blocks and streams is presented in Table 3.

The methanol-water separation is fairly easy and is performed at 1.4 bar condenser pressure and 1.7 bar reboiler pressure. Txy diagram at 1.5 bar pressure is given in Figure 2. The plot gives the temperature range at which the distillation column should operate to give higher purity of methanol in the distillate. In the simulated case, the distillation column operates in the temperature range of 74.9 to 100.15°C.

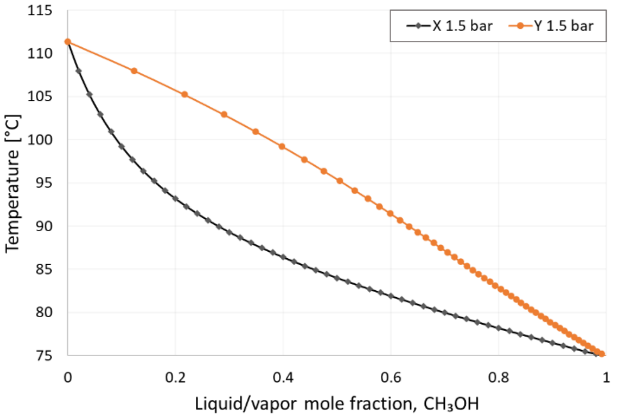

Figure 2. Txy diagram for methanol/water

A total condenser is selected for this simulation as sufficient cooling is available as the feed consists of 32.5 mass% of water at 60°C. This water is sufficient to condensate all the condensable vapor generated at the column overhead.

4 Results and discussion

Table 4 shows the mass balance for the simulated case. The table shows the yield of 2.33 tonnes of methanol per tonne of syngas ($CO+H_2$) supplied [calculated as methanol_out/(CO_in + H_2_in)]. Considering an operation of 8600 hr/year, the annual mass production of methanol is equal to 96492 tonnes. The conversion of CO, CO_2 and H_2 are 50.4%, 99.8% and 100% respectively and the results are similar to the study of Luyben (Luyben, 2010).

Table 4. Mass balance for the simulated case

Compound	In (t/hr)	Out (t/hr)
CO	2.8	1.39
CO_2	13.2	0.01
H_2	2.02	0
Methanol	0	11.22
H_2O	0	5.40

Several studies by different researchers show that methanol mainly originates from the CO_2 hydrogenation, and hardly from the CO hydrogenation (Kagan *et al.*, 1975; Nestler *et al.*, 2018). Therefore, CO conversion to methanol principally occurs via water gas shift reaction with subsequent CO_2 hydrogenation.

Simulations were performed to know the minimum number of stages for the desired recovery of methanol in distillate and the required molar reflux ratio for the desired purity of methanol in the distillate.

Figure 3 shows the minimum number of stages required to achieve the methanol recovery from 0.9 to 1. The number of minimum stages required increases linearly for up to around 98% methanol purity and increases exponentially after 98%. As most of the industrial scale, methanol synthesis plant operates at around 95% purity of methanol, which is relatively straightforward and doesn't overburden the column cost.

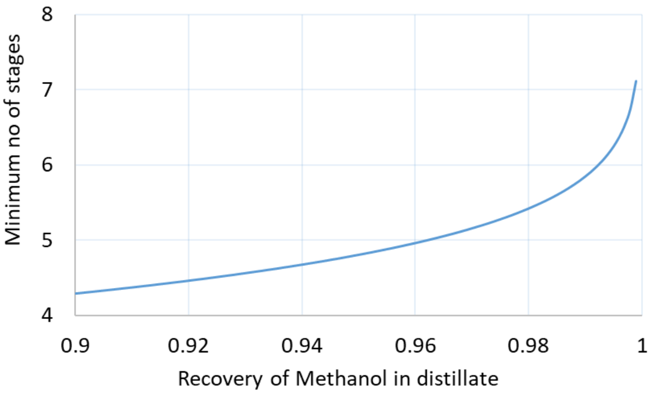

Figure 3. Minimum number of column stages required for corresponding methanol recovery

Figure 4 shows the purity of methanol for different molar reflux ratios. The purity of methanol increases with an increase in the molar reflux ratio, however the reboiler duty and cost increase linearly with an increase in reflux ratio. The purity of methanol synthesis increases steadily initially and exponentially for the higher methanol purity. Therefore, a tradeoff is required for the reflux ratio and the desired methanol purity in the column distillate.

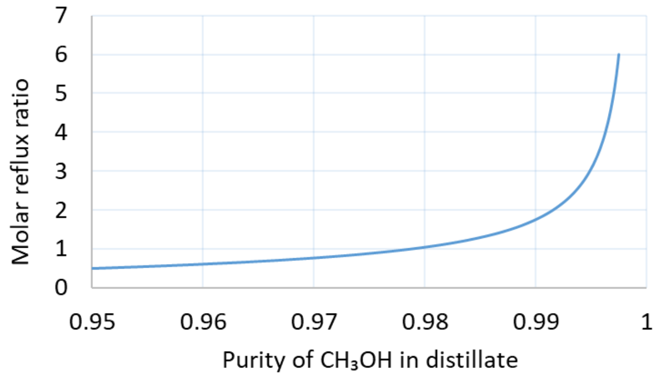

Figure 4. Molar reflux ratio vs methanol purity in distillate

As the total number of stages increases, energy costs and heat exchanger capital costs decrease, however, the total capital costs of the plant will increase. Therefore, a rigorous single distillation column with 7 stages was chosen to separate water from methanol. The selected number of stages gave the desired purity of methanol (95 mass percentage) in the distillate. The temperature profile across the stages is presented in Figure 5 and the liquid molar composition across the stages is presented in Figure 6. Stage 1 is the top of the column and stage 7 is the bottom of the distillation column.

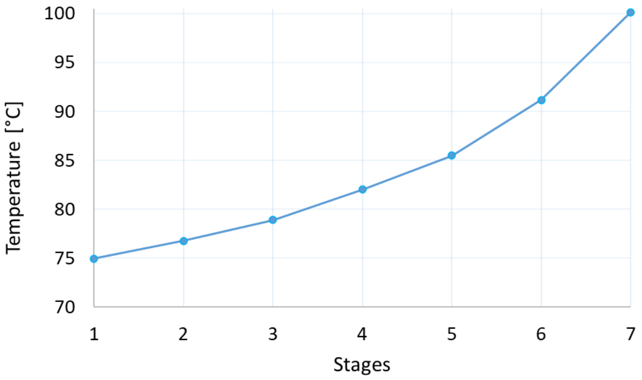

Figure 5. Column temperature profile

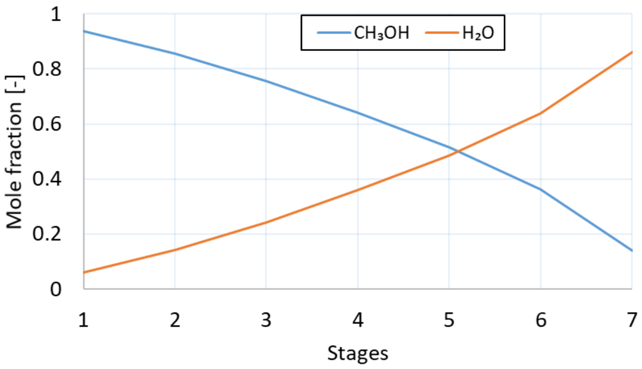

Figure 6. Column composition profile

The figure illustrates a gradual decrease in temperature from the bottom of the tower to the top of the distillation tower. The change of composition of methanol increases steadily from the bottom (stage 7) to the top (stage 1) and the mole fraction of water decreases steadily from the bottom to the top of the distillation tower.

The higher the system pressure, the smaller the reactor for a given recycle flow rate, which reduces the reactor and catalyst capital investment. However, for a given reactor size, the higher the pressure, the smaller the recycle flow rate, which reduces the recycle compressor capital investments and recycle compression energy.

Therefore, the design specification for a methanol synthesis plant depends upon the different parameters such as system pressure, temperature, reactor size, recycle flow rate, compressor energy, reflux ratio in the distillation column and the purity of methanol in the distillate.

Sensitivity analysis for the CSTR reactor showed relatively low sensitivity towards the change of temperature and pressure inside the reactor in the range of 220-280°C and 40-100 bar. The change in reactor pressure from 40 bar to 100 bar gave an increase of 1.7% in methanol production. Temperature variation from 220-280°C gave a 0.02% reduction in methanol synthesis.

5 Conclusion

A steady-state Aspen Plus™ model was developed to study the conversion of syngas into methanol. Simulations were performed to analyze the conversion process. The model was used to study the different integral parts of a methanol synthesis reactor such as compressor, heater, reactor, separator, and distillation column. The desired purity of methanol in the distillate was 95%. In order to achieve this for the given mass flow rate, a 7-stage rigorous two-phase single column was used.

The following results were obtained from the distillation column for the specified thermodynamic conditions.

- $\frac{CH_3OH \text{ in distillate}}{CH_3OH \text{ in feed}}$: 87.1%
- Distillate to feed ratio: 0.5
- Reflux ratio (molar): 1.2
- Purity of methanol in distillate: 96.4%
- Methanol production: 96492 tonnes/year

A cooling duty of 23.62 GJ/hr was required for the given flowrate specifications and a reactor size of 5 m³.

The model can further be improved by adding a suitable catalyst in the reactor, selecting/optimizing the reaction kinetics as well as performing the sensitivity analysis for the synthesis reactor. The distillation column can be optimized further based on the required specification for the methanol plant.

Acknowledgments

The authors would like to thank the University of South-Eastern Norway (USN) for providing the necessary software for the simulation works. The authors would like to acknowledge the Bio4Fuels projects in Norway.

References

S. Al-Sobhi and A. Elkamel. Simulation and optimization of natural gas processing and production network consisting of LNG, GTL, and methanol facilities. *Journal of Natural Gas Science and Engineering 23*, 500-508, 2015. doi.org/10.1016/j.jngse.2015.02.023.

X. Cui and S. K. Kær. A comparative study on three reactor types for methanol synthesis from syngas and CO2. *Chemical Engineering Journal*, *393*, 124632, 2020. doi.org/10.1016/j.cej.2020.124632.

O. Dessens, G. Anandarajah and A. Gambhir. Limiting global warming to 2° C: What do the latest mitigation studies tell us about costs, technologies and other impacts? *Energy Strategy Reviews*, *13*, 67-76, 2016. doi.org/10.1016/j.esr.2016.08.004.

S. Hoseiny, Z. Zare, A. Mirvakili, P. Setoodeh and M. Rahimpour. Simulation–based optimization of operating parameters for methanol synthesis process: application of response surface methodology for statistical analysis. *Journal of Natural Gas Science and Engineering, 34*, 439-448, 2016. doi.org/10.1016/j.jngse.2016.06.075.

Y. B. Kagan, L. Liberov, E. Slivinskii, S. Loktev, G. Lin, A. Y. Rozovskii, and A. Bashkirov. Mechanism of methanol synthesis from carbon dioxide and hydrogen.[Tracer study of conversion over Cu--Zn--aluminium oxide SNM-1 catalyst]. *Dokl. Chem.(Engl. Transl.);(United States), 221*. 1975

A. K. Kralj, and P. Glavič. Multi-criteria optimization in a methanol process. *Applied Thermal Engineering*, *29*(5-6), 1043-1049, 2009. doi.org/10.1016/j.applthermaleng.2008.05.015.

P. Kumari and B. Mohanty. Maximization of hydrogen production from pine needles steam gasification based on response surface methodology. *Biomass Conversion and Biorefinery*, 1-14, 2020. doi.org/10.1007/s13399-020-00761-7.

J.-P. Lange. Methanol synthesis: a short review of technology improvements. *Catalysis Today*, *64*(1-2), 3-8, 2001. doi.org/10.1016/S0920-5861(00)00503-4.

C. Li, H. Bai, Y. Lu, J. Bian, Y. Dong, and H. Xu. Life-cycle assessment for coal-based methanol production in China. *Journal of Cleaner Production*, *188*, 1004-1017, 2018. doi.org/10.1016/j.jclepro.2018.04.051.

W. L. Luyben. Design and control of a methanol reactor/column process. *Industrial & Engineering Chemistry Research*, *49*(13), 6150-6163, 2010. doi.org/10.1021/ie100323d.

F. Manenti, S. Cieri, and M. Restelli. Considerations on the steady-state modeling of methanol synthesis fixed-bed reactor. *Chemical Engineering Science*, *66*(2), 152-162, 2011. doi.org/10.1016/j.ces.2010.09.036.

F. Nestler, M. Krüger, J. Full, M. J. Hadrich, R. J. White, and A. Schaadt. Methanol synthesis–industrial challenges within a changing raw material landscape. *Chemie Ingenieur Technik*, *90*(10), 1409-1418, 2018. doi.org/10.1002/cite.201800026.

G. A. Olah. Beyond oil and gas: the methanol economy. *Angewandte Chemie International Edition*, *44*(18), 2636-2639, 2005. doi.org/10.1002/anie.200462121.

F. G. Ortiz, A. Serrera, S. Galera, and P. Ollero. Methanol synthesis from syngas obtained by supercritical water reforming of glycerol. *Fuel*, *105*, 739-751, 2013. doi.org/10.1016/j.fuel.2012.09.073.

J. H. Pauls, N. Mahinpey, and E. Mostafavi. Simulation of air-steam gasification of woody biomass in a bubbling fluidized bed using Aspen Plus: A comprehensive model including pyrolysis, hydrodynamics and tar production. *Biomass and bioenergy*, *95*, 157-166, 2016. doi.org/10.1016/j.biombioe.2016.10.002.

M. Puig-Gamero, J. Argudo-Santamaria, J. Valverde, P. Sánchez, and L. Sanchez-Silva. Three integrated process simulation using aspen plus®: Pine gasification, syngas cleaning and methanol synthesis. *Energy conversion and management*, *177*, 416-427, 2018. doi.org/10.1016/j.enconman.2018.09.088.

V. S. Sikarwar, M. Zhao, P. S. Fennell, N. Shah, and E. J. Anthony. Progress in biofuel production from gasification. *Progress in Energy and Combustion Science*, *61*, 189-248, 2017. doi.org/10.1016/j.pecs.2017.04.001.

É. S. Van-Dal, and C. Bouallou. Design and simulation of a methanol production plant from CO2 hydrogenation. *Journal of Cleaner Production*, *57*, 38-45, 2013. doi.org/10.1016/j.jclepro.2013.06.008.

X. Wu, J. Lang, Y. Jiang, Y. Lin, and Y. H. Hu. Thermo–Photo Catalysis for Methanol Synthesis from Syngas. *ACS Sustainable Chemistry & Engineering*, *7*(23), 19277-19285, 2019. doi.org/10.1021/acssuschemeng.9b05657.

S. Yang, B. Li, J. Zheng, and R. K. Kankala. Biomass-to-Methanol by dual-stage entrained flow gasification: Design and techno-economic analysis based on system modeling. *Journal of Cleaner Production*, *205*, 364-374, 2018. doi.org/10.1016/j.jclepro.2018.09.043.

C. Wu-Hsun. Methanol Production and Use. *Dekker*, 1994.

Paper VIII

Experimental evaluation of wood and grass pellets in a bubbling fluidized bed gasifier

Ramesh Timsina, Rajan Jaiswal, Rajan K. Thapa, Britt M. E. Moldestad, Ashish Bhattarai, Mladen Jecmenica*, Marianne S. Eikeland

Submitted to *Chemical Science*

Short overview

The paper contains the results from the gasification of wood pellets and grass pellets in the BFB gasification reactor. The pilot-scale gasifier has a capacity of 20 kW and is located at USN. Wood pellets and grass pellets were gasified in the temperature range of 750-900°C at atmospheric conditions. The product gas compositions and the gasifier performance (based on the mass balance of N_2 in the inlet and outlet gas) were measured and analyzed at different equivalence ratios. Gasifier performance was calculated in terms of product gas yield, LHV, CCE, CGE, and energy rate. Wood pellets showed reasonable results at a temperature of around 850°C with a carbon conversion of around 60%.

Not available online

Doctoral dissertation no. 118
2022

Modelling and simulations of bubbling fluidized bed and entrained flow biomass gasification reactors

Dissertation for the degree of Ph.D

Ramesh Timsina

ISBN: 978-82-7206-644-3 (print)
ISBN: 978-82-7206-645-0 (online)

usn.no